Functional analysis of DDR2 mutations leading to Warburg Cinotti syndrome

Ziteng Hao

Cardio-Respiratory Interface

National Heart and Lung Institute

Imperial College London

Dr Birgit Leitinger

A thesis submitted for the degree of

Doctor of Philosophy

March 2024

Statement of Originality

I Ziteng Hao declare that all the work presented in this thesis is my own, and any contributions from others are acknowledged.

Copyright declaration

The copyright of this thesis rests with the author. Unless otherwise indicated, its contents are licensed under a Creative Commons Attribution-Non Commercial 4.0 International Licence (CC BY-NC).

Under this licence, you may copy and redistribute the material in any medium or format. You may also create and distribute modified versions of the work. This is on the condition that: you credit the author and do not use it, or any derivative works, for a commercial purpose.

When reusing or sharing this work, ensure you make the licence terms clear to others by naming the licence and linking to the licence text. Where a work has been adapted, you should indicate that the work has been changed and describe those changes.

Please seek permission from the copyright holder for uses of this work that are not included in this licence or permitted under UK Copyright Law.

Abstract

Warburg Cinotti syndrome is described as a severe connective tissue disorder, with symptoms related to the hearing system, vision, skin and joints. Exome sequencing of patients revealed that two heterozygous variants (c.1829T>C; p.Leu610Pro and c.2219A>G; p.Tyr740Cys) located within the discoidin domain receptor 2 (DDR2) tyrosine kinase domain were responsible for this disease. We hypothesised that these two mutations may modify the inactive conformation and result in constitutive DDR2 kinase activity as well as changed cellular behaviour through enhanced matrix-induced signalling. In this project, constitutive activities of DDR2-L610P and DDR2-Y740C were observed in both an overexpression system using HEK293 cells and endogenous expression in patient primary fibroblasts. Biochemical and enzymological analysis of soluble recombinant DDR2 kinase constructs revealed the enhanced autophosphorylation and substrate phosphorylation rates found in DDR2-Y740C compared to DDR2-WT. Compared to WT cells, altered cellular behaviours were found in patient fibroblasts, including increased cell migration on 2D surfaces and enhanced cell-induced collagen gel contraction. Intriguingly, neither of the changes was primarily dependent on DDR2 kinase activity. Moreover, preliminary data revealed a potential relationship between DDR2 and integrin-mediated focal adhesion. These results suggested a kinase-independent role of DDR2 in regulating some of the functions of Warburg Cinotti fibroblasts. Our data support the hypothesis of constitutive mutant DDR2 kinase activity and changed cellular behaviour as the underlying mechanism of Warburg Cinotti syndrome.

Acknowledgements

I would like to express my deepest gratitude to my supervisor, Dr Birgit Leitinger, whose expertise and support have been indispensable during my research and writing of my final thesis. With her guidance, I have become more professional and independent as a scientist. Secondly, I am thankful to Prof Erhard Hohenester for his help with recombinant protein purification. I would also like to thank Prof Cecilie Bredrup from the University of Bergen for kindly providing the patient cells.

I am very grateful to Dr David Gaboriau at the Imperial College FILM facility for his help in cell imaging and guidance on wound healing assay quantification. Additionally, I would like to thank Dr Alessia David for her help in predicting the structure of the disease variants. Thank you also to Dr Valerie Good at the Baculovirus Facility and Dr Jessica Rowley at the Flow Cytometry Facility for the use of their facilities and for their generous help.

I would also like to thank all the previous and current lab members, Dr Fuad Mosis and Yuxuan Feng, for their support and friendship during my study. A special thank you goes to Dr Douglas Sammon for his help and guidance during the early stage of my research. It was a pleasure to work with such wonderful people. Thank you also to the people from the Cardio-Respiratory Interface section, including Ben, Narmin, Sek-Shir, Sally, Akif, Renos, Krisna, Nuun, and Mandy.

To my friends outside the lab, thank you for the support and encouragement during my PhD study. Specifically, I would like to thank Jieying, Jiaqi, Lina, Mengxuan, and Shuhan.

To my partner, Tianhao Gao, thank you for your unwavering support and for always standing by me through all the hardships I have experienced. I would also like to thank my pets, Peanut, Boba, Tiffany, and Pepper, for their company and many cuddles!

Finally, I would like to thank my grandparents, Daidi Li, Lianbin Hao, and Xinglan Li; my aunt and uncle, Xiaohang Hao and Xidong Sun; and my parents, Haiyan Liu and Yidong Hao, for their unconditional love, encouragement, patience, as well as the financial support. I dedicate this thesis to them.

Table of Contents

Statement of Originality **2**

Copyright declaration **3**

Abstract **4**

Acknowledgements **5**

Table of Contents **6**

Table of figures **9**

List of tables **11**

Abbreviations **12**

Chapter 1 Introduction **16**

1.1 Cell-surface receptors **16**

1.2 Receptor tyrosine kinases **17**

1.2.1 The structure of RTKs 17

1.2.2 The kinase domain structure and conformations 19

1.2.3 The regulation of kinase domain activity in RTKs 21

1.2.4 RTK activation and downstream signalling 23

1.2.5 RTKs in disease 26

1.3 Discoidin domain receptors **27**

1.3.1 DDR tissue expression and functions 28

1.3.2 DDR structure and domains 30

1.3.3 DDR activation and regulation 35

1.3.4 DDR downstream signalling 38

1.3.5 DDRs in disease 40

1.4 Warburg Cinotti Syndrome **43**

1.5 Hypothesis and aims **46**

1.5.1 Chapter aims 46

Chapter 2 Materials and Methods **47**

2.1 Materials **47**

2.1.1 Cell culture reagents 47

2.1.2 Molecular biology reagents 47

2.1.3 Buffer chemicals, solutions and reducing agents 48

2.1.4 Protein purification buffers 49

2.1.5 Peptides and inhibitors 49

2.1.6 Protein assay buffers 50

2.1.7 Gel running and Western blotting reagents 51

2.1.8 Flow cytometry and immunofluorescence reagents 52

2.1.9 Antibodies 53

2.2 Cloning **56**

2.2.1 Site-directed mutagenesis and subcloning 56

2.2.2 In-Fusion cloning 60

2.3 Soluble DDR2 construct expression **62**

2.3.1 Viral amplification and small-scale protein expression test 62
2.3.2 Large-scale protein purification 63
2.3.3 Optimization experiments for increasing DDR2-L610P-K protein solubility 64
2.3.4 Recombinant DDR2-L610P-K protein production in mammalian cells and *in vitro* functional analysis 64
2.4 Recombinant kinase protein autophosphorylation assay 65
2.5 Western blotting 65
2.6 Native gel electrophoresis 66
2.7 Protein kinase kinetic analysis 66
2.8 Mammalian cell culture 67
2.8.1 Cell passaging 67
2.8.2 Cell freezing and thawing 67
2.8.3 Cell seeding 68
2.8.4 Cell counting 68
2.9 Primary cell genotyping 68
2.10 DDR2 autophosphorylation assay 69
2.11 Deglycosylation assay 70
2.12 Flow cytometry 70
2.13 Phospho-array assay 71
2.14 Quantitative PCR 72
2.15 Immunofluorescence imaging 72
2.16 Wound healing assay 73
2.17 Cell morphology imaging 74
2.18 Collagen gel contraction assay 74
2.19 Cell adhesion assay 76
2.20 Statistical analysis 77

Chapter 3 Investigation of Warburg Cinotti Syndrome related DDR2 mutant activities 78
3.1 Introduction 78
3.2 Results 81
3.2.1 Locations of Warburg Cinotti mutants on DDR2 kinase domain 81
3.2.2 Production of recombinant soluble DDR2 kinase 84
3.2.3 Recombinant DDR2-L610P-K protein is unstable 90
3.2.4 DDR2 kinase has similar activation mechanism as DDR1 kinase 99
3.2.5 DDR2-Y740C kinase is more active than DDR2-WT kinase 105
3.2.6 Full-length Warburg Cinotti DDR2 mutants are constitutively active in the absence of collagen stimulation 110
3.2.7 Warburg Cinotti mutants can express on cell surface 113
3.2.8 DDR2 kinase inhibitors can block both recombinant and full-length DDR2 activity 116
3.3 Discussion 119

Chapter 4 Investigation of Warburg Cinotti Syndrome related DDR2 variants in patient primary dermal fibroblasts 125
4.1 Introduction 125
4.2 Results 126

4.2.1 Ligand-independent DDR2 phosphorylation in patient HDF cells can be blocked by VU6015929 126
4.2.2 Investigation of patient cell migration on two-dimensional surfaces 131
4.2.3 HDF cells expressing DDR2-Y740C exhibit increased collagen gel contraction..... 141
4.2.4 DDR2-Y740C expressing HDF cells induced collagen gel contraction via a DDR2 kinase activity-independent manner 146
4.2.5 Investigation of β1 integrin activities in Patient HDF cells 152
4.3 Discussion 157

Chapter 5 Regulation of signalling by Warburg Cinotti Syndrome DDR2 variants in patient primary dermal fibroblasts 162
5.1 Introduction 162
5.2 Results.....163
5.2.1 Determination of signalling molecules' phosphorylation or expression levels in HDF cells 163
5.2.2 Determination of selected gene expression levels in HDF cells 168
5.3 Discussion 170

Chapter 6 Final discussion 173
6.1 DDR2 kinase undergoes in *cis* activation loop autophosphorylation 173
6.2 Catalytic-independent functions of DDR2 kinase and potential issues in kinase inhibitor application for Warburg Cinotti syndrome.....174
6.3 DDR2 association with cytoskeleton and focal adhesion 176
6.4 Summary 178

Chapter 7 Appendix.....179

.....183

Reference list 191

Table of figures

Figure 1. 1 RTK subfamilies and their members 18
Figure 1. 2 Kinase domain structure 21
Figure 1. 3 Ligand-induced receptor dimerisation models 24
Figure 1. 4 DDR structure and isoforms 31
Figure 1. 5 Crystal structure of DDR1 DS and DS-like domains 33
Figure 1. 6 Sequence alignments of DDR1 and DDR2 kinase domains 35
Figure 1. 7 DDR1 phosphosites interaction with binding partners 39

Figure 2. 1 Schematic diagram illustrating different types of mutagenic primers used. 56
Figure 2. 2 Schematic diagram illustrating the key fragment locations on the pOPIN construct. 61
Figure 2. 3 Example images and equation used for collagen gel contraction assay quantification. 76

Figure 3. 1 The JM4 region is highly conserved. 79
Figure 3. 2 Warburg Cinotti syndrome affected DDR2 amino acid conservation and location. 82
Figure 3. 3 Warburg Cinotti syndrome variants are predicted to be damaging by structural analysis. 83
Figure 3. 4 Generation of soluble recombinant DDR2 kinase constructs. 85
Figure 3. 5 Large-scale purification of soluble recombinant DDR2-WT-K. 87
Figure 3. 6 Large-scale purification of soluble recombinant DDR2-Y740C-K. 89
Figure 3. 7 Recombinant DDR2-L610P-K is insoluble when expressed in Sf9 cells. 91
Figure 3. 8 Expression test for GST-tagged and SUMO-tagged DDR2-L610P-K generated in Sf9 cells. 93
Figure 3. 9 Expression test for MBP-tagged DDR2-L610P-K generated in Sf9 cells. 94
Figure 3. 10 Large-scale purification of soluble recombinant DDR2-L610P-K. 95
Figure 3. 11 Expression test for fusion-tagged DDR2-L610P-K in mammalian cells. 97
Figure 3. 12 *In vitro* kinase activity of soluble recombinant DDR2 kinase constructs. 98
Figure 3. 13 DDR2 kinase has similar activation mechanism as DDR1 (1 µM protein autophosphorylation assay). 100
Figure 3. 14 DDR2 kinase has similar activation mechanism as DDR1 (100 µM protein autophosphorylation assay). 102
Figure 3. 15 DDR2 JM4 and activation loop both undergo protein concentration independent autophosphorylation. 104
Figure 3. 16 DDR2-Y740C-K autophosphorylates quicker than DDR2-WT-K. 106
Figure 3. 17 Temperature impacts on DDR2-WT-K and DDR2-Y740C-K substrate phosphorylation rates. 108
Figure 3. 18 Determination of DDR2-WT-K and DDR2-Y740C-K catalytic activities. 109
Figure 3. 19 Full-length DDR2-Y740C and DDR2-L610P are constitutively active in the absence of collagen stimulation. 112
Figure 3. 20 Surface expressed DDR2-Y740C and DDR2-L610P are detected by immunofluorescence. 114
Figure 3. 21 Surface expressed DDR2-Y740C and DDR2-L610P are detected by flow cytometry. 115
Figure 3. 22 Dasatinib and VU6015929 block both DDR2-WT and DDR2-Y740C kinase abilities to phosphorylate substrate. 117
Figure 3. 23 DDR-specific inhibitor VU6015929 can block collagen-induced full-length DDR2 activation in the overexpression system. 118

Figure 4. 1 Verification of Warburg-Cinotti syndrome associated DDR2 heterozygous mutations by Sanger Sequencing. 127
Figure 4. 2 DDR2 autophosphorylation in WT and Warburg Cinotti patient cells. 130
Figure 4. 3 HDF cells wound healing assay on a non-collagen-coatedplate. 132
Figure 4. 4 HDF cells wound healing assay on a collagen-coated plate. 134
Figure 4. 5 Comparisons of gap closure percentages between cells migrating on non-collagen-coated and on collagen-coated surfaces. 135
Figure 4. 6 HDF cells wound healing assay on a non-collagen-coated plate in the presence of 100 nM VU6015929. 137
Figure 4. 7 Comparisons of gap closure percentages between cells cultured in DMSO medium and 100 nM VU6015929 medium (non-coated surface). 138
Figure 4. 8 HDF cells wound healing assay on a non-collagen-coated plate with 200 nM dasatinib treatment. 140
Figure 4. 9 HDF cell morphology change upon 200 nM dasatinib treatment. 141
Figure 4. 10 Schematic diagram of three collagen gel contraction assay models. 143
Figure 4. 11 Collagen gel contraction by HDF cells in the floating matrix model. 144
Figure 4. 12 Collagen gel contraction by HDF cells in the stressed matrix model. 145
Figure 4. 13 Collagen gel contractions by HDF cells in the stressed matrix model in the presence of 100 nM VU6015929. 147
Figure 4. 14 Comparisons of the gel contraction between cells cultured in DMSO medium and 100 nM VU6015929 medium. (stressed matrix model) 148
Figure 4. 15 Investigations of myofibroblast features. 150
Figure 4. 16 Collagen gel contractions by HDF cells in the stressed matrix model in the presence of 200 nM dasatinib. 151
Figure 4. 17 Collagen gel contractions by HDF cells in the stressed matrix model in the presence of 10 µg/mL P5D2 antibody. 153
Figure 4. 18 Mutant HDF cells exhibited changed adhesion to medium- and low-affinity integrin-specific collagen peptides. 155
Figure 4. 19 HDF cell surface expressed collagen-binding integrin subunits detection by flow cytometry. 156

Figure 5. 1 Detection of phosphorylation or expression status of selected signalling molecules by phospho-array. 164
Figure 5. 2 Quantification of phosphorylation or expression signal intensity of selected signalling molecules by phospho-array. 165
Figure 5. 3 Protein phosphorylation and expression analysis of key DDR2 downstream signalling molecules. 167
Figure 5. 4 Selected gene expression analysis in WT and Warburg Cinotti patient cells. 169

Figure 7. 1 Single cell RNA expressions for DDR1 and DDR2. 179

List of tables

Table 1. 1 Small molecule kinase inhibitors 27
Table 1. 2 A selection of Warburg Cinotti syndrome clinical features 45

Table 2. 1 Sequences of synthetic triple-helical collagen-derived integrin-selective peptides and control peptide (Xu et al., 2012, Xu et al., 2011) 50
Table 2. 2 List of primary antibodies 53
Table 2. 3 List of secondary antibodies and fluorescent dyes 55
Table 2. 4 Primer sequences 57
Table 2. 5 List of pOPIN constructs and their protein constructs name 61

Table 3. 1 Apparent K_{cat} and K_m values for Axltide peptide and ATP. 110
Table 3. 2 IC_{50} values from the dasatinib and VU6015929 inhibitor assays for blocking DDR2-WT-K and DDR2-Y740C-K kinase abilities to phosphorylate substrate. 117

Table 7. 1 Signalling protein names and their phosphorylation sites 180

Abbreviations

2D	two-dimensional
3D	three-dimensional
A.C.	African clawed
Acry/Bis	Acrylamide/Bis-acrylamide
ALK	anaplastic lymphoma kinase
APS	ammonium persulfate
Arg	arginine
Asp	aspartic acid
ATP	Adenosine triphosphate
Axl	tyrosine-protein kinase receptor UFO
Bcr-Abl	breakpoint cluster region Abelson
BPB	bromophenol blue
BSA	Bovine serum albumin
C-	carboxy
CAFs	Cancer-associated fibroblasts
Chk-2	checkpoint kinase-2
Comparative CT	ΔΔCT
CREB	cAMP-response element binding protein
CSF1R	colony-stimulating factor 1 receptor
DD	Dupuytren's disease
DDR	discoidin domain receptor
DFG	Asp-Phe-Gly
DMEM/F-12	Dulbecco's modified eagle medium/nutrient mixture F-12
DMSO	Dimethyl sulfoxide
dNTPs	deoxynucleotide triphosphates
DTT	dithiothreitol
ECD	extracellular domain
ECM	extracellular matrix
EDTA	ethylenediaminetetraacetic acid
EGFR	epidermal growth factor receptor
EMT	epithelial to mesenchymal transition
Endo H	Endoglycosidase H
eNOS	Endothelial nitric oxide synthase
Eph	Ephrin receptor
ER	endoplasmic reticulum
Erb	erythroblastic leukemia viral oncogene homologue
Erk	extracellular signal-regulated kinase
EtOH	ethanol
FAK	focal adhesion kinase
FBS	Fetal bovine serum
FC	Flow cytometry
FGFR	fibroblast growth factor receptor
FLT3	fms-like tyrosine kinase 3

GC	gel contraction assay
Glu	glutamic acid
Gly	glycine
GPCRs	G protein-coupled receptors
GSK-3β	glycogen synthase kinase 3β
HCC	Hepatocellular carccinoma
HCl	Hydrogen chloride
HDF	Human dermal fibroblast
HEK	Human embryonic kidney
HEPES	4-(2-Hydroxyethyl)piperazine-1-ethanesulfonic acid
HER	human epidermal growth factor receptor
His	histidine
HRD	His-Arg-Asp
HRV	human rhinovirus
Hsp90	heat shock protein 90 kD
IF	Immunofluorescence
Ig CAMs	cell adhesion immunoglobulin-like cell adhesion molecules
IGF1R	insulin-like growth factor 1
IMAC	immobilized metal affinity chromatography
InsR	insulin receptor
InsRR	insulin receptor-related receptor
IP	immunoprecipitation
IPF	idiopathic pulmonary fibrosis
IRE1	inositol-requiring enzyme type 1
IRS-1	insulin receptor substrate 1
JM	juxtamembrane
JNK	Jun N-terminal kinase
KCl	potassium chloride
KH_2PO_4	potassium phosphate monobasic
LB	Lysogeny broth
Lck	lymphocyte cell-specific protein-tyrosine kinase
LTK	leukocyte receptor tyrosine kinase
mAb	monoclonal antibody
MAPK	mitogen-activated protein kinase
MDCK	Madin-Darby canine kidney
MeOH	methanol
MET	mesenchymal epithelial transition factor
$MgCl_2$	magnesium chloride
MMP	matrix metalloprotease
$MnCl_2$	manganese chloride
MSK	mitogen- and stress-activated kinase
MuSK	muscle-specific kinase
N-	amino
NA	not available
Na_2HPO_4	sodium phosphate dibasic

NaCl	sodium chloride
NaF	sodium fluoride
NaH_2PO_4	sodium phosphate monobasic
NaOH	sodium hydroxide
Nck2	non-catalytic region of tyrosine kinase adaptor protein 2
ND	not determined
NEB	New England Biolabs
NF1	neurofibromatosis type 1
NGF	nerve growth factor
Ni-NTA	nickel-nitrilotriacetic acid
NSCLC	non-small-cell lung cancer
nTPM	normalised transcripts per million
ON	osteonectin
PARP1	poly(ADP-ribose)polymerase-1
PBS	Phosphate-buffered saline
PBS-T	PBS-Tween
PCR	Polymerase chain reaction
PDB	protein data bank
PDGFR	platelet derived growth factor receptor
PEI Max	Polyethylenimine Max
PFA	paraformaldehyde
Phe	phenylalanine
PI3-K	phosphoinositide 3-kinase
PIK3C2α	phosphatidylinositol-4-phosphate 3-kinase C2 domain containing α polypeptide
PKD	protein kinase D
PLCL-2	phospholipase C like 2
PLC-γ1	phospholipase C-γ1
PRAS40	proline-rich Akt substrate of 40 kDa
PTK7	protein tyrosine kinase 7
pY	phospho-tyrosine
PYK	Pyruvate kinase
qPCR	Quantitative PCR
RasGAP	Ras-specific GTPase-activating protein
Ret	rearranged during transfection
RhoA	Ras homolog family member A
ROCK	Rho-associated protein kinase
Ron	receptor d'origine kinase
Ror	receptor tyrosine kinase like orphan receptor
RSK	ribosomal s6 kinase
RTKs	receptor tyrosine kinases
Ryk	related to receptor tyrosine kinase
SCF	stem cell factor
SCP	single-cell proteomics
scRNA-seq	single-cell RNA sequencing

SDS	sodium dodecyl sulfate
Sf9	*Spodoptera frugiperda* 9
SFK	Src family kinases
SFM	serum-free medium
SHIP-1/2	SH2-containing 5'-inositol phosphatase-1/2
SHP	Src homology region 2 domain-containing phosphatase
SMED-SL	Spondylo-meta-epiphyseal dysplasia with short limbs
Stat	signal transducers and activators of transcription
T25	25cm2 tissue culture flask
T75	75cm2 tissue culture flask
TAB1	transforming growth factor-β-activated protein kinase 1-binding protein
TAE	Tris-Acetate-EDTA
TAZ	transcriptional coactivator with PDZ-binding motif
TBRI	TGF-β receptor I
TCEP	Tris(2-carboxyethyl)phosphine hydrochloride
TEMED	N,N,N',N'-Tetramethyl ethylenediamine
TGF-β1	transforming growth factor-β1
TIE	tyrosine kinase with immunoglobulin like and EGF like domains
TM	transmembrane
TN-C	Tenascin-C
Tris	Trizma base
Trk	tropomyosin receptor kinase
Tyr	Tyrosine
Tyro3	Tyrosine-protein kinase receptor 3
UV	ultraviolet
VEGFR	vascular endothelial growth factor receptor
WB	Western blot
WNK1	lysine deficient protein kinase
WT	wildtype
YAP	yes-associated protein
YFP	yellow fluorescent protein
α-SMA	alpha smooth muscle actin

Chapter 1 Introduction

1.1 Cell-surface receptors

In the human body, a fundamental cellular process is to sense environmental information and adapt to changes by altering cellular behaviours (Ullo and Case, 2023). To coordinate and communicate information between organs and tissues, cells express various surface receptors to sense and process different signals (Miller and Lappin, 2024). Extracellular signals include electrical, mechanical, and chemical factors, of which chemical signals are the majority in nature (Nair et al., 2019). Chemical signals consist of various ligand molecules, such as soluble factors (hormones, proteins, sugars, etc.) and components from the extracellular matrix (ECM) (Nair et al., 2019). Different ligands often bind to the extracellular region of the surface receptors with distinct binding patterns, resulting in conformational change to the receptor cytoplasmic region (Miller and Lappin, 2024). Once the ligand binding initiates activation of the receptor intracellular domain, signals can be transmitted rapidly downstream, or communication can occur between cells over a long distance (Ullo and Case, 2023).

The surface receptors responding to distinct ligand signals can be divided into four groups: ion channel receptors, adhesion receptors, G protein-coupled receptors (GPCRs) and enzyme-linked receptors (Ullo and Case, 2023). The ion channel receptors contain a special membrane-spanning region that opens a pore in the plasma membrane upon ligand (i.e. neurotransmitter) binding, allowing ions or lipid membrane-impermeable molecules to exchange (Li et al., 2014). The adhesion receptors include cadherin and cell adhesion immunoglobulin-like cell adhesion molecules (Ig CAMs) for cell-cell adhesion, sugar-binding selectins for immune cell arrestment, and integrins for cell-matrix attachment (Patel et al., 2003, Harjunpaa et al., 2019, Leitinger, 2011). These receptors act as a physical linker between the extracellular environment and intracellular cytoskeleton proteins (Kim et al., 2011). For instance, integrins can transduce intracellular signals through inside-out signalling to change their adhesiveness to the matrix or sense ligand binding signals to recruit downstream proteins, such as focal adhesion kinase (FAK) and Fyn, in an outside-in signalling direction (Luo et al., 2007, Pang et al., 2023). The GPCRs, also known as seven-pass transmembrane (TM) domain receptors, contain seven TM-spanning helices that pass through the plasma membrane seven times, connected via three loops for extracellular signal detection and three loops to associate with the intracellular heterotrimeric G protein (Rosenbaum et al., 2009). Ligand binding of GPCRs results in the

activation and release of the G protein, which subsequently induces the production of secondary messenger molecules to propagate the signals (Hilger et al., 2018, Rosenbaum et al., 2009). Finally, the enzyme-linked receptors contain a catalysis site within the cytosolic domain, with tyrosine kinase as the most common type (Miller and Lappin, 2024). Receptor tyrosine kinases (RTKs) are single-span TM proteins that activate their intracellular kinase domain upon ligand binding, delivering phosphorylation signals to downstream targets (Lemmon and Schlessinger, 2010). This chapter will start with the general activation mechanisms of typical RTKs and their kinase domain, followed by detailed information on an atypical RTK subfamily, the discoidin domain receptors (DDRs). A severe connective tissue disorder, Warburg Cinotti Syndrome, will be introduced at the end of this chapter, as mutations within the kinase domain of a DDR subfamily member (DDR2) have been reported to be responsible for this syndrome (Xu et al., 2018).

1.2 Receptor tyrosine kinases

1.2.1 The structure of RTKs

RTKs regulate several critical cellular processes, including proliferation, differentiation, cell metabolism, cell survival, cell migration, and cell cycle control (Lemmon and Schlessinger, 2010). The general structure of RTKs consists of a ligand-biding extracellular domain (ECD), a single-span TM segment, an intracellular catalytic tyrosine kinase domain with a short unstructured carboxy (C-) terminal tail region, as well as an extracellular and intracellular juxtamembrane (JM) region (**Figure 1. 1**) (Lemmon and Schlessinger, 2010). In humans, there are 55 known RTKs with highly conserved topology, and the diversity in their ECD architecture groups these RTKs further into 19 subfamilies (Lemmon and Schlessinger, 2010, Trenker and Jura, 2020, Wendler et al., 2021). The ECDs from different RTK subfamilies contain discrete structural domains with various sizes, providing a structural basis for the receptors to recognise distinct protein ligands in the human body (Trenker and Jura, 2020). For example, the EGFR ECD has four domains (DI-DIV) that form an autoinhibited conformation in the absence of ligand, in which ligand binding reorients the ECD and leads to the formation of a dimerisation arm between the ECDs from two EGFR monomers (**Section 1.2.4**). In most RTKs,

ligand binding to the ECD triggers the dimerisation of receptor monomers, which in turn leads to the close proximity of the intracellular kinase domains, facilitating transphosphorylation on

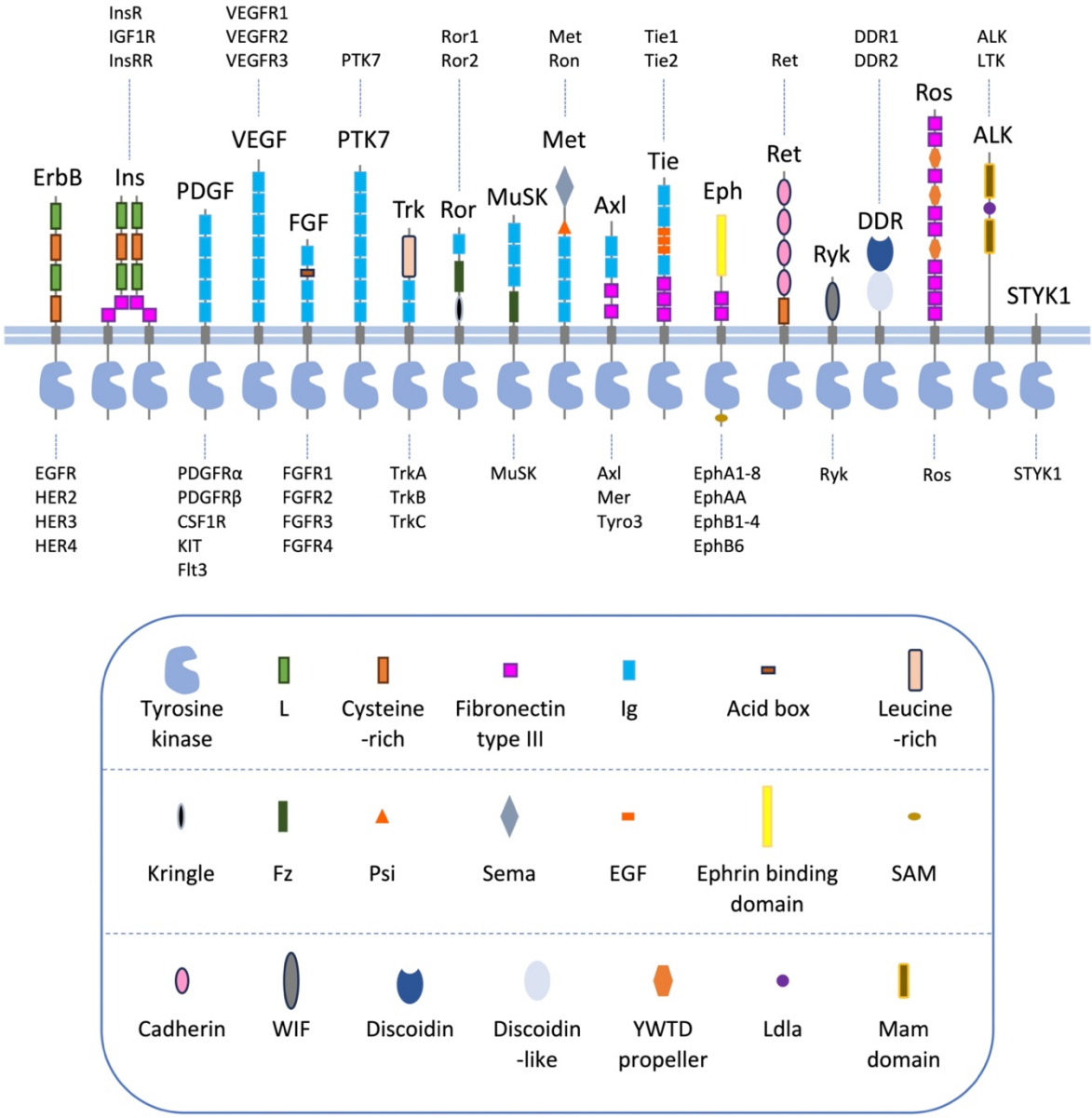


Figure 1. 1 RTK subfamilies and their members
Schematic diagram showing the molecular architecture of 19 RTK subfamilies with their members indicated on the top or bottom. Structural domains depicted by different shapes and colours are presented in the bottom box. Erb, erythroblastic leukemia viral oncogene homologue; EGFR, epidermal growth factor receptor; HER, human epidermal growth factor receptor; InsR, insulin receptor; IGF1R, insulin-like growth factor 1; InsRR, insulin receptor related receptor; PDGFR, platelet derived growth factor receptor; CSF1R, colony-stimulating factor 1 receptor; Flt3, fms-like tyrosine kinase 3; VEGFR, vascular endothelial growth factor receptor; FGFR, fibroblast growth factor receptor; PTK7, protein tyrosine kinase 7; Trk, tropomyosin receptor kinase; Ror, receptor tyrosine kinase like orphan receptor; MuSK, muscle-specific kinase; Met, mesenchymal epithelial transition factor; Ron, receptor d'origine kinase; Axl, tyrosine-protein kinase receptor UFO; Tyro3, tyrosine-protein kinase receptor 3; Tie, tyrosine kinase with immunoglobulin like and EGF like domains; Eph, ephrin receptor; Ret, rearranged during transfection; Ryk, related to receptor tyrosine kinase; ALK, anaplastic lymphoma kinase; LTK, leukocyte receptor tyrosine kinase; STYK1, Ser/Thr/Tyr kinase 1. This figure was made with PowerPoint and is adapted from (Lemmon and Schlessinger, 2010).

tyrosine residues, the first step in RTK signal transduction (Lemmon and Schlessinger, 2010). The TM segment also contributes to signalling transduction by stabilising receptor dimers and altering the orientation of the intracellular JM region or the catalytic region into a signalling-competent structure (Li and Hristova, 2006, Trenker et al., 2016). For example, introducing simultaneous mutations to the amino (N-) terminal dimerisation motif in the TM domain of EGFR abolished the receptor activity in response to EGF signals (Endres et al., 2013). The intracellular JM region acts as a linker between the TM segment and the catalytic kinase domain. Additionally, it can play an essential role in activating downstream proteins and/or regulating kinase activity (Li and Hristova, 2006). The kinase domain has a highly conserved architecture among most RTKs (Trenker and Jura, 2020). Autoinhibitory interactions and intracellular phosphatase activities work together to maintain the kinase domain in an inactive state in the absence of ligand stimulation (Lemmon and Schlessinger, 2010). An active receptor undergoes autophosphorylation on its intracellular JM and kinase domain, in which the phosphorylated tyrosine residues act as a docking site for cytoplasmic signalling proteins containing Src homology-2 (SH2) or phosphotyrosine-binding (PTB) domains (Lemmon and Schlessinger, 2010, Pawson, 2004). These molecules then activate downstream signalling cascades to regulate different cellular processes (Heldin et al., 2016, Lemmon and Schlessinger, 2010).

1.2.2 The kinase domain structure and conformations

All protein kinases are highly dynamic proteins that are structurally conserved. This protein family includes the tyrosine kinase domain in RTKs, the non-receptor tyrosine kinases, and the serine/threonine kinases (Kornev and Taylor, 2010). Protein kinases are flexible proteins consisting of two lobes: an N-lobe at the N-terminal end composed of a β-sheet with five strands and a single α-helix (termed αC-helix), and a larger C-lobe at the C-terminal end, consisting predominantly of α-helices and loops (McClendon et al., 2014). These two lobes are connected by a linker, with the active site being sandwiched in the middle cleft (termed catalytic cleft) (Endicott et al., 2012). Some key segments for kinase catalysis will be introduced in this chapter. These include N-lobe motifs such as the αC-helix, the P loop (a glycine-rich loop, Gly-rich loop), and the β3 strand. In the C-lobe, key regulatory segments include the activation loop with a DFG (aspartic acid-phenylalanine-glycine, Asp-Phe-Gly) motif and the

catalytic loop with an HRD (histidine-arginine-aspartic acid, His-Arg-Asp) motif (Endicott et al., 2012).

The active kinases share a very similar conformation, where the N-lobe and C-lobe adopt a 'packed' conformation to position the ATP and peptide substrate. To achieve the active state (**Figure 1. 2A**), the αC-helix moves to a closed position against the β-sheets of the N-lobe, which is often called the 'C-IN' conformation, in which the conserved glutamic acid (Glu) residue in the αC-helix interacts with the lysine (Lys) residue located on the β3 strand. This interaction stabilises the position of the Lys residue to an optimal distance for coordinating the α- and β-phosphate groups of adenosine triphosphate (ATP) (Endicott et al., 2012). The N-terminus of the activation loop consists of a conserved DFG motif, which is the key coordinator for ATP (Kornev et al., 2006). The Asp residue on the DFG motif faces into the active site and chelates a Mg^{2+} ion to interact with the α- and γ-phosphate groups of ATP. In addition, the P loop located in between the β1 and β2 strands also participates in stabilising the β- and γ-phosphate groups. By stabilising the ATP conformation with multiple interactions, the phosphate groups are oriented out of the adenosine pocket for γ-phosphate transfer to the peptide substrate (Kornev et al., 2006, Endicott et al., 2012). To coordinate the peptide substrate, the C-terminus of the activation loop moves to an extended conformation, which is triggered by activation loop phosphorylation. Additional interactions between the Asp residue of the HRD motif and a proton from the peptide substrate further stabilise the catalysis reaction (Jura et al., 2011). Different from the conserved kinase active conformation, the inactive kinases are often structurally diverse (**Figure 1. 2B**) (Noble et al., 2004, Kornev et al., 2006, Jura et al., 2011). This is because the inactive kinase structure is not constrained by catalytic requirements, allowing for different conformations to share a common theme (Endicott et al., 2012). The αC-helix can rotate into a position away from the C-lobe, with the interactions between Lys residue on the β3 strand and Glu residue on the αC-helix disrupted, which is often called the 'C-OUT' conformation. Apart from this, the movement of the DFG motif is a pivot point for determining the active or inactive state (Arter et al., 2022). In the active kinase, the Asp residue of the DFG motif points into the active site to form the 'DFG-IN' configuration (Endicott et al., 2012). Conversely, in the inactive state, the DFG motif flips into the 'DFG-OUT' configuration, with the Asp residue moving away from the ATP binding site (Vijayan et al., 2015). Both DFG-IN and DFG-OUT configurations can be presented together

with different αC-helix positions (i.e. C-IN or C-OUT), while only DFG-IN and C-IN together forming an active kinase (Arter et al., 2022).

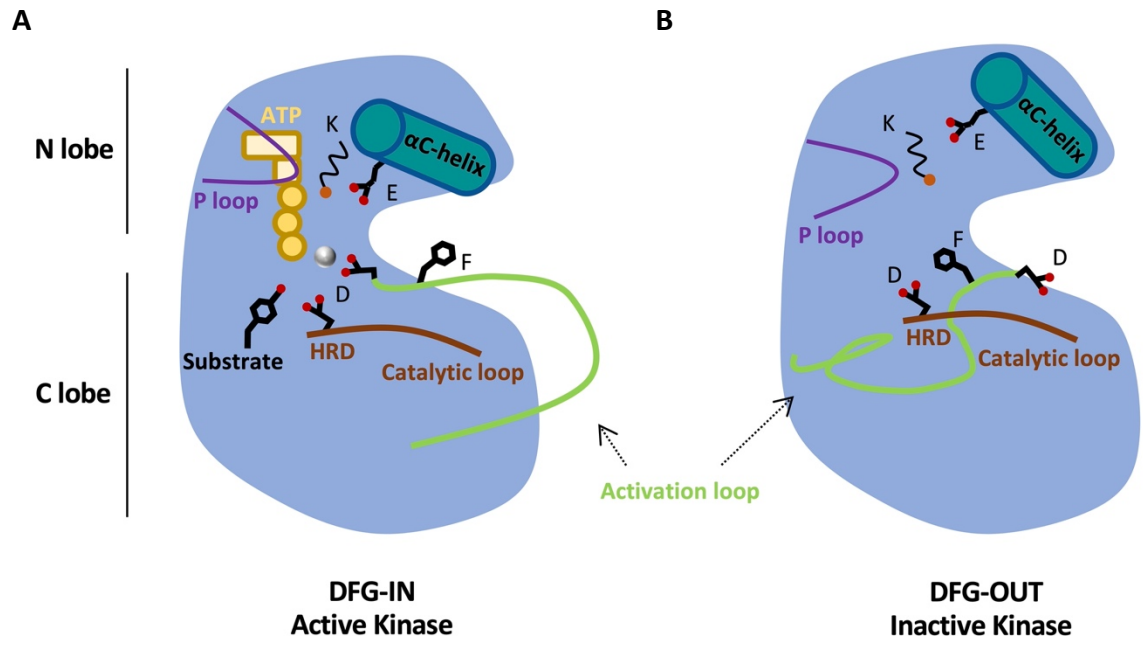


Figure 1. 2 Kinase domain structure
Schematic diagram showing the active and inactive kinase conformation with key segments and residues highlighted.
A. In the active kinase, the Lys residue on the β3 strand forms a salt bridge to the Glu residue on the αC-helix (teal), which stabilises the Lys residue to coordinate ATP (yellow) α- and β-phosphates. The activation loop (green) is phosphorylated, and the Asp residue of the DFG motif interacts with a Mg^{2+} ion (silver circle) to coordinate ATP. The P loop (purple) stabilises the ATP β- and γ-phosphate groups. The Asp residue of the HRD motif located on the catalytic loop (brown) interacts with a proton from the peptide substrate.
B. In the inactive kinase, the DFG motif flips to a DFG-OUT conformation, and the activation loop interacts with the Asp residue on the HRD motif to stabilise the inactive conformation. Orientation of the αC-helix and P loop disrupts the interaction between Lys and Glu residues.
This figure was made with PowerPoint and is adapted from (Jura et al., 2011)

1.2.3 The regulation of kinase domain activity in RTKs

The kinase domain catalytic activity is tightly regulated to avoid receptor activation in the absence of ligand binding (Lemmon and Schlessinger, 2010). Within a receptor monomer, intramolecular interactions are in place for *cis*-autoinhibition of the kinase domain (Hubbard, 2002). These can include the involvement of the kinase activation loop, intracellular JM domain, and the C-terminal tail (Hubbard, 2002, Bayliss et al., 2015).

The activation loop contributes to kinase catalysis and contains between one and three tyrosine residues as phosphorylation sites (Lemmon and Schlessinger, 2010). In the absence of phosphorylation, the activation loop is locked to a position that blocks access for both ATP

and peptide substrate (**Figure 1. 2B**) (Lemmon and Schlessinger, 2010). For example, the middle tyrosine residue in the activation loop of InsR tyrosine forms hydrogen bonds with adjacent residues in the active site, and *cis*-autophosphorylation (by its own kinase domain) on this residue is prevented by the DFG-OUT conformation (Hubbard et al., 1994). Although the unphosphorylated activation loop suppresses kinase catalytic activity in most kinases, the specific ways it does this can vary. A different mechanism to the InsR kinase is employed by the FGFR activation loop autoinhibition, in which the C-terminal end of the activation loop interferes with the peptide substrate binding site without occluding the ATP-binding site (Mohammadi et al., 1996). The *cis*-autoinhibition of kinase activity by the activation loop can be released by ligand-induced dimerisation or conformational change, in which *trans*-phosphorylation of activation loop results from close proximity of the kinase domains, which triggers movement of the activation loop away from its inhibitory conformation (**Figure 1. 2A**) (Lemmon and Schlessinger, 2010, Kavran et al., 2014).

Although the activation loop is a key structural element for regulating RTK activity, research has shown additional *cis*-autoinhibition mechanisms contributed by regulatory elements outside the kinase domain (Hubbard, 2004, Lemmon and Schlessinger, 2010). The intracellular JM region varies in size and length between different RTK subfamilies and often contains tyrosine residues (Hubbard, 2004). These residues serve as the docking site for downstream signalling proteins but can also participate in forming autoinhibitory interactions in some RTKs, such as Eph, MuSK, and KIT (Lemmon and Schlessinger, 2010, Till et al., 2002, Wybenga-Groot et al., 2001). In the EphB2 receptor, the JM region interacts with both the N-lobe and C-lobe of the kinase domain, resulting in a kinked αC-helix with the Lys-Glu salt bridge being disrupted and the activation loop being stabilised into the inactive conformation (Wybenga-Groot et al., 2001). In the MuSK receptor, instead of direct contact with the kinase domain, the JM region displays a different autoinhibitory mechanism by stabilising the interaction between the MuSK kinase domain and a MuSK signalling repressor (Till et al., 2002). Structural analysis of the KIT receptor cytoplasmic region revealed that the JM domain inserts into the kinase active site and stabilises the inactive configuration (Mol et al., 2004). This *cis*-autoinhibition on the JM region can be disrupted by ligand-induced dimerisation and *trans*-autophosphorylation.

The autoinhibitory role of the C-terminal tail was first reported in tyrosine kinase with TIE2 (Niu et al., 2002). The activation loop of TIE2 is not restrained in an inactive configuration, whilst the P loop is positioned to block ATP binding (Shewchuk et al., 2000). In addition, the tyrosine residues in its C-terminal tail block the peptide substrate binding site (Shewchuk et al., 2000). Similar to the relieve of JM region autoinhibition by its autophosphorylation, autophosphorylation of the C-terminal tail disrupts its interaction with the kinase domain and results in an active kinase conformation (Niu et al., 2002).

1.2.4 RTK activation and downstream signalling

A crucial question in RTK research is how ligand binding to the receptor extracellular region results in the phosphorylation of the intracellular kinase domain. For most RTKs, ligand binding is thought to promote the dimerisation of receptor monomers, in which autophosphorylation occurs between neighbouring RTKs (Lemmon and Schlessinger, 2010). However, the particular dimerisation method varies between RTK family members, and not all RTKs are activated by ligand-induced dimerisation. This section will include information for canonical ligand-induced dimerisation, ligand-induced receptor conformational change, ligand-induced oligomerisation, and downstream signalling.

Several ligand-induced receptor dimerisation models have been proposed. The most extreme 'ligand-mediated' model involves a bivalent ligand cross-linking the receptor monomers without allowing them to interact directly (Lemmon and Schlessinger, 2010). For instance, the dimeric nerve growth factor (NGF) is the ligand for TrkA, and TrkA dimerisation is accomplished by NGF contact with the Ig2 domain from each monomer (**Figure 1. 3A**) (Wehrman et al., 2007, Wiesmann et al., 1999). In contrast, receptor dimerisation can be entirely 'receptor-mediated, with no requirement for the ligand to participate in the dimer interface (Lemmon and Schlessinger, 2010). EGFR dimer serves as a typical representation of this model (**Figure 1. 3B**). The extracellular region of this receptor consists of four domains (DI-IV), and the bivalent ligand contacts the DI and DIII in one monomer, which unmasks the dimerisation arm in DII. Instead of cross-linking two monomers with one bivalent ligand, a 'back-to-back' dimer is induced (Garrett et al., 2002, Ogiso et al., 2002, Burgess et al., 2003). Alternatively, ligand binding can also cause an intermediate conformation with both ligand and receptor involved in the dimerisation (Lemmon and Schlessinger, 2010). For example, the KIT ligand (stem cell factor, SCF) binds to the membrane-distal domains (D1-3), subsequently

leading to the reorientation of the membrane-proximal domains (D4 and D5). D4 and D5 then form additional associations between receptor monomers (**Figure 1. 3C**) (Yuzawa et al., 2007, Liu et al., 2007). In addition to these three classic models, the dimerisation of FGFR revealed another mechanism that requires the involvement of both ligand (FGF) and an accessory molecule, heparin (**Figure 1. 3D**) (Lemmon and Schlessinger, 2010). The extracellular region of FGFR contains three Ig-like domains (D1-D3). A structural analysis presented a dimeric complex with FGFR1c extracellular region: FGF2: heparin in a 2:2:2 ratio (Schlessinger et al., 2000). Unlike NGF and SCF, FGF ligands are monomeric and contact both receptor monomers in the dimer, with the attachments stronger with one than the other. The two monomers interact directly through their D2 domain, further stabilising the dimerisation. Moreover, heparin forms interaction with both two ligands and two monomers in the dimer complex.

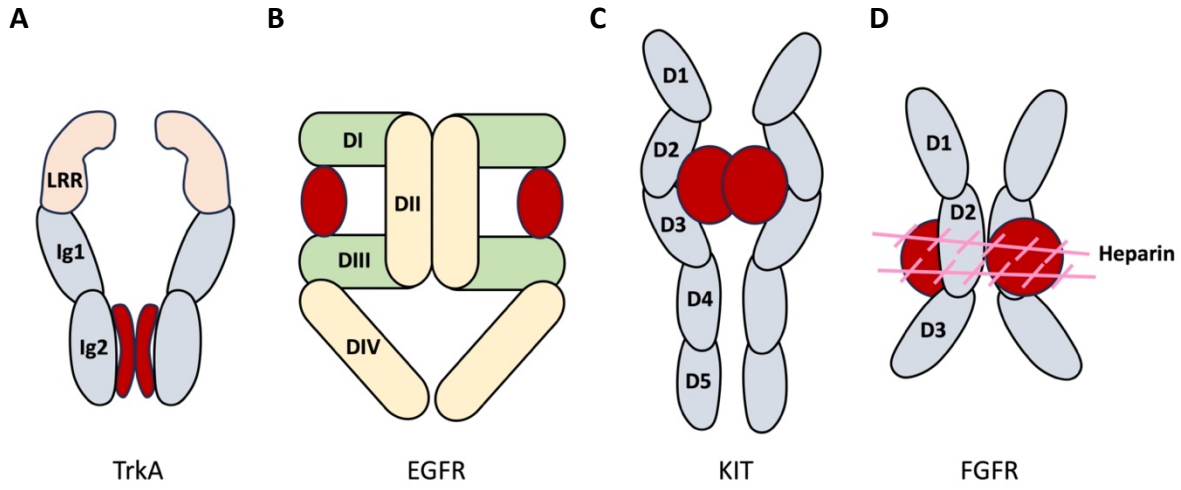


Figure 1. 3 Ligand-induced receptor dimerisation models
Schematic diagram showing the four ligand-induced receptor dimerisation models.
A. TrkA contains two Ig domains (grey) and one leucine-rich domain (orange) in its ECD region. Two receptor monomers bind to NGF (red) without direct receptor-receptor contact.
B. EGFR contains two L domains (green) and two cysteine-rich domains (yellow) in its ECD region. Two receptor monomers bind to EGF (red) and form a dimer with only receptor-receptor interactions through DII domain.
C. KIT contains five Ig domains in its ECD region. SCFs (red) binding to D2 and D3 domains results in an association formed by D4 and D5 domains between receptor monomers.
D. FGFR contains three Ig domains in its ECD region. The dimerisation of FGFR requires both FGF (red) and heparin (pink) involvement. This figure was made with PowerPoint and is adapted from (Lemmon and Schlessinger, 2010).

Ligand-induced dimerisation is a typical mechanism for most RTK activation, however, this is not a universal process. Some RTKs, such as InsR, form ligand independent covalent dimers (De Meyts, 2000). Ligand-binding dramatically changes both the receptor extracellular and intracellular conformation to stabilise the active kinase configuration; however, the

mechanism has not yet been completely understood (Yunn et al., 2023). Additionally, ligands are also capable of inducing the formation of higher-order oligomers. For example, the Eph receptor binds to the ephrin ligand expressed on the neighbouring cells instead of binding to soluble ligands (Stein et al., 1998). Structural analysis of EphA2 revealed two interfaces between adjacent receptors in an oligomer, including the 'dimerisation' and 'clustering' interfaces (Himanen et al., 2010, Seiradake et al., 2010). Taken together, RTK activation can be achieved in various ways, including ligand-dependent dimerisation, oligomerisation, and ligand-induced conformational change.

Upon receptor activation, the kinase domain undergoes autophosphorylation to disrupt the *cis*-inhibitory interactions (**Section 1.2.3**). This process stabilises the kinase into an active conformation and subsequently enhances its catalytic activity. The phosphorylated tyrosine residues then recruit signalling molecules containing SH2 or PTB domains (Lemmon and Schlessinger, 2010). As one RTK often contains several autophosphorylation sites, different SH2 and PTB domain-containing proteins can be recruited. This results in a complicated signalling network downstream of a signalling RTK. In addition, signalling downstream of the same receptor can vary depending on which ligand promotes receptor activation, as most RTKs can bind and be activated by multiple ligands (Trenker and Jura, 2020). For example, three ErbB receptors respond to a subset of 13 ligands, such as EGF, transforming growth factor (TGF)-α, and epigen (Wieduwilt and Moasser, 2008). This allows the same receptor expressed in different tissues to obtain various information from the environment. Moreover, binding to different ligands results in distinct receptor dimer conformation and unique phosphorylation states of tyrosines located on the C-terminal tail, which subsequently induce different downstream signalling and cell responses (Trenker and Jura, 2020). For example, EGFR binding to epigen forms a weaker dimer than when it binds to EGF and TGF-α (Freed et al., 2017). This weakened dimerisation leads to more sustained signalling and induces cell differentiation, compared to cell proliferation promoted by EGF-induced transient signalling (Freed et al., 2017). Moreover, the downstream signalling pathways activated by different RTKs are often overlapping (Lemmon and Schlessinger, 2010, Trenker and Jura, 2020). However, specific effects in cellular responses to different RTK signals vary due to the involvement of multiple positive and negative feedback mechanisms. For example, NGF receptor activation promotes cell differentiation, whilst EGFR activation results in cell

proliferation (Marshall, 1995). The mechanism by which RTKs utilise limited signalling pathways to induce specific cellular responses remains poorly understood.

1.2.5 RTKs in disease

Dysregulated RTK signalling is the underlying cause of numerous human diseases, making RTKs popular targets for therapeutic intervention (Du and Lovly, 2018). An extensive range of inhibitors have been investigated based on structural and biochemical studies of RTKs (Pottier et al., 2020). These inhibitors include monoclonal antibodies (mAbs) that target the receptor extracellular regions to disrupt activation and small molecule inhibitors that block the function of the kinase domain (Yamaoka et al., 2018).

The antibody development of the HER family presented a great example for targeting cancer-related RTK abnormal activation (Fauvel and Yasri, 2014). Within this subfamily, HER2 and HER3 undergo different activation mechanisms, in which the kinase-defective HER3 only participates in ligand binding-induced dimerisation, whilst HER2 does not bind to extracellular ligands but forms heterodimers with HER3 (Way and Lin, 2005). In breast tumours, overexpression of HER2 is an indicator of poor prognosis (Rubin and Yarden, 2001). An antibody called pertuzumab was designed to block ligand-induced HER2/HER3 heterodimerisation and inhibit HER3 signalling (Adams et al., 2006, Agus et al., 2002). In addition, trastuzumab results in downregulation of HER2 expression levels on the cell surface and directs the cells to the immune system for antibody-dependent cell-mediated cytotoxicity of tumour cells (Cuello et al., 2001, Arnould et al., 2006). Interestingly, trastuzumab binding can inhibit intracellular signalling pathways without blocking HER2 dimerisation with other HER family members (Gajria and Chandarlapaty, 2011, McLarty et al., 2009). The investigation of these inhibitors showed how mAbs can interfere with RTK activation and signalling.

Over the past few decades, six groups of small molecule inhibitors (**Table 1. 1**) have been designed to target the kinase active site and prevent the phosphorylation of downstream signalling proteins (Pottier et al., 2020, Roskoski, 2016). The ATP-competitive inhibitors bind in the ATP binding site, with type I inhibitors targeting the active DFG-IN conformation and type II inhibitors targeting the inactive DFG-OUT conformation (Pottier et al., 2020). Although these types of inhibitors have been clinically useful, the highly conserved kinase structure often results in inhibitors being promiscuous and thus leading to off-target effects (Hanson et

al., 2019). Both type III allosteric inhibitors and type V covalent inhibitors are designed to be potent and highly selective (Pottier et al., 2020). However, inhibitor resistance can rapidly arise by activating by-pass signalling or the existence of additional RTK mutations (Yamaoka et al., 2018). For instance, inhibition of HER2 leads to a compensatory upregulation of HER3 and activation of downstream signalling molecules (Garrett et al., 2011). Applying allosteric inhibitors can overcome the resistance induced by additional RTK mutations. For example, allosteric inhibitor cetuximab, instead of the original first-line medicine gefitinib (type I inhibitor), is more effective in treating non-small-cell lung cancer (NSCLC) with additional EGFR mutation (T790M) (Kris et al., 2003, Jia et al., 2016). Thus, investigation of RTK and kinase activation mechanisms contributes to the design of inhibitors to overcome potential resistance.

Table 1. 1 Small molecule kinase inhibitors
Six groups of small molecule kinase inhibitors are shown with their binding site and examples indicated. NA, not available. This is adapted from (Roskoski, 2016).

Type	Binding	Example
I	ATP-competitive inhibitor, binds to DFG-IN conformation	Dasatinib (Roskoski, 2016)
II	ATP-competitive inhibitor, binds to DFG-OUT conformation	Imatinib (Roskoski, 2016)
III	Allosteric inhibitor, binds next to the ATP-site	Trametinib (Zhao et al., 2017)
IV	Allosteric inhibitor, no effect on ATP or peptide binding	Asciminib (Das et al., 2022)
V	Bivalent inhibitor, binds to two kinase regions	NA
VI	Covalent inhibitor	Afatinib (Roskoski, 2016)

1.3 Discoidin domain receptors

The discoidin domain receptors, DDR1 and DDR2, are RTKs named after their extracellular globular discoidin (DS) domain (Fu et al., 2013b, Leitinger, 2014, Agarwal et al., 2019). The DS domain was first discovered as the discoidin I protein of the slime mould *Dictyostelium discoideum* (Poole et al., 1981). The DDRs have several unique features that distinguish them

from typical RTKs. Firstly, instead of binding to soluble growth factors like other RTKs, the DDRs bind to different types of collagens, which are the most abundant proteins present in the ECM (Shrivastava et al., 1997, Vogel et al., 1997, Kadler et al., 2007). By binding to large triple helical collagens, the DDRs undergo ligand-induced activation (autophosphorylation) with unusually slow kinetics (in the order of hours), while typical RTKs are activated within seconds to minutes (Lemmon and Schlessinger, 2010, Shrivastava et al., 1997, Vogel et al., 1997). Moreover, activation by canonical ligand-induced receptor dimerisation does not apply to the DDRs, as they exist as constitutive non-covalently-linked dimers on the cell surface without collagen stimulation (Noordeen et al., 2006, Mihai et al., 2009, Xu et al., 2014). These characteristics suggest the atypical activation and regulation mechanisms of DDRs.

1.3.1 DDR tissue expression and functions

The DDRs are widely expressed in different tissues during embryo development and the adult body (Leitinger, 2014, Franceschi et al., 2023, Cario, 2018). DDR1 is mostly found in epithelial cells located in the brain, lung, kidney, spleen, and placenta (Di Marco et al., 1993, Johnson et al., 1993, Laval et al., 1994, Perez et al., 1994, Leitinger, 2014), while DDR2 is highly expressed in cells located in connective tissue cells of mesenchymal origin, such as found in skeletal and heart muscle, cartilage, kidney, and lung (Lai and Lemke, 1994, Karn et al., 1993, Alves et al., 1995, Leitinger, 2014). Based on the single cell RNA data from The Human Protein Atlas (Appendix, **Figure 7. 1**), DDR1 and DDR2 mRNA expression was mostly exclusive in different cell types, with only astrocytes showing comparable DDR1 and DDR2 mRNA expression levels. In line with the protein level evidence introduced above, DDR1 and DDR2 showed overall high mRNA expression levels in epithelial cells and mesenchymal cells, respectively.

During development, DDR1 and DDR2 play a key role in organogenesis and bone growth, respectively (Leitinger, 2014). The DDR1 knockout mouse model displays multiple defects in mammary gland development, including reduced cell motility, reduced collagen synthesis, and hyperproliferative epithelium, all of which lead to branching abnormalities (Vogel et al., 2001, Faraci-Orf et al., 2006). Further defects in kidney and inner ear structure can also be observed in Ddr1 -/- mice (Gross et al., 2004, Meyer zum Gottesberge et al., 2008). In humans, less is known about developmental disorders related to DDR1. Recent studies using coexpression network analysis with a transcriptomic database from the human brain revealed the possible role of DDR1 expression in schizophrenia and bipolar disorder by regulating

oligodendrocyte precursor cells and astrocytes proliferation (Muntane et al., 2021, Aranda et al., 2024). As DDR2 is expressed in connective tissue cells, such as fibroblasts and bone cells, the Ddr2 -/- mice exhibit dwarfism with reduced chondrocyte proliferation (Labrador et al., 2001). Moreover, DDR2 was found to regulate osteoblast differentiation and chondrocyte maturation, which influences skeletal development through endochondral ossification (Zhang et al., 2011). A recent study revealed the cell-autonomous functions of DDR2 in resting and proliferative chondrocyte colonies and skeleton progenitor cells, in which DDR2 regulates chondrocyte organisation, cell maturation and bone development (Mohamed et al., 2022, Mariadoss and Wang, 2023). In humans, four DDR2 mutations have been identified to be responsible for a rare genetic disorder called spondylo-meta-epiphyseal dysplasia with short limbs (SMED-SL) (Bargal et al., 2009). These mutations lead to collagen binding-deficient DDR2 (E113K) or trafficking defects (T731I, I726R, and R752C mutations), with DDR2 being retained on the endoplasmic reticulum before being degraded (Ali et al., 2010).

Apart from their contribution to development, both DDRs are found in immune cells and regulate certain immunological functions (Leitinger, 2014, Majo and Auguste, 2021). For instance, DDR1 is expressed on activated T cells and can mediate T cell migration in a three-dimensional (3D) collagen matrix (Kamohara et al., 2001, Hachehouche et al., 2010). Moreover, DDR1 was found to enhance T lymphocyte migration *in vitro* and *in vivo*, by activating p38 MAPK and the RhoA/ROCK/MAPK/ERK (Ras homolog family member A/Rho-associated protein kinase/mitogen-activated protein kinase/extracellular signal-regulated kinase) pathway (El Azreq et al., 2016). Similarly, neutrophil migration in a 3D collagen matrix has been shown to require functional DDR2 (Afonso et al., 2013). In addition to immune cell migration, DDRs are also critical mediators for matrix metalloprotease (MMP) production and activation (Leitinger, 2014, Majkowska et al., 2017, Mariadoss and Wang, 2023). MMPs in humans consist of 23 family members that are zinc-dependent proteases, which can be divided into groups of collagenases (MMP1, 8, 13, 18), gelatinases (MMP2, 9), stromelysins (MMP3, 10, 11), matrilysins (MMP7, 26), enamelysins (MMP20), divers groups (MMP19, 21, 23A, 23B, 27, 28), and membrane type MMPs (MT-MMPs) (MMP14, 15, 16, 17, 24, 25) (Hey and Linder, 2024). MMPs are able to cleave cell surface proteins and ECM components, therefore play an essential role in physiological and pathological processes involving tissue remodelling (Hey and Linder, 2024). DDR-regulated MMPs participate in tissue remodelling by

degrading ECM components and facilitating cell migration or invasiveness (Leitinger, 2014, Itoh, 2018). For instance, collagen IV induced DDR1 activation in MDA-MB-231 breast cancer cells results in an upregulation of MMP2 and MMP9 secretion, which subsequently promoted cancer cell invasion (Castro-Sanchez et al., 2011). DDR2 is required for collagen production and MMP2 expression in dermal fibroblast cells, with both collagen and MMPs contributing to tissue homeostasis and regeneration during wound healing (Olaso et al., 2002). Moreover, DDR2 expression and activity was found to positively mediate collagen-induced MMP14 (MT1-MMP) activation in fibroblast cells (Majkowska et al., 2017). Overall, both DDR1 and DDR2 can control cell functions in different tissues, such as migration, proliferation, and differentiation (Leitinger, 2014). Although studies have unmasked DDR functions in tissue development and regeneration (i.e. in brain, skin, and bones) (Vilella et al., 2019, Cario, 2018, Mariadoss and Wang, 2023), the primary investigations have been focused on pathological rather than physiological conditions (Leitinger, 2014). An in-depth understanding of the DDR function in adult tissues is crucial for future research.

1.3.2 DDR structure and domains

Like all RTKs, DDRs are single-span TM proteins with an intracellular tyrosine kinase domain (**Figure 1. 4**) (Lemmon and Schlessinger, 2010, Leitinger, 2014). Although the DDR kinase domains are most similar to that of the TrkA receptor (about 45% amino acid identity), their extracellular regions do not contain any Ig-like domains or other structural motifs (fibronectin domains or cysteine-rich domains) that are seen in many RTKs (Lemmon and Schlessinger, 2010, Leitinger, 2014). Instead, the DDRs contain two unique globular domains in the extracellular region: the N-terminal DS domain which is connected to a DS-like domain (**Figure 1. 4**) (Carafoli et al., 2012, Carafoli and Hohenester, 2013). A poorly conserved extracellular JM segment of about 50 (DDR1) or 30 (DDR2) amino acids links the DS-like domain with the TM domain (Carafoli and Hohenester, 2013) (**Figure 1. 4**). The DS-like domain and extracellular JM region contain several predicted N- and O-glycosylation sites (**Figure 1. 4**)(Carafoli and Hohenester, 2013, Fu et al., 2013b, Leitinger, 2014). The intracellular region starts with a long flexible JM segment of up to 171 (varies in length between DDR1 isoforms) or 142 (DDR2) amino acids. This is followed by a tyrosine kinase domain and a very short C-terminal tail (eight amino acids for DDR1, six amino acids for DDR2) with no tyrosine residues (**Figure 1. 4**) (Leitinger, 2014, Fu et al., 2013b).

The human *DDR1* gene has 17 exons located on chromosome 6 (6p21.3), with five different DDR1 isoforms (DDR1a-e) due to alternative splicing (**Figure 1. 4**) (Playford et al., 1996). The extracellular and TM regions are identical between DDR1 isoforms, while their main differences exist in the cytoplasmic regions (Leitinger, 2014). DDR1a and DDR1b are the most common isoforms, and DDR1b has a 37 amino acid insertion in its intracellular JM region

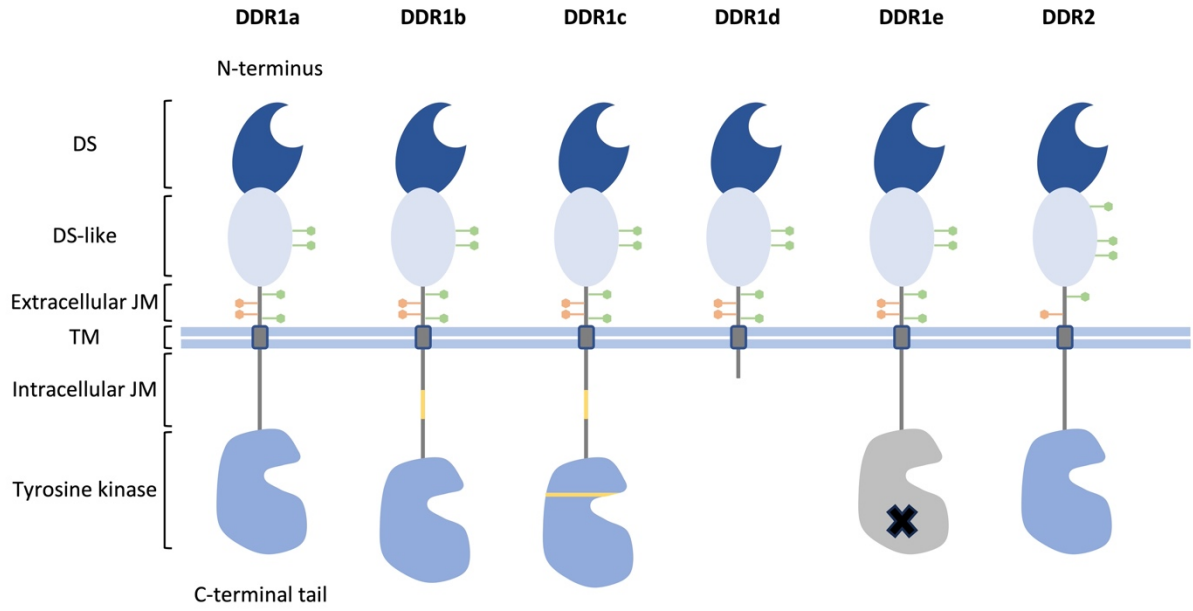


Figure 1. 4 DDR structure and isoforms
The DDRs consist of an extracellular DS domain followed by a DS-like domain, an extracellular JM domain and a TM domain. The intracellular part is composed of a flexible intracellular JM domain and a catalytic tyrosine kinase domain with a very short C-terminal tail. The green and orange symbols represent predicted N- and O-glycosylation sites. There are five isoforms of DDR1: DDR1a, b, c, d, and e. The intracellular JM domain of DDR1b and DDR1c contain extra 37 amino acids (compared with DDR1a), which are shown in yellow blocks. The tyrosine kinase domain of DDR1c comprises of additional 6 amino acids (shown in yellow). DDR1d and DDR1e exhibit incomplete or inactive kinase domains, respectively. Only a single isoform exists for DDR2. This figure was made with PowerPoint and is adapted from (Leitinger, 2014).

compared to DDR1a (Alves et al., 1995). In addition to DDR1b, DDR1c has six extra amino acids inserted in its kinase domain, making it the longest DDR1 isoform (Alves et al., 1995). In contrast to DDR1a-c, which are full-length functional receptors, DDR1d and DDR1e are inactive truncated proteins lacking the entire kinase domain (DDR1d) or parts of the intracellular JM segment and the ATP binding site (DDR1e). The human *DDR2* gene has 19 exons located on chromosome 1 (1q23.3), and no alternatively spliced DDR2 isoforms have been identified (**Figure 1. 4**) (Leitinger, 2014, Carafoli and Hohenester, 2013).

As mentioned above, most RTKs are stimulated by soluble proteins, such as growth factors (e.g. EGF), proteoglycan (e.g. agrin), and hormones (e.g. insulin) (Trenker and Jura, 2020).

However, DDRs are activated by different types of collagen (see below) (Vogel et al., 1997, Shrivastava et al., 1997). Collagens are the most abundant structural proteins in the ECM, compared to other ECM components, including elastin, proteoglycans, laminin, and fibronectin (Frantz et al., 2010, Kular et al., 2014). During early investigation, it was believed that these matrix components had only a structural function (i.e. being responsible for the biophysical properties of different types of matrices) (Piez, 1997). However, further research has revealed that some matrix components, including collagen, play a signalling role by directly interacting with cell-surface receptors (Hynes, 2009). Both DDRs are considered adhesion molecules due to their ability to binding collagen. For example, DDR1-null mice showed significantly reduced mesangial cell adhesion to collagen (Curat and Vogel, 2002). In chondrocytes, DDR2 was found to mediate direct cell attachment to collagen-containing fibrils (Woltersdorf et al., 2017). Besides DDRs, there are three more collagen receptors: collagen binding β1 integrins, glycoprotein VI, and leukocyte-associated immunoglobulin-like receptor-1 (Leitinger, 2011). These receptors have diverse structures and recognise specific collagens via different motifs. Here, I introduce the molecular basis for DDR to recognise collagens.

DDR1 and DDR2 have a high amount of homology in their DS (59% amino acid identity) and DS-like domain (51% amino acid identity) (Carafoli and Hohenester, 2013). The structures of these two globular domains are established at atomic level resolution (Carafoli et al., 2012, Carafoli et al., 2009, Ichikawa et al., 2007), and the first structure was obtained for unliganded DDR2 DS domain (Ichikawa et al., 2007). DDRs bind to fibrillar and non-fibrillar collagen via their DS domains. Unlike fibrillar collagens (I-III) that both DDR1 and DDR2 can recognise, some non-fibrillar collagens can only bind to one of the DDR receptors (Shrivastava et al., 1997, Vogel et al., 1997). For instance, DDR1, but not DDR2, recognises and binds to basement membrane collagen IV, whilst DDR2 binds to collagen X (Leitinger and Kwan, 2006, Shrivastava et al., 1997, Vogel et al., 1997). Native-folded collagen consists of three polypeptide α chains that coil around one another to form a triple helical structure, which is required for DDR binding (Shrivastava et al., 1997, Vogel et al., 1997, Brodsky and Persikov, 2005). Studies have mapped the DDR binding sites in fibrillar collagen and identified the minimal binding sequence as being GVMGFO (O is hydroxyproline) (Agarwal et al., 2002, Leitinger et al., 2004, Farndale et al., 2008, Konitsiotis et al., 2008, Xu et al., 2011). This allowed the development of a collagen-mimetic peptide with the sequence of GVNleGFO (methionine to norleucine (Nle)

substitution for increased DDR2 binding), which was then used to co-crystallise with the DDR2 DS domain (Carafoli et al., 2009). Later, the crystal structure of a tandem complex of DDR1

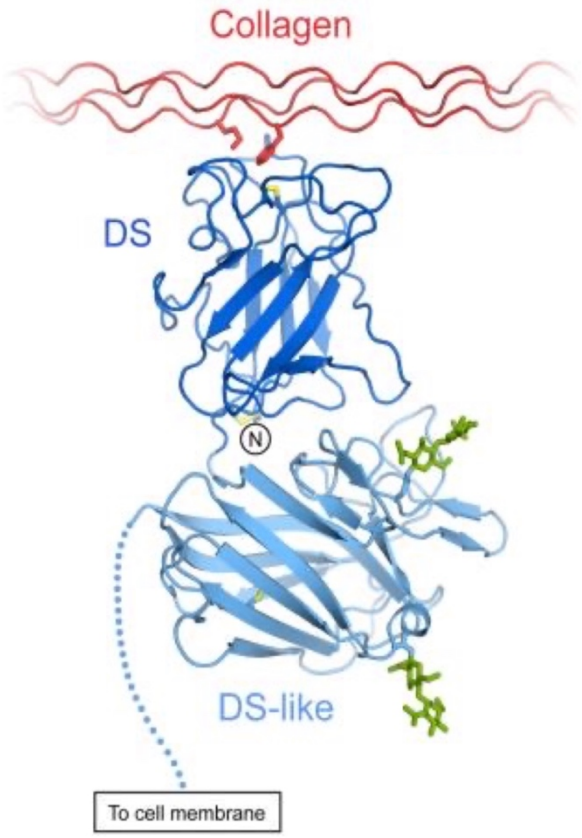


Figure 1. 5 Crystal structure of DDR1 DS and DS-like domains
This composite structure was generated by superposing DDR1 DS/DS-like domains (PDB: 4AG4) (Carafoli et al., 2012) onto the DDR2 DS domain binding to a collagen peptide (PDB:2WUH) (Carafoli et al., 2009). The side chains of essential collagen residues (Met21 of the leading chain and Phe23 of the middle chain) are shown. Disulfate bounds are shown in yellow. The N-linked glycans are shown in green. The DDR1 N-terminus is indicated. The dashed line represents the extracellular JM domain. This figure is taken from (Leitinger, 2014).

DS/DS-like domain with an anti-DDR1 antibody fragment was also determined (Carafoli et al., 2012). From the structures (**Figure 1. 5**), the DS domain comprises in total eight β-strands forming two antiparallel β-sheets (Carafoli et al., 2009). The N- and C-terminus of the DS domain are linked at the bottom of the barrel structure by a disulphide bond (**Figure 1. 5**) (Carafoli and Hohenester, 2013). The collagen binding region at the top of the barrel structure consists of five protruding loops, forming an amphipathic trench for the binding of the GVMGFO motif (Carafoli et al., 2009). The amino acid residues at the periphery binding trench are less conserved than the main binding residues, therefore resulting in different DDR specificities to non-fibrillar collagens (Xu et al., 2011, Leitinger, 2014).

From a structural perspective, the DDR1 DS-like domain shares a similar β-barrel fold with the DS domain, though their sequences are not conserved (**Figure 1. 5**) (Carafoli et al., 2012). The anti-DDR1 antibody used for crystallising binds to the DS-like domain and prevents DDR kinase activation without blocking collagen binding (Carafoli et al., 2012). The flexible extracellular JM segment allows the projection of DDR globular domains far from the cell surface, which could potentially allow the DS domain to reach the ECM environment (Carafoli et al., 2012).

Like most single-span TM proteins that dimerise through specific motifs (SmxxxSm, x is any amino acid, and Sm can be glycine, alanine, serine, or threonine) (Li et al., 2012), DDRs contain a GxxxA motif and an additional dimerisation motif, a leucine-based 'zipper' in their TM domain segment (Noordeen et al., 2006). Introducing alanine to valine substitution to the GxxxA motif did not disrupt DDR dimerisation, whilst mutations designed to disrupt helix interactions through the leucine zipper severely disrupted DDR1 dimerisation and collagen-induced phosphorylation (Noordeen et al., 2006). The large intracellular JM region contains several tyrosine residues (seven for DDR1 and four for DDR2), and two tyrosines (Tyr569 and Tyr586) in the DDR1b JM region have been shown to play an important autoinhibitory role in regulating the kinase activity (see **Section 3.1**) (Sammon et al., 2020). Most structural analyses for DDR kinases focused on DDR1, showing a typical kinase structure with a small N-lobe and a bigger C-lobe (**Section 1.2.2**). Due to the high conservation of their kinase domains (**Figure 1. 6**), DDR1 and DDR2 have similar kinase structures and key catalysis elements. The DDR1 N-lobe contains elements such as the P loop, the catalytically essential Lys residue in the β3 strand, and the αC-helix (**Figure 1. 6**). The DDR1 C-lobe contains an activation loop with three tyrosine residues. DDR1 kinase domain was found to be stable in the inactive DFG-OUT conformation, making it promiscuous to many inhibitors (Hanson et al., 2019). The middle tyrosine residue (Tyr796) on the DDR1 activation loop interacts with adjacent Asp (Asp766) to stabilise the inactive conformation (Sammon et al., 2020). In addition, an *in vitro* study using recombinant DDR2 cytosolic region revealed the important autoinhibitory role of the DDR2 middle tyrosine residue of the activation loop (Tyr740) (Yang et al., 2005). As no tyrosine residues exist on the DDR C-terminal tail, the intracellular JM region and the activation loop are the only two autoinhibitory motifs known for DDR1 (Sammon et al., 2020).

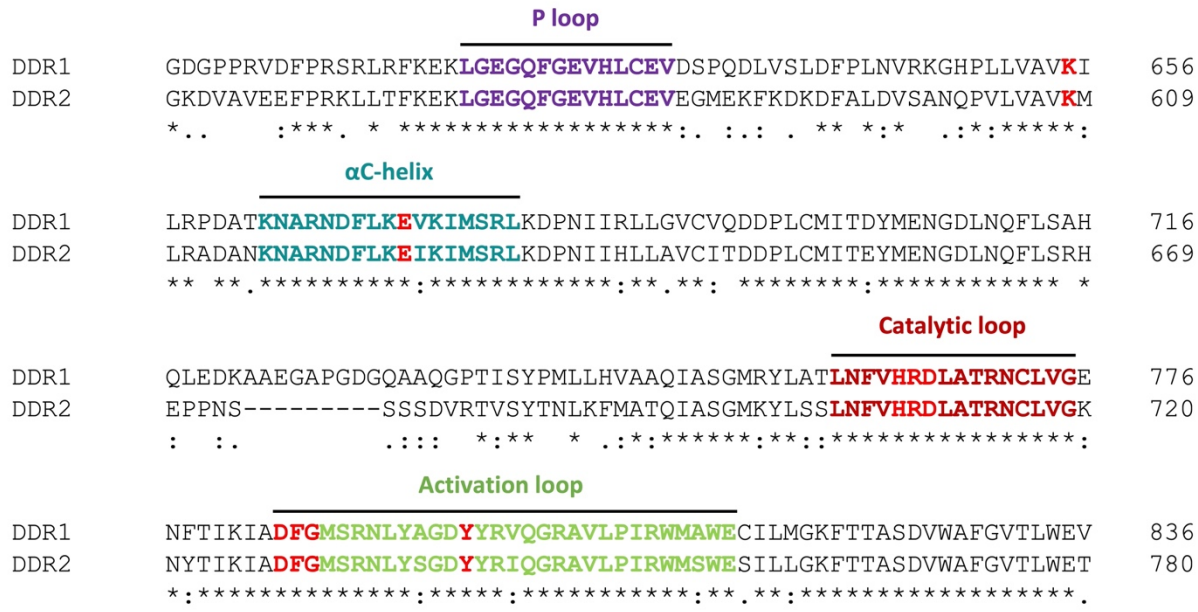


Figure 1. 6 Sequence alignments of DDR1 and DDR2 kinase domains
Part of the sequences of DDR1 kinase domain (amino acid 598 to 836) and DDR2 kinase domain (amino acid 550 to 780) were aligned using Clustal Omega. Key conserved elements are indicated with different colours. The conserved Lys residue on the β3 strand, the Glu residue on the αC-helix, the HRD motif on the catalytic loop, the DFG motif on the activation loop, and the activation loop middle tyrosine residue (Tyr796 for DDR1 and Tyr740 for DDR2) are indicated in red. Sequence numbers are shown to the right. '*' (asterisk); fully conserved residue. ':' (colon); conserved substitutions. '.' (period); less well conserved substitution.

1.3.3 DDR activation and regulation

As described above, DDRs exist as constitutive non-covalent dimers in the absence of collagen, therefore the typical activation mechanism through ligand-induced receptor dimerisation does not apply to DDRs (Noordeen et al., 2006, Lemmon and Schlessinger, 2010, Xu et al., 2014). DDR dimer formation is likely to occur during the early stages of biosynthesis, before transportation to the cell surface (Noordeen et al., 2006). Multiple contacts in the extracellular, TM, and intracellular region are found within a DDR dimer, with the most important interaction identified as the strong helix-helix association via the leucine zipper motif of the TM domain, as described above (**Section 1.3.2**) (Noordeen et al., 2006). This self-association was later confirmed as the strongest among all the RTK TM interactions (Finger et al., 2009).

As a dimeric RTK in the absence of ligands, as is the case for the DDRs, the InsR is activated through the ligand-induced conformational change of its extracellular and intracellular regions (**Section 1.2.4**). However, for the DDRs, collagen binding only leads to limited structural changes to the DS domain, and little contribution was found within the extracellular JM region to DDR activation, ruling out the possibility that DDRs undergo similar activation as the InsR

(Carafoli and Hohenester, 2013). Another possible activation mechanism for RTKs is through the formation of ligand-induced higher-order oligomers, as seen in Eph receptors (**Section 1.2.4**). Indeed, recent studies have observed DDR1 cluster formation upon collagen binding (Corcoran et al., 2019, Yeung et al., 2019). Corcoran et al. have dissected DDR1 activation into two stages and explained the possible mechanism for the slow kinetics of DDR activation. In the first stage, DDR1 is redistributed into small clusters within five minutes of collagen binding. In the second stage, which requires 45-60 minutes of collagen stimulation, further aggregation occurs and results in dense clusters (Corcoran et al., 2019). This could allow phosphorylation to happen between neighbouring DDR dimers, as has been shown biochemically (Juskaite et al., 2017). However, the DDR activation does not require the fibrillar collagen structure (higher order ligand conformation); instead, collagen-mimetic peptide (GVMGFO), which mimics single triple helices of collagen, can also induce receptor activation with a similar slow kinetics (Xu et al., 2011). Thus, the DDR clustering is unlikely to be triggered by the fibrillar collagen structure. It remains unclear how collagen binding triggers DDR oligomerisation. Nevertheless, a mutagenesis study showed that the DDR2 DS/DS-like domain contains binding site for an allosteric inhibitor, in which the binding abolished DDR2 extracellular domain oligomerisation and kinase activation (Grither and Longmore, 2018). Therefore, the DS/DS-like domain interface could play an essential role in regulating DDR clustering.

Both the intracellular JM region and activation loop has been shown to stabilise the DDR1 inactive conformation (Canning et al., 2014, Sammon et al., 2020). Studies have shown that DDRs may require association with Src as a binding partner for full kinase activation (Dejmek et al., 2003, Lu et al., 2011a, Ikeda et al., 2002, Yang et al., 2005). Thus, the ligand binding induced Src recruitment could be essential for DDR activation.

In general, RTK signals are regulated through receptor internalisation and lysosomal degradation to avoid aberrant and prolonged activation (Lu et al., 2011a). However, the DDRs undergo slow activation, and the signal can be detected for days, suggesting that rapid degradation is unlikely to happen in DDRs (Shrivastava et al., 1997, Vogel et al., 1997). Whether DDRs are internalised upon collagen binding remains controversial. Studies have shown DDR1b-YFP (DDR1 tagged with yellow fluorescent protein) was co-localised with an overexpressed endosomal marker, and the dynamin-dependent endocytosis inhibitor could block ligand-induced DDR1b-YFP endocytosis (Mihai et al., 2009, Yeung et al., 2013). Fu et al.

used a biochemical assay to demonstrate the internalisation of DDR1b-Myc (Fu et al., 2014). Due to the sustained DDR activation signals, the authors proposed that collagen binding results in DDR internalisation, in which the receptor activation occurs on endosomes but not on cell membranes (Mihai et al., 2009, Fu et al., 2014). However, Corcoran et al. were able to image collagen binding induced-DDR1b (untagged) clustering on the cell surface, and the autophosphorylation took place exclusively on the cell membrane (Corcoran et al., 2019). Thus, further investigations are required to clarify the difference between these studies and the role of endocytosis in DDR signal regulation.

Another receptor signalling regulatory mechanism, ectodomain shedding, reduces the availability of ectodomains of cell surface proteins (Clark, 2014). This process occurs at or near the plasma membrane, in which the receptor ectodomains are cleaved by a protease to regulate the number of available receptors for ligand binding (Miller et al., 2017, Itoh, 2021). DDR1 ectodomain has been reported to shed upon collagen binding which may enable termination of DDR1 regulated signalling (Vogel, 2002, Shitomi et al., 2015). Constitutive DDR1 ectodomain shedding has also been investigated in multiple studies (Alves et al., 1995, Fu et al., 2013a, Shitomi et al., 2015). Fu et al. showed constitutive DDR1 shedding in COS1 cells and T47D breast cancer cells is mediated by overexpressed MMP14 (Fu et al., 2013a). However, they failed to verify endogenous MMP14-regulated DDR1 shedding in HCC1806 cells (Fu et al., 2013a). Similarly, Shitomi et al. later demonstrated that endogenous MMP14 cannot mediate constitutive or collagen-induced DDR1 shedding in A431 cells, indicating a possibility that the findings from Fu et al. study were affected by experimental conditions (i.e. overexpression) (Shitomi et al., 2015). Instead of MMP14, Shitomi et al. found the ADAM metallopeptidase domain 10 (ADAM10) can promote collagen-induced DDR1 shedding, which subsequently terminates DDR1 signalling (Shitomi et al., 2015). Intriguingly, the collagen binding potential of the DDR1 DS domain is not diminished by shedding, which could still regulate collagen structure (Abbonante et al., 2013). Indeed, a recent study showed that DDR1 ectodomain shedding results in a highly organised and aligned stromal ECM within the tumour microenvironment of breast cancer, which excludes immune cells from accessing the tumour targets (Sun et al., 2021, Leitinger, 2022, Liu et al., 2023). This points out the additional role of DDRs in disease progression and tissue remodelling, in addition to receptor activation-induced downstream signalling (Leitinger, 2022).

1.3.4 DDR downstream signalling

Like other RTKs, 'classical' DDR downstream signalling starts from the recruitment of SH2 and PTB domain-containing proteins to the intracellular phosphorylated tyrosine residues (Leitinger, 2014). There are up to 15 tyrosines in the DDR1 intracellular region, with eight located in the kinase domain and the rest in the intracellular JM region (five in DDR1a, seven in DDR1b/c). The DDR2 contains ten tyrosines in the kinase domain and four in the intracellular region. However, among all these tyrosine residues, only three on the DDR1 JM region (Tyr513 on DDR1b/c; Tyr569 and Tyr586 on DDR1b) and three on the DDR1 and DDR2 activation loop (Tyr792, Tyr796, and Tyr797 on DDR1; Tyr736, Tyr740, and Tyr741 on DDR2) have been demonstrated in cell experiments as collagen-induced phosphorylation sites (Iwai et al., 2013b, Lemeer et al., 2012, Xu et al., 2014, Sammon et al., 2020). The current explorations of the proteins that can be recruited to the DDRs remain incomplete, with most studies focused on DDR1. Nevertheless, several binding partners have been identified for DDR1, such as ShcA, non-catalytic region of tyrosine kinase adaptor protein 2 (Nck2), Src homology region 2 domain-containing phosphatase (SHP)-1, and SHP-2, etc (Vogel et al., 1997, Koo et al., 2006, Abbonante et al., 2013, Wang et al., 2006). Lemeer et al. identified an extended range of potential proteins that bind to DDR1 using a library of phospho-peptides generated based on the potential DDR1 tyrosine phosphorylation sites (**Figure 1. 7**) (Lemeer et al., 2012). Very little is known about DDR2 signalling, with only ShcA, SHP-2, Nck1, Lyn, and phospholipase C like 2 (PLCL-2) being shown to interact with DDR2 intracellular region (Ikeda

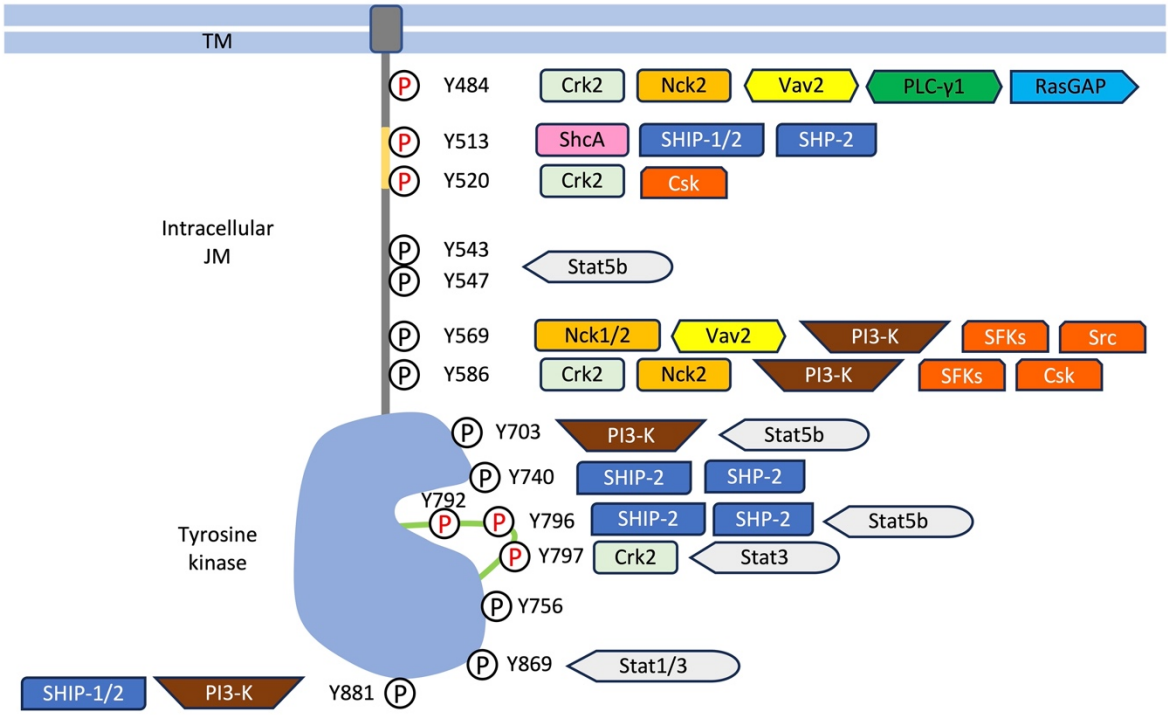


Figure 1. 7 DDR1 phosphosites interaction with binding partners
The DDR1b intracellular region is presented with the JM region in grey (DDR1b-specific insert in yellow), the kinase domain in blue, and the activation loop in green. The potential phosphorylation sites are indicated by circles with 'P', where a red P indicates the biochemically verified sites. Binding partners with SH2 and PTB domains were identified by phosphotyrosine peptide pulldowns in human placenta tissue (Lemeer et al., 2012). PLC-γ1 (phospholipase C-γ1), RasGAP (Ras-specific GTPase-activating protein), SHIP-1/2 (SH2-containing 5'-inositol phosphatase-1/2), SFK (Src family kinases), Stat (signal transducers and activators of transcription), PI3-K (phosphoinositide 3-kinase). This figure was made with PowerPoint and is adapted from (Leitinger, 2014).

et al., 2002, Iwai et al., 2013b). Detailed information on which signalling pathway these adaptor proteins are involved in remains poorly understood. Current knowledge of DDR-related pathways exhibits distinct signalling outcomes for a single type of DDR, depending on the ligand used for stimulation and cell type (Leitinger, 2014, Itoh, 2018). For instance, DDR1b-dependent MAPK activation in human embryonic kidney (HEK) cells can be stimulated with collagen IV instead of collagen I (Ongusaha et al., 2003). Furthermore, the core signalling molecule in MAPK pathway, Erk 1/2, can be activated by DDR1 in smooth muscle cells, mammary epithelium, transfected HEK cells, and megakaryocytes (Abbonante et al., 2013, Hilton et al., 2008, Lu et al., 2011a, Ongusaha et al., 2003); whilst its activity is likely to be repressed by DDR1 in mesangial cells (Curat and Vogel, 2002). Limited research has been conducted on DDR2-regulated signalling pathways. Nevertheless, in chondrocytes, DDR2 has been shown to activate p38 and c-Jun N-terminal kinase (JNK) to induce interleukin-12 expression (Poudel et al., 2013), while activates p38 and Erk 2 for upregulating MMP13

expression (Xu et al., 2005, Xu et al., 2007). Moreover, deletion of DDR2 disrupted the FAK/YAP/TAZ (focal adhesion kinase/yes-associated protein/transcriptional coactivator with PDZ-binding motif) signalling in mesenchymal lineage cells (Pagani et al., 2022).

Besides recruiting downstream proteins, crosstalk between surface receptors also contributes towards signalling (Volinsky and Kholodenko, 2013, Natarajan and Berk, 2006). For instance, collagen-induced DDR2 activation can be promoted by the insulin signalling pathway (Iwai et al., 2013a). Crosstalk was also identified between DDRs and the major collagen receptor, β1 integrin (Leitinger, 2014). Although β1 integrin has no contribution to DDR activation, integrin-mediated cellular functions have been shown to be positively and negatively regulated by DDRs in a cell type-dependent manner (Leitinger, 2014). For example, suppression of α2β1 integrin-mediated cell functions (migration, spreading, and adhesion) in Madin-Darby canine kidney (MDCK) cells are regulated by DDR1 through different downstream signalling molecules (Wang et al., 2006, Wang et al., 2005, Yeh et al., 2009). However, in pancreatic cancer cells, both α2β1 and DDR1 contribute to the upregulation of JNK-mediated N-cadherin expression, which in turn promotes epithelial to mesenchymal transition (EMT)-like cell scattering (Shintani et al., 2008). Furthermore, overexpression of DDR1 and DDR2 in HEK cells positively regulates integrin-mediated cell adhesion to collagen I (Xu et al., 2012). A recent study using Caenorhabditis elegans utse-seam tissue showed collagen IV-induced DDR2 activity strengthens integrin-mediated cell adhesion (Park et al., 2023). In cancer associated fibroblasts (CAFs), DDR2 was found to control β1 integrin activity through Ras-related protein 1 (RAP1) mediated talin1 and kindlin2 activation (Bayer et al., 2019). Similarly, β1 integrin-regulated cell migration can be promoted by DDR1 interaction with the focal adhesion protein, talin (Borza et al., 2022).

1.3.5 DDRs in disease

Besides their regulation of embryo development mentioned in **Section 1.3.1**, both DDRs have been found to contribute to human disease progression and have been studied in many disease models, such as animal models for cancer, osteoarthritis, and fibrotic disease (Borza and Pozzi, 2014, Wu et al., 2022, Xiao et al., 2021, Coelho et al., 2019). As DDRs positively contribute to disease progression, discovering small-molecule inhibitors against DDR activation is an important topic. Besides the broad-range inhibitors which target many kinases in their DFG-IN or DFG-OUT conformation, several selective and potent DDR inhibitors have

been developed (Elkamhawy et al., 2021, Shenoy et al., 2023, Liu et al., 2024). However, no DDR-specific inhibitors have been investigated clinically, given that the pathological roles of DDRs and their downstream signalling pathways remain less well understood.

Cancer

Overexpression and increased activity of DDRs have been observed in various types of cancer, such as NSCLC, breast, ovarian, and pancreatic cancers (Valiathan et al., 2012). The altered DDR functions are likely to play a role in tumorigenesis, as well as promoting metastasis, chemotherapy resistance, and prosurvival signals (Valiathan et al., 2012, Cader et al., 2013, Ongusaha et al., 2003).

The high expression of DDRs has been reported in multiple cancers, such as lung, breast, and ovarian cancers, in which the expression is often linked to poor patient prognosis and progression to malignancy (Valiathan et al., 2012). Thus, several studies have proposed DDR expression as a prognostic biomarker (Ben Arfi et al., 2022, Quan et al., 2011, Romayor et al., 2022, Fan et al., 2016). Indeed, DDR1 knockdown showed reduced glioblastoma invasiveness (Ma et al., 2018) and the percentage of malignant melanomas (Reger de Moura et al., 2019). Although the understanding of DDR overexpression in cancers remain incomplete, a few factors that could potentially regulate DDR cancer expression have been suggested, including the loss of DDR suppressor miRNA, a hypoxia environment, and the involvement of a cancer-promoting tetraspanin (Deng et al., 2017, Ren et al., 2014, Yang et al., 2017). The dysregulated DDR expression can lead to altered receptor phosphorylation. For instance, a phosphoproteomic study of NSCLC showed that both DDRs are among the most phosphorylated RTKs (Rikova et al., 2007). DDR-mediated signalling has been shown to regulate multiple cellular processes (Valiathan et al., 2012). In breast cancer cells that express DDR2, collagen stimulation to DDR2 results in Erk2-mediated SNAIL1 phosphorylation, which in turn promotes cancer cell migration and invasion (Zhang et al., 2013). Thus, the application of small-molecule DDR inhibitors in cancer therapy could be attractive.

It is important to note that the specific roles that DDR play in cancer tissue could be cell-type dependent. For instance, DDR1 overexpression in breast cancer cells was linked to increased metastasis in one study (Gadiya and Chakraborty, 2018), whilst another study showed DDR1 expression in tumour surrounding tissues led to reduced breast cancer metastasis (Takai et al.,

2018). Moreover, upregulated collagen III expression through DDR1 signalling was found to maintain the non-linear ECM organization and cellular dormancy of head and neck squamous cell carcinomas (Di Martino et al., 2022). These studies suggest that DDR roles in cancer progress may be muti-faceted, and DDRs may have tissue-specific or cancer-specific different roles, which could bring difficulties in taking DDRs as treatment targets for cancer therapy (Trono et al., 2024). Apart from the DDR-mediated signalling and cell functions that include pro-tumour and anti-tumour roles in cancer, DDRs can also regulate tumour immune exclusion in a kinase-independent way (Sun et al., 2021, Liu et al., 2023). Liu et al. showed that constitutive DDR1 ectodomain shedding results in a highly organized stromal ECM, which subsequently interrupts immune cell access to the tumour core (Liu et al., 2023). This indicates that applying a small-molecule kinase inhibitor might not be sufficient to reverse DDR-regulated cancer progression.

Fibrotic disease

In lung fibrotic diseases, such as idiopathic pulmonary fibrosis (IPF), both DDR1 and DDR2 have been identified as potential therapeutic targets (Avivi-Green et al., 2006, Borza et al., 2018). DDR1-deficient mice were found to be protected from bleomycin-induced lung inflammation and fibrotic scarring (Avivi-Green et al., 2006). Similarly, DDR2-null mice are also protected from this acid-induced lung fibrosis (Jia et al., 2018, Zhao et al., 2016a). Jia et al. proposed a mechanism that DDR2 expressed in IPF fibroblasts protects the cells from apoptosis (Jia et al., 2018). However, Zhang et al. found that DDR2 TGF-β1-induced fibroblast activation (Zhao et al., 2016a).

In liver fibrosis, DDR2 plays a controversial role in regulating this disease. In a chronic liver injury model, DDR2-deficient mice were more susceptible to fibrosis compared to the wildtype (WT), indicating a protective role of DDR2 against chronic liver injury (Olaso et al., 2011). However, DDR2 was found to promote liver fibrosis by mediating hepatic stellate cell activation and proliferation in an acute liver injury model (Olaso et al., 2001). Moreover, increased DDR2 expression was associated with increased MMP2 expression, collagen deposition and ECM remodelling in an experimental alcoholic liver model (Luo et al., 2013). Taken together, these studies suggest DDR2 may play a pathogenic role in early live fibrosis, but act to be protective in chronic liver disease.

Osteoarthritis

Osteoarthritis is a chronic condition that leads to long-term pain. Current treatment mainly focuses on pain relief but not managing disease progression (Pulsatelli et al., 2013). In both mouse models and osteoarthritis patients, there is an observed increase in DDR2 expression linked to the extent of cartilage damage (Xu et al., 2007, Sunk et al., 2007). The increase in DDR2 expression was found to promote the expression of MMP-13, a key enzyme that cleaves collagen and degenerate cartilage (Xu et al., 2007). In a mouse model, DDR2 reduction or deletion could lessen cartilage degeneration (Xu et al., 2010, Manning et al., 2016). In addition, Schminke et al. found DDR1-deficient mice showed typical signs of osteoarthritis, thus proposing this as a novel osteoarthritis model (Schminke et al., 2014). It is important to note that although DDR1 could be protective for osteoarthritis, complete DDR1 knockout can result in a compensatory expression of DDR2 in chondrocytes (Schminke et al., 2014). Taken together, these studies suggest DDR2 as a therapeutic target for osteoarthritis management, however, further tests using DDR-specific inhibitors are required.

1.4 Warburg Cinotti Syndrome

Connective tissue, primarily composed of ECM components with sparse cells, is one of the basic tissues that provides internal support to the human body (Kamrani et al., 2024). Disorganised ECM composition or structure could potentially be the underlying cause of various connective tissue-related diseases (McKee et al., 2019). In 2006, a case study from Warburg et al. first described a series of new symptoms seen in a blepharophimosis patient (Warburg et al., 2006), making it different from the existing symptoms such as Penttinen syndrome, hereditary mucoepithelial dysplasia, and mucopolysaccharidoses (Johnston et al., 2015, Halawa et al., 2015, Zhou et al., 2020). This new syndrome is characterised by blepharophimosis, progressive corneal vascularisation, deafness, acroosteolysis, and subcutaneous tissue wasting in the face, hands, and feet (Warburg et al., 2006). Later in 2013, Cinotti et al. reported a new patient case with similar pathological features (Cinotti et al., 2013). This new disease was then named 'Warburg Cinotti Syndrome', and a more detailed case report was published in 2018 (Xu et al., 2018). Xu et al. provided a more extended clinical description (**Table 1. 2**) of Warburg Cinotti syndrome, with a total of six patients included in the study (Xu et al., 2018). The discovery of several features, including keloid-like plaques, excessive contractures, and acroosteolysis, made it a connective tissue-related disease (Xu et

al., 2018). Exome sequencing was performed to identify potential variants shared by Warburg Cinotti patients, with two heterozygous missense variants (c.1829T>C; p.Leu610Pro and c.2219A>G; p.Tyr740Cys) located on DDR2 identified as being responsible for the disease (Xu et al., 2018). These two novel variants are both located in the DDR2 tyrosine kinase domain and affect conserved amino acid residues. Endogenous DDR2 proteins from healthy control (WT) cells and patient cells with different Warburg Cinotti variants were examined using ELISA and Western blotting, with increased DDR2 phosphorylation signals seen in both patient samples without additional collagen stimulation treatment (Xu et al., 2018). Moreover, dasatinib treatment blocked the DDR2 phosphorylation signals from both WT and patient cell samples (Xu et al., 2018). This suggests that the identified Warburg Cinotti variants could be gain-of-function mutations associated with enhanced DDR2 kinase activity and signalling.

Table 1. 2 A selection of Warburg Cinotti syndrome clinical features

DDR2 variants are shown in short names (L610P, p.Leu610Pro; Y740C,p.Tyr740Cys). '+' and '-' represent 'presence' and 'absence' of symptoms, with degree indicated with extra '+'. NR, not reported. This table is adapted from (Xu et al., 2018).

Patient	**1**	**2**	**3**	**4**	**5**	**6**
Described by	(Warburg et al., 2006)	(Cinotti et al., 2013)	(Xu et al., 2018)	(Xu et al., 2018)	(Xu et al., 2018)	(Xu et al., 2018)
Age	63	64	37	14	9	41
DDR2 variant	L610P	Y740C	Y740C	Y740C	Y740C	L610P
Corneal vascularisation	+++	+++	++	+	+	NR
Conductive hearing loss	+	-	-	NR	NR	+
Skin with little subcutaneous tissue	+	NR	+	+	NR	+
Keloid-like plaques	+	+	+	-	-	+
Contractures	++	+++	++	+	+	+
Acroosteolysis	+	+	+	-	-	+
Thin nose	+	+	+	+	+	+
Loss of toes/toenails	+	+	+	-	-	+

1.5 Hypothesis and aims

The study showing preliminary evidence for DDR2 activation in WT and Warburg Cinotti patient cells (Xu et al., 2018), left a few questions open about the underlying cellular and biochemical mechanisms of disease induction. First, it is unclear whether and how these two variants lead to changes in DDR2 kinase catalysis. Second, it is not clear whether the patient cells harbour constitutive DDR2 activation in cells and how collagen binding regulates DDR2 signalling in these cells. Third, it remains unexplored whether these DDR2 variants lead to changes in cellular processes and how they could link to clinical features. Finally, DDR-specific inhibitors should be tested to verify whether any changes are due to altered DDR2 kinase activity. Answering these questions could provide an extended understanding of DDR2 kinase regulation, DDR2 downstream signalling and pathological roles and provide new treatment options for Warburg Cinotti Syndrome. The main hypothesis for this project is that the Warburg Cinotti DDR2 variants result in constitutive kinase activity as well as changed cellular behaviours through enhanced DDR2 receptor signalling.

1.5.1 Chapter aims

Chapter 3: 1) To analyse WT and mutant DDR2 kinase catalytic parameters using purified soluble recombinant constructs *in vitro*; 2) To analyse full-length WT and mutant DDR2 activities in transfected cells; 3) To establish whether a DDR-specific inhibitor blocks mutant DDR2 activities *in vitro* and in transfected cells.

Chapter 4: To analyse mutant DDR2 functions in cell-based functional assays and test the DDR-specific inhibitor in patient-derived human dermal fibroblast (HDF) cells.

Chapter 5: To explore DDR2-regulated signalling molecules in patient-derived HDF cells.

Chapter 2 Materials and Methods

2.1 Materials

2.1.1 Cell culture reagents

HEK293 cells and Cos-7 monkey fibroblast-like kidney cells were obtained from American tissue culture collection (ATCC), US. Primary human dermal fibroblast (HDF) cells, isolated from a healthy donor (control cells) or the Warburg-Cinotti Syndrome patients' biopsy, were obtained through collaboration from Dr Cecilie Bredrup, Haukeland University Hospital, Norway. Spodoptera frugiperda 9 (Sf9) cell stock was maintained by Valerie Good at the baculovirus facility at Imperial College London.

Dulbecco's modified eagle medium/nutrient mixture F-12 (DMEM/F-12), Opti-MEM reduced serum medium without phenol red, Pen Strep (10,000 U/mL penicillin, 10,000 µg/mL streptomycin), L-Glutamine 200 mM (100X), heat inactivated fetal bovine serum (FBS) and 0.5% trypsin-EDTA (10X) were from Gibco, ThermoFisher Scientific, UK. Insect Xpress medium was from Lonza, Belgium. Enzyme-free cell dissociation solution and 0.4% trypan blue solution were from Sigma-Aldrich, UK.

6-, 12- and 24-well tissue culture plates and 100 mm tissue culture dishes were purchased from VWR, UK. 25 cm^2 tissue culture flasks (T25) and 75 cm^2 tissue culture flasks (T75) were from Sarstedt, Germany. Corning polystyrene roller bottles were from Corning, US.

Polyethylenimine Max (PEI Max) was from Polysciences, US. Lipofectamine 3000 and Cellfectin II were from ThermoFisher, UK.

Dimethyl sulfoxide (DMSO) was from Sigma-Aldrich, UK

Collagen I from rat tail (#C7661) and collagen I solution from bovine skin (#C4243) were purchased from Sigma-Aldrich, UK

2.1.2 Molecular biology reagents

Polymerase chain reaction (PCR) and sequencing primers were from Invitrogen, UK. In-Fusion HD enzyme premix, cloneAmp HiFi PCR premix and PrimeScript reverse transcriptase were purchased from TakaraBio, Japan. Fast SYBR green master mix (2X) and Applied Biosystems MicroAmp optical 96-well reaction plates were from ThermoFisher, UK.

All restriction enzymes, CutSmart buffer, Q5 High-Fidelity DNA polymerase, 5X Q5 reaction buffer, 10 mM deoxynucleotide triphosphates (dNTPs), T4 ligase, 10X T4 ligase buffer, 6X gel loading dye, 100bp DNA ladder and 1 kb DNA ladder were purchased from New England Biolabs (NEB), UK.

Stellar™ competent cells were from TakaraBio, Japan. DH5α chemically competent cells were from ThermoFisher, UK. NEB 5-alpha competent cells (high efficiency) were from NEB, UK. Lysogeny broth (LB) agar, LB broth and ampicillin were from Sigma-Aldrich, UK.

UltraPure agarose and SYBR safe DNA gel stain were from ThermoFisher, UK.

NucleoSpin Gel and PCR clean-up kit were from Macherey-Nagel. QIAquick gel extraction kit, RNeasy Mini kit and QIAprep Miniprep, Midiprep, Maxiprep kits were purchased from Qiagen, Germany.

Endoglycosidase H (Endo H), 10X glycoprotein denaturing buffer and 10X G5 buffer were purchased from NEB, UK

2.1.3 Buffer chemicals, solutions and reducing agents

Trizma base (Tris), 4-(2-Hydroxyethyl)piperazine-1-ethanesulfonic acid (HEPES), glycine, sodium dodecyl sulfate (SDS), glycerol, ethylenediaminetetraacetic acid (EDTA), sodium phosphate monobasic (NaH_2PO_4), sodium phosphate dibasic (Na_2HPO_4), potassium phosphate monobasic (KH_2PO_4), sodium chloride (NaCl), potassium chloride (KCl), magnesium chloride ($MgCl_2$), manganese chloride ($MnCl_2$) and sodium fluoride (NaF) were purchased from Sigma-Aldrich, UK. Bovine serum albumin (BSA) and Tween-20 were from ThermoFisher, UK.

Hydrogen chloride (HCl), acetic acid, sodium hydroxide (NaOH), methanol (MeOH), ethanol (EtOH) and isopropanol were from Sigma-Aldrich.

β-mercaptoethanol was from Sigma-Aldrich, UK. Tris(2-carboxyethyl)phosphine hydrochloride (TCEP) and dithiothreitol (DTT) were purchased from ThermoFisher, UK.

2.1.4 Protein purification buffers

2.1.4.1 Small-scale protein expression test buffers

Small-scale Sf9 cells lysis buffer 1, regular: 50 mM NaH_2PO_4 pH 8.0, 300 mM NaCl, 5 mM imidazole, 1% (v/v) Tween-20, with 133 units/mL DNase I (NEB, UK) and 1 cOmplete EDTA-free protease inhibitor cocktail tablet (Roche, Switzerland) per 50 mL, freshly added before use.

Small-scale Sf9 cells lysis buffer 2, modified: Sf9 cells lysis buffer 1, with pH adjusted to 7.5 with HCl.

Small-scale Sf9 cells lysis buffer 3, modified: Sf9 cells lysis buffer 1, with pH adjusted to 7.0 with HCl.

Small-scale Sf9 cells lysis buffer 4, modified: Sf9 cells lysis buffer 1 (pH 8.0), with 10% (v/v) glycerol.

Small-scale Sf9 cells lysis buffer 5, modified: Sf9 cells lysis buffer 1 (pH 8.0), with 2% (v/v) Tween-20.

Small-scale nickel-nitrilotriacetic acid (Ni-NTA) wash buffer: 50 mM NaH_2PO_4, 300 mM NaCl, 15 mM imidazole, 0.05% (v/v) Tween-20, pH 8.0.

2.1.4.2 Large-scale protein purification buffers

Large-scale Sf9 cells lysis buffer: 500 mM NaCl, 50 mM Tris pH 7.5, 0.2% (v/v) Tween-20, with 0.05 U/mL benzonase (Sigma-Aldrich, UK) and 1 cOmplete EDTA-free protease inhibitor cocktail tablet per 50 mL, immediately added before use.

HisTrap wash buffer: 500 mM NaCl, 50 mM Tris pH 7.5.

HisTrap elution buffer: 500 mM NaCl, 50 mM Tris pH 7.5, 500 mM imidazole.

Dialysis buffer (for C3 cleavage experiments): 50 mM Tris pH 8.0, 200 mM NaCl, 0.5 mM TCEP.

Gel filtration buffer: 200 mM NaCl, 25 mM HEPES pH 7.5, 0.5 mM TCEP.

2.1.5 Peptides and inhibitors

Axltide insulin receptor substrate 1 (IRS-1) derived peptide with the amino acid sequence of KKSRGDYMTMQIG was purchased from GenScript Biotech, Netherlands. Synthetic triple-

helical collagen-derived integrin-selective peptides, as well as the control non-receptor binding peptide GPP10 (Table 1), were obtained from Prof Richard Farndale, Cambridge. These peptides were custom synthesised by (N-(9-fluorenyl)methoxycarbonyl) (Fmoc) chemistry as a C-terminal amide in the Applied Biosystems Pioneer automated synthesizer with TentaGel R RAM resin and purified as described (Raynal et al., 2006).

Dasatinib was purchased from Selleckchem, US. VU6015929 DDR-specific inhibitor was from Insight Biotechnology, UK. Both inhibitors were dissolved in DMSO with stock concentrations of 2.48 mM and 1 mM, respectively. The stocks were aliquoted into small volumes and stored at -80°C.

Table 2. 1 Sequences of synthetic triple-helical collagen-derived integrin-selective peptides and control peptide (Xu et al., 2012, Xu et al., 2011)

Name	Sequence
GFOGER	$GPC(GPP)_5$ -GFOGER-$(GPP)_5GPC$-NH_2
GLOGER	$GPC(GPP)_5$ -GLOGER-$(GPP)_5GPC$-NH_2
GMOGER	$GPC(GPP)_5$ -GMOGER-$(GPP)_5GPC$-NH_2
GAOGER	$GPC(GPP)_5$ -GAOGER-$(GPP)_5GPC$-NH_2
GLOGEN	$GPC(GPP)_5$ -GLOGEN-$(GPP)_5GPC$-NH_2
GPP10	$GPC(GPP)_{10}$-GPC-NH_2

2.1.6 Protein assay buffers

25X cOmplete protease inhibitor stock solution: 1 cOmplete EDTA-free protease inhibitor cocktail tablet dissolved in 2 mL sterile MilliQ water.

Mammalian cell lysis buffer: 150 mM NaCl, 50 mM Tris pH 7.4, 1 mM EDTA, 1% (v/v) IGEPAL CA-630 (substitution for Nonidet P-40), with 1X cOmplete protease inhibitor, 5 mM NaF, 1 mM sodium orthovanadate immediately added before use.

Recombinant protein lysis buffer: 50 mM NaH_2PO_4 pH 8.0, 300 mM NaCl, 10 mM imidazole, 1% (v/v) IGEPAL CA-630, with 1 cOmplete EDTA-free protease inhibitor cocktail tablet per 50 mL, freshly added before use.

0.5 M sodium phosphate buffer, pH 8.0: 19.82 mM NaH_2PO4, 480.2 mM Na_2HPO4.

2X binding/wash buffer: 100 mM sodium phosphate buffer pH 8.0, 600 mM NaCl, 0.02% (v/v) Tween-20.

2X sample buffer: 125 mM Tris pH 6.8, 2% (w/v) SDS, 25% (v/v) glycerol, 0.02% (w/v) bromophenol blue (BPB), with 2% (v/v) β-mercaptoethanol if reducing buffer used.

5X sample buffer: 300 mM Tris pH 6.8, 10% (w/v) SDS, 50% (v/v) glycerol, 0.1% (w/v) BPB, with 10% (v/v) β-mercaptoethanol if reducing buffer used.

ADP-Glo™ kinase assay kit and ADP-Glo™ Max kinase assay kits were purchased from Promega, US.

ATP for kinase buffer 1 and 2 was from Sigma-Aldrich. ATP for ADP-Glo^{TM} assay was from Promega, US.

Kinase buffer 1 (for 1 mM ATP reaction): 10 mM $MnCl_2$, 10 mM $MgCl_2$, 200 mM NaCl, 25 mM Tris pH 7.5, 100 µM DTT, 0.1 mg/mL BSA.

Kinase buffer 2 (for 20 mM ATP reaction): 20 mM $MnCl_2$, 20 mM $MgCl_2$, 200 mM NaCl, 25 mM Tris pH 7.5, 100 µM DTT.

ADP-Glo^{TM} kinase buffer: 25 mM Tris pH 7.5, 1 mM $MnCl_2$, 5 mM $MgCl_2$, 200 mM NaCl, 100 µM DTT, 0.1 mg/mL BSA.

ADP-Glo^{TM} Max kinase buffer: 25 mM Tris pH 7.5, 1 mM $MnCl_2$, 15 mM $MgCl_2$, 200 mM NaCl, 100 µM DTT, 0.1 mg/mL BSA.

2.1.7 Gel running and Western blotting reagents

30% Acrylamide/Bis-acrylamide (Acry/Bis), ammonium persulfate (APS) and N,N,N',N'-Tetramethyl ethylenediamine (TEMED) were purchased from Sigma-Aldrich, UK. Blue prestained protein standard ladder (11-250 kDa) was from NEB, UK.

1X Tris-Acetate-EDTA (TAE) buffer: 40 mM Tris pH 8.5, 0.1% (v/v) acetic acid, 1.3 mM EDTA.

1X Phosphate-buffered saline (PBS): 137 mM NaCl, 2.7 mM KCl, 10 mM Na_2HPO_4, 1.8 mM KH_2PO_4, pH 7.4.

SDS-PAGE resolving gel: 375 mM Tris pH 8.9, 7.5-10% (v/v) Acry/Bis, 0.1% (w/v) SDS, 0.04% (w/v) APS, 0.2% (v/v) TEMED.

SDS-PAGE stacking gel: 125 mM Tris pH 6.8, 3% (v/v) Acry/Bis, 0.1% (w/v) SDS, 0.04% (w/v) APS, 0.2% (v/v) TEMED.

SDS running buffer: 25 mM Tris, 192 mM glycine, 0.1% (w/v) SDS.

SDS blotting buffer: 25 mM Tris, 192 mM glycine, 20% (v/v) MeOH, 0.01% (w/v) SDS.

InstantBlue Coomassie stain was purchased from Abcam, UK. Intercept (PBS) blocking buffer and NewBlot Nitro stripping buffer were from LI-COR, UK. Amersham Protran 0.2 µm nitrocellulose membrane was from Cytiva, UK.

2.1.8 Flow cytometry and immunofluorescence reagents

37% formaldehyde solution, paraformaldehyde (PFA) and Triton X-100 were from Sigma-Aldrich, UK. Vectashield Vibrance antifade mounting medium with DAPI was from Vector Laboratories, US. Zombie NIR™ fixable viability dye was from Biolegend, US.

FACSWASH buffer: 1% BSA (w/v) in PBS.

FACSFIX buffer: 2% formaldehyde (v/v) in PBS.

2.1.9 Antibodies

Table 2. 2 List of primary antibodies
Western blot (WB), flow cytometry (FC), immunofluorescence (IF), gel contraction assay (GC)

Name / catalogue number	Manufacturer	Host species	Dilution factors	Application
Monoclonal anti-pY, clone 4G10 (#05-321)	Sigma-Aldrich, UK	Mouse	1:666	WB
Polyclonal anti-phospho-DDR1/DDR2, anti-pY569/521	Custom-made by Biomatik (Sammon et al., 2020)	Rabbit	1:666	WB
Polyclonal anti-phospho-DDR1/DDR2, anti-pY586/538	Custom-made by Biomatik (Sammon et al., 2020)	Rabbit	1:666	WB
Monoclonal anti-phospho-DDR1/DDR2, pY796/740 (#MAB25382)	Bio-Techne, US	Rabbit	1:666	WB
Polyclonal anti-DDR2, N-terminal epitope (#AF2538)	Bio-Techne, US	Goat	1:666	WB
Polyclonal anti-DDR2, C-terminal epitope (#PA5-79144)	Invitrogen, UK	Rabbit	1:1000	WB
Monoclonal anti-DDR1, C-terminal epitope (#sc-374618)	Santa-Cruz, US	Mouse	1:500	WB
Monoclonal anti-FLAG M2 (#F3165)	Sigma-Aldrich, US	Mouse	1:200	FC, IF
Polyclonal anti-phospho-Src (Y527) (#2105)	Cell Signaling, US	Rabbit	1:500	WB

Monoclonal anti-Src (32G6) (#2123)	Cell Signaling, US	Rabbit	1:500	WB
Monoclonal anti-Akt pan specific antibody (#MAB2055)	Bio-Techne, US	Mouse	1:1000	WB
Polyclonal anti -phospho-Akt (S473) (#AF887)	Bio-Techne, US	Rabbit	1:1000	WB
Monoclonal anti-phospho-Erk1 (T202/Y204)/Erk2 (T185/Y187) (#MAB1018)	Bio-Techne, US	Rabbit	1:1000	WB
Monoclonal anti-Erk1/Erk2 (#MAB1576)	Bio-Techne, US	Mouse	1:1000	WB
Monoclonal anti-phospho-p38 MAPK (T180/Y192) (D3F9) (#4511)	Cell Signaling, US	Rabbit	1:1000	WB
Monoclonal anti-p38 MAPK (D13E1) (#8690)	Cell Signaling, US	Rabbit	1:1000	WB
Monoclonal anti-alpha-Tubulin (DM1A) (#T6199)	Sigma-Aldrich, US	Mouse	1:2000	WB
Monoclonal anti-alpha-smooth muscle actin (1A4) (#14-9760-80)	ThermoFisher, UK	Mouse	1:500 for WB, 0.5mg/mL for IF	WB, IF
Monoclonal anti-integrin beta 1 (P5D2)	In-house produced (Xu et al., 2012)	Mouse	10 µg/mL	FC, GC
Monoclonal anti-integrin alpha 1 (FB12) (#MAB1973)	Millipore Chemicon, UK	Mouse	10 µg/mL	FC
Monoclonal anti-integrin alpha 2 (AK7) (#MCA743)	AbD Serotec, UK	Mouse	10 µg/mL	FC

Table 2. 3 List of secondary antibodies and fluorescent dyes

Name	Manufacturer	Host species	Dilution factors	Application
IRDye 680RD anti-mouse IgG (#926-68070)	LI-COR, US	Goat	1:17,500	WB
IRDye 680RD anti-goat IgG (#926-68074)	LI-COR, US	Donkey	1:17,500	WB
IRDye 800CW anti-mouse IgG (#926-32210)	LI-COR, US	Goat	1:17,500	WB
IRDye 800CW anti-rabbit IgG (#926-32213)	LI-COR, US	Donkey	1:17,500	WB
AlexaFluor 488 anti-mouse IgG1 (#A-21121)	ThermoFisher, UK	Goat	1:500	IF
AlexaFluor 488 anti-mouse IgG (H+L) (#A-11001)	ThermoFisher, UK	Goat	1:500	IF
Anti-mouse IgG-FITC (#F9006)	Sigma-Aldrich, US	Goat	1:500	FC
Rhodamine Phalloidin (#00027)	Biotium, US	-	1:200	IF

2.2 Cloning

2.2.1 Site-directed mutagenesis and subcloning

The mutant constructs, including point mutants DDR2-Y740C and DDR2-L610P, as well as insertion mutant Flag-GS-DDR2 were generated using the PCR QuickChange mutagenesis method (Liu and Naismith, 2008). The plasmid pS-DDR2, consisting of the WT DDR2 cDNA cloned into the pSP72 vector (Promega, US) (Leitinger, 2003), was used as the cloning template. All primer designs were based on the principles shown in **Figure 2. 1**. The primers are shown in **Table 2. 4**.

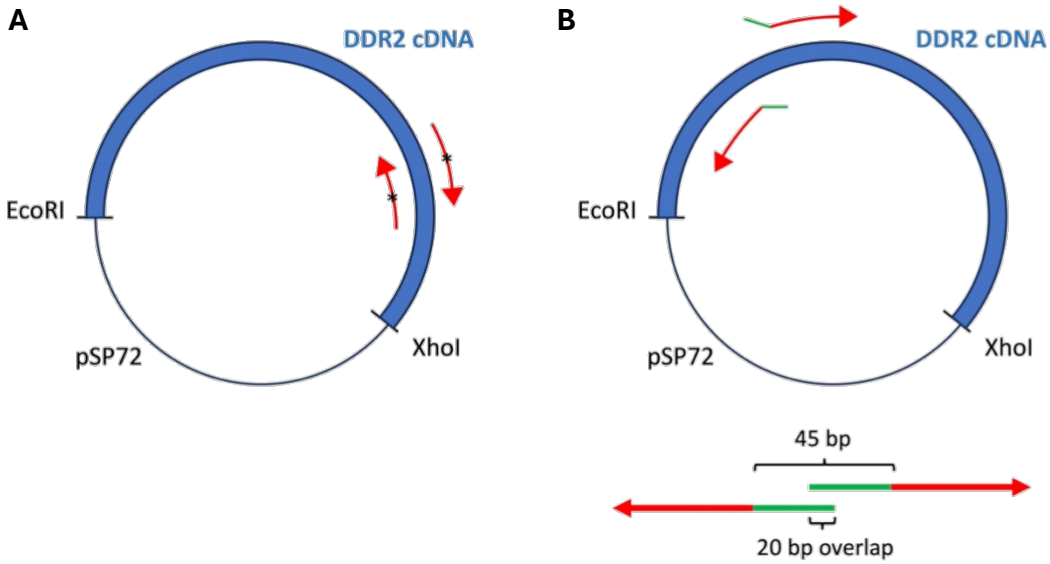


Figure 2. 1 Schematic diagram illustrating different types of mutagenic primers used.
All constructs can by analytically digested with EcoRI and XhoI, the two enzymes used to clone the DDR2 cDNA constructs into the cloning vector pSP72.
A. Both forward and reverse primers for missense mutants were designed with the mutated bases (*) in the middle.
B. For the insertion of the Flag tag and short flexible linker, the short tags were directly encoded in the primers, with the 3' regions of the insertion included in the forward primer and the 5' region in the reverse primer. The red regions depict the annealing part of the primers and the green regions the insertion. The primer pair has a 20-base overlap region.

Table 2. 4 Primer sequences

Mutagenic bases are shown in green. Flag-tag insertion are shown in red.

Primer Name	Forward primer (5'-3') Reverse primer (5'-3')	Application
DDR2Y740C	CTGTACAGTGGTGACTGTTACCGGATCCAGG CCTGGATCCGGTAACAGTCACCACTGTACAG	QuickChange Mutagenesis
DDR2L610P	GGCTGTGAAAATGCCCCGAGCAGATGCC GGCATCTGCTCGGGGCATTTTCACAGCC	
FlagGS	GATGACGATAAGAGTGGTTCTGGATCAGGTTCGC CAGCTATATGCCGCTATCCTC GAACCACTCTTATCGTCATCGTCCTTATAGTCATTA ACCTGAGCTTTTGCAGAACTCA	
spOPIN-DDR2	AAGTTCTGTTTCAGGGCCCGGTGCCCCACTATGCA GAG ATGGTCTAGAAAGCTTTACTCGTCGCCTTGTTGAA GGAGCAG	In-Fusion cloning
DDR2RT	CACCATGGACCTGCTCTCAG TGTAGTGAACTTGCCCAGCA	Genotyping
DDR2DS1	GTTTCTGCAGATTGACTTGCAC	Sanger sequencing
DDR2SEQ1	ACTACCATGAAGGTCCACTGC	
DDR2SEQ2	GGCTGCAGCGGTGTTGTGAA	
DDR2SEQ3	CTCAAGGACCCAAACATCATCCA	
T7P	TAATACGACTCACTATAGGG (Provided by GeneWiz)	
DDR2SEQ5	CCTAACTTTCAAAGAGAAGCTGG	Sanger sequencing for HDF cells genotyping
MMP2	CCAAGAACTTCCGTCTGTCC TGAACCGGTCCTTGAAGAAG	qPCR
SMAD3	TGGACGCAGGTTCTCCAAAC CCGGCTCGCAGTAGGTAAC	
ACTG2	CTGCCATGTACGTCGCCATTCA GACATTGTGGGTGACGCCATCA	

CTNNB2	GCTACTCAAGCTGATTTGATGGA	
	GGTAGTGGCACCAGAATGGATT	
TNC	ACTGACTCAGAAGCCTTGG	
	ATTTCTGGCACTTTCTCGC	
LTBP2	CTGCACAGATGACAACGAGTGTC	
	AGAGTGTAGCCAGGGTAGCAGA	
ACTA2	TGGCTATTCCTTCGTTACTACTGCT	
	CATCAGGCAACTCGTAACTCTTCTC	
GAPDH	GGTGGTCTCCTCTGACTTCAACA	
	GTTGCTGTAGCCAAATTCGTTGT	

The primers for DDR2-Y740C and DDR2-L610P contained the mutated bases in the middle to maximise the priming efficiency. The primers designed for the Flag-containing construct were based on the chimera insertion (Li et al., 2011). The insertion site of the Flag tag was located three amino acids after the predicted signal peptide cleavage site. After obtaining the pS-Flag-GS-DDR2-WT construct (WT DDR2 with Flag tag insertion, cloned into pSP72), this plasmid was then used as a template for point missense mutant generation (Flag-GS-DDR2-Y740C and Flag-GS-DDR2-L610P). The PCR reactions included 10 ng template cDNA, 0.3 µM forward and reverse primers and 1X cloneAmp HiFi PCR premix (25 µL total reaction volume). The reactions were carried out in a G-Storm thermal cycler (Somerset, UK) with the following programme:

Step	Condition	Cycle
Initial denaturation	98°C, 3 minutes	-
Denaturation	98°C, 10 seconds	X20
Annealing	55°C, 15 seconds	
Elongation	72°C, 1 minute	
Final elongation	72°C, 10 minutes	-
Hold	12°C	-

The PCR products were digested by adding 20 U of *DpnI* enzyme and incubated at 37°C for 1 hour, to destroy the template DNA. All digested products were then mixed with 1X gel loading dye and analysed on 0.8% agarose gel containing 1x SYBR safe DNA gel stain, at 100 V

for 30 minutes along with the 1 kb DNA ladder. 1X TAE buffer was used to dissolve the agarose gel powder and also acted as the agarose gel running buffer. Products (PCR mix) with correct sizes were then transformed into Stellar™ competent cells using the heat-shock protocol. In brief, 2.5 µL of PCR product was mixed with 25 µL E.*coli* and incubated on ice for 30 minutes. The mixture was then heated to 42°C for 45 seconds, followed by two minutes incubation on ice. Cells were spread onto LB agar plates containing 100 µg/mL ampicillin and grown overnight (for a maximum of 18 hours) at 37°C in an incubator (Memmert, Germany). At least three single colonies were picked from the plates and further grown in LB broth containing 100 µg/mL ampicillin at 37°C overnight, with shaking at 200 rpm in a Stuart shaking incubator (Cole-Parmer, UK). Cells were pelleted at 1,000 xg for 30 minutes at 4 °C in a CR-412 benchtop centrifuge (Jouan, US) the next morning, and the plasmid DNAs were extracted and purified using QIAprep Miniprep kit according to the manufacturer's protocol. DNA concentration was measured on a Nanodrop ND-1000 Spectrophotometer (ThermoFisher, UK).

In order to validate the size of the cDNA contained in the plasmids, 500 ng purified DNA was incubated with 10 U *EcoRI-HF* and 10 U *XhoI* enzymes (in CutSmart buffer) at 37°C for 1 hour, followed by analysing the fragments on 0.8% agarose gel (described as above). The constructs with expected size were then subjected to Sanger sequencing (conducted by GeneWiz, UK) to verify the existence of the desired mutation, as well as that no unwanted PCR-generated mutations were contained in the cDNA. All primers used for DNA sequencing are shown in **Table 2. 4**. Correct cDNA constructs were then subcloned into the mammalian expression vector pcDNA™3.1/Zeo (ThermoFisher, UK). To this end, 1-2 µg cDNA and pcDNA™3.1/Zeo vector was digested with 20 U *EcoRI-HF* and 20 U *XhoI* enzymes (in CutSmart buffer) at 37°C for at least 3 hours. The products were then separated on a 0.8% agarose gel (described above) until the loading stain reached the bottom line of the gel. DNA bands were visualized, and relevant bands isolated under a 180 W ultraviolet (UV) transilluminator (UViTec STX-20.M, UK) using a scalpel. The DNA fragments were extracted from the gel pieces and purified using a QIAquick gel extraction kit according to the manufacturer's instructions. After measuring the DNA fragment concentrations, the ligation reaction was performed as an overnight incubation at 16°C, using 3:1 (insert: vector) molar ratio with 0.04 U/mL T4 ligase and 1X T4 ligase buffer. Each ligation mixture was transformed into Stellar™ competent cells, followed by bacterial culturing and Miniprep purification (described above). Sanger sequencing was then

performed again to verify the construct's identity. The DNA constructs produced were pc-DDR2-WT, pc-DDR2-Y740C, pc-DDR2-L610P, pc-Flag-GS-DDR2-WT, pc-Flag-GS-Y740C and pc-Flag-GS-DDR2-L610P.

In order to obtain larger amounts of DNA for mammalian cell transfection 10 ng of the correct constructs in pcDNA 3.1 vector were transformed (described above) into 25 µL DH5α competent cells or NEB 5-alpha competent cells followed by colony-picking and liquid bacterial culture as described above. QIAprep Midiprep or Maxiprep kit was then used to purify the DNAs from 50 mL or 100 mL bacterial cultures according to the manufacturer's instructions.

2.2.2 In-Fusion cloning

In order to obtain baculovirus expression of soluble DDR2 kinases, constructs were cloned into pOPINF vector or other pOPIN vectors for optimal expression (Berrow et al., 2007). The constructs generated are shown in **Table 2. 5**. All pOPIN vectors were provided by the Oxford Protein Production Facility (OPPF; the current name is Protein Production UK; Link: https://www.rfi.ac.uk/projects/protein-production-uk/). The pOPIN vectors enable the expression of proteins in multiple hosts, including mammalian cells, E.*coli* and insect cells. The vectors all contained sequences encoding a His_6-tag together with a human rhinovirus (HRV) 3C protease cleavage site, which allows nickel affinity purification and further removal of the His_6-tag by 3C protease. For optimization of DDR2-L610P protein expression, all the pOPIN vectors except pOPINF contained additional tags (**Figure 2. 2, Table 2. 5**) before the 3C cleavage site to increase protein stability or solubility. The In-Fusion cloning technique (TakaraBio, Japan) was used to produce the pOPIN-constructs, which encoded the DDR2 JM4 segment with the kinase domain (residues 518-855) of WT or mutant DDR2. To achieve this, pc-DDR2-WT, pc-DDR2-Y740C and pc-DDR2-L610P were used as the PCR templates. Primers (**Table 2. 4**) contained 15 bases 5' end overlap with the linearised vector, were all designed using the online In-Fusion tool (Link: https://www.takarabio.com/learning-centers/cloning/primer-design-and-other-tools). The same procedures for PCR and *DpnI* parental DNA digestion were performed as in **Section 2.2.1**. The digested PCR products were then purified using NucleoSpin Gel and PCR clean-up kit according to the manufacturer's instructions. 50 ng of the purified product was then incubated with 100 ng linearized pOPIN vector, together with 1X In-Fusion HD enzyme premix. This 10 µL reaction was performed at

50°C in a water bath for 15 minutes. After this, 2.5 µL mixture was transformed into 25 µL Stellar™ competent cells as described in **Section 2.2.1**. The same bacterial culture, DNA purification, analytical digestion and Sanger sequencing steps were performed as in **Section 2.2.1**.

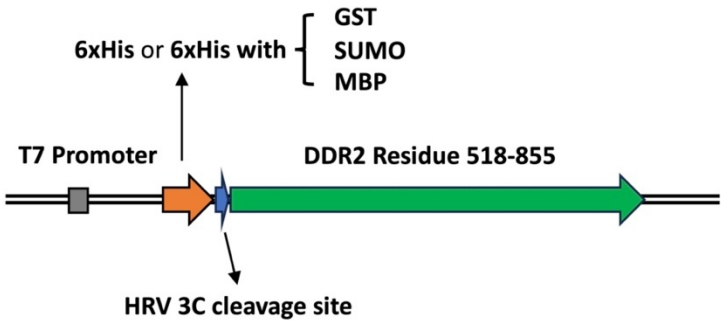


Figure 2. 2 Schematic diagram illustrating the key fragment locations on the pOPIN construct.
DDR2 JM4-kinase cDNA (encoding DDR2 residues 518-855) was inserted after the 3C cleavage site. The part labelled in orange encodes a His6-tag with or without other fusion tags, as listed in **Table 2. 5**.

Table 2. 5 List of pOPIN constructs and their protein constructs name
Glutathione S-transferase (GST), ubiquitin-like modifier (SUMO), maltose-binding protein (MBP)

DNA construct name	Tag	Protein construct name
pOPINF-DDR2-WT-K	His_6-tag	DDR2-WT-K
pOPINF-DDR2-Y740C-K		DDR2-Y740C-K
pOPINF-DDR2-L610P-K		DDR2-L610P-K
pOPINJ-DDR2-L610P-K	His_6-GST-tag	His-GST-DDR2-L610P-K
pOPINS3C-DDR2-WT-K	His_6-SUMO-tag	His-SUMO-DDR2-WT-K
pOPINS3C-DDR2-L610P-K		His-SUMO-DDR2-L610P-K
pOPINM-DDR2-WT-K	His_6-MBP-tag	His-MBP-DDR2-WT-K
pOPINM-DDR2-L610P-K		His-MBP-DDR2-L610P-K

2.3 Soluble DDR2 construct expression

2.3.1 Viral amplification and small-scale protein expression test

To obtain soluble DDR2 constructs DDR2-WT-K, DDR2-Y740C-K and DDR2-L610P-K expression in the baculovirus system, 1 µg of linearised ORF1629 Bacmid (provided by Ian Jones, University of Reading) and 1 µg of the pOPIN constructs were co-transfected into Sf9 cells grown at 1 x 10^6 cells/well in a 6-well plate. The cells were cultured in Insect Xpress medium without antibiotics, and Cellfectin II was used for transfection according to the manufacturer's protocol. The cells were incubated at 27°C for seven days in a static Innova® 42 incubator (New Brunswick Scientific, UK), followed by using a pipette to harvest the supernatant as P_0 virus for further Sf9 cells infection. In order to amplify P_1 virus, 10 mL of the Sf9 cells at 1 x 10^6 cells/mL were grown in a 125 mL Erlenmeyer flask and infected with 100 µL P_0 virus solution. The infected cells were incubated in an INFORS HT Multitron shaker at 27°C, 120 rpm for seven days. The supernatant containing P_1 virus was then separated from the cells pellet by 4°C centrifugation at 3,000 xg for 15 minutes.

A small-scale protein expression test was conducted using the P_1 virus before further virus amplification. 10 mL of the Sf9 cells cultured at 1 x 10^6 cells/mL in a 125 mL Erlenmeyer flask were infected with 10 µL or 100 µL P_1 virus solution. During the 27°C, 120 rpm incubation, 1 mL infected Sf9 cells were removed and pelleted at 14,000 xg for 1 minute on days 2, 3 and 4. The cell pellets were then lysed with 210 µL regular Sf9 lysis buffer (**Section 2.1.4.1**) at room temperature for 30 minutes, before being pelleted at 14,000 xg for 10 minutes at 4°C. Ni-NTA agarose beads (Qiagen, Germany) were washed twice with sterile MilliQ water and then resuspended with an equal volume of 1X PBS (**Section 2.1.7**) to generate a 50% bead slurry. All wash steps were performed by centrifuging at 3,000 xg for 1 minute and discarding the supernatant. 40 µL of this 50% Ni-NTA bead were then incubated with the cell lysates on a tube rotator at low speed for 30 minutes at room temperature. Beads were then washed twice with Ni-NTA wash buffer (**Section 2.1.4.1**), before being boiled with 2x reducing sample buffer for 5 minutes. The mixture was then cooled down to room temperature and centrifuged briefly to pellet the beads. The supernatant was separated on a 10% SDS-PAGE gel along with the blue prestained protein standard ladder in SDS running buffer (**Section 2.1.7**). The gels were stained with at least 25 mL InstantBlue Coomassie stain for 15 minutes, followed by washing with MilliQ water and imaging on an Odyssey FC imager (LICOR, US).

For constructs with sufficient soluble protein expression levels (DDR2-WT-K and DDR2-Y740C-K), P_2 virus was amplified using a 50 mL Sf9 cell culture following the same procedures as for P_1 virus amplification. A small-scale expression test (as above) was performed again with Sf9 cells infected with P_2 virus to confirm the ability to generate soluble proteins.

2.3.2 Large-scale protein purification

For large-scale protein production, 10 µL of the P_2 virus solution was added to each mL of the Sf9 cell suspension (0.5-1 L, at 1 x 10^6 cells/mL) in a Corning roller bottle. The cells were cultured at 27°C, with shaking at 120 rpm for three days, before being pelleted at 3,000 xg for 15 minutes at 4°C. The cell pellets were then frozen at -80°C for at least 1 hour before cell lysis. 30 mL of the large-scale Sf9 cell lysis buffer (**Section 2.1.4.2**) was used to resuspend a 500 mL cell culture pellet on ice, before sonicating on ice for 10 minutes (9 seconds on and 9 seconds off, 50% amplitude) on a Fisherbrand Q500 sonicator (with probe, ThermoFisher, UK). The sonicated lysates were then centrifuged at 30,000 xg for 1 hour at 4°C, followed by filtration through a 0.45 µm cellulose acetate filter (Sartorius, UK). On an ÄKTA Pure chromatography system (GE Healthcare, US), a 1 mL HisTrap HP column (GE Healthcare, US) was equilibrated using HisTrap wash buffer (**Section 2.1.4.2**), before running the clear protein lysates at 4°C with the flow rate of 1 mL/minute. The column was then washed with HisTrap wash buffer until the UV 280 nm absorbance reached the baseline. A further column cleaning was performed by combining HisTrap wash buffer and 3% HisTrap elution buffer (**Section 2.1.4.2**) before the final elution step with 100% HisTrap elution buffer. Protein concentration was measured on a Nanodrop ND-1000 Spectrophotometer (ThermoFisher, UK).

To remove the His_6-tag, 1 U HRV 3C protease (ThermoFisher, UK) was added to each 0.1 mg purified protein. The mixture was then transferred to a 3,500 MWCO SnakeSkin dialysis tubing (ThermoFisher, UK) and dialysed in 4-5 L of the dialysis buffer (**Section 2.1.4.2**) overnight at 4°C. Dialysis buffer was changed to fresh buffer 3-4 hours before the next purification step. The dialysed protein solution was loaded onto the 1 mL HisTrap HP column at 4°C with a flow rate of 1 mL/minute. The protein without His_6-tag was collected in the flow-through, followed by concentrating to 500 µL with a 10,000 MWCO Vivaspin centrifugal concentrator (Sartorius, UK).

Final purification was performed on a Superdex™ 200 Increase 10/300 GL column (GE Healthcare, US) by size exclusion chromatography. The column was first equilibrated with at least 50 mL gel filtration buffer (**Section 2.1.4.2**), before running the protein samples at 0.75 mL/minute flow rate. Protein fractions were collected and concentrated using a 10,000 MWCO Vivaspin concentrator (as described above) before snap-freezing in liquid nitrogen.

2.3.3 Optimization experiments for increasing DDR2-L610P-K protein solubility

Construct DDR2-L610P-K failed to produce soluble protein in initial experiments. To check for protein expression and the presence of aggregated DDR2-L610P-K, cell pellets after lysis and Ni-NTA washes were checked on 10% SDS-PAGE along with the material obtained with Ni-NTA purification. To achieve this, cell pellets were resuspended with 15 µL 2x reducing sample buffer and sonication for 5 minutes (10 seconds on 10 seconds off) in a water sonicator (VWR, US), before boiling at 100°C for 5 minutes. 10 µL of the Ni-NTA washes were mixed with 2.5 µL 5X reducing sample buffer prior to boiling (as above).

The bands indicated potential DDR2-L610P-K expression were only observed from the cell pellet fractions, suggesting most of the DDR2-L610P-K protein molecules were insoluble with the current expression system or purification method. In order to establish whether changing the purification method could overcome this problem, procedures after the step of pelleting the Sf9 culture were optimized. The cell pellets were either lysed immediately or frozen at -80°C for 1 hour before lysis to increase protein extraction efficiency. Sf9 cells lysis buffer was also modified (see **Section 2.1.4.1**) in an attempt to increase protein solubility and to reduce protein aggregation. The modifications included a range of different pH, addition of glycerol or higher concentration of detergent (Hofmann et al., 2018, Vagenende et al., 2009).

2.3.4 Recombinant DDR2-L610P-K protein production in mammalian cells and *in vitro* functional analysis

As soluble DDR2-L610P-K was unable to be obtained via the baculovirus expression system, the pOPIN constructs encoding DDR2-L610P-K with various fusion tags were then expressed in HEK293 cells, in order to check whether soluble protein could be detected in the cytosol. Expressing DDR2-L610P-K in HEK293 cells allowed the protein to be immunoprecipitated from mammalian cells for *in vitro* autophosphorylation assays to confirm the recombinant DDR2-L610P-K kinase is catalytically active. 3 µg of the pOPIN constructs were transfected with 9 µg

of PEI into HEK293 cells grown in a 6-well plate (**Section 2.10**). After two days of incubation, cells were collected and frozen at -80 °C for at least 1 hour, before lysing with recombinant protein lysis buffer (**Section 2.1.6**) at 4°C on a spin rotor. The cells were then pelleted through 4°C centrifugation at 6,000 xg for 30 minutes. During the spin, 50 uL cobalt-based immobilized metal affinity chromatography (IMAC) Dynabeads™ (ThermoFisher, UK) were prepared according to manufacturer's instructions. 300 µL of clear lysates were then diluted with 2X binding/wash buffer (**Section 2.1.6**), before incubating with the Dynabeads at room temperature on a spin rotor for 5 minutes. The beads were then washed 4 times with 1X binding/wash buffer (**Section 2.1.6**) on a DynaMag™ magnet (ThermoFisher, UK) according to the manufacturer's protocol. The beads/protein mixtures were either resuspended with 40 µL PBS and boiled with 15 µL 5X sample buffer for 5 minutes, or they were incubated in 40 µL kinase buffer 1 with or without 1 mM ATP (**Section 2.1.6**) at room temperature for 30 minutes before boiling with 20 µL 5X sample buffer. The samples were then analysed on 10% SDS-PAGE followed by Western blotting (**Section 2.5**).

2.4 Recombinant kinase protein autophosphorylation assay

To find autophosphorylation differences between constructs, purified soluble recombinant protein DDR2-WT-K, DDR2-Y740C-K as well as DDR1-WT-K (provided by Douglas Sammon, previous lab member) at 0.1 and 1 µM concentration were incubated at 20°C in kinase buffer 1 (**Section 2.1.6**) with or without 1 mM ATP for up to 60 minutes. A longer time course (up to 180 minutes) experiment was performed with 100 µM DDR1-WT-K and DDR2-WT-K in the presence of 20 mM ATP in kinase buffer 2 (**Section 2.1.6**). To establish whether DDR2 JM4 and kinase regions undergo protein concentration dependent autophosphorylation, DDR2-WT-K at 125-1000 nM concentration were incubated with 1 mM ATP in kinase buffer 1 (**Section 2.1.6**) at 20°C for 10 or 30 minutes. The reactions were either terminated by boiling samples with 5X reducing sample buffer followed by analysis on 10% SDS-PAGE and Western blotting (**Section 2.5**), or by mixing with 80 mM EDTA solution as well as non-reducing 5X sample buffer (no SDS) and analysis on 7.5% native-PAGE followed by Coomassie staining (**Section 2.6**)

2.5 Western blotting

Protein samples were separated on SDS-PAGE gels (7.5% or 10%) using a Mini-PROTEAN tetra vertical electrophoresis tank (BioRad, UK) with SDS running buffer (**Section 2.1.7**) at 120 V for 1.5 hours. The sample containing gels were then transferred onto 0.2 µm nitrocellulose

membrane using a Mini Trans-Blot tank with SDS blotting buffer (**Section 2.1.7**) on ice at 200 mA for 1 hour. The membranes were blocked with Intercept (PBS) blocking buffer at room temperature for 1 hour, before primary antibody overnight incubation at 4°C. Primary antibodies (**Table 2. 2**) were prepared in Intercept blocking buffer with 0.2% (v/v) Tween-20. Membranes were then washed 3 times for 10 minutes with PBS containing 0.1% (v/v) Tween-20 (PBS-T), followed by secondary antibody incubation at room temperature for 1 hour in the dark. Secondary antibodies (**Table 2. 3**) were prepared in 0.1% PBS-T. Membranes were then washed 4 times with 0.1% PBS-T for 5 minutes in the dark. The blot images were obtained on an Odyssey Fc imager using the 700 or 800 nm channel. Intensity quantification was performed using ImageStudio Lite software (LICOR, US).

2.6 Native gel electrophoresis

Native-PAGE gels were prepared with 7.5% resolving gel and 3% stacking gel without SDS addition (**Section 2.1.7**). Samples were prepared (**Section 2.4**) and separated on the gel in non-SDS running buffer at 90 V for 3 hours at 4°C. Gels were then stained with at least 25 mL InstantBlue Coomassie stain for 15 minutes at room temperature, followed by washing with MilliQ water and imaging on the Odyssey FC imager (700 nm channel).

2.7 Protein kinase kinetic analysis

To investigate the catalytic differences between soluble DDR2 constructs, ADP-Glo™ assays or ADP-Glo™ Max assays were performed. The ADP-Glo assay measures the luminescent signals from kinase reaction-produced ADP and allows a wide range of ATP concentration (up to 1 mM for ADP-Glo™, up to 5 mM for ADP-Glo™ Max) to be used. The reactions were done in 25 µL volumes, where 0.1 µM of the recombinant DDR2 protein was independently incubated with a range of Axltide peptide concentration (0-1.04 mM) in the presence of a fixed ATP concentration (1 mM), or a range of ATP concentration (0-5 mM) in the presence of a fixed Axltide peptide concentration (520 µM). The reactions were performed at room temperature (21°C to 24°C) in 96-well Cellstar® plates (Greiner, Germany) and stopped at indicated times (up to 40 minutes). Either ADP-Glo™ kinase buffer or ADP-Glo™ Max kinase buffer (Section 2.1.6) was used to dilute the reagents. After the indicated reaction time, 25 µL of the ADP-Glo™ reagent was added and incubated for 40 minutes, followed by 60 minutes incubation with 50 µL Kinase detection reagent. An ADP standard curve was generated by mixing pure ATP and ADP in the reaction according to manufacturer's protocol. Luminescence signals were

then measured on a Spark® plate reader (Tecan, Switzerland). The luminescence readings were converted to ADP concentrations according to the ADP standard curve. The initial rates at each ATP or peptide concentration were determined by linear regression ($nM*min^{-1}$) and plotted as specific activity ($nM*min^{-1}*mg^{-1}$). The data was fitted with the Michaelis-Menten equation using GraphPad Prism 9 software.

IC_{50} values of type-II kinase inhibitor dasatinib as well as DDR-specific inhibitor VU6015929 were also investigated using the ADP-Glo™ assay. The 25 µL reactions were performed by incubating 0.1 µM of the recombinant DDR2 protein with a range of inhibitor concentrations (0.28 nM-50 µM for dasatinib, 0.056 nM-10 µM for VU6015929) in the presence of ATP (100 µM or 1 mM) and Axltide peptide (250 µM). The same incubation time and procedures were used as described above. The data were plotted as the percentage of inhibition, with IC_{50} calculated using GraphPad Prism 9 software.

2.8 Mammalian cell culture

2.8.1 Cell passaging

HEK293, Cos-7 and primary human dermal fibroblast (HDF) cells were cultured in complete medium, consisting of DMEM/F-12 medium with 10% (v/v) FBS, 2 mM L-Glutamine, 100 U/mL penicillin and 100 µg/mL streptomycin. Cells were grown in T25 or T75 flasks under the condition of 5% CO_2, 100% humidity, 37°C. Cell passaging was performed once the cells reached 90-95% confluency. HEK293, COS-7, and HDF cells were diluted 1:5, 1:10, or 1:3, respectively, for passaging. Cell medium was removed, followed by PBS rinsing. Thereafter, 0.5 mL (into T25) or 1.5 mL (into T75) of the 0.5% trypsin-EDTA solution was then added to the cells and incubated for 1-3 minutes at room temperature (HEK293 cells) or 37°C (Cos-7 and HDF cells). The trypsinization was then stopped by adding 4.5 mL (into T25) or 13.5 mL (into T75) complete medium, followed by seeding the cells into new flasks.

2.8.2 Cell freezing and thawing

Cells were grown in T75 flasks to full confluency before being collected by trypsinization (**Section 2.8.1**). The cells were then centrifuged at 300 xg for 5 minutes, followed by resuspending in 2-3 mL freezing medium (complete medium with 10% DMSO). 500 µL of the cell solution was then aliquoted into Nunc™ Cryogenic tubes (ThermoFisher, UK), and frozen overnight at -80°C prior to transfer into liquid nitrogen.

Cells from liquid nitrogen storage were quickly thawed in a 37°C water bath, and then immediately diluted into 10 mL complete medium. The cells were then centrifuged at 300 xg for 5 minutes and resuspended with fresh complete medium, before being transferred into a culture flask.

2.8.3 Cell seeding

Cells were trypsinized and resuspended into complete medium as described in Section 2.8.1. HEK293 cells were 1:4 diluted with complete medium and seeded into 6-well plates (2 mL/well) for DDR2 autophosphorylation assay and flow cytometry. Cos-7 cells were 1:13 diluted and seeded into 24-well plates (0.5 mL/well) for immunofluorescence assay. HDF cells were either 1:3 diluted and seeded into 100 mm dishes for autophosphorylation assay, or were seeded with specific cell numbers for indicated experiments.

2.8.4 Cell counting

A 20 µL aliquot of cells collected as described in Section **2.8.1** was mixed with an equal volume of 0.4% trypan blue. The mixtures were then loaded onto a haemocytometer (Assistant, Germany), and the cells were manually counted using an Olympus CKX41 microscope.

2.9 Primary cell genotyping

To confirm the identify of control and mutant HDF cells, total RNAs were extracted from primary HDF-WT, HDF-Y740C and HDF-L610P cell lines using RNeasy Mini kit according to manufacturer's protocol. Total RNA concentrations were measured on a Nanodrop ND-1000 Spectrophotometer. RNA samples were kept on ice during experiments and stored in -80°C to prevent degradation. For reverse transcription from RNA to cDNA, 500 ng of the total RNA was mixed with 1X PrimeScript RT mastermix in a 10 µL volume. The reactions were performed in a peqSTAR thermal cycler (VWR, US) with the following programme: 37°C for 40 minutes, 85°C for 5 seconds and 4°C on hold.

cDNA products were then used as templates for target fragment amplification. Primers (**Table 2. 4**) were designed to amplify the DDR2 sequence that encodes the protein sequence starting before residues Leu610 and ending after Tyr740. A 50 µL reaction was performed by mixing 250 ng cDNAs in 1X Q5 reaction buffer, together with 200 µM dNTPs, 0.5 µM forward and reverse primers as well as 0.02 U/pL Q5 High-Fidelity DNA polymerase. The reactions were performed in a peqSTAR thermal cycler (VWR, US) with the following programme:

Step	Condition	Cycle
Initial denaturation	98°C, 30 seconds	-
Denaturation	98°C, 10 seconds	X35
Annealing	68°C, 30 seconds	
Elongation	72°C, 20 seconds	
Final elongation	72°C, 2 minutes	-
Hold	4°C	-

The products were checked on 1.5% agarose gel along with 100bp DNA ladder, followed by bands isolation and gel purification (**Section 2.2.1**). Sanger sequencing was performed as described in **Section 2.2.1**.

2.10 DDR2 autophosphorylation assay

The collagen stimulation assays were performed either with DDR2-expressing HEK293 cells or primary HDF cells. HEK293 cells were transfected with 2 µg (WT) or 3 µg (mutants) full-length DDR2 constructs in pcDNA3.1 vector using the PEI transfection method. PEI is a stable positively charged polymer (Boussif et al., 1995) which can condense DNA into particles and bind to negatively charged cell surface. PEI stock was prepared in sterile MilliQ water with the concentration of 1 mg/mL. PEI stock was diluted into 100 µL Opti-MEM and incubated at room temperature for 5 minutes, before being added to 100 µL DNA containing Opti-MEM. The optimal ratio was 3:1 of PEI to DNA (w/w). The mixture was then incubated at room temperature for 20 minutes, followed by dropwise addition to the cells. Transfected HEK293 cells were further cultured for 24 hours and then serum starved for 16 hours by replacing the culture medium with serum free medium (SFM). SFM consisted of DMEM/F-12 medium with 2 mM L-Glutamine, 100 U/mL penicillin and 100 µg/mL streptomycin. HDF cells growing in 100 mm dishes were serum starved when 80% confluency was observed.

Collagen stock was prepared by using a stock solution that contained collagen I from rat tail in 0.1 M acetic acid. Cells were stimulated with SFM containing 10 µg/mL (HEK293 cells) or 20 µg/mL (HDF cells) collagen I and 10 mM HEPES pH 7.2. Vehicle control groups were incubated in SFM together with 1 mM (HEK293 cells) or 2 mM (HDF cells) acetic acid and 10 mM HEPES pH 7.2. The reactions were carried out at 37°C for 90 minutes (HEK293 cells) or 4 hours (HDF

cells). For inhibitor experiments, cells were treated with SFM containing 100 nM VU6015929 inhibitor or 0.01% DMSO (vehicle control) at 37°C for 45 minutes before collagen stimulation. After simulation, cells were harvested on ice followed by lysing with mammalian cell lysis buffer (**Section 2.1.6**) for 40 minutes. The cells were then pelleted by centrifuging at 14,000 xg for 10 minutes at 4°C. The supernatants were transferred to fresh tubes and analysed immediately by Western blotting or stored at -20 °C for further analysis. 10 µL of the cell lysates was mixed with 2.5 µL of the 5X reducing sample buffer and boiled at 100°C for 5 minutes, before being checked by Western blotting (**Section 2.5**).

2.11 Deglycosylation assay

To monitor the extent of oligosaccharide processing of the full-length DDR2 proteins, Endo H was used to deglycosylate the immature proteins. The digested proteins had smaller sizes that can be observed via Western blotting. HEK293 cells were transfected and lysed as described in **Section 2.10**. 18 µL cell lysates was boiled with 1X glycoprotein denaturing buffer at 100°C for 5 minutes, before being divided into 2 fresh tubes. Samples were then incubated with 1X G5 buffer and 10 U of Endo H at 37°C for 3 hours. Control samples were incubated under the same condition but with 1X G5 Buffer alone. After the incubation, all samples were boiled with the appropriate amount of 5X reducing sample buffer for 5 minutes, followed by analysis on SDS-PAGE and Western blotting (**Section 2.5**)

2.12 Flow cytometry

To confirm the surface expression of the full-length DDR2 constructs expressed in HEK293 cells, Flag-GS-DDR2 constructs were generated (**Section 2.2.1**) and used in this assay due to the lack of antibodies binding to native DDR2 on the cell surface. Flag-GS-DDR2 constructs were single-transfected (**Section 2.10**) or co-transfected with a construct encoding non-tagged DDR2-WT into HEK293 cells. For co-transfection, 0.75 µg of pc-DDR2-WT was mixed with 2.25 µg pc-Flag-GS-DDR2 mutant construct, before being transfected with 9 µg PEI. Cells were collected after 2 days of transfection by incubating with 1 mL cell dissociation solution at room temperature and then pelleted by centrifuging at 300 xg for 5 minutes at 4 °C. All the steps were performed on ice or at 4°C afterwards. The cell pellets were resuspended in FACSWASH buffer and divided into fresh tubes, followed by further centrifugation at 300 xg for 5 minutes. The pellets were then resuspended and incubated with either FACSWASH alone (secondary antibody only staining) or the same buffer containing mouse anti-Flag M2 antibody (**Table 2.**

2) for 30 minutes. Cells were then washed twice with FACSWASH by centrifuging at 300 xg for 5 minutes with the supernatant discarded. Anti-mouse IgG-FITC antibody (**Table 2. 3**) was diluted in FACSWASH and incubated with cells for 30 minutes in the dark. This was followed by one wash with FACSWASH and one wash with PBS. The cells were then incubated with 1:1,000 Zombie NIR™ dye in PBS for 20 minutes in the dark, before being washed once with FACSWASH and then fixed with FACSFIX. Data were collected on a BD Accuri C6 plus (BD Life Science, US) using BD Accuri C6 Plus software and further analysed by Flowjo software (BD Life Science, US).

HDF cells were also analysed by flow cytometry to confirm the surface expression level of integrin receptors. HDF cells grown in T75 flasks were collected by trypsinization, followed by incubating in complete medium at 37°C for 30 minutes to enable receptor recycling back to the plasma membrane. Cells were pelleted the same way as described above. Anti-integrin beta 1 P5D2, anti-integrin alpha 1 FB12 and anti-integrin alpha 2 AK7 (**Table 2. 2**) diluted in FACSWASH were used for primary antibody incubation. The same procedures for secondary antibody and Zombie dye incubation as well as cell fixing were used as described above. Data were collected on a BD LSRFortessa cell analyzer (BD life science, US; from the Flow Cytometry Facility, Imperial College London) using BD FACSDiva software and further processed using Flowjo software.

2.13 Phospho-array assay

To determine potential differences in phosphorylation levels of a specific set of signalling molecules, a kinase profile assay from Bio-Techne was used. HDF cells were grown in 100 mm dishes and stimulated with or without collagen before lysis, as described in **Section 2.10**. The cells were lysed, followed by protein concentration measurements using the Pierce BCA protein assay kit according to the manufacturer's instructions. The lysates were then analysed using the Proteome Profiler human phospho-kinase array kit. The assay was performed according to the manufacturer's instructions. In brief, 270 µg cell lysates were incubated overnight with membranes that contained capture or control antibodies. The membranes were washed to remove unbound proteins, before being incubated with a mixture of biotinylated detection antibodies. Signals were produced by further incubation with IRDye 800CW Streptavidin (LICOR, US) and captured on an Odyssey FC imager. Spot intensities were analysed using ImageStudio Lite software.

2.14 Quantitative PCR

Total RNA extraction from HDF cells and cDNA reverse transcription were performed as described in **Section 2.9**. Quantitative PCR (qPCR) reactions were prepared by mixing 23 ng cDNA, 0.2 µM forward and reverse primer (**Table 2. 4**), and 1X Fast SYBR green master mix in a total volume of 10 µL in a MicroAmp® Fast 96-well reaction plate. The reactions were carried out in a 7500 Fast Real-time PCR system (ThermoFisher, UK) using 7500 Fast software with the following programme:

Step	Condition	Cycle
Holding stage	95°C, 20 seconds	-
Cycling stage	95°C, 3 seconds	X40
	60°C, 30 seconds	
Melt curve stage (continuous)	95°C, 15 seconds	-
	60°C, 1 minute	-
	95°C, 15 seconds	-
	60°C, 15 seconds	-

C_T values were exported into Excel, and the comparative C_T ($\Delta\Delta C_T$) were calculated by normalizing the C_T values of the target gene to the endogenous reference (GAPDH) gene, followed by further calculating the relative-fold change of target gene expression levels from the patient samples *versus* the expression obtained from the control samples using the $2^{-\Delta\Delta CT}$ methods (Livak and Schmittgen, 2001).

2.15 Immunofluorescence imaging

To confirm the surface expression of Flag-tagged DDR2 constructs, Cos-7 cells were seeded onto 13 mm coverslips (VWR, US) and cultured in 24-well plates (**Section 2.8.3**). When cells reached ~40% confluency, 500 ng DNA constructs were mixed with 1 µL P3000 reagent and 1 µL Lipofectamine 3000 in 50 µL Opti-MEM medium at room temperature for 10 minutes, before being added dropwise to the cells. After 2 days of incubation, cell-containing coverslips were washed with ice-cold PBS followed by incubating with anti-Flag M2 antibody in 5% BSA/PBS on ice for 1 hour. The coverslips were then washed for 3 times with PBS and the cells were fixed with 4% PFA/PBS at room temperature for 15 minutes. Cells were then washed 3

times with PBS before being blocked with 5% BSA/PBS at room temperature for 1 hour. The secondary antibody incubation was performed by incubating cells with AlexaFluor 488 anti-mouse IgG1 in 5% BSA/PBS at room temperature for 1 hour in the dark. Cells were then washed with PBS for final 3 times followed by mounting the coverslips onto the microscope slides (ThermoFisher, UK) with Vectashield Vibrance antifade mounting medium (with DAPI). The slides were allowed to dry at room temperature overnight in the dark before being transferred into 4°C storage boxes. Widefield images were acquired using an Olympus BX51 microscope with Simple-PCI acquisition software. Images were prepared using FIJI software.

To observe the alpha smooth muscle actin (α-SMA) expression levels, HDF cells were seeded at 10,000 cells/cm^2 density onto the coverslips. The coverslips were washed with ice-cold PBS on the next day, followed by fixing the cells with 4% PFA/PBS at room temperature for 15 minutes. The cells were then washed with PBS for 3 times and then permeabilized with 0.1% Triton X-100/PBS (v/v) at room temperature for 10 minutes. Cells were then washed 3 times with PBS before being blocked with 5% BSA/PBS at room temperature for 1 hour. The primary antibody incubation was performed by incubating cells with anti-alpha-smooth muscle actin 1A4 in 5% BSA/PBS at room temperature for 1.5 hours. Cells were then washed for 3 times with PBS and incubated with AlexaFluor 488 anti-mouse IgG (H+L) as well as Rhodamine-coupled phalloidin in 5% BSA/PBS at room temperature for 1 hour in the dark. Cells were then washed and mounted the same way as described above. Widefield images were acquired using a Zeiss Axio Observer microscope (in the Facility for Imaging by Light Microscopy, Imperial College London) equipped with an EC Plan-Neofluar 10X/0.30 Ph1 objective and Zen pro software (Zeiss, Germany). Images were prepared using Zen 3.5 blue edition software (Zeiss, Germany).

2.16 Wound healing assay

The wound healing assay was performed using 2 well culture inserts (#80209, ibidi GmbH, Germany) to create 500 µm cell-free gaps. The 24-well plates were either used directly with the inserts or coated with collagen I before usage. The coating was performed by adding 500 µL of the 20 µg/mL collagen prepared in 0.1 M acetic acid to the wells of the 24-well plate, followed by incubating at room temperature for 1 hour. The coating solution was then removed, and the wells were washed twice with sterile PBS. The coated plate was dried completely before applying the inserts. The inserts were manually attached to each well

centre, followed by seeding 5,000 HDF cells per insert well in a volume of 70 µL. The cells were then allowed to reach full confluency (around 20 hours) before being serum-starved by replacing the culture medium with SFM for 24 hours. After serum starvation, the inserts were carefully removed with a pair of tweezers, and the cells were gently washed twice with SFM. For normal conditions, SFM medium with 0.5% FBS (v/v) was used during the wound closure incubation period. For inhibitor treatment, cells were incubated with 0.5%FBS/SFM and 100 nM VU6015929 inhibitor or 200 nM dasatinib. 0.01% DMSO in 0.5% FBS/SFM was used as the vehicle control. Widefield images were acquired using a Zeiss Axio Observer equipped with an EC Plan-Neofluar 10X/0.30 Ph1 objective after 0, 10 and 24 hours of insert removal. The wound sizes were measured using FIJI software with the Scratch/Wound assay macro (designed by Facility for Imaging by Light Microscopy, Imperial College London). Data were presented as the percentage of closure, and the images were prepared using FIJI software.

2.17 Cell morphology imaging

The HDF cells were seeded on coverslips as described in **Section 2.16** and allowed to reach around 90% confluency before serum starvation. After 24 hours incubation with SFM, cells were either incubated with 0.5% FBS/SFM and 200 nM dasatinib or 0.01% DMSO (vehicle control) for 4 days. Widefield images were acquired using an EVOS XL Core imaging system (ThermoFisher) at the same area on the coverslips daily during the incubation. Images were prepared using FIJI software.

2.18 Collagen gel contraction assay

HDF cells were embedded into 3D collagen gels to create models of analysing fibroblast-induced collagen contraction. Firstly, a gel formation test was performed with NaOH titration to find the optimal volume required to generate a well-solidified gel. 3 mg/mL collagen I solution from bovine skin (stock purchased in 0.01 M HCl with a pH of 2.0) was diluted in SFM to the final concentration of 1 mg/mL in a volume of 600 µL. 1-8 µL of 1 M NaOH was added to each tube containing collagen, followed by mixing and immediately transferring 500 µL to pre-labelled 24-well plate. The gels were allowed to solidify at 37°C for 1 hour. After incubation, the least volume of NaOH required to generate a solidified gel was chosen as the standard for further gel contraction assay.

HDF cells were trypsinized and counted as described in **Section 2.8**. For each individual gel, 50,000 cells were mixed into the solution containing 1 mg/mL collagen I (from 3 mg/mL stock) and a pre-determined volume of NaOH in a volume of 600 µL on ice, followed by transferring 500 µL to the 24-well plate. The gels were allowed to solidify at 37°C for 1 hour. For the floating model, gels were released immediately after the one hour of solidification. This was performed carefully using a P10 pipette tip and then the gels were transferred to a 12-well plate containing 1.5 mL 0.5% FBS/SFM in each well. For the stressed matrix model, 0.5 mL of the 0.5% FBS/SFM was added on top of the gels retained in the 24-well plate and incubated for 2 days with the culture medium changed daily, before processing as described in the floating model. For inhibitor and antibody treatments, gels were incubated in 0.5% FBS/SFM containing 100 nM VU6015929 inhibitor or 200 nM dasatinib or 10 µg/mL anti-integrin beta 1 P5D2 antibody. 0.01% DMSO in 0.5% FBS/SFM was used as a vehicle control for the inhibitor experiment.

To acquire images of the gels, culture medium was removed carefully with the gel remaining at the centre of the well. Plates were placed on a black surface, and images were collected from the top of the plates using an iPhone 11 Pro (Apple, US). Phone holder with a flexible arm was used to stabilise the iPhone, which allowed the pictures to be taken with a consistent distance above the plate. Build-in level tool from iPhone was used to ensure the phone was positioned horizontally without an angle. Fresh culture medium (prepared as above) was added to the gels after the imaging for further incubation. Images were acquired at various time points indicated in each experiment. Gel areas were measured using the 'Freehand selections' and 'Measure' functions in FIJI software. Gel area size was normalized to the area size of the culture well border from the same image, and the data was presented as the percentage of the original gel area obtained on day zero (**Figure 2. 3**). Images were prepared using FIJI software.

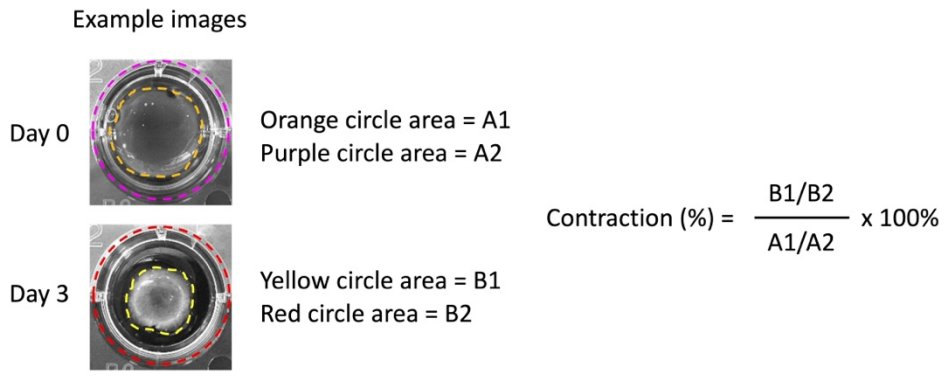


Figure 2. 3 Example images and equation used for collagen gel contraction assay quantification.
Gel areas were circled using the 'Freehand selections' in FIJI software, as shown in the example images. The culture well border was also circled, and the area size was used for data normalization. The percentage of contraction was calculated based on the equation shown on the right-hand side.

2.19 Cell adhesion assay

Wells in a 96-well Immulon® 2HB plate (ThermoFisher, UK) were coated with 50 µL 10 µg/mL collagen I in 50 mM Tris pH 7.5, 100 mM NaCl solution or 10 µg/mL of various of integrin-specific collagen peptides as well as non-receptor binding peptide GPP10 in 0.01 M acetic acid at 4°C overnight. The plate was then washed twice with 150 µL PBS and blocked with 50 µL 0.1% BSA/PBS (w/v) for at least 1 hour at room temperature. During the blocking, HDF cells were trypsinized and counted as described in **Section 2.8**. Cells were then washed once with Opti-MEM and resuspended in an appropriate volume of 0.1% BSA/Opti-MEM. Calcein-AM cell-permeant dye (ThermoFisher, UK; 6µM final concentration) was then added to the cell suspension and incubated at 37°C for 40 minutes in the dark. After the incubation, cells were washed twice with 0.1% BSA/Opti-MEM and resuspended in 0.1% BSA/Opti-MEM to reach the desired cell density. The blocked plate was washed twice with PBS, followed by adding 40 µL 0.1% BSA/Opti-MEM to each well. 40 µL (around $3.5x10^4$ cells) of the labelled cells were then added to the coated wells and further incubated at 37°C for 1 hour in the dark. The plate was then washed carefully four times with PBS using a multichannel pipette. After the final wash, 100 µL PBS were added to each well, and 40 µL of the labelled cells were added to the uncoated well for total fluorescence detection. Fluorescence signals (absorbance at 485 nm, emission at 520nm) were measured on a Spark® plate reader. Data were normalized to the total fluorescence reading and presented as the percentage of cell adhesion.

2.20 Statistical analysis

GraphPad Prism 9 was used to perform the comparison tests and establish the statistical significance between groups. Different tests were used as stated in the figure legends. A p-value smaller than 0.05 was judged as ‘significant’.

Chapter 3 Investigation of Warburg Cinotti Syndrome related DDR2 mutant activities

3.1 Introduction

RTKs play fundamental roles in multiple cellular processes, including cell proliferation, differentiation, migration and metabolism (Lemmon and Schlessinger, 2010, Diwanji et al., 2019). The catalytic activity of these receptors is tightly controlled by several auto-inhibitory mechanisms, which prevent unwanted signalling (Hubbard, 2002, Du and Lovly, 2018). In general, receptor dimerisation or oligomerisation upon ligand binding juxtaposes the cytoplasmic tyrosine kinase domains, facilitating *trans*-phosphorylation of tyrosine residues located in the juxtamembrane region and activation loop to release the autoinhibition (Hubbard and Miller, 2007, Maruyama, 2014).

The kinase activation loop acts as a main autoinhibitory motif that has been first characterised by the structural study of InsR (Hubbard et al., 1994). The InsR kinase contains three tyrosine residues on the activation loop, with the key one, Tyr1162, positioned in the kinase active site and forming hydrogen bonds with neighbouring arginine and aspartic acid residues in the catalytic loop. Those interactions maintain the activation loop in a DFG-OUT conformation to block ATP binding, which prevents *cis*-autophosphorylation. This autoinhibition is released upon *trans*-phosphorylation of the activation loop, resulting in a conformation that coordinates ATP and permits substrate binding (Hubbard et al., 1994, Hubbard, 1997). DDR2 kinase is highly homologous to the kinase domain of the InsR, and the highly conserved activation loop tyrosine residue Tyr740 (Tyr796 in DDR1) was found to inhibit DDR2 *cis*-autophosphorylation (Yang et al., 2005). Structural analysis of DDR1 kinase revealed that the Tyr796 adopts a conserved pseudosubstrate position and forms a hydrogen bond with the catalytic loop Asp766 (Canning et al., 2014, Sammon et al., 2020). Phosphorylation or mutation of this key tyrosine is considered to free the activation loop, which then adopts the 'active' configuration (Yang et al., 2005, Iwai et al., 2013b). The αC-helix located in the kinase N-lobe also reorients, enabling the conserved Glu residue (Glu625 in DDR2) to interact with the Lys residue (Lys608 in DDR2) in the β3-strand, which then stabilises ATP binding (Hubbard, 1997, Knighton et al., 1991).

Apart from the tyrosine kinase domain that is directly responsible for RTK catalytic activity, RTK activity can be regulated by structural elements outside the kinase domain. For instance, the JM region of some RTKs can act as an autoinhibitory element through a variety of mechanisms (Mori et al., 1993, Baxter et al., 1998, Binns et al., 2000). For DDR1, the last quarter of the intracellular JM segment (residues 566 to 591), located closest to the kinase domain, was found deeply inserted into the kinase active site in inactive DDR1, which reinforced the autoinhibition of the activation loop (Sammon et al., 2020). This important JM segment, named JM4, is very highly conserved between DDR1 and DDR2, indicating a similar activation mechanism involving the JM4 segment for both DDR1 and DDR2 in kinase autoinhibition (**Figure 3. 1**). In contrast to JM4, the other JM segments are much less well conserved between DDR1 and DDR2.

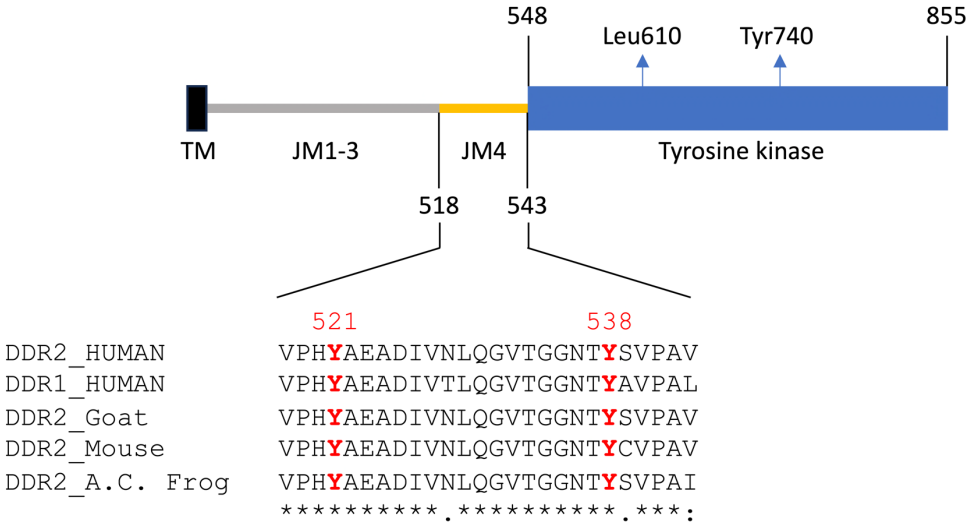


Figure 3. 1 The JM4 region is highly conserved.
Top, the DDR2 cytosolic region (amino acid 400 to 855) is shown as a schematic diagram with amino acid boundaries of the JM4 and the kinase indicated. TM, transmembrane domain.
Bottom, sequence alignment of the human DDR2 (UniprotKB Q16832) JM4 region. Alignment (Clustal Omega) was performed with paralog human DDR1 (Q08345) and DDR2 sequences from other species. Goat; *Capra hircus* (A0A452FL91). Mouse; *Mus musculus* (Q62371). African clawed (A.C.) frog; *Xenopus laevis* (A0A1L8GGW0). '*' (asterisk); fully conserved residue. ':' (colon); conserved substitutions. '.' (period); less well conserved substitution.

Point mutations in the cytoplasmic domain of RTKs can lead to constitutive receptor activity, which is the underlying cause of numerous diseases. For example, hypochondroplasia-associated gain-of function mutation Asn540Lys in the FGFR3 kinase domain results in increased receptor phosphorylation and substrate phosphorylation (Bellus et al., 1995). This mutation leads to a release of the restriction on the N-lobe movement and provides an optimal position of the DFG motif (Mohammadi et al., 1996, Hubbard, 2002). Point mutation

Val665Ala on the kinase domain of PDGFRB leads to ligand-independent receptor activity, which has been reported to be responsible for the Penttinen syndrome (Johnston et al., 2015). Patients with Penttinen syndrome suffer from a series of premature ageing and skin-related symptoms similar to what has been described in the Warburg Cinotti syndrome cases (Warburg et al., 2006, Cinotti et al., 2013, Xu et al., 2018, Johnston et al., 2015, Aggarwal et al., 2022). In a recent report, Xu et al. performed exome sequencing for the Warburg Cinotti syndrome patient samples and discovered two gain-of-function mutations, Leu610Pro and Tyr740Cys, located on the DDR2 kinase domain, which are thought to be disease-causing mutations (Xu et al., 2018). Limited protein and biochemical studies were included in the report. Therefore, more evidence of how these two mutants would affect the DDR2 kinase catalytic activity is required, in order to get a deeper mechanistic understanding.

In this chapter, the hypothesis to be addressed was that the Warburg Cinotti syndrome related DDR2 mutants (Leu610Pro and Tyr740Cys) have higher intrinsic kinase activity than WT DDR2 kinase and result in constitutive activation of the receptor. The aims were: (1) to obtain the soluble DDR2 kinase constructs; (2) to determine the catalytic parameters of WT and mutant DDR2 kinases; (3) to analyse the mutant DDR2 activities in the presence and absence of collagen stimulation; (4) to establish whether commercial kinase inhibitors block the mutant DDR2 kinase activities.

3.2 Results

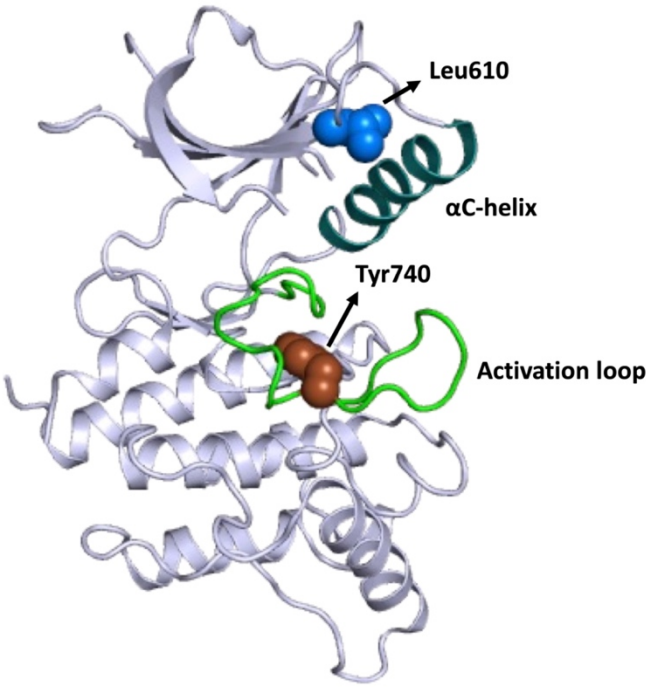
3.2.1 Locations of Warburg Cinotti mutants on DDR2 kinase domain

The Warburg Cinotti syndrome related missense variants affect highly conserved residues (Leu610, Tyr740) located on the DDR2 tyrosine kinase domain (**Figure 3. 2A**). Only one experimentally determined DDR2 kinase structure is available in the Protein Data Bank (PDB, code: 7AYM), and this structure solved the DDR2 kinase region only, without the JM4 region (Nawrotek, 2020). The locations of DDR2-L610 and DDR2-Y740 are shown in **Figure 3. 2B**. The structural analysis was conducted with the help of Dr Alessia David, Imperial College London. Leu610 locates close to the conserved Lys608 of the β3 strand that forms a salt bridge with αC-helix residue Glu625 in the active kinase conformation. The leucine to proline mutation is predicted to be structurally damaging and to affect the correct folding on the kinase N-lobe (**Figure 3. 3A**). This mutation affects the folding stability of the domain, and the predicted change in folding energy is ΔΔG- 3 Kcal (ELASPIC prediction tool: http://elaspic.kimlab.org/). Misfolding of the mutant protein could lead to early degradation (Goldberg, 2003). However, if the mutant protein is produced, the insertion of a proline at this position may affect the positioning of the αC-helix relative to the activation loop and the rest of the N-lobe. Tyr740 is the key tyrosine residue located on the activation loop (**Figure 3. 2B**), which contributes to kinase autoinhibition (Yang et al., 2005). It forms hydrogen bond interactions with Asp710 and Arg714 to maintain the activation loop position (**Figure 3. 3B**). Substitution to cysteine abolishes these hydrogen bonds, thus likely affecting the conformation of the activation loop. Both substitutions are predicted to be damaging evolutionarily by sequence-based tools (SIFT tool: https://sift.bii.a-star.edu.sg/; CADD tool: https://cadd.gs.washington.edu/snv) (SIFT score =0, CADD score =31 for L610P; SIFT score =0, CADD score =30 for Y740C).

A

```
                          610                                 740
DDR2_Human          VAVKMLRADANKNARNDFLKEIK---SRNLYSGDYYRIQGR
DDR1_Human          VAVKILRPDATKNARNDFLKEVK---SRNLYAGDYYRVQGR
DDR2_Goat           VAVKMLRADANKNARNDFLKEIK---SRNLYSGDYYRIQGR
DDR2_Mouse          VAVKMLRADANKNARNDFLKEIK---SRNLYSGDYYRIQGR
DDR2_A.C. Frog      VAVKMLRADANKNARNDFLKEIK---SRNLYSGDYYRIQGR
DDR2_Electric Eel   VAVKMLRADANKNARNDFLKEIK---SRNLYSGDYYRIQGR
DDR2_Fruit Fly      VAVATLRPGANDHLRKEFRSKAK---NRSAYASDYCQLEGF
                    ***  ** .*..: *::* .: *   .*. *:.** :::*
```

B



PDB code: 7AYM

Figure 3. 2 Warburg Cinotti syndrome affected DDR2 amino acid conservation and location.
A. Sequence showing Warburg Cinotti syndrome related human DDR2 (UniprotKB Q16832) kinase region. Alignment (Clustal Omega) was performed with paralog human DDR1 (Q08345) and DDR2 sequences from other species. Goat; *Capra hircus* (A0A452FL91). Mouse; *Mus musculus* (Q62371). African clawed (A.C.) frog; *Xenopus laevis* (A0A1L8GGW0). Electric eel; *Electrophorus electricus* (A0A4W4EQ84). Fruit fly; *Drosophila melanogaster* (Q59DZ7). '*' (asterisk); fully conserved residue. ':' (colon); conserved substitutions. '.' (period); less well conserved substitution.
B. Crystal structure of DDR2 kinase domain. Figure generated with PyMOL using PDB code 7AYM. The activation loop is shown in green. The αC-helix is shown in cyan and labelled with 'αC'. Residues that are mutated in Warburg Cinotti Syndrome, are labelled as 'Leu610' and 'Tyr740', with Leu610 in blue located before the αC-helix and Tyr740 in brown on the activation loop.

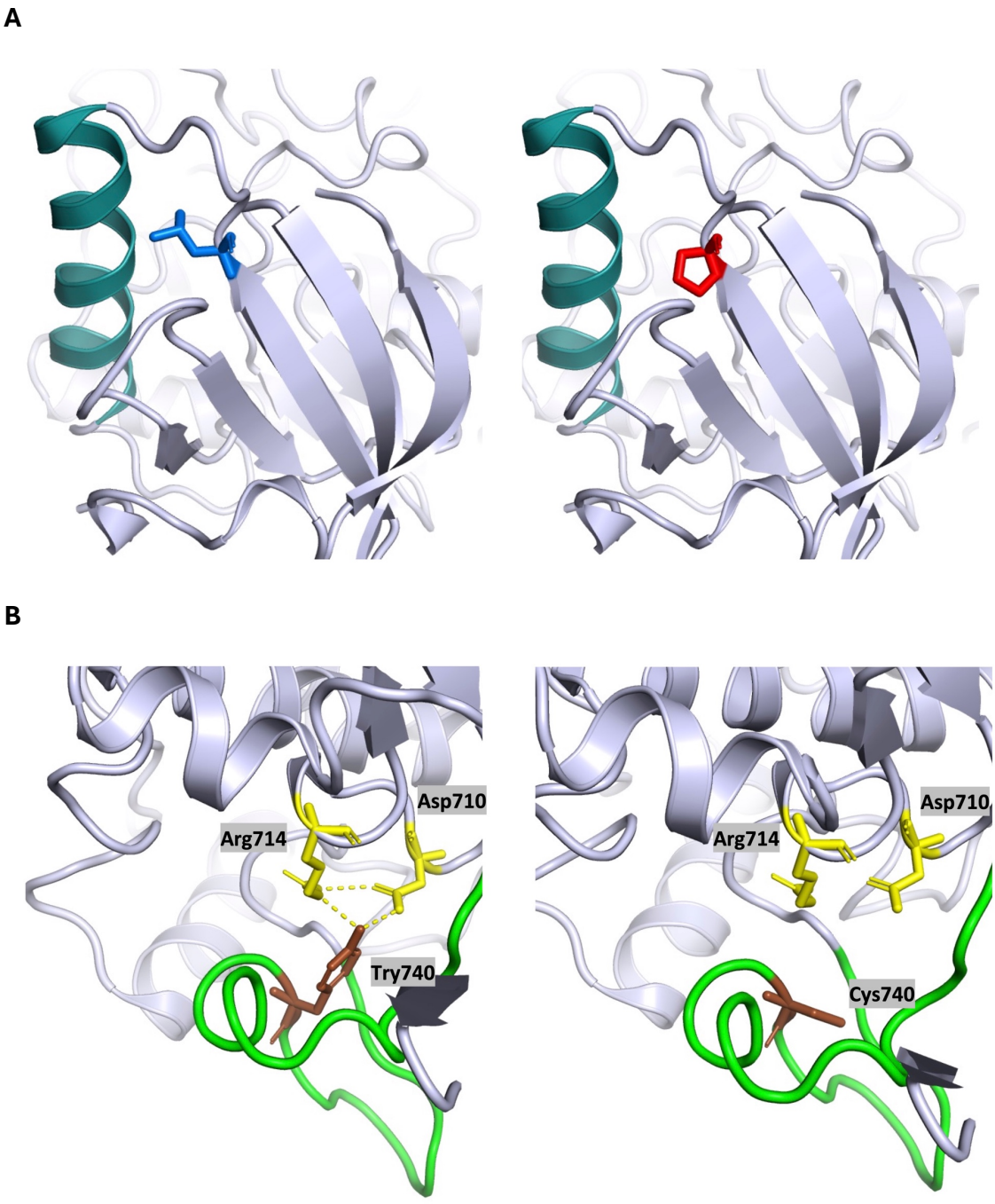


Figure 3. 3 Warburg Cinotti syndrome variants are predicted to be damaging by structural analysis.
A. p.L610P mapped on experimental structure 7AYM. The αC-helix is shown in cyan. Leu610 is presented in blue on the left and pro610 in red on the right.
B. Left: WT Tyr740 (in brown) forms hydrogen bonds with Asp710 and Arg714 (both in yellow). The activation loop is presented in green. Right: Hydrogen bonds are destroyed due to the substitution with Cys740.

3.2.2 Production of recombinant soluble DDR2 kinase

A recent study defined the kinetic parameters of DDR1 kinase (Sammon et al., 2020); however, similar information for DDR2 is still lacking. To investigate the catalytic activities of both DDR2 WT and mutant kinases, several recombinant DDR2 constructs were designed for *in vitro* studies. Previous studies from our lab showed a production difficulty for soluble cytosolic DDR1 constructs via several bacterial expression systems (B Leitinger lab, unpublished), which was later overcome by generating the soluble DDR1 kinase protein from baculovirus-infected Sf9 cells (Sammon et al., 2020). Thus, all soluble DDR2 proteins were obtained using the same baculovirus expression system. The constructs generated were: DDR2-WT-K, DDR2-Y740C-K and DDR2-L610P-K. These expression constructs (DDR2 residues 518-855) contained either the WT or mutant DDR2 kinase together with the highly conserved JM4 segment.

The cDNAs encoding DDR2 intracellular JM4 region as well as the kinase domain (**Figure 3. 1**) were first cloned into the pOPINF vector using In-Fusion cloning method (**Figure 3. 4A, B**). The pOPINF vector contains sequences encoding a His_6-tag, a HRV 3C cleavage site, and the baculovirus ORF1629 gene (**Figure 2. 2**). The pOPINF constructs were co-transfected with linearised ORF1629-deficient bacmid into Sf9 cells for baculovirus production. The P_0 virus successfully replicated as the bacmid function was restored by recombination with the ORF1629-containing pOPINF constructs (Zhao et al., 2003). Following P_0 virus production, it was used for P_1 virus amplification and protein expression was assessed as shown in **Figure 3. 4C**. 10 or 100 µL of the P_1 virus suspension was used to infect 10 mL of the Sf9 cells. During the incubation, 1 mL of the infected Sf9 cells was taken on day 2, day 3 and day 4 for small-scale protein purification. His_6-tagged DDR2 proteins were extracted from the cells and subsequently pulled down using Ni-NTA beads. Non-specific protein binding was removed by washing the beads in buffer containing low concentration of imidazole. Protein/beads were then boiled in sample buffer and analysed on SDS-PAGE with Coomassie staining. Both DDR2-WT-K and DDR2-Y740C-K showed clearly visible protein bands on all incubation days (**Figure 3. 4C**). However, there were no expected bands observed for DDR2-L610P-K.

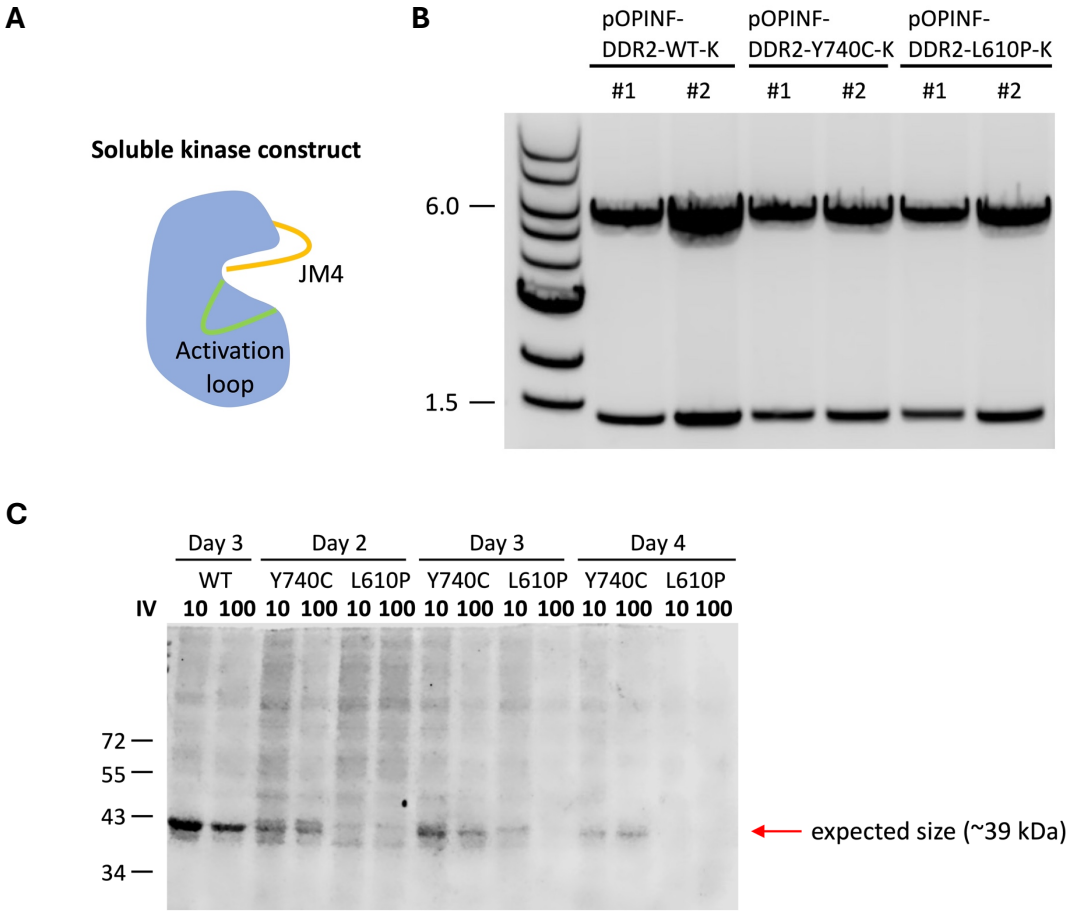


Figure 3. 4 Generation of soluble recombinant DDR2 kinase constructs.
A. Schematic diagram showing the recombinant DDR2 construct consisting of the JM4 region (in yellow) and the kinase domain (in blue, with the activation loop shown green). **B.** Analytical digestion of the pOPINF constructs. PCR reactions were performed to amplify the sequences encoding DDR2 JM4 and kinase domain (DDR2-K constrcuts). The PCR products were then cloned into the pOPINF vector. DNA Minipreps were generated and verified by analytical digestion. All pOPINF constructs were digested with *XbaI* and analysed on 0.8% agarose gel. The expected band sizes for DDR2 inserts (coding for residue 518-855) are ~1.4 kb and ~4.8 kb for the pOPINF vector. DNA sequences were verified by Sanger sequencing.
C. Expression test to verify soluble DDR2-K construct production. His_6-tagged DDR2 proteins were extracted from the P_1 virus infected Sf9 cells and purified using Ni-NTA beads. Purified proteins were then boiled in sample buffer and analysed by SDS-PAGE with Coomassie staining. The positions of molecular weight markers (in kDa) are shown on the left. Recombinant DDR2 proteins were found with the size around 39 kDa (red arrow). IV, infection volume (in µL).

Since DDR2-WT-K and DDR2-Y740C-K bands were observed, P_2 virus for DDR2-WT-K and DDR2-Y740C-K were amplified and used for large-scale protein production. 1 L of Sf9 cells were infected with 10 µL virus per mL of cells for 3 days. Cells were then harvested and lysed, followed by centrifugation and subsequent filtration to remove cell debris. Clear lysates were loaded onto a HisTrap HP column which was then washed to remove low affinity protein interactions (**Figure 3. 5A, Figure 3. 6A**). His_6-tagged proteins were then eluted with buffer containing 500 mM imidazole. Protein fractions were analysed on SDS-PAGE with Coomassie

staining (**Figure 3. 5B, Figure 3. 6B**), showing production of the soluble DDR2 proteins with expected size around 40 kDa. The fractions containing DDR2-WT-K or DDR2-Y740C-K were then combined and dialysed overnight, and the His_6-tag was cleaved with C3 protease during dialysis. After C3 cleavage, the proteins without His_6-tag were then loaded again onto the HisTrap HP column, with the flow-through containing soluble DDR2 proteins collected (**Figure 3. 5C, Figure 3. 6C**). This process was named reverse His-Trap purification, with any non-cleaved material remaining on the HisTrap column. Contaminating proteins were eluted from the column as fractions. Both fractions and flow-through were checked on SDS-PAGE, with the proteins with the expected molecular weight seen from the flow-through samples (**Figure 3. 5D, Figure 3. 6D**). In the final purification step, the flow-through of the reverse His-Trap was concentrated and purified by gel filtration. Pure DDR2 proteins were eluted with a sharp peak presented in the chromatography diagrams (**Figure 3. 5E, Figure 3. 6E**). The fractions containing proteins with expected size (**Figure 3. 5F, Figure 3. 6F**) were combined and concentrated, followed by aliquoting and snap-freezing in liquid nitrogen.

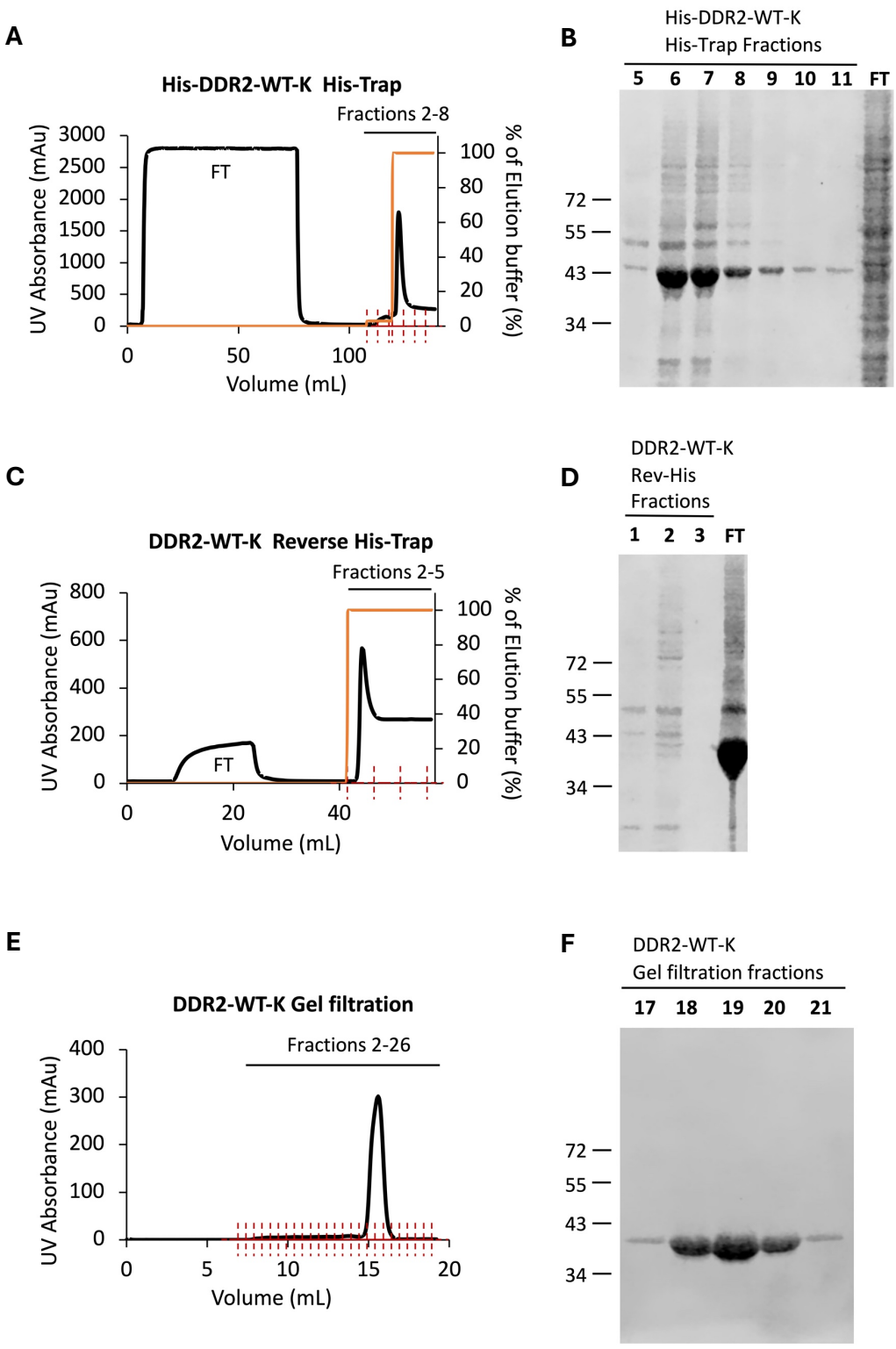


Figure 3. 5 Large-scale purification of soluble recombinant DDR2-WT-K.
Cell lysates were loaded onto a HisTrap HP column on an ÄKTA pure system.
A. The His-Trap chromatogram is shown with UV absorbance (A_{280}, mAU) in black and conductance (mS/cm) in orange. The column was washed until the UV reading reached the baseline.
Proteins were eluted with buffer containing 500 mM imidazole.
B. Aliquots of His-Trap fractions (5-11 in **A.**) and purification flowthrough were boiled in sample buffer and analysed on 10% SDS-PAGE with Coomassie staining.
Continued on the next page.

Figure 3.5. continued
C. The reverse His-Trap purification was performed with cleaved His-Trap purified proteins. The chromatogram is shown with UV absorbance (A_{280}, mAU) in black and conductance (mS/cm) in orange. The recombinant DDR2-WT-K protein was collected from the flowthrough. Contaminant proteins that bound to the column were eluted with buffer containing 500 mM imidazole.
D. Aliquots of reverse His-Trap fractions (1-3 in **C.**) and purification flowthrough were boiled in sample buffer and analysed on 10% SDS-PAGE with Coomassie staining.
E. Gel filtration (size exclusion chromatography) was performed with the reverse His-Trap purified protein. Chromatogram from gel filtration is shown with UV absorbance (A_{280}, mAU) in black.
F. Aliquots of gel filtration fractions (17-21 in **E.**) were boiled in sample buffer and analysed on 10% SDS-PAGE with Coomassie staining. The position of molecular weight markers (in kDa) are shown on the left. Recombinant DDR2-WT-K protein was found with the size around 39 kDa. FT, flowthrough.

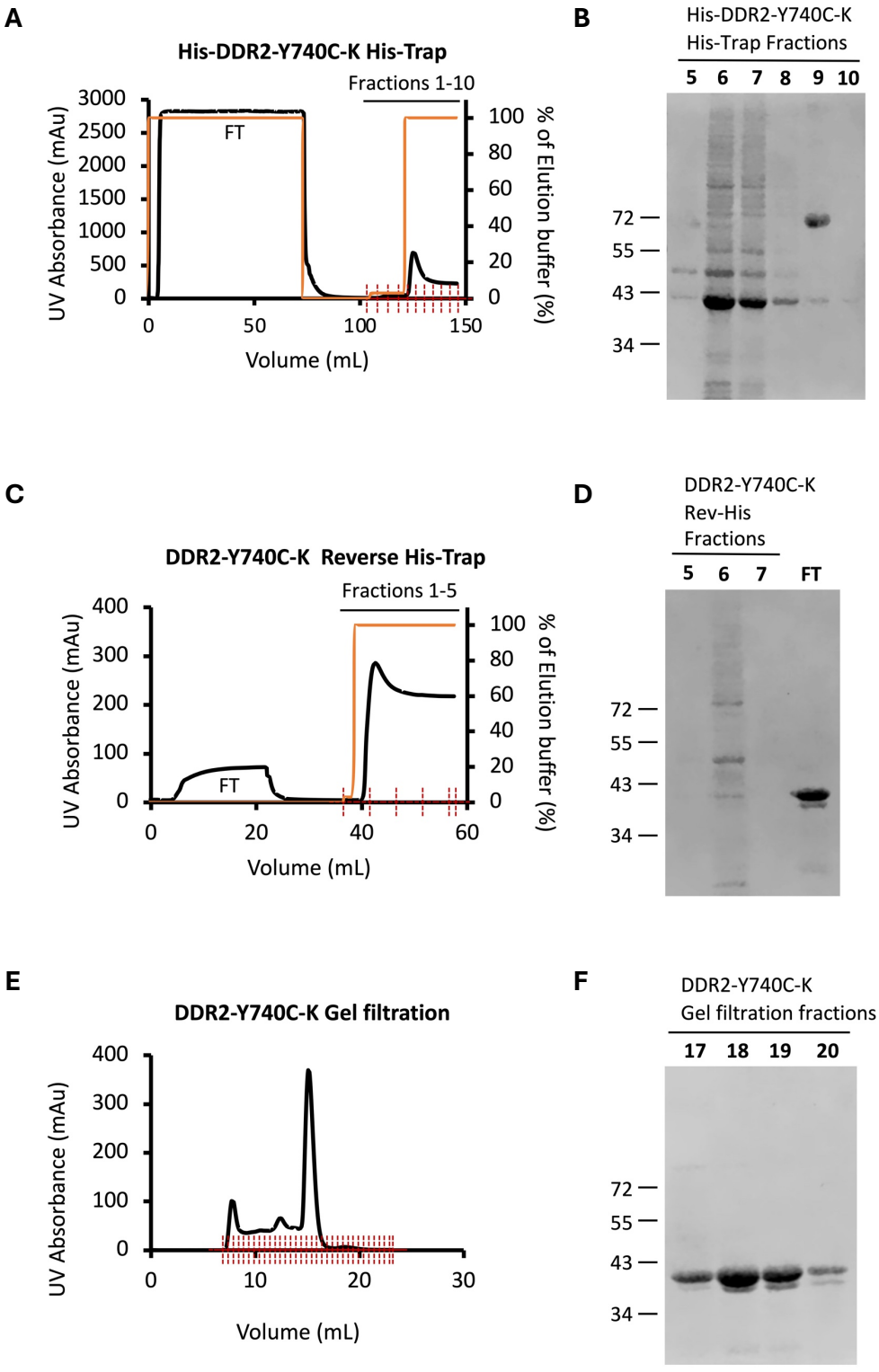


Figure 3. 6 Large-scale purification of soluble recombinant DDR2-Y740C-K.
Cell lysates were loaded onto HisTrap HP column on an ÄKTA pure system.
A. The His-Trap chromatogram is shown with UV absorbance (A_{280}, mAU) in black and conductance (mS/cm) in orange. The column was washed until the UV reading reached the baseline. Proteins were eluted with buffer containing 500 mM imidazole.
B. Aliquots of His-Trap fractions (5-10 in **A.**) and purification flowthrough were boiled in sample buffer and analysed on 10% SDS-PAGE with Coomassie staining.
Continued on the next page.

Figure 3.6. continued
C. The reverse His-Trap purification was performed with cleaved His-Trap purified proteins. The chromatogram is shown with UV absorbance (A_{280}, mAU) in black and conductance (mS/cm) in orange. The recombinant DDR2-Y740C-K protein was collected from the flowthrough. Contaminant proteins that bound to the column were eluted with buffer containing 500 mM imidazole.
D. Aliquots of reverse His-Trap fractions (5-7 in **C.**) and purification flowthrough were boiled in sample buffer and analysed on 10% SDS-PAGE with Coomassie staining.
E. Gel filtration (size exclusion chromatography) was performed with the reverse His-Trap purified protein. Chromatogram from gel filtration is shown with UV absorbance (A_{280}, mAU) in black.
F. Aliquots of gel filtration fractions (17-20 in **E.**) were boiled in sample buffer and analysed on 10% SDS-PAGE with Coomassie staining. The position of molecular weight markers (in kDa) are shown on the left. Recombinant DDR2-Y740C-K protein was found with the size around 39 kDa. FT, flowthrough.

3.2.3 Recombinant DDR2-L610P-K protein is unstable

The absence of soluble DDR2-L610P-K protein production from the initial expression test (**Figure 3. 4C**) brought us to the question of whether the protein was unable to be generated in Sf9 cells or was lost during the Ni-NTA purification. Cell pellets containing insoluble cellular materials and aliquots of the first wash fraction from the Ni-NTA purification were analysed together with the Ni-NTA purified samples on SDS-PAGE followed by Coomassie staining. Strong bands with the expected size of DDR2-L610P-K were found in cell pellet samples (**Figure 3. 7A**), indicating the insolubility of the DDR2-L610P-K protein with the current expression system or lysis conditions. In an attempt to rescue the proteins from the insoluble fractions, adjustments of lysis pre-treatment as well as different buffer compositions were applied. Infected Sf9 cells were either frozen for 1 hour or immediately lysed in a variety of lysis buffers aiming to reduce protein aggregation (**Figure 3. 7B, C**). However, none of the approaches led to an increase in DDR2-L610P-K solubility, as the protein was still only found in the insoluble pellet fractions.

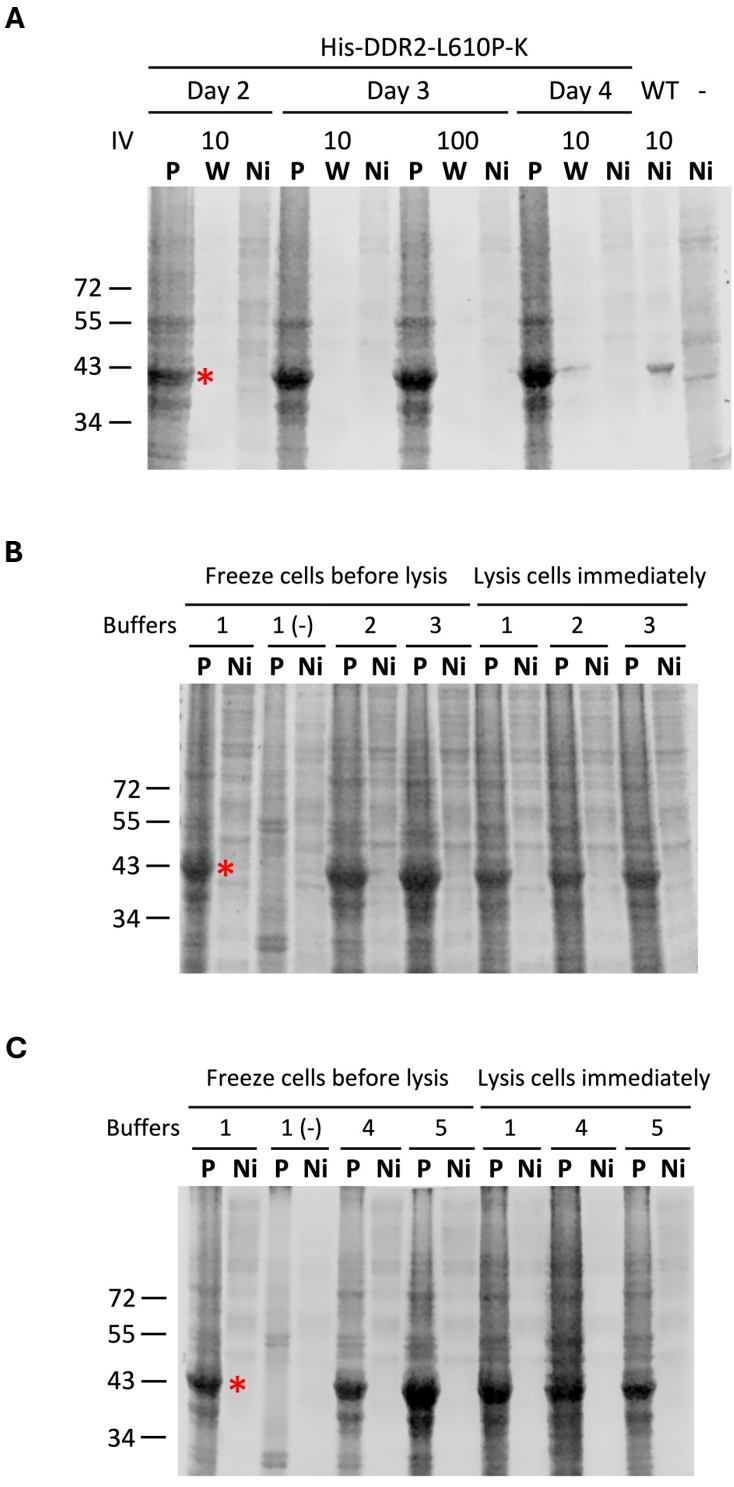


Figure 3. 7 Recombinant DDR2-L610P-K is insoluble when expressed in Sf9 cells.
A. Expression test to verify His-DDR2-L610P-K construct production. Protein was extracted from the P_1 infected Sf9 cells and purified using Ni-NTA beads. The cell pellets (sonicated), aliquots of the first wash during protein purification, and the purified proteins were boiled in sample buffer and analysed by SDS-PAGE with Coomassie staining. The protein purified from DDR2-WT-K P_1 virus infected Sf9 cells was included as a positive control. The protein purified from non-infected Sf9 cells was included as a negative control (-).
B. C. To increase the recombinant protein solubility, different approaches were applied during the Ni-NTA purification. The cells were either frozen before lysis or lysed immediately in a variety of lysis buffers.
Continued on the next page.

Figure 3.7. continued.
The cell pellets (sonicated) and the purified proteins were boiled in sample buffer and analysed by SDS-PAGE with Coomassie staining. The protein purified from non-infected Sf9 cells was included as a negative control (-). The positions of molecular weight markers (in kDa) are shown on the left. Bands with expected size of recombinant His-DDR2-L610P-K protein are indicated with a red asterisk (*). P, cell pellet; W, first wash; Ni, Ni-NTA purified protein.

The usage of fusion tags in recombinant protein production has the well-known advantages of increasing protein stability and solubility (Esposito and Chatterjee, 2006). Therefore, pOPIN-vectors with additional tags were used to generate the recombinant DDR2-L610P-K protein. DDR2-WT-K was also cloned into the same pOPIN vectors as positive controls. The fusion tag-encoding sequence was located in between the His_6-tag and the HRV C3 cleavage site (**Figure 2. 2**), enabling the cleavage after the first His-Trap purification. The new constructs were expressed in the same way as described before. P_1 virus passages were used to assess protein expressions, which was performed by analysing the cell pellet fractions and Ni-NTA purified products together on SDS-PAGE with Coomassie staining (**Figure 3. 8, Figure 3. 9**). Proteins with expected size were observed only in the insoluble pellet fractions for both GST-tagged and SUMO-tagged constructs (**Figure 3. 8**), whereas MBP-tagged DDR2-L610P-K showed a detectable level of soluble protein production (**Figure 3. 9, day 3 samples**). However, the bands detected for soluble and insoluble MBP-tagged DDR2-L610P-K were still much weaker than those detected for the corresponding DDR2-WT-K constructs. Since some soluble protein was detected in the MBP-tagged DDR2-L610P-K expression test, the large scale protein production was attempted. To this end, the P_2 virus for MBP-tagged DDR2-L610P-K was amplified and used for large-scale protein production. The same cell lysis and filtration methods were used as described before. His-Trap purification was performed with the protein eluted into fractions (**Figure 3. 10A**). Dialysis was then performed with the eluted His-Trap fractions pooled together and incubated with or without C3 protease. However, precipitates were observed from both of the dialysed samples the following morning, indicating the cleavage by C3 protease was not the reason of protein precipitation. The dialysed sample with precipitates was centrifuged to obtain the supernatant for reverse His-Trap purification (**Figure 3. 10C**), in case the precipitated material was not related to DDR2-L610P-K. The precipitates were boiled with sample buffer and analysed together with the aliquots of His-Trap fraction samples on SDS-PAGE. Unfortunately, a clear band with the expected size (around 80 kDa) was found in the precipitate sample, indicating a loss of soluble DDR2-L610P-

K protein (**Figure 3. 10B**). Analysis of the flowthrough from the reverse His-trap purification showed no protein with the expected molecular weight found for DDR2-L610P-K, which confirmed the loss of soluble DDR2-L610P-K during overnight dialysis. (**Figure 3. 10D**). To this point, we concluded that the recombinant DDR2-L610P-K protein obtained from the baculovirus expression system was unstable and could therefore not be obtained and used for the following *in vitro* kinase assays.

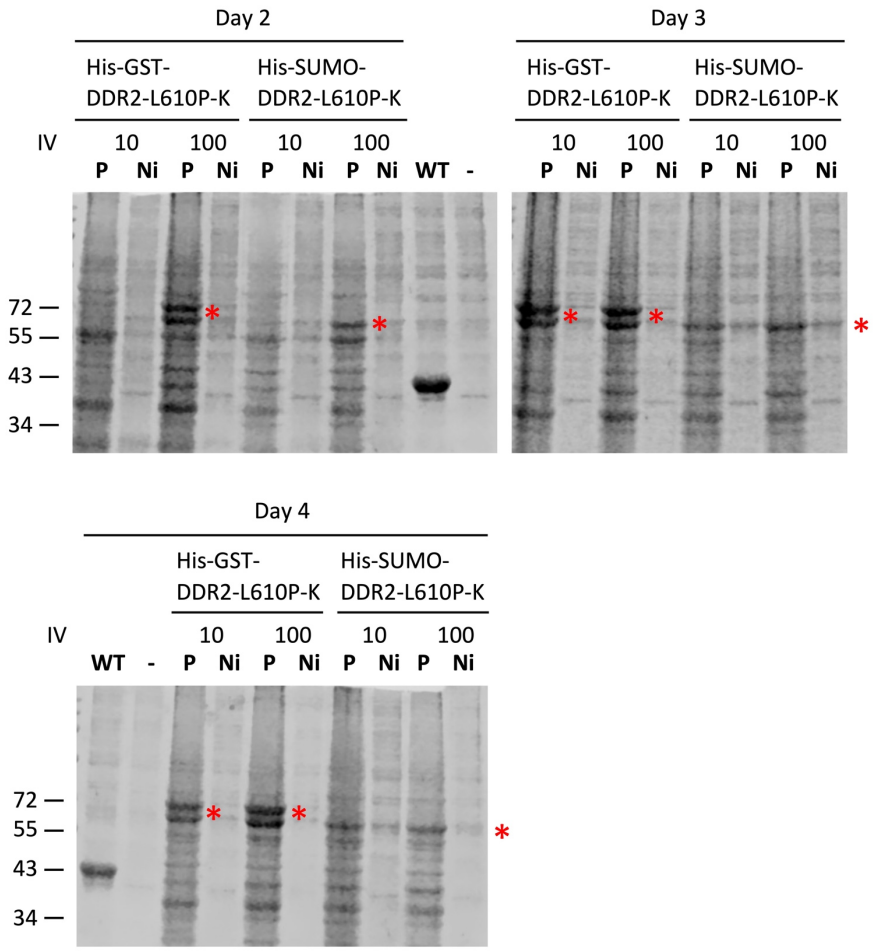


Figure 3. 8 Expression test for GST-tagged and SUMO-tagged DDR2-L610P-K generated in Sf9 cells.
Expression test to verify soluble His-GST-DDR2-L610P-K and His-SUMO-DDR2-L610P-K construct production. Proteins were extracted from the P_1 virus infected Sf9 cells and purified using Ni-NTA beads. The cell pellets (sonicated) and the purified proteins were boiled in sample buffer and analysed by SDS-PAGE with Coomassie staining. The protein purified from DDR2-WT-K P_1 virus infected Sf9 cells was included as a positive control. The positions of molecular weight markers (in kDa) are shown on the left. Bands with expected size of recombinant His-GST-DDR2-L610P-K or His-SUMO-DDR2-L610P-K protein are indicated with a red asterisk (*). IV, infection volume (in µL); P, cell pellet; Ni, Ni-NTA purified protein.

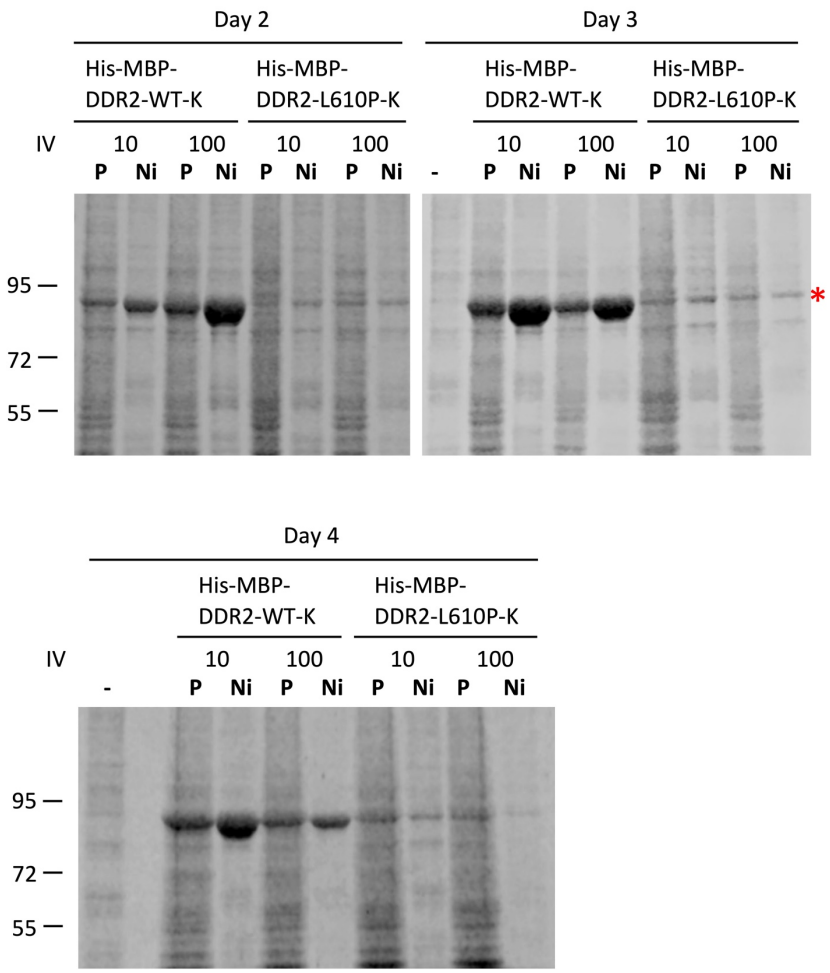


Figure 3. 9 Expression test for MBP-tagged DDR2-L610P-K generated in Sf9 cells.
Expression test to verify soluble His-MBP-DDR2-WT-K and His-MBP-DDR2-L610P-K construct production. Proteins were extracted from the P_1 virus infected Sf9 cells and purified using Ni-NTA beads. The cell pellets (sonicated) and the purified proteins were boiled in sample buffer and analysed by SDS-PAGE with Coomassie staining. The protein purified from non-infected Sf9 cells was included as a negative control (-). The positions of molecular weight markers (in kDa) are shown on the left. Bands with expected size of recombinant His-MBP-DDR2-L610P-K protein are indicated with a red asterisk (*). IV, infection volume (in µL); P, cell pellet; Ni, Ni-NTA purified protein.

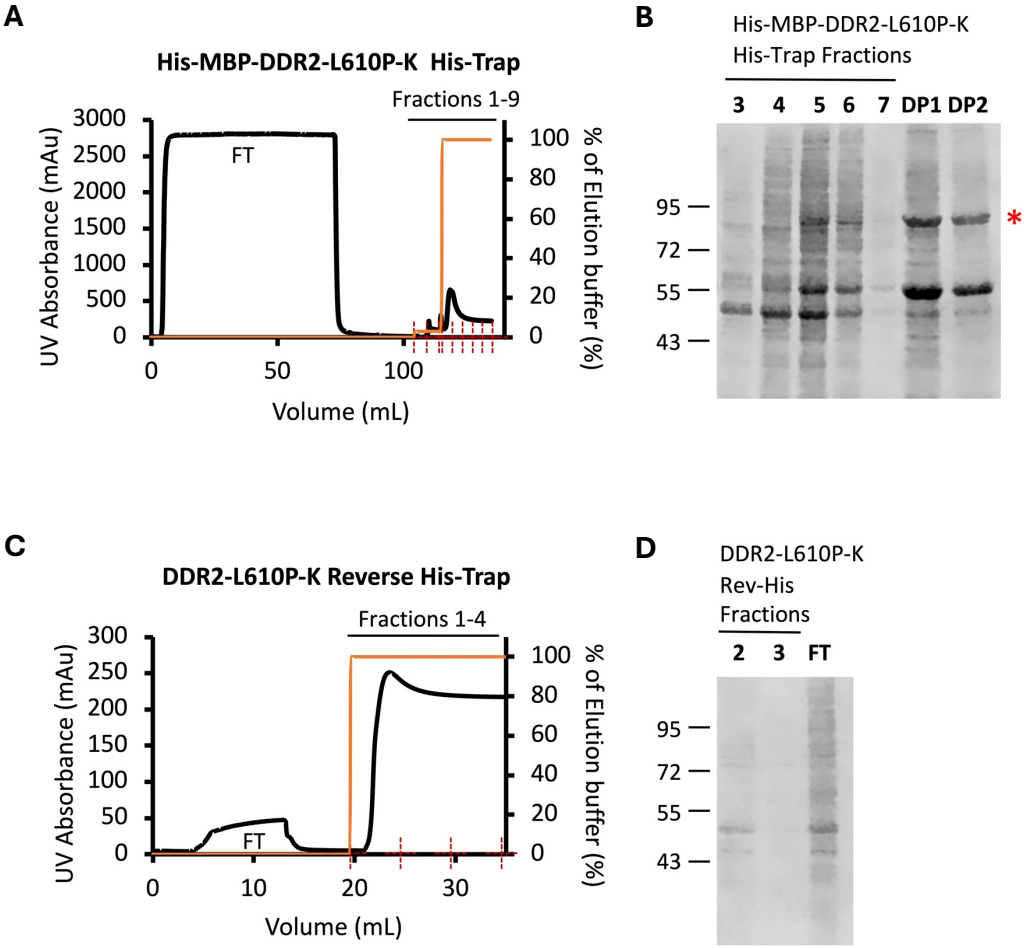


Figure 3. 10 Large-scale purification of soluble recombinant DDR2-L610P-K.
Cell lysates were loaded onto HisTrap HP column on an ÄKTA pure system.
A. The His-Trap chromatogram is shown with UV absorbance (A_{280}, mAU) in black and conductance (mS/cm) in orange. The column was washed until the UV reading reached the baseline. Proteins were eluted with buffer containing 500 mM imidazole.
B. His-Trap purified proteins were dialysed overnight with or without C3 protease. Precipitates were found in both dialysed samples. Aliquots of His-Trap fractions (3-7 in **A.**) and dialysis precipitates (DP1 for precipitates collected from dialysis samples with C3 protease cleavage, DP2 for precipitates collected from dialysis samples without C3 protease incubation) were boiled in sample buffer and analysed on 10% SDS-PAGE with Coomassie staining.
C. The reverse His-Trap purification was performed with cleaved His-Trap purified proteins. The chromatogram is shown with UV absorbance (A_{280}, mAU) in black and conductance (mS/cm) in orange.
D. Aliquots of reverse His-Trap fractions (2-3 in **C.**) and purification flowthrough were boiled in sample buffer and analysed on 10% SDS-PAGE with Coomassie staining. The positions of molecular weight markers (in kDa) are shown on the left. Bands with expected size of recombinant His-MBP-DDR2-L610P-K protein are indicated with a red asterisk (*). FT, flowthrough; DP, dialysis precipitates.

In the hope that using a mammalian cell expression system can help obtain small-scale soluble DDR2-L610P-K protein for simple *in vitro* assays, all pOPIN constructs generated before were transfected into HEK293 cells, followed by protein extraction and purification. His_6-tagged proteins were isolated from the cell lysates with cobalt-based immobilised metal affinity chromatography (IMAC) Dynabeads. As before, cell pellet samples, purification flowthrough and purified materials were analysed on SDS-PAGE followed by Western blotting. Similarly, most of the His_6-tagged DDR2-L610P-K protein was found from the insoluble pellet fraction, but both His_6-tagged DDR2-WT-K and DDR2-Y740C-K showed clearly visible soluble protein production (**Figure 3. 11A**). GST-tagged DDR2-L610P-K exhibited minor soluble protein production (**Figure 3. 11A**), whereas greater soluble levels were observed from both SUMO and MBP-tagged DDR2-L610P-K proteins, with the highest soluble protein production seen from SUMO-tagged DDR2-L610P-K (**Figure 3. 11B**). SUMO-tagged DDR2-WT-K construct was then made as a control for the use in *in vitro* kinase assays. Again, the SUMO-tagged constructs as well as the His_6-tagged DDR2-WT-K and DDR2-Y740C-K were individually expressed in HEK293 cells followed by cell lysis and protein purification with IMAC Dynabeads as described above to obtain the purified soluble recombinant proteins for further analysis. To assess the ability of the mutant and WT constructs to carry out autophosphorylation, these small-scale purified proteins, still bound to the Dynabeads, were stimulated by ATP and analysed by Western blotting with phospho-tyrosine (pY) specific antibodies (**Figure 3. 12**). Clear *in vitro* phosphorylation of His-tagged and SUMO-tagged DDR2-WT-K was observed for both JM4 phosphorylation (anti-pY521 blot) and activation loop phosphorylation (anti-pY740 blot). For His-tagged DDR2-Y740C-K, only JM4 phosphorylation was detected, but the activation loop phosphorylation signal was missing. The DDR2-Y740C protein has no Y740 available for phosphorylation; therefore, it is not surprising that no phosphorylation was detected with anti-pY740 antibody. However, this antibody cross-reacts with other activation loop tyrosines (Y736, Y741), and higher concentrations of DDR2-Y740C-K on blots show anti-pY740 signals (see **Figure 3.16**). For the SUMO-tagged DDR2-L610P-K, only minimal phosphorylation of JM4 tyrosine Y521 was seen and no phosphorylation observed on the activation loop (**Figure 3. 12**). This indicates a loss of kinase functions of this particular recombinant DDR2-L610P-K construct. Taken together, the recombinant DDR2-L610P-K protein was unstable, with a loss of kinase function, in agreement with the structural analysis which predicted the reduced protein folding stability (**Section 3.2.1**).

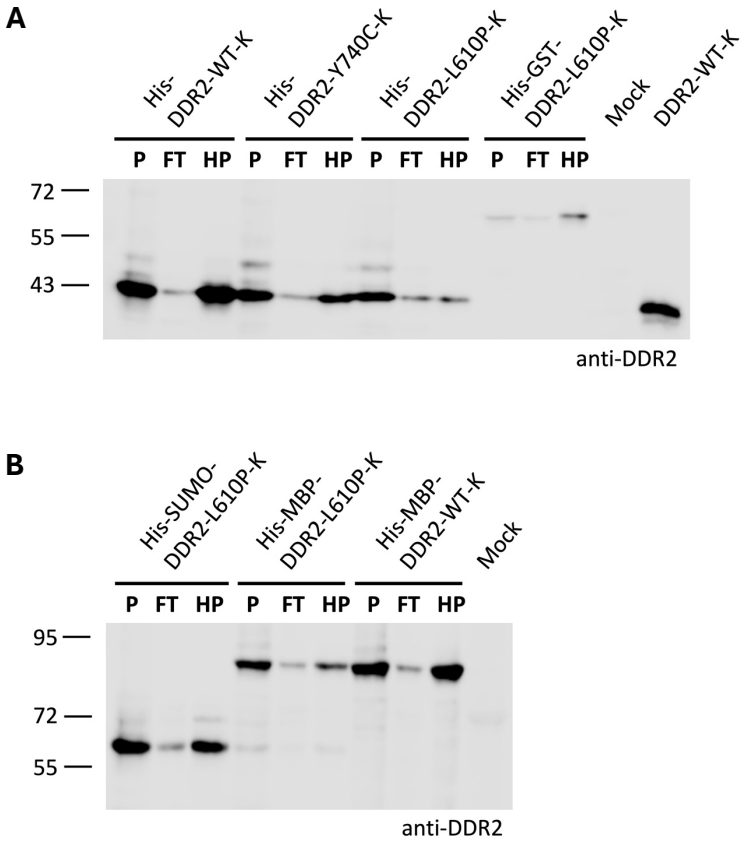


Figure 3. 11 Expression test for fusion-tagged DDR2-L610P-K in mammalian cells.
A. B. Constructs encoding His-tagged DDR2-WT-K, His-tagged DDR2-Y740C-K, His-tagged DDR2-L610P-K, GST-tagged DDR2-L610P-K, SUMO-tagged DDR2-L610P-K, MBP-tagged DDR2-WT-K and MBP-tagged DDR2-L610P-K were independently transfected into HEK293 cells. The His-tagged proteins were then isolated from the cell lysates with cobalt-based immobilized metal affinity chromatography (IMAC) Dynabeads. The cell pellets (after sonication), aliquots of the first wash during protein purification, and the purified proteins were boiled in sample buffer and analysed by Western blotting with anti-DDR2 antibody. The purified DDR2-WT-K protein was included as a positive control. The sample purified from non-transfected cells was included as a negative control (Mock). The positions of molecular weight markers (in kDa) are shown on the left. P, cell pellet; FT, flowthrough, HP, purified protein.

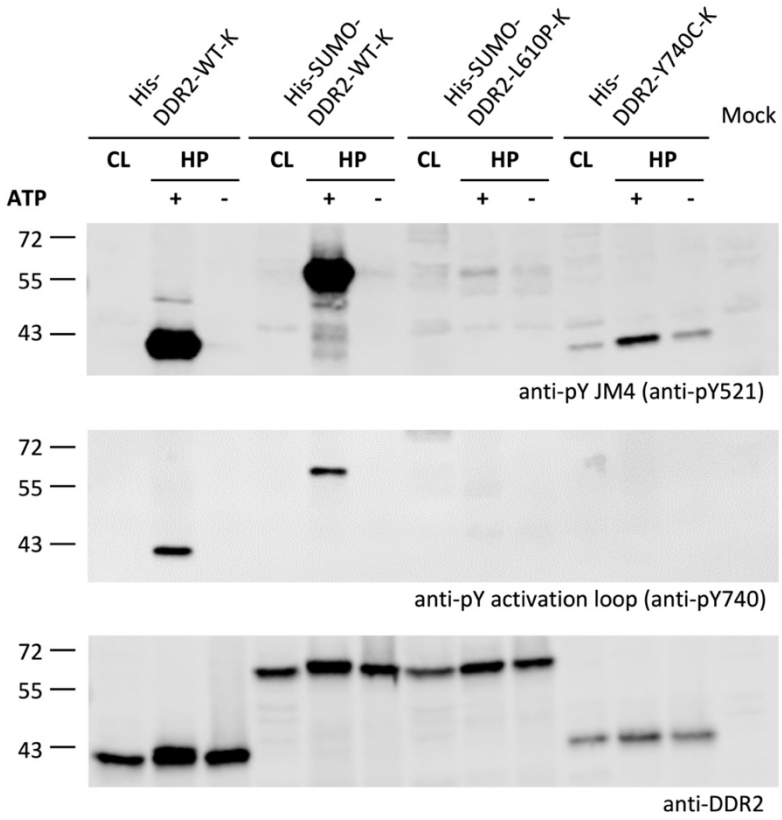


Figure 3. 12 *In vitro* kinase activity of soluble recombinant DDR2 kinase constructs.
Constructs encoding His-tagged DDR2-WT-K, SUMO-tagged DDR2-WT-K, SUMO-tagged DDR2-L610P-K and His-tagged DDR2-Y740C-K were independently transfected into HEK293 cells. The His-tagged proteins were then isolated from the cell lysates with cobalt-based immobilized metal affinity chromatography (IMAC) Dynabeads. The purified proteins were then stimulated with 1 mM ATP in kinase buffer for 30 minutes at 23°C. Samples were boiled in sample buffer and analysed by SDS-PAGE and Western blotting with the JM4-specific and activation loop-specific anti-pY antibodies, as indicated. Total DDR2 levels were detected using an anti-DDR2 antibody. The sample purified from non-transfected cells was included as a negative control (Mock). The positions of molecular weight markers (in kDa) are shown on the left. Experiments were repeated three times with similar results. CL, cell lysate; HP, purified His-tagged protein.
Note that DDR2-Y740C-K does not react with the activation loop antibody because this antibody mainly reacts with phosphorylated Y740 and cross-reacts with other activation loop tyrosine residues (phosphorylated Y736, Y741). The His-Y740C-K protein expression level was not high enough on this blot for the antibody to bind to the other activation loop tyrosines.

3.2.4 DDR2 kinase has similar activation mechanism as DDR1 kinase

A recent study from our lab showed that DDR1 kinase is first phosphorylated in the JM4 segment, followed by activation loop phosphorylation (Sammon et al., 2020). To investigate whether DDR2 undergoes the same activation steps as DDR1, the DDR2-WT-K protein was assessed for its ability to autophosphorylate *in vitro*. Previously generated recombinant DDR1-WT-K protein (received from Douglas Sammon, Leitinger lab) was included in this assay to compare potential kinase catalytic differences between DDR1 and DDR2. The DDR1 and DDR2 constructs were incubated at 1 µM in the presence of 1 mM ATP over a time course (0-60 minutes) at 20°C. Reactions were stopped by boiling the samples at each time point, followed by Western blotting with pY specific antibodies. Tyrosine residues located in the kinase-preceding JM4 region (Y569 and Y586 for DDR1, Y521 and Y538 for DDR2), as well as the activation loop of the kinase domain (Y796 in DDR1, corresponding to Y740 in DDR2; **Figure 3. 13A**), are highly conserved, and the phospho-specific antibodies that react with relevant DDR1 tyrosine residues also react with respective DDRR2 residues. Phosphorylation was observed from all three tyrosine residues on both DDR1-WT-K and DDR2-WT-K proteins, reflecting successful kinase activation (**Figure 3. 13B**). For DDR1 kinase, phosphorylation increased at Y569 and Y586 over time, while only minimal phosphorylation was observed from the activation loop tyrosine (pY796) (**Figure 3. 13B**), in agreement with the previous study (Sammon et al., 2020). On the other hand, DDR2 kinase exhibited faster activation than DDR1 kinase, with clear activation loop phosphorylation observed within 5 minutes (anti-pY740; **Figure 3. 13B**).

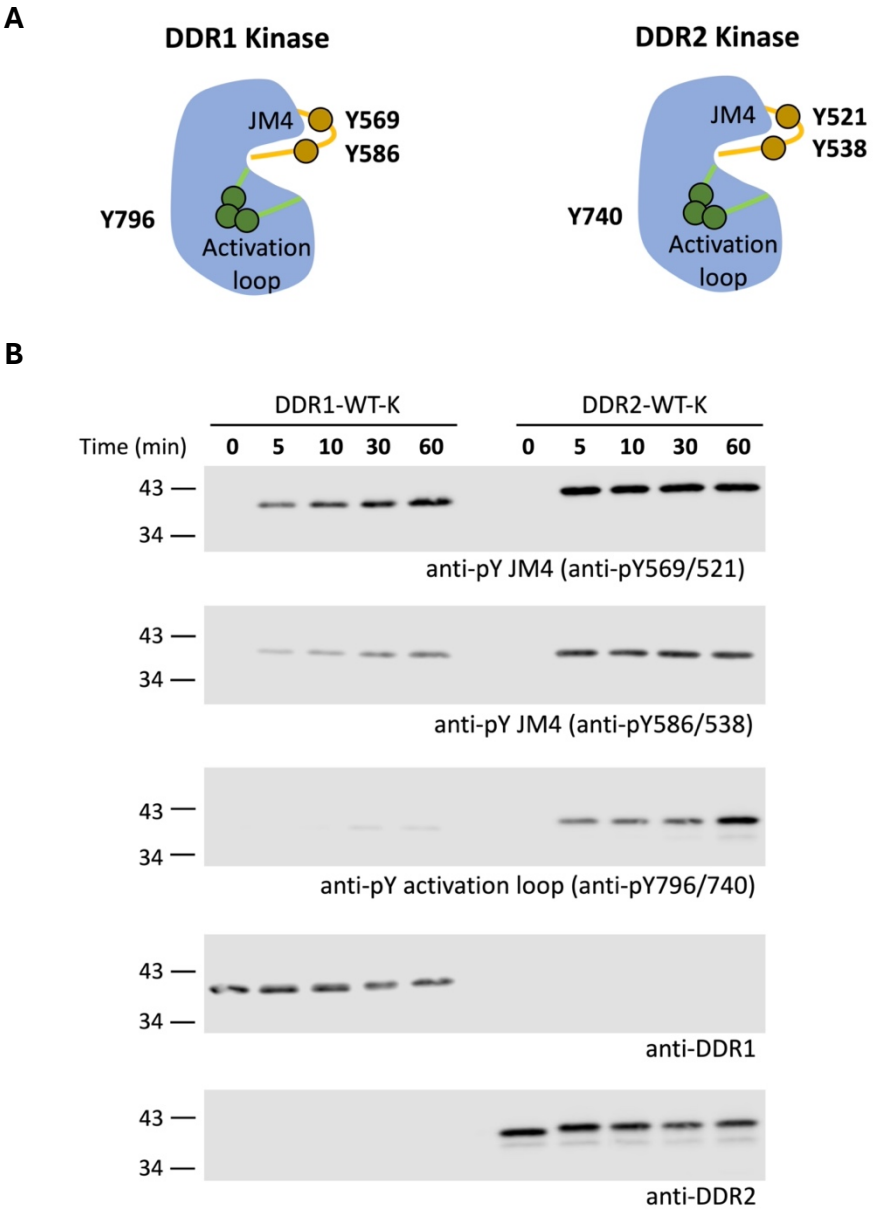


Figure 3. 13 DDR2 kinase has similar activation mechanism as DDR1 (1 µM protein autophosphorylation assay).

A. Schematic diagrams showing the location of JM4 and activation loop tyrosine residues in DDR1-WT-K and DDR2-WT-K constructs.

B. The *in vitro* autophosphorylation assay was performed by incubating 1 µM protein constructs with 1 mM ATP in kinase buffer 1 at 20°C over a 60 minutes time course. The reactions were stopped at indicated time points by boiling with sample buffer. Samples were then analysed by SDS-PAGE and Western blotting with the JM4-specific and activation loop-specific anti-pY antibodies. Total DDR levels were detected using anti-DDR1 or anti-DDR2 antibodies. The positions of molecular weight markers (in kDa) are shown on the left. Experiments were repeated three times with similar results.

To further establish the autophosphorylation differences, the constructs were incubated at 100 µM in the presence of 20 mM ATP over a longer time course (0-180 minutes). The samples were either analysed on native-PAGE with Coomassie staining or boiled to be analysed by

Western blotting with phospho-specific antibodies. Native-PAGE separates the proteins according to their charge, which allowed us to identify protein forms with different numbers of tyrosines in the phosphorylated form. Similar as above, DDR1-WT-K underwent slow activation towards the fully phosphorylated form (**Figure 3. 14, left panels**), again, in agreement with the published DDR1 kinase study (Sammon et al., 2020). The second phospho-form was clearly observable around 30 minutes of ATP stimulation, and the final state was observable at 180 minutes. Moreover, the DDR2-WT-K showed quicker activation which the conversion to the final phosphorylated form seen from 30 minutes of ATP incubation (**Figure 3. 14, right panels**). Taken together, these data demonstrate that DDR2 kinase follows the same activation mechanism as DDR1, but with a higher autophosphorylation rate.

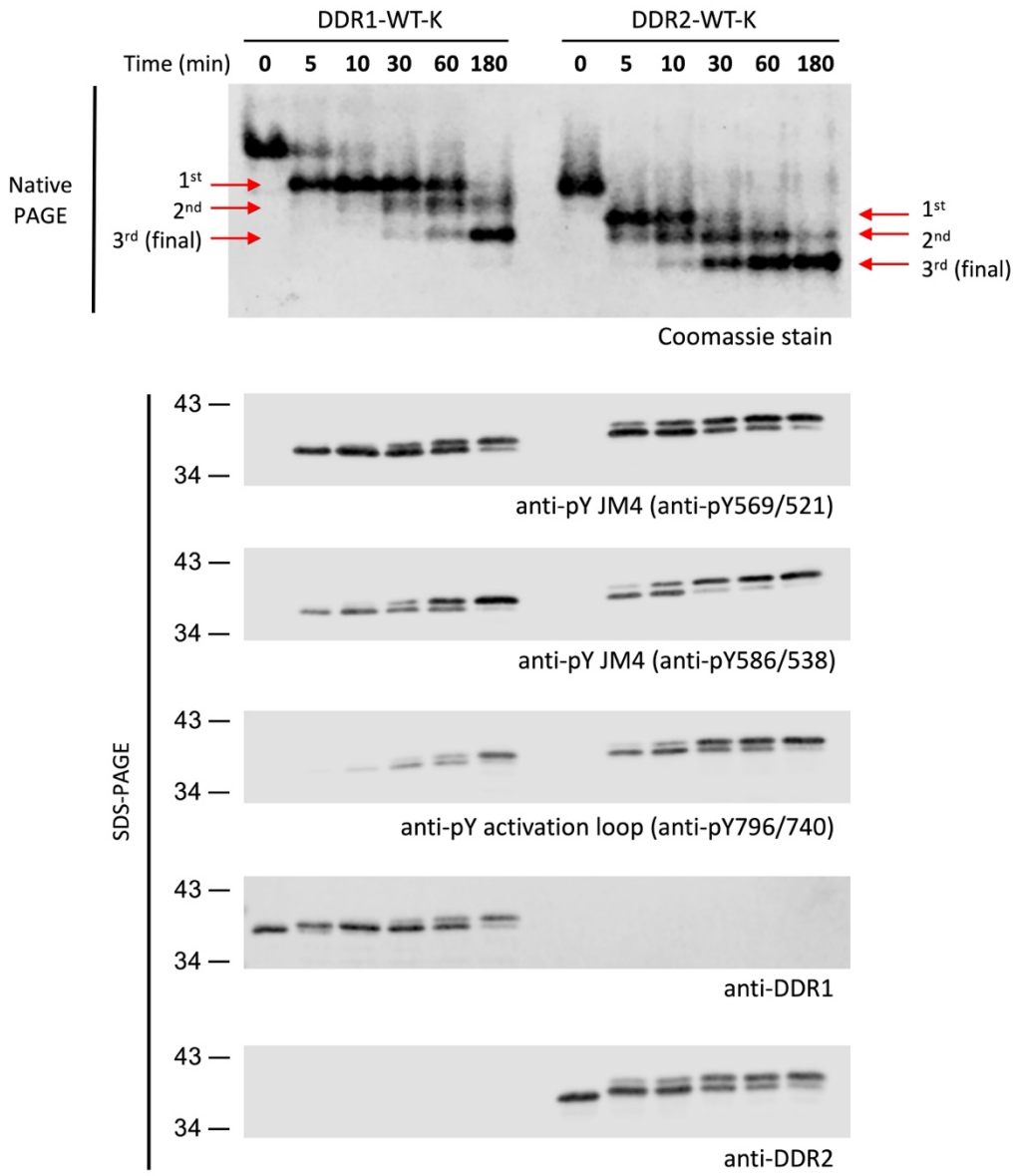


Figure 3. 14 DDR2 kinase has similar activation mechanism as DDR1 (100 µM protein autophosphorylation assay).

The *in vitro* autophosphorylation assay was performed by incubating 100 µM protein constructs with 20 mM ATP in kinase buffer 2 at 20°C over a 180 minutes time course. The reactions were stopped at indicated time points by adding 80 mM EDTA (for native-PAGE) or boiling with sample buffer (for SDS-PAGE). Samples were either separated by native-PAGE with Coomassie staining (upper image) or analysed by SDS-PAGE and Western blotting with the JM4-specific and activation loop-specific anti-pY antibodies (lower image). Different DDR phosphorylated forms are indicated with red arrows. Total DDR1 levels were detected using an anti-DDR1 antibody. The positions of molecular weight markers (in kDa) are shown on the left. As limited DDR1-WT-K was available, there was only enough material to perform this experiment once.

Protein phosphorylation can occur through an intramolecular (in *cis*) reaction or an intermolecular (in *trans*) reaction. The *cis*-autophosphorylation is not affected by increasing protein concentrations, however, a higher *trans*-autophosphorylation level can be observed with an increase in protein concentration (Reinhardt and Leonard, 2023). Previously, the DDR1 JM4 region and activation loop were proven to undergo *cis*-autophosphorylation and *trans*-autophosphorylation, respectively (Douglas Sammon and Birgit Leitinger, unpublished data). To establish whether DDR2 JM4 and the activation loop exhibit the same behavior, the DDR2-WT-K construct at 125-1000 nM were incubated with 1 mM ATP at 20°C for 10 or 30 minutes (**Figure 3. 15A**). No significant differences in JM4-specific pY521 and activation loop-specific pY740 signals were found across all protein concentrations (**Figure 3. 15B**). This indicated both DDR2 JM4 region and activation loop autophosphorylation occurs intramolecularly (in *cis*), in contrast to what was observed in DDR1 where only JM4 was observed to be phosphorylated in *cis*.

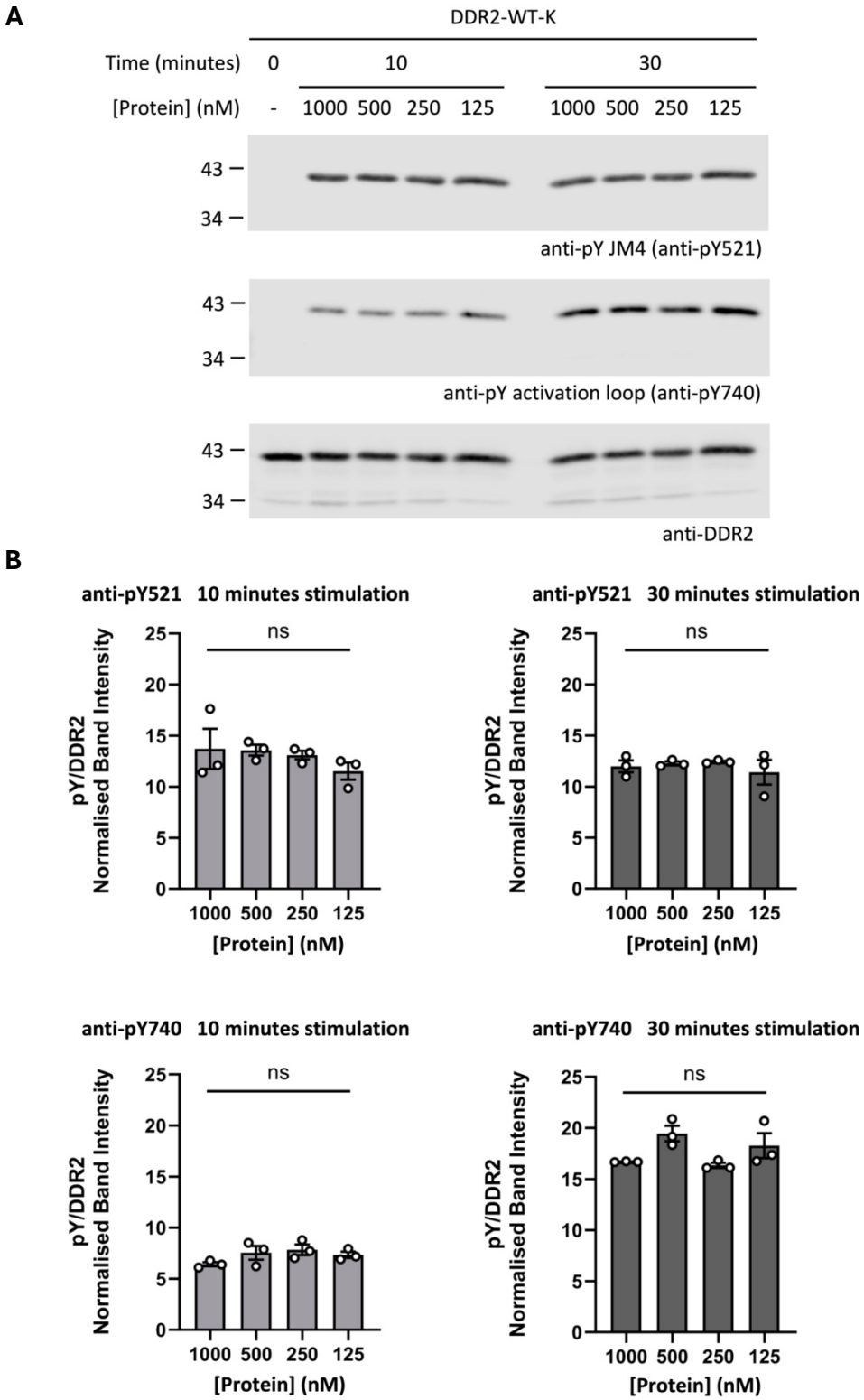


Figure 3. 15 DDR2 JM4 and activation loop both undergo protein concentration independent autophosphorylation.

A. The soluble DDR2-WT-K was titrated from 125-1000 nM and incubated with 1 mM ATP in kinase buffer 1 at 20°C for 10 or 30 minutes. The sample incubated with kinase buffer 1 in the absence of ATP was included as a negative control (-). The reactions were stopped by boiling with sample buffer. Samples were then analysed by SDS-PAGE and Western blotting with the JM4-specific and activation loop-specific anti-pY antibodies. Total DDR2 levels were detected using anti-DDR2 antibodies. The positions of molecular weight markers (in kDa) are shown on the left.

Continued on the next page.

Figure 3.15 continued
B. Quantification of the JM4 specific anti-pY521 and activation loop specific anti-pY740, signals normalised to respective anti-DDR2 signals. The anti-pY signal is expressed as a percentage of the sum of all bands on a blot, with mean and standard error of the mean shown (n=3). No statistically significant differences (ns) were found between any groups. One-way ANOVA with Tukey's multiple comparisons test.

3.2.5 DDR2-Y740C kinase is more active than DDR2-WT kinase

To investigate any potential differences in autophosphorylation rates between DDR2-WT-K and DDR2-Y740C-K, further *in vitro* kinase assays were performed. Both proteins were incubated at 0.1 mM in the presence of 1 mM ATP over a time course. As DDR2 phosphorylates itself more rapidly (**Figure 3. 13, Figure 3. 14**), the time course was shortened to 0-15 minutes. Again, DDR2-Y740C-K showed phosphorylation of both JM4 tyrosine (Y521 and Y538, data not shown for anti-pY538 blot) and activation loop tyrosine (Y736 and Y741), revealing kinase activation (**Figure 3. 16A**). The rate differences can be observed within 2 minutes of ATP addition, showing significantly quicker DDR2-Y740C JM4 and kinase activation at early time points of 15s, 30s, and 1 minute (**Figure 3. 16B**). Furthermore, the DDR2-Y740C-K activation loop phospho-signal plateaued after 2 minutes, but the signal for the WT protein was more linear across the time course (**Figure 3. 16B, right**). This indicated that DDR2-Y740C-K rapidly achieved complete activation loop phosphorylation, which is in line with our initial hypothesis that the tyrosine substitution disrupts the autoinhibitory structure, and hence allows much faster phosphorylation of other kinase tyrosines.

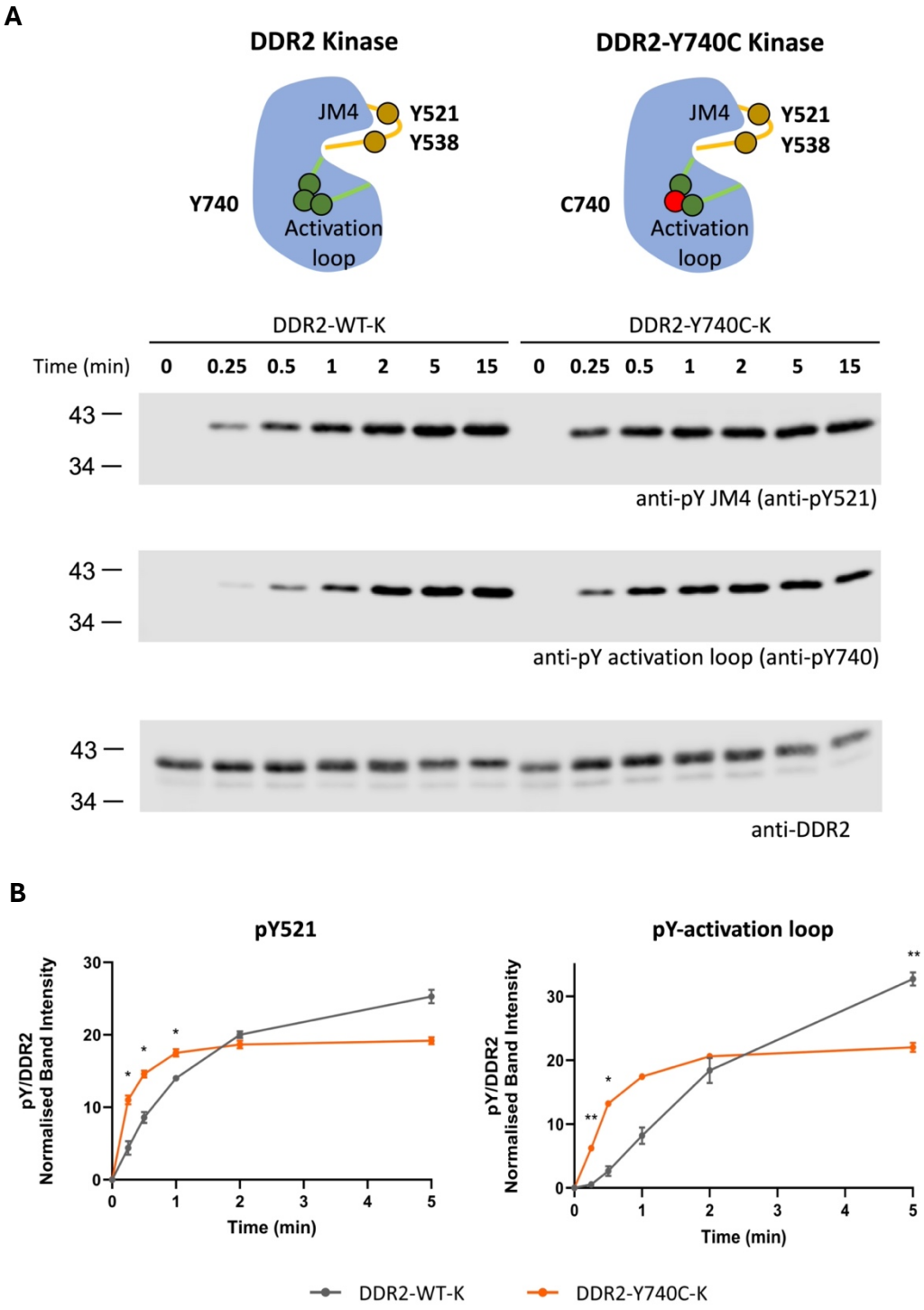


Figure 3. 16 DDR2-Y740C-K autophosphorylates quicker than DDR2-WT-K.
A. Schematic structure of the recombinant DDR2 constructs. JM4 tyrosines (Y521, Y538) and activation loop tyrosines (mutated to C740 in DDR2-Y740C-K) are labelled. The soluble DDR2-WT-K and DDR2-Y740C-K proteins were incubated at 0.1 µM in the presence of kinase buffer and 1 mM ATP for the indicated time course (0-15 minutes) at 20 °C. Protein was then boiled in sample buffer and analysed by SDS-PAGE and Western blotting. The molecular weight of the molecular markers is shown in kDa on the left side of each blot. Experiments were repeated three times with similar results.
B. Quantification of the JM4 specific anti-pY521 and activation loop specific anti-pY740, signals normalised to respective anti-DDR2 signals. The anti-pY signal is expressed as a percentage of the sum of all bands on a blot, with mean and standard error of the mean shown (n=3). Statistically significant differences ($P < 0.05$)
Continued on the next page.

Figure 3.16. continued
between the DDR2-WT-K and DDR2-Y740C-K signals are indicated by asterisks (left graph, *P = 0.0389, t = 0.25 min; *P = 0.0270, t = 0.5 min; *P = 0.0400, t = 1 min. Right graph, **P = 0.0067, t = 0.25 min; *P = 0.0170, t = 0.5 min; **P = 0.0099, t = 5 min). Two-way ANOVA with Šídák's multiple comparisons test.

The rapid kinase autophosphorylation observed from the mutant protein DDR2-Y740C-K raised the question of whether any differences in the abilities to phosphorylate substrate can be seen between this kinase and WT DDR2 kinase. Therefore, a kinetic analysis of the DDR2-WT-K and DDR2-Y740C-K substrate phosphorylation using the ADP-Glo™ assay was performed. Axltide peptide, a derivative of IRS-1, was used as the substrate peptide in this assay, as it can function as a DDR2 substrate *in vitro* (Iwai et al., 2013b). The soluble kinase proteins were incubated with Axltide peptide and ATP, followed by measuring the reaction-formed ADP that correlated with kinase activity. To find the optimal incubation temperature and check the potential impact of temperatures on DDR2 kinase activities, the kinase proteins were incubated with 200 µM Axltide peptide in the presence of 1 mM ATP. These reactions were carried out at 21, 30, and 37°C over a 40 minute time course. The initial rates were determined and plotted as specific activity (nmol min^{-1} mg^{-1}). DDR2-Y740C-K showed significantly higher specific activities than DDR2-WT-K across all three incubation temperatures (**Figure 3. 17**). Furthermore, while the different incubation temperatures did not change the DDR2-WT-K specific activity, DDR2-Y740C-K exhibited significantly higher activity at 30°C compared with 21°C (**Figure 3. 17**). To avoid reaching saturation of kinase activity, the following *in vitro* experiments were performed at 21°C.

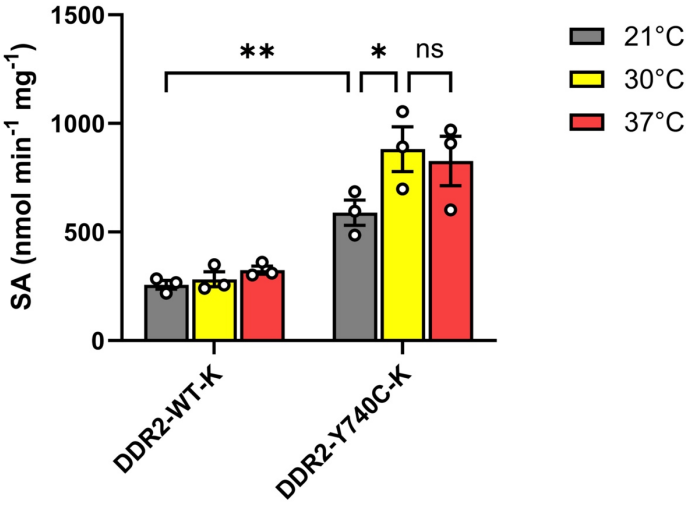


Figure 3. 17 Temperature impacts on DDR2-WT-K and DDR2-Y740C-K substrate phosphorylation rates.
In vitro kinase activity of DDR2-WT-K and DDR2-Y40C-K was assessed at different temperatures (21°C, 30°C, and 37°C) using the ADP-Glo™ assay. Initial velocities were determined by incubating 0.1 µM kinase proteins with 200 µM Axltide peptide and 1 mM over a 40 minutes time course (0, 10, 20, 40 minutes). Data are shown as specific activity (SA) with mean and standard error of the mean shown (n=3). Statistically significant differences ($P < 0.05$) between DDR2-WT-K and DDR2-Y740C-K signals are indicated by asterisks (*P = 0.0287; **P = 0.0054; ns, non-significant). Two-way ANOVA with Tukey's multiple comparisons test.

Kinetic analysis was then performed using the ADP-Glo™ or ADP-Glo™ Max assays. The proteins were independently incubated with a range of Axltide peptide concentrations (0-1.04 mM) in the presence of a fixed ATP concentration (1 mM; **Figure 3. 18A**), or a range of ATP concentrations (0-5 mM) in the presence of a fixed Axltide peptide concentration (520 µM; **Figure 3. 18B**). ADP production after different incubation times (0-40 minutes) was then quantified. The initial rates at each ATP or peptide concentration were again determined and plotted as specific activity (nmol min^{-1} mg^{-1}). All the experimental conditions in this assay were previously determined for DDR1 kinase by Douglas Sammon from Leitinger Lab. The DDR2-Y740C-K displayed higher specific activities only towards peptide but not ATP substrate, when compared with DDR2-WT-K (**Figure 3. 18**). Moreover, DDR2-WT-K showed around 4-fold higher K_m value towards peptide substrate compared with DDR2-Y740C-K, with little difference in K_m towards ATP substrate (**Table 3. 1**). Although substrate affinity was not directly measured, a lower K_m could suggest a higher protein to substrate affinity. The K_m differences suggested that DDR2-Y740C-K had higher peptide affinity than DDR2-WT-K, but there was no difference in ATP affinity between the two proteins. This can be explained based on the kinase structure, where DDR2-Y740C only loses the ability of stabilising the activation loop but the ATP binding site is likely not affected by the mutation of the activation loop Tyr740. When comparing the catalytic parameters (**Table 3. 1**) of DDR2-WT-K to the published

data for DDR1 (Sammon et al., 2020), the unphosphorylated DDR2-WT kinase has similar catalytic rates to the fully phosphorylated DDR1-WT kinase, which is in agreement with the earlier *in vitro* autophosphorylation analysis (**Figure 3. 13, Figure 3. 14).** Taken together, the mutant DDR2-Y740C kinase showed much higher activities in both kinase autophosphorylation as well as substrate phosphorylation compared with DDR2-WT kinase, which is consistent with our initial hypothesis.

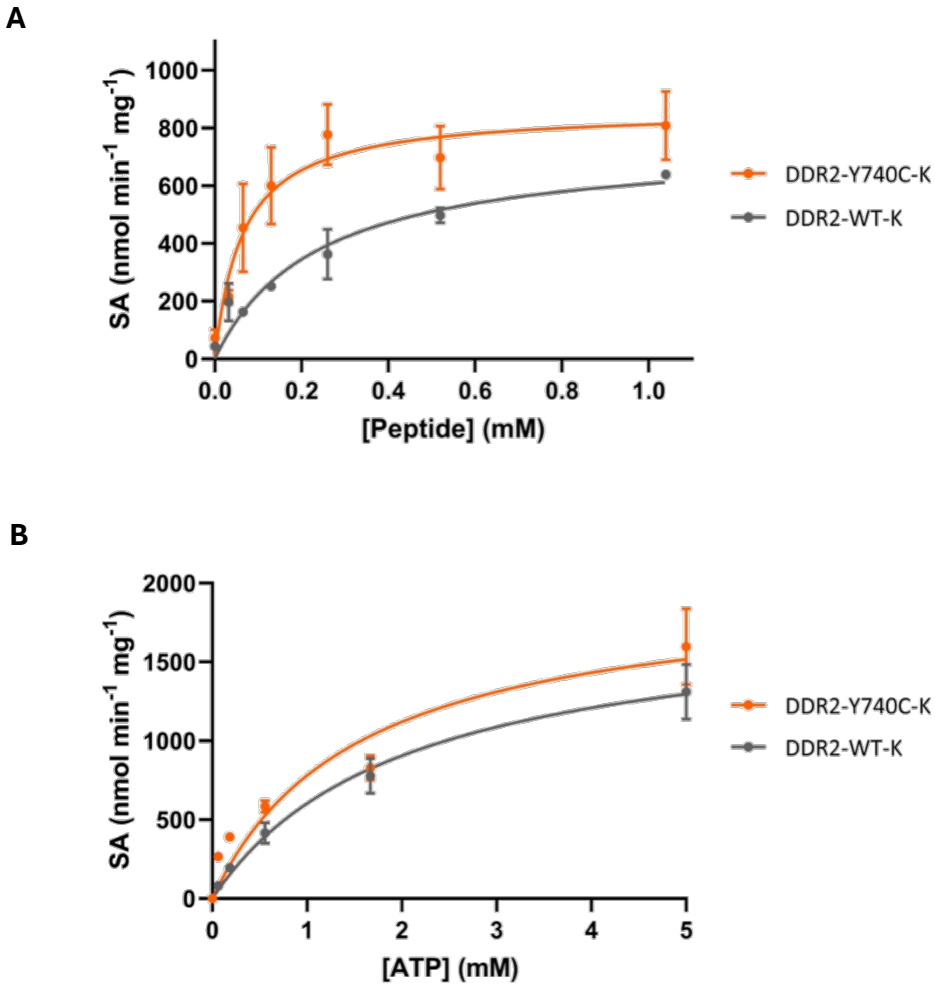


Figure 3. 18 Determination of DDR2-WT-K and DDR2-Y740C-K catalytic activities.
In vitro kinase activity of DDR2-WT-K and DDR2-Y40C-K was assessed using the ADP-Glo™ assay. Initial velocities were determined at 20°C.
A. over a range of Axltide peptide concentrations (0-1.04 mM) in the presence of a fixed ATP concentration (1 mM), or **B.** over a range of ATP concentrations (0-5 mM) in the presence of a fixed Axltide peptide concentration (520 µM). Data were then fitted with the Michaelis-Menten equation. Mean and standard error of the mean shown (n=3). SA, specific activity.

Table 3. 1 Apparent K_{cat} and K_m values for Axltide peptide and ATP.
Kinetic parameters for the Axltide peptide and ATP were calculated by fitting initial rate data (mM min-1) with the Michaelis-Menten equation. The mean and 95% confidence intervals are shown for 3 independent experiments. Parameters of DDR1-WT-K and fully phosphorylated DDR1-WT-K were obtained from (Sammon et al., 2020). ND, not determined; NA, not available.

Substrate	Kinetic parameter	DDR2-WT-K	DDR2-Y740C-K	DDR1-WT-K	Fully phosphorylated DDR1-WT-K
Peptide	K_{cat} (min^{-1})	29.0 (23.0 – 38.2)	33.3 (27.1 – 41.1)	ND	4.2 (3.6 - 5)
	K_m (mM)	0.2 (0.1 – 0.5)	0.06 (0.03 – 0.1)	ND	0.1 (0.08 – 0.2)
	V_{max} (nmol min^{-1})	2.9	3.3	NA	NA
ATP	K_{cat} (min^{-1})	70.3 (54.2 – 100.3)	76.6 (54.3 – 128.2)	ND	6.2 (5 – 7.8)
	K_m (mM)	2.0 (1.0 – 4.3)	1.5 (0.6 – 4.8)	ND	0.2 (0.08 – 0.3)
	V_{max} (nmol min^{-1})	7.0	7.7	NA	NA

3.2.6 Full-length Warburg Cinotti DDR2 mutants are constitutively active in the absence of collagen stimulation

Following the confirmation of upregulated kinase specific activities in mutant DDR2-Y740C-K, the full-length DDR2 receptor proteins were assessed in cell-based assays for their abilities to autophosphorylate in basal state and following collagen binding. Therefore, full-length DDR2 constructs were produced in a mammalian expression vector: DDR2-WT, DDR2-Y740C and DDR2-L610P. These constructs were individually expressed in HEK293 cells, which were then stimulated with soluble collagen I at 37°C for 90 minutes. The cells were harvested and lysed, followed by separating the lysates on SDS-PAGE and analysing by Western blotting with pY-specific antibodies (anti-4G10) as well as anti-DDR2 antibody. A marked increase in phosphorylation level was seen from the stimulated DDR2-WT compared with the unstimulated control, indicating the successful detection of collagen-induced receptor activation (**Figure 3. 19A**), in line with published literature (Vogel et al., 1997, Shrivastava et al., 1997, Leitinger, 2003, Leitinger et al., 2004, Leitinger and Kwan, 2006, Konitsiotis et al., 2008, Ali et al., 2010). Interestingly, even though recombinant DDR2-L610P-K showed no catalytic activity when expressed as soluble proteins (**Figure 3. 12**), collagen-independent phosphorylation was seen in both full-length DDR2-Y740C and DDR2-L610P, and collagen

stimulation did not lead to a significant increase in phosphorylation levels, indicating the constitutive activities of both mutant receptors (**Figure 3. 19A**).

DDR2 was found as three molecular forms, which expressed equally in the wild-type constructs, as expected (Konitsiotis et al., 2008, Leitinger, 2003, Noordeen et al., 2006). However, both mutant DDR2s showed much lower proportion of the higher molecular form, even though clear phosphorylation was still observed (**Figure 3. 19A, left lower panel**). We reasoned that the mutant proteins had higher proportion of immature DDR2 protein, compared with WT DDR2. This was then verified by EndoH digestion. The cell lysates were incubated with EndoH, which deglycosylates the immature, high-mannose glyco-forms in N-linked glycosylated proteins, and results in a visible shift of the protein size that can be detected by SDS-PAGE and Western blotting. The proteins that have undergone complete glycosylation with mature, complex glycans, should be resistant to EndoH digestion (Freeze and Kranz, 2010). As expected, only the lowest molecular weight bands of all three DDR2 constructs shifted to lower molecular weight forms after EndoH digestion, indicating the presence of the immature DDR2 proteins (**Figure 3. 19B**). These data showed that for both of the DDR2 mutant constructs, the majority of protein molecules were present as immature biosynthetic precursors.

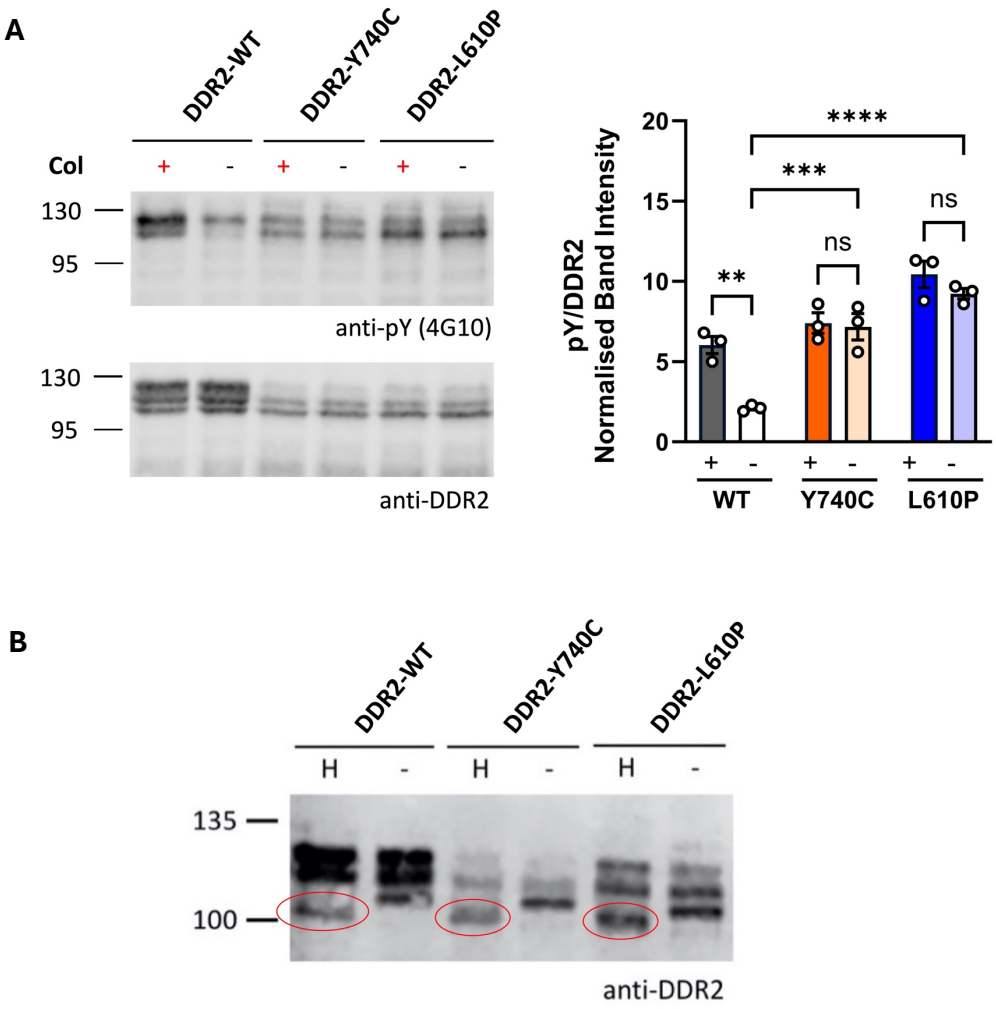


Figure 3. 19 Full-length DDR2-Y740C and DDR2-L610P are constitutively active in the absence of collagen stimulation.

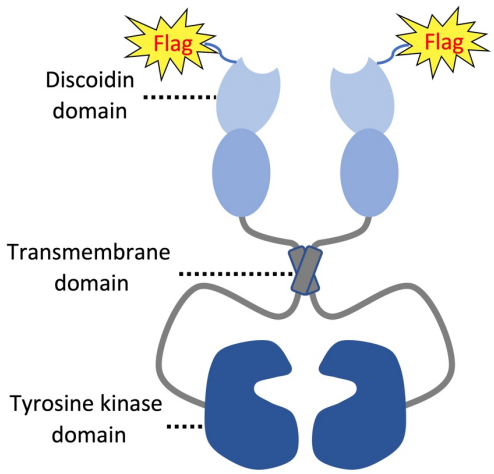
A. Left: DDR2-WT, DDR2-Y740C, DDR2-L610P were transfected into HEK293 cells. Transfected cells were cultured for 24 hours, and then serum staved for at least 16 hours. After starvation, the cells were stimulated with 10 µg/mL soluble collagen I at 37°C for 90 minutes. Cell lysis was performed with the lysates boiled in sample buffer and analysed by SDS-PAGE and Western Blotting with anti-pY antibody. Total DDR2 levels were then detected using an anti-DDR2 antibody. The positions of molecular weight markers (in kDa) are shown on the left. **Right:** Quantification of the anti-pY (4G10) antibody signals, normalised to respective anti-DDR2 signals. Statistically significant differences ($P < 0.05$) between signals are indicated by asterisks (**P = 0.0060; ***P = 0.0007; ****P < 0.0001; ns, non-significant). Two-way ANOVA with Tukey's multiple comparisons test.

B. DDR2-WT, DDR2-Y740C, DDR2-L610P were transfected into HEK293 cells. The cells were lysed after 2 days of transfection. The lysates were treated with EndoH (H) or left untreated (-), followed by boiling in sample buffer and analysed by Western Blotting with anti-DDR2 antibody. Clear shifts of the lowest band are detected (circled with red). Bands that are resistant to EndoH digestion are mature glyco-forms of DDR2, EndoH sensitive forms relate to the immature biosynthetic precursor forms. The positions of molecular weight markers (in kDa) are shown on the left.

3.2.7 Warburg Cinotti mutants can express on cell surface

Although mutant DDR2s showed constitutive activities in the absence of collagen, the relatively low expression of the mature proteins brought us the question of whether the mutant DDR2-Y740C and DDR2-L610P proteins had any additional trafficking issues with reaching the cell surface. To analyse whether the disease mutants are able to reach the cell surface, immunofluorescence was used. For this assay. Cos-7 cells expressing Flag-tagged DDR2 constructs (**Figure 3. 20A**) were used, as there is no commercially available antibody that can bind to the native conformation of the DDR2 extracellular region. Flag-DDR2-WT, Flag-DDR2-Y740C and Flag-DDR2-L610P were singly expressed in Cos-7 cells and the surface staining was performed with anti-Flag antibody to indicate the presence of DDR2. All three constructs were found to be expressed on the cell surface (**Figure 3. 20B**). I next used flow cytometry to test whether the mutant DDR2s expressed similar amounts of surface proteins as the WT. Therefore, the Flag-tagged DDR2 constructs were either independently expressed or co-expressed with the untagged DDR2-WT in HEK293 cells. This co-expression was designed to check whether the formation of heterodimers with WT DDR2 could increase the mutant DDR2 surface expression levels. Cells were labelled with anti-Flag and then a FITC-conjugated secondary antibody, followed by analysis with flow cytometry. Interestingly, both mutants showed comparable levels of surface expression as WT DDR2, when expressed as single proteins, and the co-expression with untagged DDR2-WT did not result in any increase of the mutants' surface expression (**Figure 3. 21**). These data demonstrated that DDR2-Y740C and DDR2-L610P are expressed on the cell surface, despite the fact that smaller proportions of mature protein were observed by Western blotting.

A



B

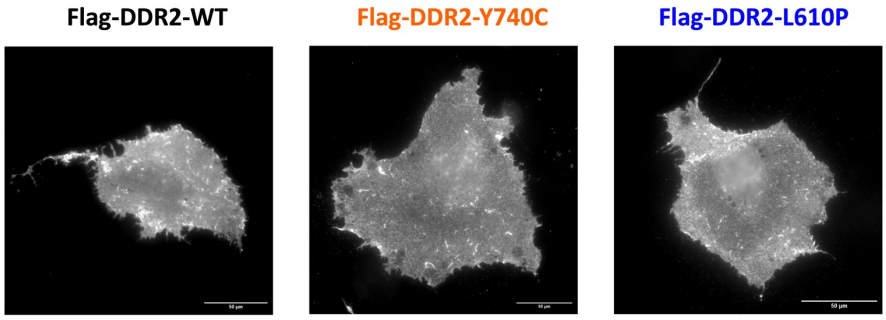


Figure 3. 20 Surface expressed DDR2-Y740C and DDR2-L610P are detected by immunofluorescence.
A. Schematic structure of the Flag-tagged full-length DDR2 construct. The Flag tag was fused to the N-terminus of the construct, with a short linker between the Flag tag and DDR2.
B. Flag-DDR2-WT, Flag-DDR2-Y740C and Flag-DDR2-L610P were singly transfected into Cos-7 cells. Cells were subsequently stained with anti-Flag antibody, followed by AlexaFluor 488 anti-mouse IgG1 secondary antibody. Scale bar = 50 µm. Widefield images were acquired using an Olympus BX51 microscope with Simple-PCI acquisition software.

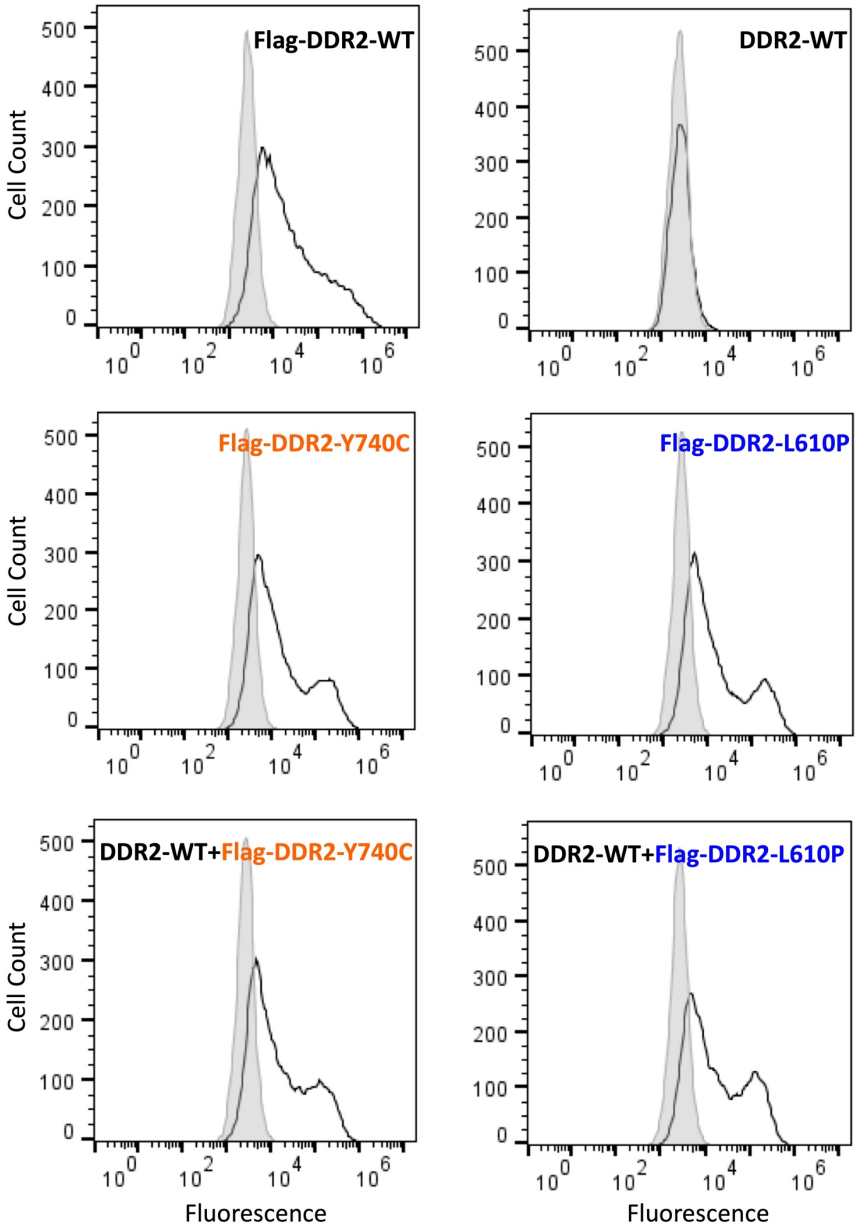


Figure 3. 21 Surface expressed DDR2-Y740C and DDR2-L610P are detected by flow cytometry.
Flag-DDR2-WT, Flag-DDR2-Y740C and Flag-DDR2-L610P were singly transfected into HEK293 cells. Untagged DDR2-WT was expressed on its own or co-expressed with Flag-DDR2-Y740C or Flag-DDR2-L610P. Cells were subsequently stained with anti-Flag antibody, followed by FITC-labelled anti-mouse-Fc antibody and analysed by flow cytometry. The filled grey histograms represent secondary antibody only staining, while the open histograms represent anti-Flag and secondary antibody staining.

3.2.8 DDR2 kinase inhibitors can block both recombinant and full-length DDR2 activity

Thus far, I showed that recombinant soluble DDR2-Y740C-K and both full-length mutant DDR2s had higher phosphorylation activities than the respective WT proteins. I next established whether commercial kinase inhibitors can block the excess activities. The ATP competitive type-I kinase inhibitor dasatinib as well as DDR-specific inhibitor VU6015929 were tested (Jeffries et al., 2020). Unlike the highly selective VU6015929, dasatinib is a non-selective kinase inhibitor that has been shown to block DDR2 kinase activity (Day et al., 2008, Jeffries et al., 2020). For the *in vitro* assays, proteins were independently incubated with a range of dasatinib concentrations (0.28 nM-50 µM) or a range of VU6015929 concentrations (0.056 nM-10 µM) in the presence of ATP (100 µM or 1 mM) and 250 µM Axltide peptide. Again, ADP production was recorded using the ADP-Glo^{TM} assay. Both DDR2-WT-K and DDR2-Y740C-K could be inhibited by dasatinib with similar IC_{50} (**Figure 3. 22A, Table 3. 2**). The IC_{50} of dasatinib for DDR2-WT was also previously determined in a study using TR-FRET assay with 100 µM ATP, showing a very similar value of 1.4 ± 0.3 nM (Day et al., 2008); compare with 3.5nM and 1.4nM obtained here for DDR2-Wt-K and DDR2-Y740-K respectively). The DDR-specific inhibitor VU6015929 could also block soluble DDR2 kinase activities (**Figure 3. 22B, Table 3. 2**). This inhibitor was then assessed for its ability to block autophosphorylation of full-length DDR2 constructs expressed in HEK293 cells. After transfection, cells were treated with or without 100 nM of the VU6015929 inhibitor at 37°C for 45 minutes before collagen stimulation. This was then followed by cell lysis and Western blotting analysis with pY-specific antibodies as well as anti-DDR2 antibody. Inhibitor treatment abolished the collagen-induced receptor activation (**Figure 3. 23**). Taken together, these data demonstrated the abilities of commercial kinase inhibitors to block the substrate phosphorylation induced by soluble DDR2-WT and DDR2-Y740C kinases, and collagen-induced autophosphorylation from the full-length WT and mutant DDR2 proteins.

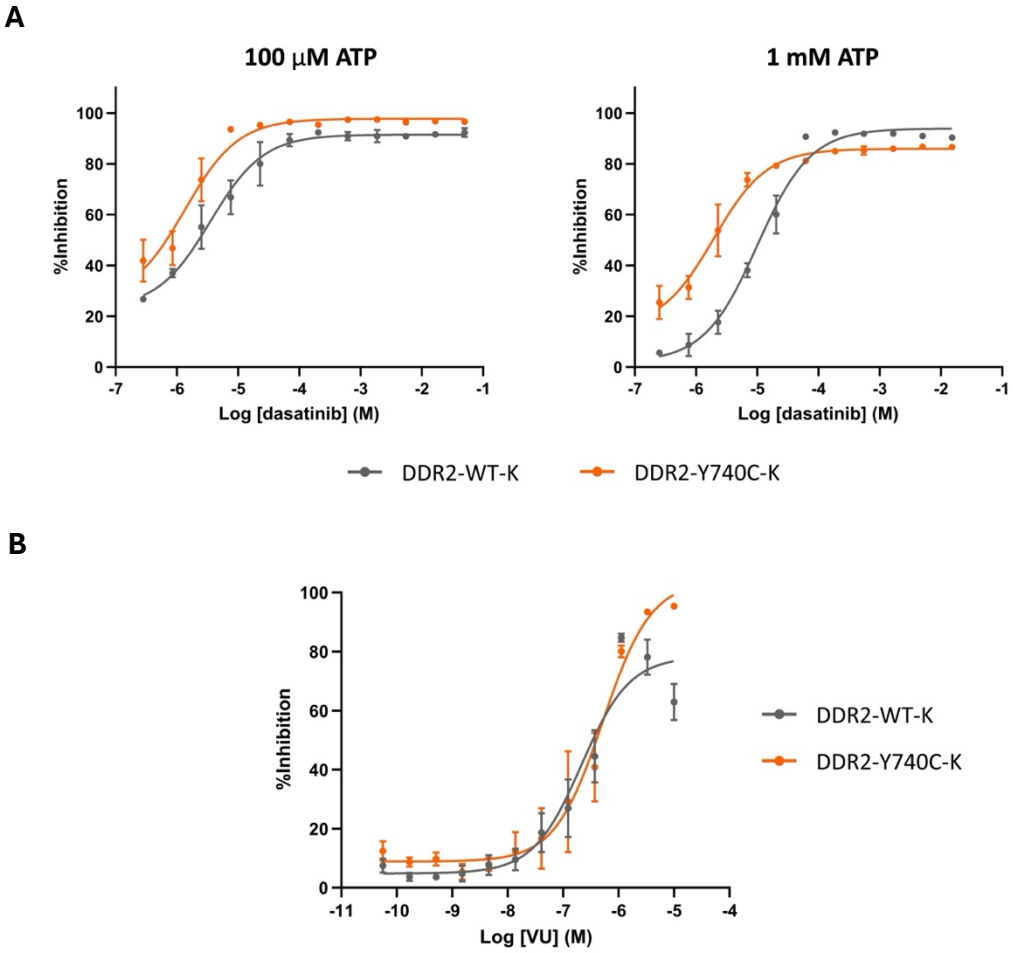


Figure 3. 22 Dasatinib and VU6015929 block both DDR2-WT and DDR2-Y740C kinase abilities to phosphorylate substrate.

DDR2-WT-K and DDR2-Y40C-K were independently incubated with a range of **A.** dasatinib concentrations (0.28 nM -50 µM) or **B.** VU6015929 concentrations (0.056 nM-10 µM) in the presence of fixed ATP concentrations (100 µM or 1 mM for dasatinib test, 100 µM for VU6015929 test) and Axltide peptide concentration (250 µM) at 20 °C. ADP production was recorded using ADP-Glo™ assay. Data is shown as percentage of inhibition. n=3; mean and standard error of the mean shown.

Table 3. 2 IC_{50} values from the dasatinib and VU6015929 inhibitor assays for blocking DDR2-WT-K and DDR2-Y740C-K kinase abilities to phosphorylate substrate.

ATP		DDR2-WT-K	DDR2-Y740C-K
100 µM	IC_{50} (Dasatinib)	3.5 nM	1.4 nM
1 mM		10.0 nM	2.0 nM
100 µM	IC_{50} (VU6015929)	213.3 nM	520.9 nM

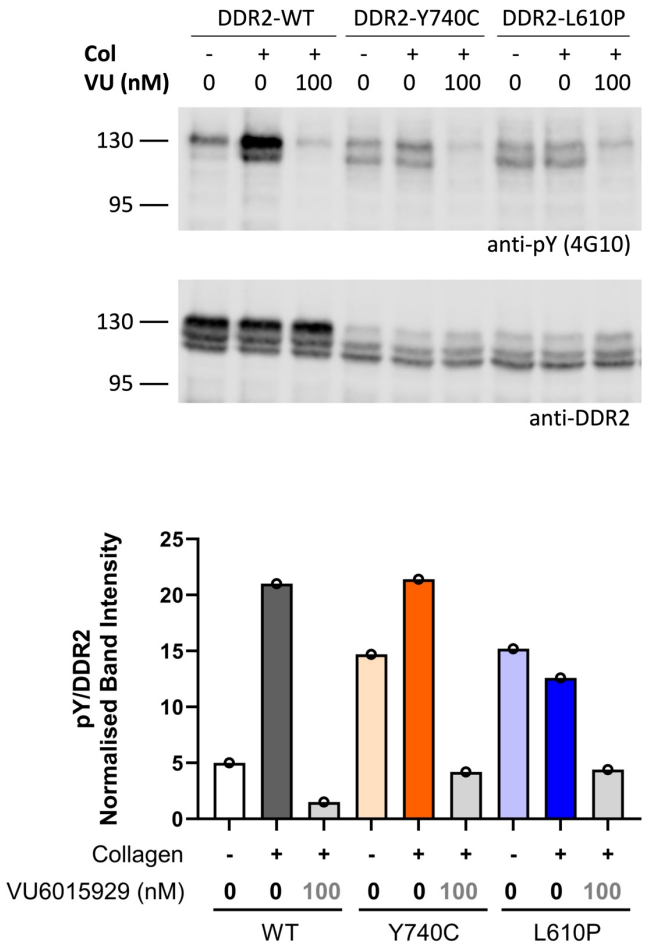


Figure 3. 23 DDR-specific inhibitor VU6015929 can block collagen-induced full-length DDR2 activation in the overexpression system.

Upper image: DDR2-WT, DDR2-Y740C, or DDR2-L610P were singly transfected into HEK293 cells. Transfected cells were cultured for 24 hours, and then serum staved for at least 16 hours. After starvation, the cells were treated with or without 100 nM VU6015929 (VU) inhibitors for 45 minutes before being stimulated with 10 µg/mL soluble collagen I at 37°C for 90 minutes. Cell lysis was performed with the lysates boiled in sample buffer and analysed by SDS-PAGE and Western Blotting with anti-pY antibody. Total DDR2 levels were then detected using an anti-DDR2 antibody. The positions of molecular weight markers (in kDa) are shown on the left. n=1.

Lower chart: Quantification of the anti-pY antibody, signal normalised to respective anti-DDR2 signals.

3.3 Discussion

Gain-of-function missense variants in the kinase domain of RTKs can lead to aberrant receptor signalling, which is the underlying cause of numerous human disorders (McDonell et al., 2015, Neben et al., 2019, Stefl et al., 2013). Those mutations mostly cluster in evolutionally conserved residues that are tightly involved in the regulation of kinase catalytic activity (Medves and Demoulin, 2012, Lahiry et al., 2010, Izarzugaza et al., 2009). For example, missense variant in FGFR3 kinase domain (Lys650Glu) leads to ligand independent receptor activation and causes thanatophoric dysplasia II (Iwata et al., 2000). In endothelial-specific receptor tyrosine kinase, TIE2, mutations (Arg849Trp, Tyr897Ser) result in multiple cutaneous and mucosal venous malformations (Wouters et al., 2010). RTK gain-of-function variants are also seen in cancers, for example multiple kinase domain activating mutations in EGFR are characterised in non-small cell lung cancer cases (Wang et al., 2011). For Warburg Cinotti syndrome, a severe connective tissue disorder (Warburg et al., 2006, Cinotti et al., 2013), two missense variants located on the DDR2 tyrosine kinase domain were identified as disease-causing variants, but limited protein studies were conducted in the original report (Xu et al., 2018). In this chapter, biochemical assays using recombinant soluble protein kinase constructs revealed the increase of kinase catalytic activity found in DDR2 carrying the Tyr740Cys mutation. Furthermore, ligand-independent receptor activation was observed in transiently transfected mammalian cells expressing the full-length TM proteins of DDR2-Y740C and DDR2-L610P.

First, the prediction of the structural effects of Leu610Pro and Tyr740Cys mutations was performed based on the experimentally determined DDR2 kinase structure (PDB code: 7AYM) (Nawrotek, 2020). Both mutations were identified to be damaging to the kinase autoinhibitory conformation. Leu610 is located at the end of the kinase β3 strand (**Figure 3. 3**), where the proline substitution is disfavoured. In most cases, introducing proline into α-helices or β-sheets, especially at their centre, breaks the secondary structure of the protein (Choi and Mayo, 2006). However, the natural presence of proline residues at the edge strands of the β-sheet is believed to help avoid aggregation (Richardson and Richardson, 2002, Shamsir and Dalby, 2007). Despite the instability predicted from the proline substitution in DDR2-L610P, the location of this mutation before the αC helix reduces the flexibility of the nearby regulatory motifs due to the conformational rigidity of proline (Melnikov et al., 2016). In a

previous study, recombinant DDR2 cytosolic protein expressed in Sf9 cells was used to demonstrate the autoinhibitory role of the Tyr740 residue in DDR2 kinase activity (Yang et al., 2005). This led us to perform *in vitro* kinase assays with soluble recombinant DDR2 kinase proteins containing the Warburg Cinotti syndrome mutants. While the structural analysis was performed with the DDR2 kinase only structure (i.e in the absence of any regulatory elements outside the kinase domain), and the Yang et al study used soluble recombinant protein of the entire DDR2 cytosolic region (Yang et al., 2005), I designed the recombinant constructs for *in vitro* analysis to contain the regulatory DDR2 JM4 region in addition to the kinase domain. The constructs were cloned into the pOPIN vector and expressed in the baculovirus system. Previously, OPPF helped our lab perform an initial screening with several DDR1 constructs cloned in pOPINF vector, including different length of JM region (JM1 to JM4) with the DDR1a or DDR1b kinase domain, and expressed in E. *coli*, mammalian, and baculovirus system (unpublished data). Only the constructs containing the DDR1 kinase domain together with the JM4 region showed sufficient expression in the baculovirus system. Thus, the important role of JM4 in DDR1 catalytic activity was characterised (Sammon et al., 2020). The JM1 to JM3 region is located away from the kinase domain, with poor conservation between DDR1 and DDR2. As the essential JM4 segment is a highly conserved region (**Figure 3. 1**), protein constructs of DDR2 JM4 and kinase domain (DDR2-K constructs) were expressed, and the *in vitro* results can be directly compared with our previous DDR1 study (Sammon et al., 2020). We were especially interested to characterise DDR2 Leu610Pro, in which the mutant kinase behaviour is less clearly predictable compared with DDR2 Try740Cys. However, the recombinant DDR2-L610P-K construct with the pOPINF vector failed to be purified as a soluble protein when expressed in the baculovirus system (**Figure 3. 4C).** OPPF provided us with other pOPIN vectors that contain additional fusion tags before the HRV 3C cleavage site. The GST tag (pOPINJ) was shown to help protein folding and stabilise protein structure (Terpe, 2003, Harper and Speicher, 2011). The SUMO (pOPINS3C) and MBP (pOPINM) tags are useful protein solubility partners (Paraskevopoulou and Falcone, 2018, Fox et al., 2003). However, even with the help of these fusion tags, no soluble DDR2-L610P-K construct could be obtained from the baculovirus system. (**Figure 3. 7-Figure 3. 10**). Furthermore, the SUMO-tagged DDR2-L610P-K construct was successfully purified as a soluble protein when expressed in mammalian cells, but the kinase lost its function (**Figure 3. 11, Figure 3. 12**). While this recombinant protein showed instability, ligand-independent phosphorylation signals could be detected from the

full-length DDR2-L610P TM receptor expressed in mammalian cells (**Figure 3. 19**). A possible explanation could be that expressing the full-length form might help protein folding, especially when the damaging residue is located away from the N-terminal portion of the protein, which may fold sooner after protein translation (Zhang and Ignatova, 2011, Waudby et al., 2019).

The regulatory role of JM4 region to DDR1 kinase domain catalytic activity has been investigated in detail (Sammon et al., 2020). This JM4 region was shown to bind tightly to the DDR1 kinase domain in the inactive state, and act as an autoinhibitory segment. Multi-step autophosphorylation is required for complete DDR1 kinase activation. In this case, the JM4 needs to be phosphorylated first in order to move away from the kinase active site. This is then followed by activation loop phosphorylation and results in a fully activated DDR1 kinase domain (Sammon et al., 2020). A similar mechanism also exists in PDGFRA and c-Kit kinase activation, where the JM region phosphorylates before the activation loop (Liang et al., 2016, Mol et al., 2003). In this chapter, DDR2 kinase was shown to undergo the same two-step activation as DDR1 (**Figure 3. 13, Figure 3. 14**). However, DDR2 kinase showed much quicker activation loop phosphorylation, compared with DDR1, in *in vitro* data (**Figure 3. 13, Figure 3. 14**). The slow DDR1 activation loop phosphorylation occurs intermolecularly, and the activation loop is atypically stable in the inactive conformation (Sammon et al., 2020, Hanson et al., 2019). In contrast, both JM4 and activation loop in DDR2-WT-K are autophosphorylated via an intramolecular mechanism (**Figure 3. 15**). Moreover, in the Yang et al., 2005 study, recombinant DDR2 cytoplasmic region showed *cis*-autophosphorylation (i.e. an intramolecular reaction) (Yang et al., 2005), in agreement with the data provided in this thesis chapter. Taken together, this may explain why DDR2 activation loop phosphorylation occurs with rapid kinetics.

In most RTKs, phosphorylation on activation loop tyrosines stabilises the loop in a conformation for optimal ATP and substrate binding (Hubbard and Till, 2000), with a few exceptions seen in EGFR (Tyr845) and KIT (Tyr823), where the role of activation loop tyrosine is only to stabilise the open conformation (Maruyama, 2014, Klug et al., 2018). In DDR2, Tyr740 forms hydrogen bonds with neighbouring residues so that the activation loop stays in the position that blocks the binding of peptide substrates (**Figure 3. 3B**). The DDR2-Y740C-K construct exhibited significantly quicker autophosphorylation on both JM4 and activation loop tyrosine residues, with the differences from the DDR2-WT-K construct seen within 1 minute

of the reaction (**Figure 3. 16**). Moreover, rapid kinetics of peptide substrate phosphorylation by the Y740C construct was found (**Figure 3. 18, Table 3. 1**), indicating an overall higher kinase catalytic activity caused by the Tyr740Cys mutation. It remains unclear whether the higher catalytic rate of DDR2-Y740C-K predominantly relies on quick kinase autophosphorylation or on higher intrinsic kinase enzymatic activity. In future studies, the fully phosphorylated DDR2-WT-K construct could be produced and purified for further ADP-Glo assays, as was done for DDR1 (Sammon et al., 2020); using the fully phosphorylated form in substrate phosphorylation assays would eliminate any confounding effects of kinase autophosphorylation during the substrate phosphorylation reactions.

DDRs are unique RTK family members that present on cell surface as constitutive dimers and undergo slow collagen-induced receptor activation (Shrivastava et al., 1997, Vogel et al., 1997, Noordeen et al., 2006, Mihai et al., 2009, Xu et al., 2014). In the absence of collagen, DDR1 is found on the cell surface as punctate clusters, which then redistribute into dense clusters upon collagen stimulation (Corcoran et al., 2019, Yeung et al., 2019). Unlike DDR1, DDR2 was not found to form clusters post-collagen binding (Yeung et al., 2019), but the absence of suitable antibodies that bind native DDR2 on the surface of cells limits current insight into potential DDR2 ligand-independent and ligand-dependent clustering. Collagen-induced DDR1 clustering results in *trans*-phosphorylation between DDR1 dimers (Yeung et al., 2019, Juskaite et al., 2017). The detailed mechanism of how clustering leads to DDR activation is still poorly understood. It will be interesting to investigate the potential differences in clustering between full-length WT and mutant DDR2 proteins. Flag-tagged DDR2 constructs used for immunofluorescence analysis in **Figure 3. 20** showed evidence of DDR2 protein surface expression, and these constructs could be used in more detailed imaging analysis. Alternative protein-labelling systems, such as SpyCatcher-SpyTag system, which can avoid the use of antibodies in labelling could be applied for more precise imaging (Zakeri et al., 2012).

One of the initial hypotheses for this study is that Warburg Cinotti DDR2 mutants lead to constitutive receptor activation due to the gain-of-function nature of these two mutants. When the recombinant DDR2 constructs were expressed in HEK293 cells for *in vitro* kinase assay, ATP-independent phosphorylation signals were observed on JM4 Tyr521 from His-DDR2-Y740C-K (**Figure 3. 12, top panel**). This can be considered as a clue for constitutive mutant kinase activity. Moreover, full-length TM receptors were expressed in HEK293, where

both DDR2-L610P and DDR2-Y740C exhibited collagen-independent autophosphorylation, as expected (**Figure 3. 19B**). Surprisingly, only a small proportion of mutant DDR2 proteins were seen as the mature form by Western blotting, which was also confirmed by EndoH digestion (**Figure 3. 19C**). Similarly, PDGFRB gain-of-function mutation, Val665Ala, showed a reduced amount of mature protein seen in Western blotting analysis, which was later shown to be associated with deficient cell surface expression (Johnston et al., 2015, Nedelec et al., 2022). However, here, comparable surface expression levels were seen from the mutant DDR2s to that of WT DDR2 (**Figure 3. 21**). It is possible that the loss of mature DDR2-Y740C and DDR2-L610P in cell lysates is linked to reduced protein solubility in non-ionic detergent, leading to loss of protein that is loaded onto the SDS-PAGE gel. A possible approach to increase the protein extraction is to lyse the cell pellet in SDS loading buffer with β-mercaptoethanol and boil it for 15 minutes before loading the sample onto a gel. Proteins associated with the cytoskeleton often result in decreased solubility in detergent (Hommelgaard et al., 2004). DDR1 was found to co-localise with linear invadosome, which is an F-actin structure and aligns along collagen fibrils (Juin et al., 2012, Juin et al., 2014). In another study, an interaction between DDR1 and cytoskeletal protein talin was observed (Borza et al., 2022). However, not much information exists in the literature addressing the co-localisation of DDR2 with the cytoskeleton. In future studies, interactions between Warburg Cinotti syndrome DDR2 mutants and cytoskeletal components could be investigated.

An extensive range of tyrosine kinase inhibitors have been developed to target the disease-associated dysregulated receptors and non-receptor kinases (Grimminger et al., 2010, Bhullar et al., 2018). A wide range of commercial inhibitors originally developed for breakpoint cluster region Abelson (Bcr-Abl) tyrosine kinase (Desogus et al., 2015), such as dasatinib, imatinib, and nilotinib, have been reported to cross-react and block both DDR1 and DDR2 kinase activity with low IC_{50} (Day et al., 2008). However, distinct mutations of the same receptor can react differently to certain inhibitors. Conventional type II inhibitor imatinib and regorafenib were shown to effectively target JM domain mutations on KIT (Val559Ala and Val560Asp) but was resisted by KIT activation loop mutation Asp816Val (Sandoval-Perez et al., 2022). Other activating mutations in PDGFRA or FLT3 also exhibited resistance to type II inhibitors (Klug et al., 2018). Applications of type I inhibitors such as dasatinib can target active kinase conformation caused by gain-of-function mutations (Laurini et al., 2013). However, off-target

inhibitions are difficult to avoid with these broad-range ATP-competitive inhibitors, as the kinase ATP binding site is extremely well conserved (Hanson et al., 2019, Lemmon and Schlessinger, 2010). Therefore, type I inhibitor dasatinib and DDR2-specific inhibitor VU6015929 were tested for recombinant and full-length DDR2s. For both inhibitors, similar IC_{50} values were seen between WT and Y740C kinases for the *in vitro* assay and notable full-length receptor inhibition was observed from cell experiments (**Figure 3. 22, Figure 3. 23**).

In this chapter, full-length DDR2 autophosphorylation capabilities were assessed in transiently transfected cells. The overexpression system is a straightforward tool for basic cell biology studies, which have been used broadly for RTK signalling investigation (Prelich, 2012). However, this overly simplistic model can obliterate possible protein crosstalk and, on the other hand, exaggerate weak interactions (Gibson et al., 2013, Dumont et al., 2002). For example, low level phosphorylation signals were observed from full-length DDR2-WT without collagen stimulation, which is likely due to receptor overexpression (**Figure 3. 19A**). Therefore, mutant receptor behaviours in cells endogenously expressing DDR2 must be assessed.

In summary, the soluble recombinant DDR2-Y740C kinase has been shown to exhibit higher catalytic activity than WT kinase, and the constitutive activity of both Warburg Cinotti syndrome-associated full-length DDR2 mutants has been demonstrated.

Chapter 4 Investigation of Warburg Cinotti Syndrome related DDR2 variants in patient primary dermal fibroblasts

4.1 Introduction

In **Chapter 3**, ligand-independent autophosphorylation of both Warburg Cinotti variants DDR2-L610P and DDR2-Y740C was demonstrated. However, the behaviour of the mutant DDR2 proteins in the context of endogenous cell expression was not assessed. DDR expression in the human body varies among different cell types: while DDR1 is mainly expressed in epithelial cells and activated T cells, DDR2 is mainly found in cells of connective tissues, such as fibroblasts and mesenchymal cells (Alves et al., 1995, Chetoui et al., 2011, Makino et al., 2013). Warburg Cinotti syndrome, as described earlier, is a rare but severe connective tissue disorder. Patients suffer from symptoms such as progressive corneal vascularisation, acro-osteolysis, and various dermatological conditions (Warburg et al., 2006, Cinotti et al., 2013). The first few signs of this syndrome, such as keloid-like plaques on the skin, can occur as a mild condition in childhood that slowly progresses to a more severe condition throughout adulthood (Xu et al., 2018, Ours et al., 2022).

Fibroblasts, primary residents in connective tissues, are widespread across different organs and tissues and synthesise key ECM components such as collagens, fibronectin and microfibrillar proteins (Plikus et al., 2021, Lendahl et al., 2022). Fibroblasts also contribute to ECM structure remodelling by secreting enzymes such as MMPs and MMP inhibitors (Lu et al., 2011b). During dermal wound healing, after the initial inflammatory stage, fibroblasts migrate into the wounded area through ECM and differentiate into myofibroblasts (activated fibroblasts), which are tightly involved in the formation of new tissue but also pathological contracture formations (Muller et al., 2012, Tomasek et al., 2002, Van De Water et al., 2013). Keloid-like lesions and severe contractures, which are known to harbour myofibroblast cells (Nangole and Agak, 2019, Shin and Minn, 2004), have been reported in multiple Warburg Cinotti patient cases (Xu et al., 2018, Ours et al., 2022).

Multiple RTKs have been reported to be essential in regulating fibroblast functions and wound repair progress (Muller et al., 2012). For example, a gain-of-function mutation in the PDGFRB kinase activation loop leads to enhanced dermal cell proliferation and migration, promoting the formation of granulation tissue after acute injury (Chiara et al., 2004, Krampert et al.,

2008). For the FGFR study in the injured palatal tissue, basic FGF was widely expressed at the wounded site, and strong expression of FGFR1 was found in myofibroblast nuclei (Kanda et al., 2003). DDRs also participate in tissue homeostasis and skin disease progression (Cario, 2018). Increased DDR1 expression and phosphorylation levels were found in keloid tissue-derived fibroblasts (Chin et al., 2000). In addition, DDR2 has been shown to regulate the proliferation, migration, and activation of dermal fibroblasts, as shown in a DDR2 knockout (KO) mouse model (Olaso et al., 2002).

In this chapter, primary HDF cells isolated from Warburg Cinotti patient biopsies were used to investigate the role of mutant DDR2 proteins in regulating cell functions. It was hypothesised that Warburg Cinotti mutants result in constitutive DDR2 activities as well as changed cellular behaviour in patient fibroblasts. The aims were: (1) to analyse DDR2 phosphorylation status and test the efficacy of the DDR-specific inhibitor in patient HDF cells; (2) to determine patient HDF cell behaviours via functional cell models.

4.2 Results

4.2.1 Ligand-independent DDR2 phosphorylation in patient HDF cells can be blocked by VU6015929

To investigate Warburg Cinotti DDR2 mutants at an endogenous expression level, I obtained primary HDF cells through collaboration with Dr Cecilie Bredrup, Haukeland University Hospital, Norway. The cells were either isolated from a healthy donor (control cells) or from Warburg Cinotti Syndrome patients' biopsies. Informed consent was obtained. After receipt of the cells, verification of the DDR2 heterozygous mutation state was performed. Total RNA was isolated from all three cell groups, followed by reverse transcription and PCR amplification of the DDR2 transcript region that encodes the protein region starting before residue 610 and ending after residue 740. The PCR products were then subjected to Sanger sequencing (**Figure 4. 1**). As expected, no changes, compared with the reference sequence, were found at the target region in the healthy donor's sample (**Figure 4. 1A**). DDR2 heterozygous missense substitutions were found in the patient samples, with the expected single substitution in each sample and no additional substitutions in the other locus (**Figure 4. 1B, C**). In the following

context, HDF cells from the healthy donor are named as WT cells, and cells from Warburg Cinotti patients 1 and 2 referred to as L610P and Y740C cells, respectively.

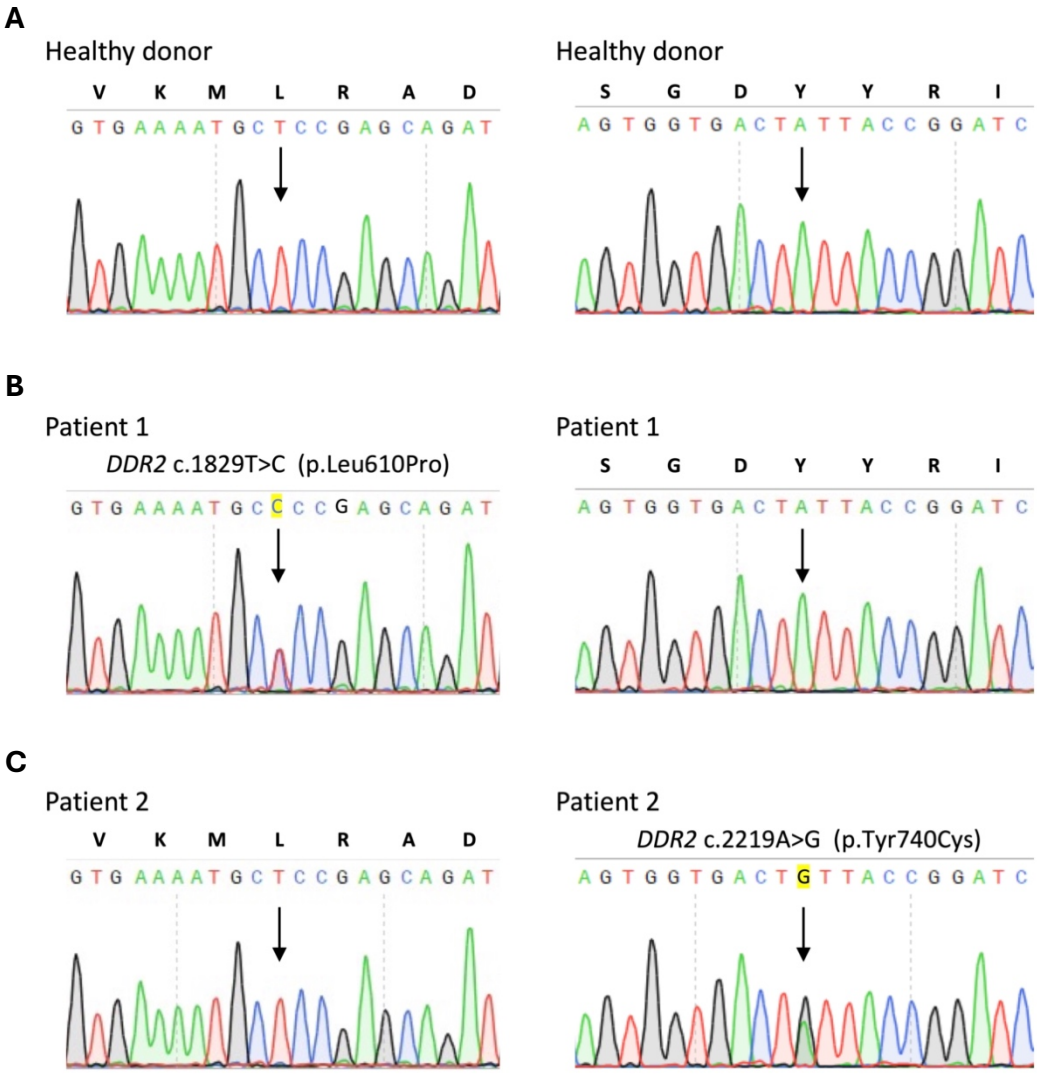


Figure 4. 1 Verification of Warburg-Cinotti syndrome associated DDR2 heterozygous mutations by Sanger Sequencing.
Total RNA was extracted from three HDF cell groups: cells from a healthy donor, Warburg Cinotti patient cells carrying the L610P variant, and Warburg Cinotti patient cells carrying the Y740C variant. Reverse transcription was performed, followed by PCR amplification of the DDR2 transcript region that encodes the receptor kinase domain. The PCR products were analysed by Sanger Sequencing. Amino acid regions from Val607 to Asp613 and from Ser737 to Ile743 are shown in this figure (left and right, respectively).
A. Wild-type DNA sequence shown for healthy donor with no extra peaks at either locus.
B. A heterozygous missense substitution (c.1829T>C) was confirmed from the patient cells with L610P variant. No additional peaks were found at the c.2219A (Y740) location.
C. A heterozygous missense substitution (c.2219A>G) was confirmed from the patient cells with Y740C variant. No additional peaks were found at the c.1829T (L610) location.

I then confirmed the DDR2 expression and autophosphorylation in HDF cells. The DDR-specific inhibitor VU6015929 was also tested in this assay. A challenge in using Western blotting to study DDR2 from primary cells was the low endogenous protein expression levels. I attempted to concentrate DDR2 proteins by immunoprecipitation (IP). However, this was unsuccessful, possibly due to the low affinity between DDR2 and the antibody (data not shown). To obtain optimal amounts of DDR2 protein for Western blotting detection, HDF cells were cultured in various sizes of culture plates/dishes and lysed in different volumes of lysis buffer. For total DDR2 signal detection, I tested the same anti-DDR2 antibody as used in the HEK293 cell experiment (**Figure 3. 23**). Preliminary experiments showed that DDR2 expression could only be detected when cells were grown in two to three 100 mm culture dishes and lysed in a total volume of 40 µL of lysis buffer. I then optimised stimulation conditions by incubating HDF cells with SFM containing 10, 20, or 100 µg/mL collagen I for 2, 4, or 8 hours at 37°C. A pan anti-pY antibody (anti-4G10) and the activation loop-specific anti-pY antibody (anti-pY740) were tested for Western blotting detection. Weak but detectable phosphorylation signals were observed among all stimulation conditions (data not shown). The anti-pY740 antibody was chosen to focus on DDR2-specific phosphorylation signals. Among all the stimulation conditions, the optimal signals from Western blotting with anti-pY740 antibody were observed from HDF cells stimulated with SFM containing 20 µg/mL collagen I for 4 hours at 37°C. For inhibitor treatment, the same condition used in the experiment with HEK293 cells (**Figure 3. 23**) was applied to HDF cells. Therefore, the above conditions were used for the DDR2 autophosphorylation assay with HDF cells. In brief, HDF cells were grown in multiple 100 mm culture dishes and serum starved for 24 hours before treatment. Then, the cells were pre-treated with 100 nM VU6015929 for 45 minutes at 37°C before being stimulated with 20 µg/mL collagen I for 4 hours at 37°C. The cells were then lysed and analysed on SDS-PAGE followed by Western blotting with the anti-pY740 antibody and the anti-DDR2 antibody (**Figure 4. 2A**). A significant increase in DDR2 phosphorylation level was seen from the stimulated WT cells compared with the unstimulated control, as expected, and the inhibitor treatment blocked collagen-induced DDR2 phosphorylation (**Figure 4. 2B**). For Y740C and L610P cells with no collagen stimulation, the DDR2 phosphorylation levels were higher than unstimulated WT cells (**Figure 4. 2B**). However, these differences were not statistically significant, which may be due to the weak signals on the Western blots obtained for the anti-pY740 antibody (**Figure 4. 2A**). Upon collagen stimulation, DDR2 phosphorylation levels were

significantly upregulated in Y740C cells (**Figure 4. 2B**). It is important to note that the anti-pY740 antibody cannot detect very well the phosphorylation signals from DDR2-Y740C protein due to the tyrosine-to-cysteine substitution. Thus, the DDR2 autophosphorylation signals in Y740C cells detected by Western blotting are likely predominantly from the WT DDR2 present in the cells. However, whilst the detection of Y740C phosphorylation signals may have been missing in this experiment, the top band from the total DDR2 signal was stronger in unstimulated Y740C samples in the absence of inhibitor (**Figure 4. 2A, bottom panel, lane 5**) compared with unstimulated DDR2-WT without inhibitor treatment (**Figure 4. 2A, bottom panel, lane 1**), which indicated a high proportion of phosphorylated DDR2s were presented in Y740C cells in the absence of collagen stimulation. Protein phosphorylation often results in a visible mobility shift from the lower molecular band to the higher band in Western blotting analysis due to the addition of phosphate groups and a decreased protein binding with SDS (Lee et al., 2019). A previous study has shown that both DDR1 and DDR2 are able to phosphorylate adjacent DDRs in *trans* (Juskaite et al., 2017). Therefore, the top DDR2 band in lane 5 could represent a mixture of constitutively phosphorylated DDR2-Y740C and DDR2-WT activated by DDR2-Y740C in *trans* (**Figure 4. 2A, bottom panel, lane 5**). DDR2 phosphorylation level in L610P cells were not increased upon collagen stimulation (**Figure 4. 2B**), in line with the constitutive DDR2-L610P autophosphorylation obtained in experiments with HEK293 cells (**Figure 3. 19**). The appearance of the total DDR2 bands from WT and L610P cell samples were very similar, and the top DDR2 bands in unstimulated L610P cells in the absence of the inhibitor (**Figure 4. 2A, bottom panel, lane 9**) were not as strong as in unstimulated Y740C cells. Moreover, DDR2 in Y740C cells reacted to collagen stimulation better than in L610P cells (**Figure 4. 2B**). These data suggested that the patient cells carrying different Warburg Cinotti mutations responded to collagen stimulation differently. For both patient cell groups, DDR2 phosphorylation was sensitive to inhibitor treatment, with both basal and collagen-induced phosphorylation being reduced compared with respective untreated samples (**Figure 4. 2B**). Taken together, HDF cells received from our collaborator expressed the expected DDR2 variants, and constitutive DDR2 activation was observed in L610P cells and indicated in Y740C cells. Moreover, DDR2 autophosphorylation in patient HDF cells could be blocked by the DDR-specific inhibitor VU6015929.

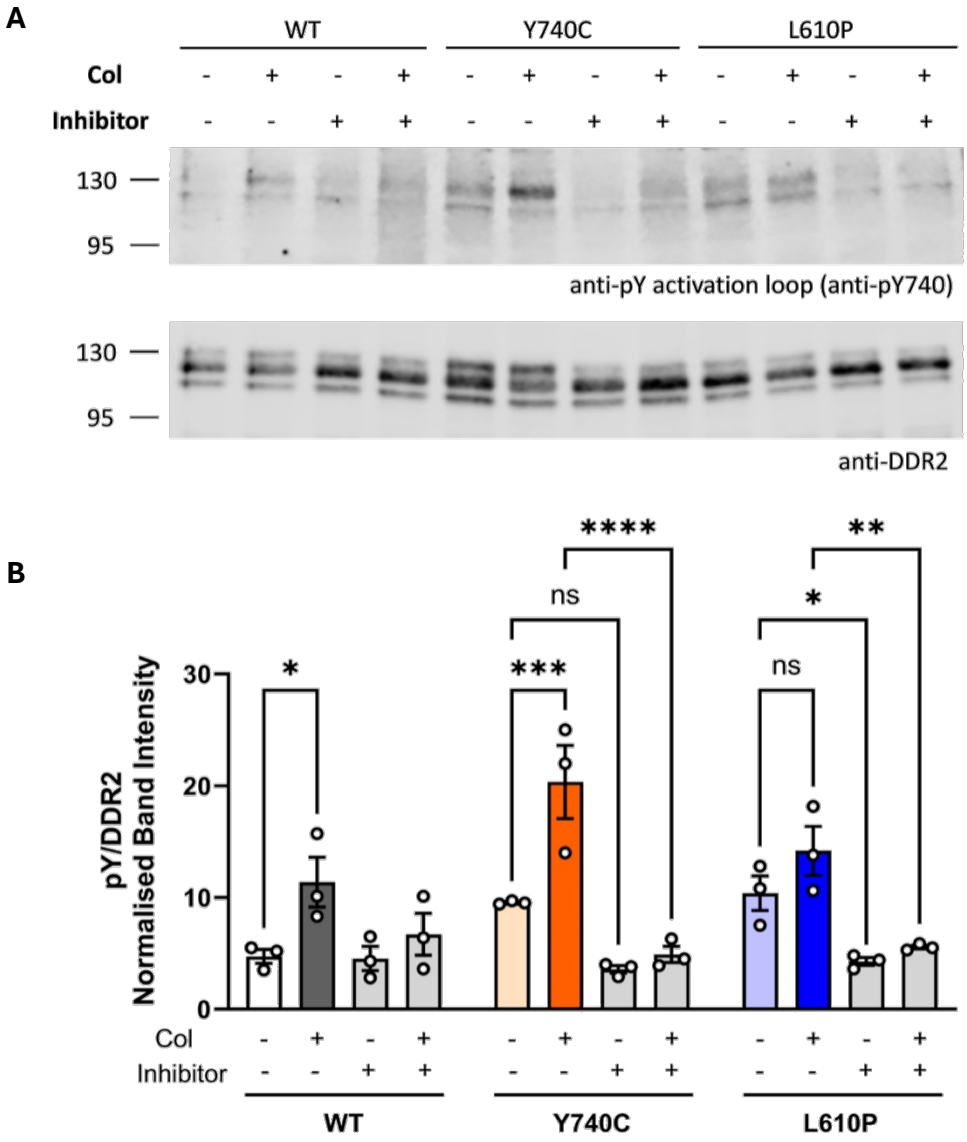


Figure 4. 2 DDR2 autophosphorylation in WT and Warburg Cinotti patient cells.

HDF cells were serum-starved prior to 100nM inhibitor/vehicle treatment at 37°C for 45 minutes, followed by stimulation for 4 hours with 20 µg/mL collagen I/vehicle.

A. Cells were then lysed, and the proteins were analysed by SDS-PAGE and Western blotting with activation loop-specific anti-pY antibody as well as anti-DDR2 antibody. The position of molecular weight markers (in kDa) is shown on the left.

B. Quantification of the anti-pY activation loop antibody signals, normalised to respective anti-DDR2 signals. The normalised signal is expressed as a percentage of the sum of all bands on a blot, with mean and standard error of the mean shown (n=3). Two-way ANOVA with Tukey's multiple comparisons test was performed. WT (-) Col I vs WT (+) Col I; p=0.0277 (*). Y740C (-) Col I vs Y740C (+) Col I; p=0.0003 (***). Y740C (-) Col I (-) inhibitor vs Y740C (-) Col I (+) inhibitor; p=0.0537 (ns). Y740C (+) Col I (-) inhibitor vs Y740C (+) Col I (+) inhibitor; p<0.0001 (****). L610P (-) Col I vs L610P (+) Col I; p=0.3263 (ns). L610P (-) Col I (-) inhibitor vs L610P (-) Col I (+) inhibitor; p=0.0469 (*). L610P (+) Col I (-) inhibitor vs L610P (+) Col I (+) inhibitor; p=0.0032 (**).

4.2.2 Investigation of patient cell migration on two-dimensional surfaces

Fibroblast migration towards the wounded area has been described as one of the essential cellular behaviours that participate in normal wound healing or disease progression (Gomes et al., 2021). For example, enhanced fibroblast migration was found in lungs with fibrotic lesions derived from IPF patients (Barkauskas and Noble, 2014). A study using human foreskin fibroblasts showed that DDR2 is required for fibroblast migration on two-dimensional (2D) surfaces, regardless of the adhesive ligand used for surface coating (Herrera-Herrera and Quezada-Calvillo, 2012). Another study found that DDR2 kinase activity is partially involved in CAFs migration through 3D Matrigel (Barcus et al., 2021). However, the correlation between DDR2 kinase activity and fibroblast migration rate remains poorly understood. Therefore, to establish whether Warburg Cinotti patient HDF cells exhibit a higher migration rate than WT cells, a wound healing assay on 2D surfaces was performed. Although the 3D migration system provides a highly *in vivo*-like environment, this system often requires the design of 3D matrices, which can be time-consuming (Wu et al., 2018). The wound healing assay on a 2D surface is a cost-effective method, and the 'wound' can be introduced by either manually removing cells with a pipette tip (scratch-wound assay) or creating a cell-free gap using commercial inserts. However, the wound size and shape obtained from the scratch-wound assay varies, while the commercial insert can create a linear cell-free area with a consistent width of around 500 µm (**Figure 4. 3A**) (Radstake et al., 2023). Therefore, the HDF cells were seeded into the insert wells attached to an uncoated or collagen I-coated cell culture plate and grown in complete medium until full confluency. To suppress cell proliferation, the HDF cells were cultured in SFM for 24 hours preceding the insert removal. After removing the insert, cells were cultured in medium containing a decreased amount of serum to minimise cell proliferation and maintain cell viability. Images of the cell-free gap area were taken at 0, 10, and 24 hours, followed by quantification of the cell-free gap area using FIJI software with a custom-made macro (**Section 2.1.6**). For cells growing on the non-coated surface, L610P cells exhibited significantly faster gap closure than WT cells starting from 10 hours, while Y740C cells showed a significantly higher gap closure rate only at 24 hours (**Figure 4. 3C**). For cells grown on the collagen-coated surface, there were no differences in gap closure rate between the WT and mutant cell groups (**Figure 4. 4B**). Moreover, WT cells displayed a significantly quicker gap closure on the collagen-coated surface compared with its gap closure rate on the non-coated surface (**Figure 4. 5A**).

Both mutant cells exhibited similar gap closure rates on the surface with or without collagen coating (**Figure 4. 5B, C**). These data suggested that WT and mutant HDF cells migrate at similar rates in a collagen-rich environment, but L610P cells have increased migration potential in a weak adhesive environment (in the absence of a coated matrix).

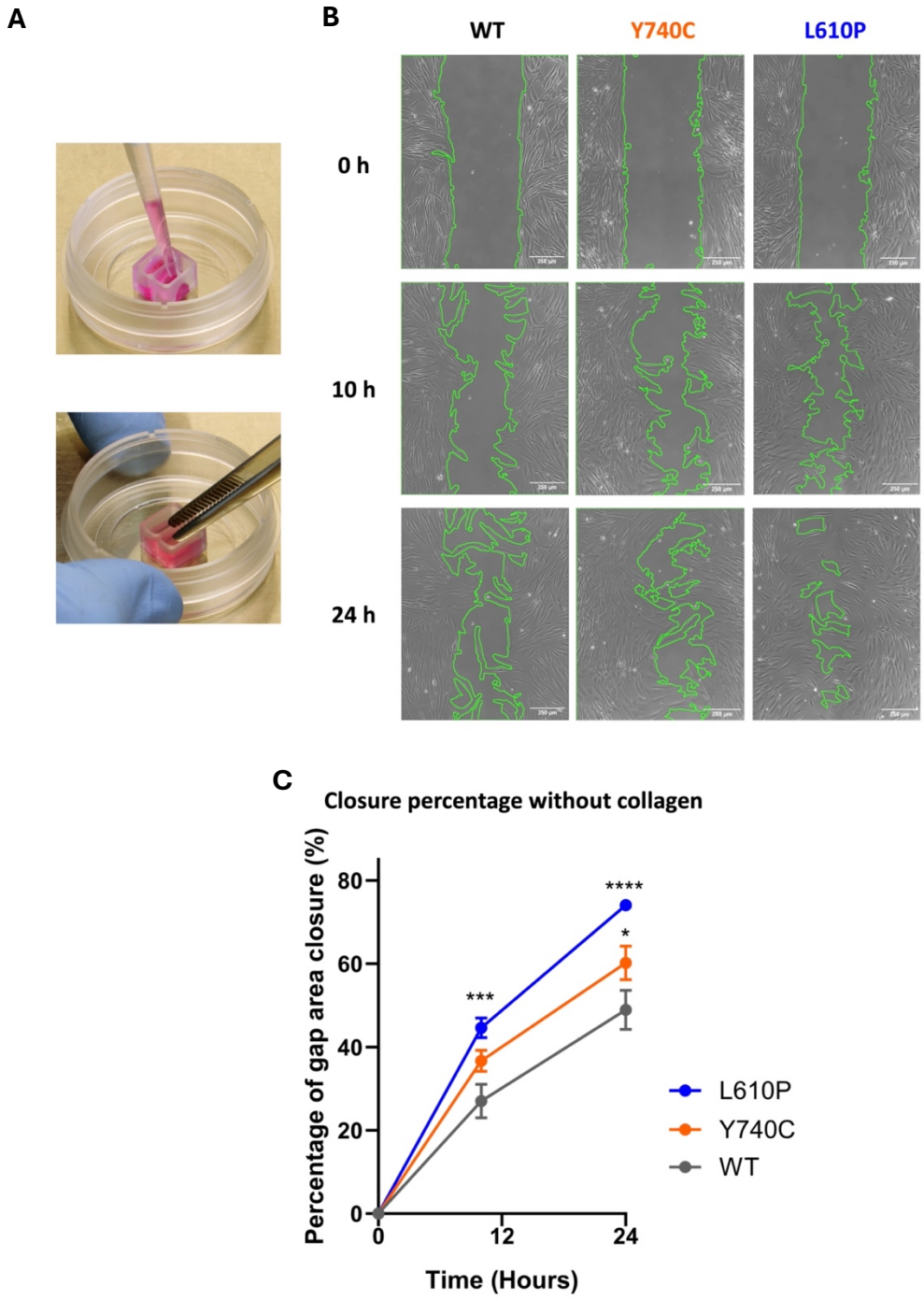


Figure 4. 3 HDF cells wound healing assay on a non-collagen-coatedplate.
Continued on the next page.

Figure 4.3. continued

A. Images showing the ibidi culture insert used for the wound healing assay. Images are from https://ibidi.com/culture-inserts/25-25-culture-inserts-2-well-for-self-insertion.html.

B. HDF cells were seeded into commercial wound healing inserts, placed into a 24-well cell culture plate and allowed to grow until full confluence. 24 hours of serum starvation was performed before removing the inserts. The cells were then allowed to migrate at 37°C, with widefield images taken at 0, 10, and 24 hours using a Zeiss Axio Observer equipped with an EC Plan-Neofluar 10X/0.30 Ph1 objective. Representative images are shown with the cell-free gap areas indicated with green lines. The cell-free gap areas were analysed using FIJI software with a macro obtained from the Facility for Imaging by Light Microscopy (FILM) at Imperial College London. The macro package can be downloaded from: https://www.imperial.ac.uk/medicine/facility-for-imaging-by-light-microscopy/software/fiji/.

C. The cell-free gap area from different time points is expressed as a percentage of the area at 0 hours with mean and standard error of the mean shown (n=3). Two-way ANOVA with Tukey's multiple comparisons test was performed. Statistically significant differences between WT and L610P gap closure percentages were found at both 10 and 24 hours (***, p=0.0003; ****, p<0.0001). *, p=0.0268 statistically significant difference was found between WT and Y740C gap closure percentage.

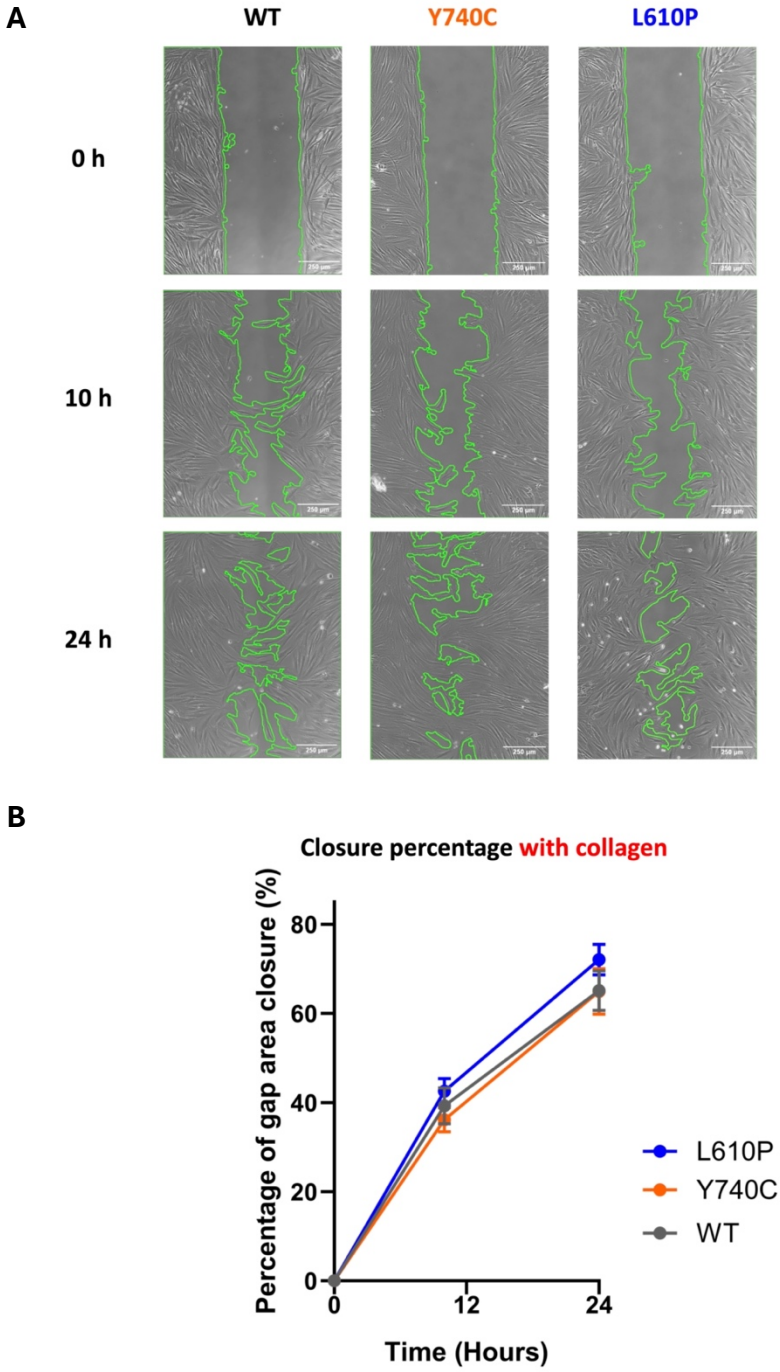


Figure 4. 4 HDF cells wound healing assay on a collagen-coated plate.

A. HDF cells were seeded into commercial wound healing inserts, placed into a collagen-coated 24-well cell culture plate and allowed to grow until full confluence. 24 hours of serum starvation was performed before removing the inserts. The cells were then allowed to migrate with widefield images taken at 0, 10, and 24 hours using a Zeiss Axio Observer equipped with an EC Plan-Neofluar 10X/0.30 Ph1 objective. Representative images are shown with the cell-free gap areas indicated with green lines. The cell-free gap areas were analysed using FIJI software with a macro obtained from the Facility for Imaging by Light Microscopy (FILM) at Imperial College London.

B. The cell-free gap areas from different time points is expressed as a percentage of the area at 0 hours with mean and standard error of the mean shown (n=3). Two-way ANOVA with Tukey's multiple comparisons test was performed. No significant differences were found between WT and mutant gap closure percentage at 10 and 24 hours.

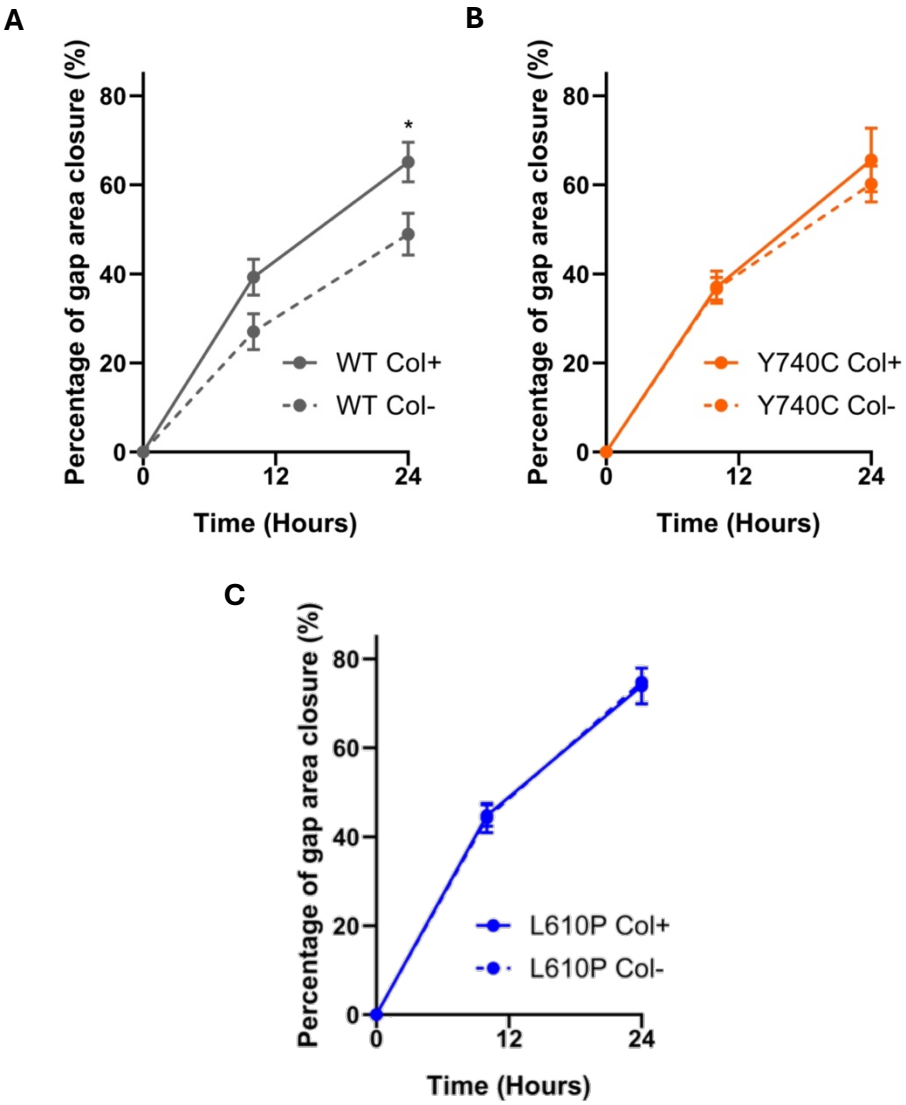


Figure 4. 5 Comparisons of gap closure percentages between cells migrating on non-collagen-coated and on collagen-coated surfaces.

Comparisons of the gap closure percentages between WT cells (**A**) or Y740C cells (**B**) or L610P cells (**C**) migrating on non-collagen-coated (Col-) and on collagen-coated (Col+) surfaces. Two-way ANOVA with Šídák's multiple comparisons test was performed. For WT cells, no significant difference was found at 10 hours of gap closure. *, p=0.0129 statistically significant difference was found at 24 hours of gap closure. For Y740C and L610P cells, no significant differences were found at both 10 and 24 hours of gap closure.

I then tested whether the increased HDF cell migration is dependent on DDR2 kinase activity. Cells were seeded into the inserts attached to an uncoated culture plate. Following insert removal, cells were cultured in medium containing 100 nM VU6015929, or 0.01% DMSO (vehicle control), over the imaging time. Again, when treated with vehicle control, L610P cells showed significantly quicker gap closure compared to the WT cells at 24 hours (**Figure 4. 6B**), but the differences were not as pronounced as obtained in the previous set of experiments with untreated cells, and there were no differences in gap closure rate of Y740C cells compared with WT cells (compare with **Figure 4. 3C**). For cells treated with VU6015929, no significant differences were found between the WT and mutant cell groups (**Figure 4. 6B**). I then compared the gap closure rate for each cell group cultured in vehicle control and VU6015929 medium (**Figure 4. 7A-C**). An increase in WT gap closure rate with VU6015929 treatment was observed, but the differences were not statistically significant (**Figure 4. 7A**). Similar gap closure rates were seen from L610P cells cultured with or without VU6015929 (**Figure 4. 7C**). These data suggested that the differences between WT and L610P migration on the non-coated surface (**Figure 4. 3C**) are not mediated by DDR2 kinase activity. However, Y740C cells exhibited a significantly higher gap closure rate at 24 hours with VU6015929 treatment compared with the vehicle treatment group (**Figure 4. 7B**). This unexpected increase indicated that DDR2 kinase activity may negatively regulate Y740C cell migration. However, further experiments would be needed to confirm whether these results are consistently obtained.

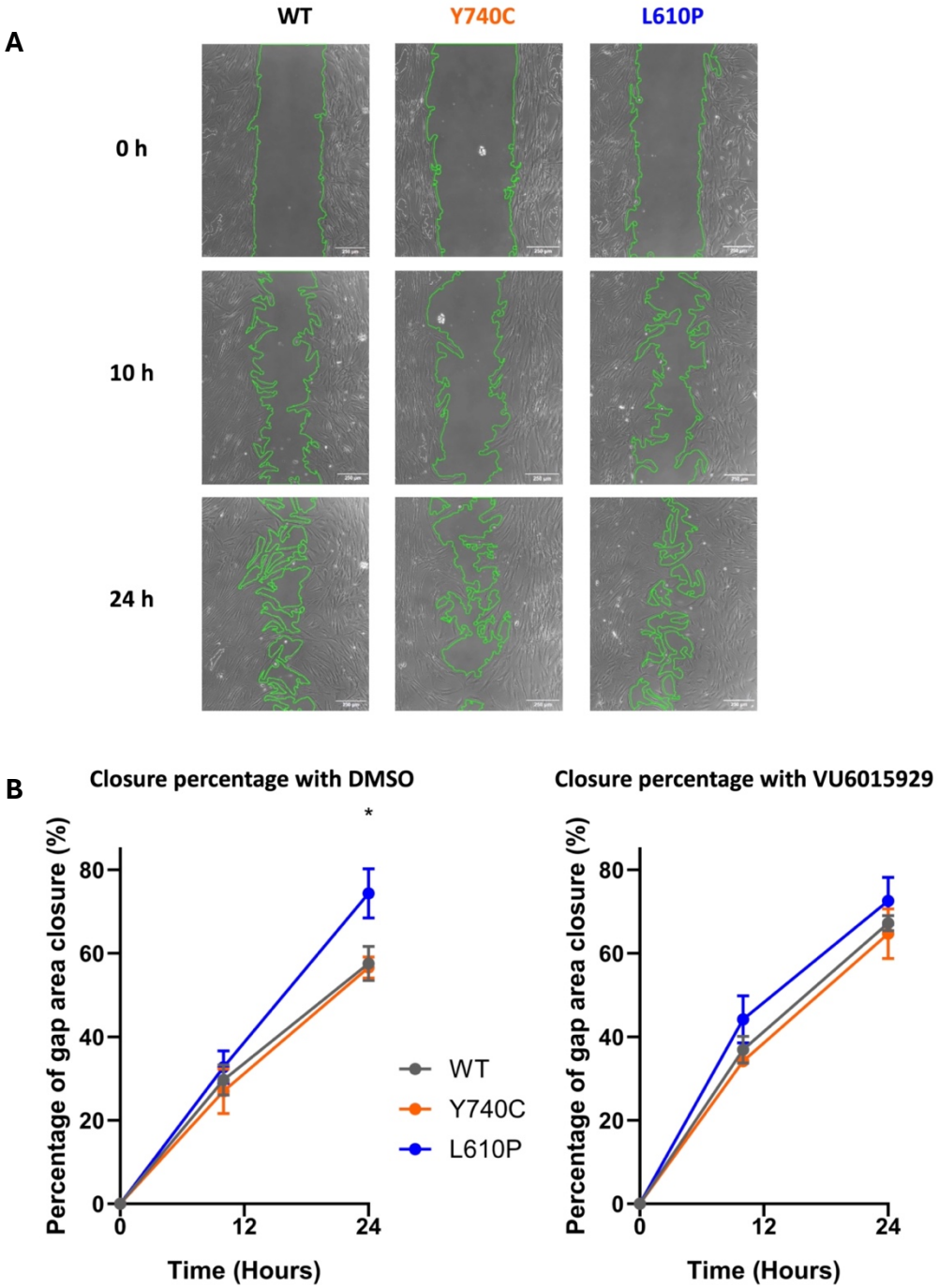


Figure 4. 6 HDF cells wound healing assay on a non-collagen-coated plate in the presence of 100 nM VU6015929.

A. HDF cells were seeded into commercial wound healing inserts, placed into collagen-coated 24-well cell culture plate and allowed to grow until full confluence. 24 hours of serum starvation was performed before removing the inserts. The cells were then cultured in medium solution containing 0.01% DMSO or 100 nM VU6015929 and allowed to migrate with widefield images taken at 0, 10, and 24 hours using a Zeiss Axio Observer equipped with an EC Plan-Neofluar 10X/0.30 Ph1 objective. Representative images are shown with the cell-free gap areas indicated with green lines. The cell-free gap areas were analysed using FIJI software with a macro obtained from the Facility for Imaging by Light Microscopy (FILM) at Imperial College London.

B. The cell-free gap areas from different time points is expressed as a percentage of the area at 0 hours with mean and standard error of the mean shown (n=3). Two-way ANOVA with Tukey's multiple comparisons test was performed. *, p=0.0101 statistically significant difference of the gap closure percentage between WT and L610P cells cultured in DMSO medium was found at 24 hours. No significant differences were found between cells cultured in VU6015929 medium.

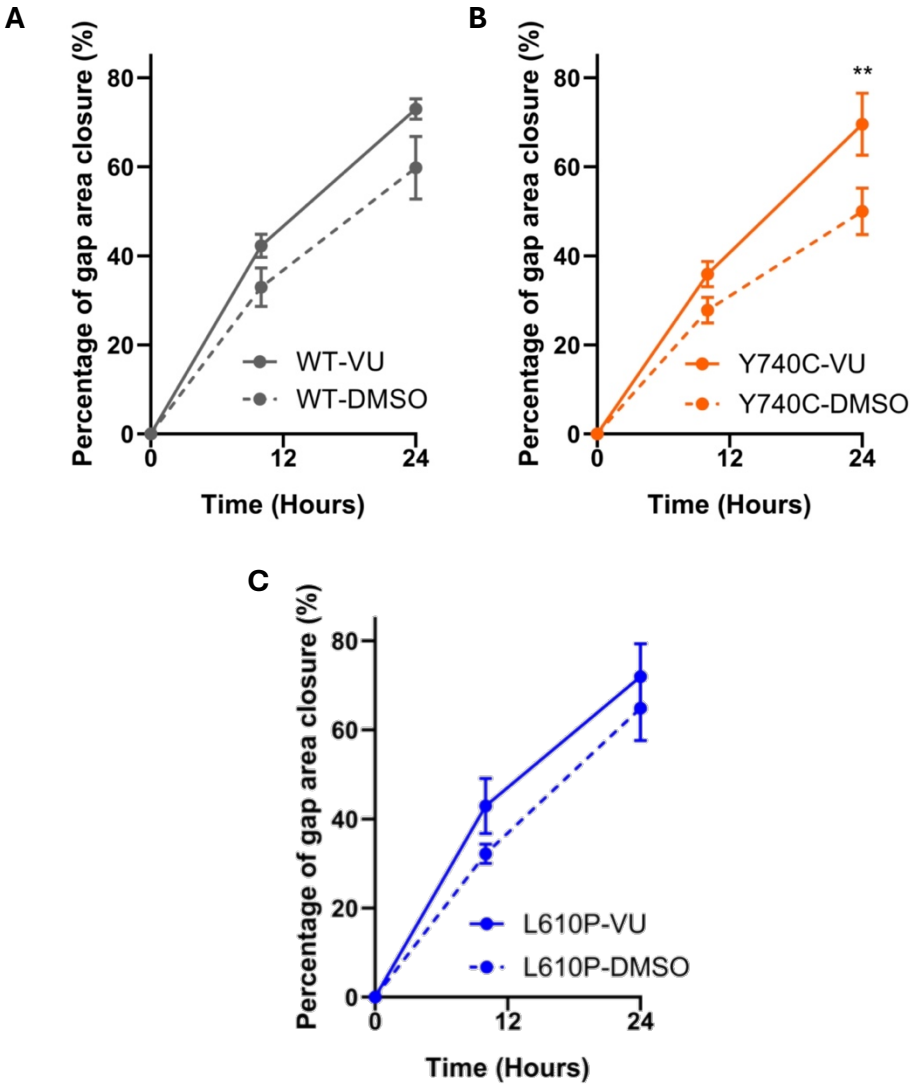


Figure 4. 7 Comparisons of gap closure percentages between cells cultured in DMSO medium and 100 nM VU6015929 medium (non-coated surface).

Comparisons of the gap closure percentages between WT cells (**A**) or Y740C cells (**B**) or L610P cells (**C**) cultured in DMSO medium and medium containing 100 nM VU6015929. Two-way ANOVA with Šídák's multiple comparisons test was performed. For WT and L610P cells, no significant differences were found at both 10 and 24 hours of gap closure. For Y740C cells, no significant difference was found at 10 hours of gap closure. **, p=0.0074 statistically significant difference was found at 24 hours of gap closure.

As the increased L610P cell migration on the non-coated surface was not regulated by DDR2 kinase activity, I then asked whether blocking other kinase activities using the broad kinase inhibitor dasatinib could reduce the L610P gap closure rate. In addition, testing inhibitors other than VU provides insight into whether applying inhibitors in this wound healing assay is sufficient to induce any changes in gap closure rate. The wound healing assay on an uncoated surface was performed with the medium containing 200 nM dasatinib, or 0.01% DMSO (vehicle control), over the imaging time. Due to time constraints, this assay was only performed once. The optimal dasatinib concentration was chosen based on a preliminary experiment (data not shown). Cell migration across 24 hours of incubation was inhibited in all three cell groups, with notable cell loss seen in Y740C and L610P cells (**Figure 4. 8**). These data suggested that dasatinib-targeted kinase activity is required for HDF cell migration to occur on the non-coated surface.

When performing the experiment, I observed cell morphology changes that are not noticeable in **Figure 4. 8**. To further investigate the morphology change, cells were then cultured in the medium containing 200 nM dasatinib or 0.01% DMSO, and images were recorded in the same area on the culture wells for four days. Similar to what was observed in the wound healing assay (**Figure 4. 8**), both mutant cells showed an obvious cell number reduction on day one, with L610P cells being more sensitive to dasatinib treatment than Y740C cells (**Figure 4. 9**). WT cell numbers were also somewhat reduced by the inhibitor treatment as observed on day one, with no apparent changes in cell numbers over the course of the experiment when cultured in the presence of dasatinib. This is in contrast to both mutant cell groups, which exhibited visible increases in cell numbers under dasatinib treatment conditions, starting from day two (**Figure 4. 9**). Moreover, after four days of dasatinib treatment, Y740C cells had grown to full confluency, similar to the vehicle treatment group (**Figure 4. 9, day four images**). These data suggested that both patient cells might be able to become resistant to dasatinib treatment and recover from the dasatinib-induced proliferation stop. However, the data presented here are preliminary, and cell proliferation assays would be required to confirm this observation.

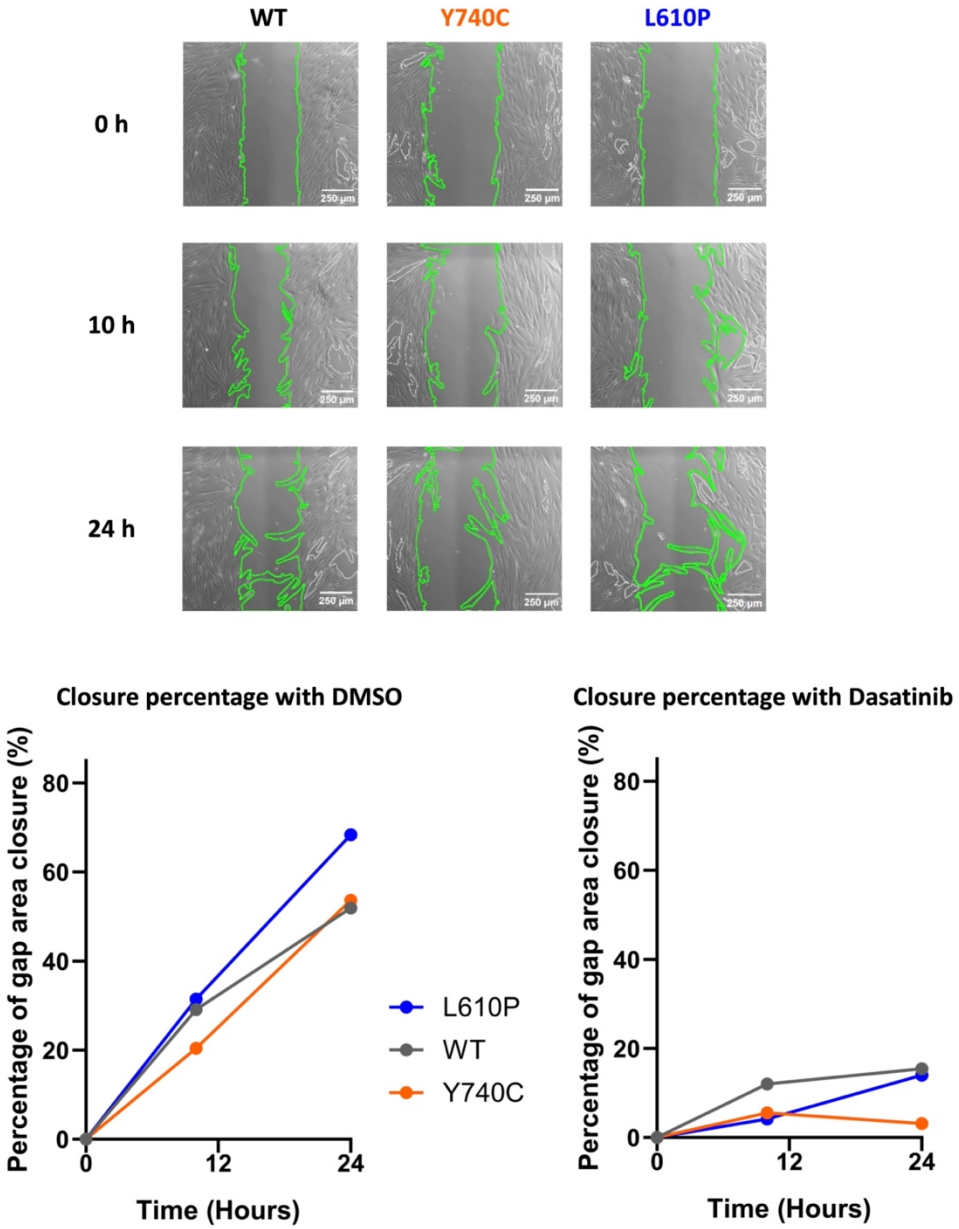


Figure 4. 8 HDF cells wound healing assay on a non-collagen-coated plate with 200 nM dasatinib treatment. HDF cells were seeded into commercial wound healing inserts, placed into collagen-coated 24-well cell culture plate and allowed to grow until full confluence. 24 hours of serum starvation was performed before removing the inserts. The cells were then cultured in medium solution containing 0.01% DMSO or 200 nM dasatinib and allowed to migrate with widefield images taken at 0, 10, and 24 hours using a Zeiss Axio Observer equipped with an EC Plan-Neofluar 10X/0.30 Ph1 objective. Representative images are shown with the cell-free gap areas indicated with green lines. The cell-free gap areas were analysed using FIJI software with a macro obtained from the Facility for Imaging by Light Microscopy (FILM) at Imperial College London. The cell-free gap areas from different time points is expressed as a percentage of the area at 0 hours (n=1).

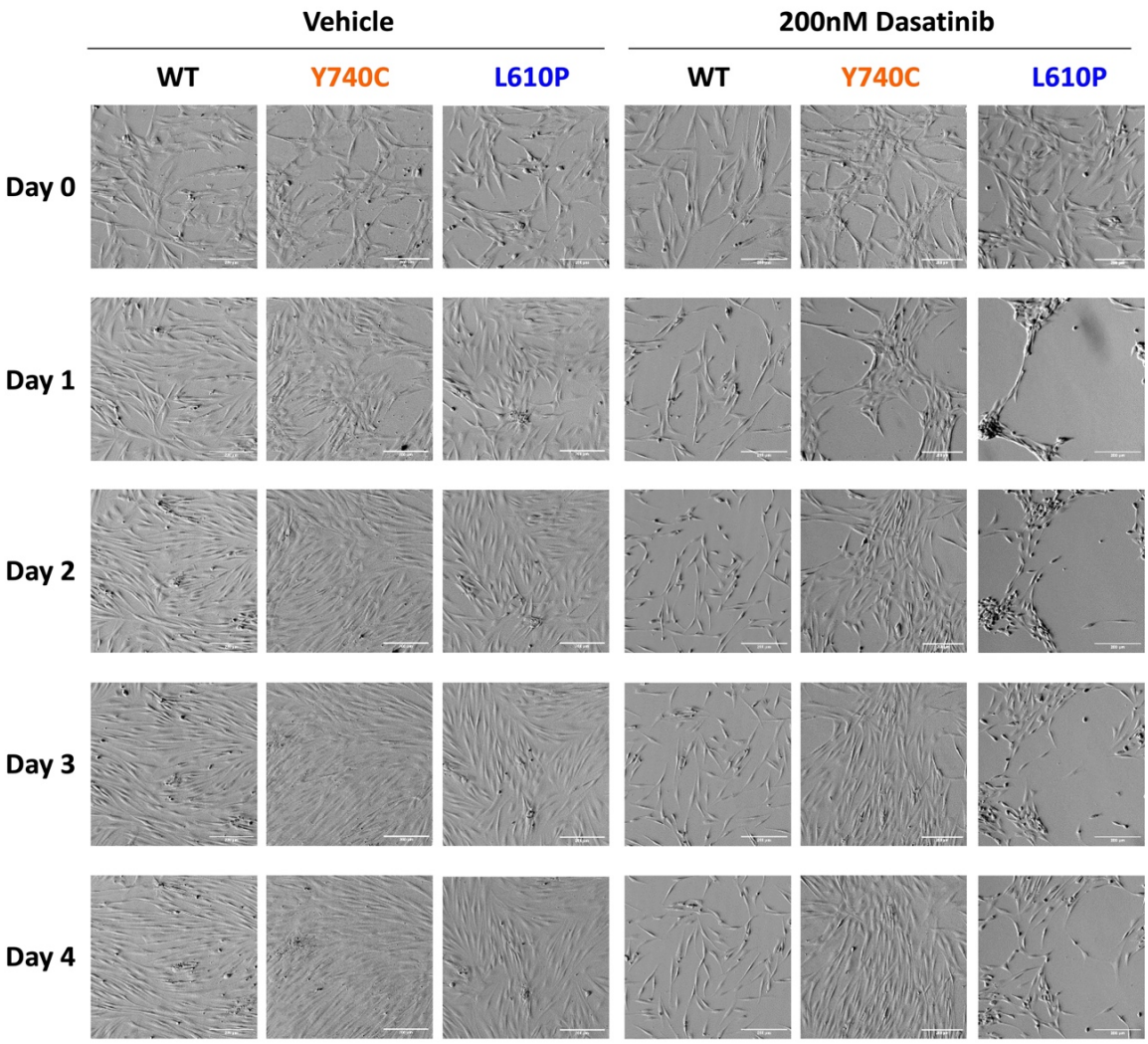


Figure 4. 9 HDF cell morphology change upon 200 nM dasatinib treatment.
HDF cells were seeded onto coverslips and allowed to grow until full confluence. 24 hours of serum starvation was then performed. The cells were then cultured in medium solution containing 0.01% DMSO (vehicle) or 200 nM dasatinib. Widefield images were taken using an EVOS XL Core imaging system at the same area on the coverslips daily for four days. Experiment was performed once.

4.2.3 HDF cells expressing DDR2-Y740C exhibit increased collagen gel contraction

During the wound healing process, fibroblasts are the major players in the proliferation and remodelling stages, and fibroblast-induced tissue contraction enables wound closure (Bainbridge, 2013). However, excessive contraction can lead to scarring and even contracture formation (Van De Water et al., 2013, Chitturi et al., 2015), as seen in Warburg Cinotti syndrome patient cases (Xu et al., 2018, Ours et al., 2022). Therefore, I examined the HDF cells' ability to contract collagen gels, as a mimic for tissue contraction, to check whether this cellular behaviour is exaggerated in patient HDF cells, compared with WT cells. The *in vitro* models of fibroblast-populated collagen matrix contraction were considered valid mimics of

real-life tissue contraction (Ngo et al., 2006, Levi-Schaffer et al., 1999, Garbuzenko et al., 2002). There are three standard models for performing collagen gel contraction assays that are widely used: the floating, the attached, and the stressed matrix models, as illustrated in **Figure 4. 10** (Howard et al., 2003). In the floating matrix model, gels are mechanically released from the culture plate immediately after polymerisation, leaving the gel floating and contracting without restriction. In contrast, gels are kept adhesive to the culture plate in the attached and stressed matrix models, thereby building up isometric tension in the horizontal dimension (Zhang et al., 2022). The compaction in the attached matrix model only happens in the vertical dimension due to mechanical resistance (Toki et al., 2013). However, in the stressed matrix model, gels are released two days after the initial attaching period, allowing rapid contraction to dissipate the isometric tension. These three models are widely used as a mimic for certain aspects of the *in vivo* processes, i.e., the initial wound contraction, the granulation tissue contraction, and the end of wound contraction, respectively (Zhang et al., 2022, Howard et al., 2003). The gels from the attached matrix models are not released from the culture plate, making it difficult for data collection. Thus, the floating and the stressed matrix models were used to investigate Warburg Cinotti patient HDF cell collagen gel contractility. The HDF cells were embedded into collagen gels, which were then polymerised at 37°C for 1 hour. The gels were then released immediately (floating model) or remained attached (stressed model) for two days before releasing, followed by culturing in the medium with a decreased amount of serum for the indicated time at 37°C. Daily images were taken from the top of the gels, which were then analysed by measuring the gel area with FIJI software (**Figure 2. 3**). The data was presented as the percentage of the original area at the start of the assay (day zero). In the floating matrix assay, the Y740C cell-populated gels showed strong contraction from 10 hours of gel releasing (**Figure 4. 11**). Among all the groups, Y740C gels contracted the most, while L610P gels contracted the least (**Figure 4. 11B**). However, there were no significant differences when either of them was compared with the WT group (**Figure 4. 11B**). When the stressed matrix model was applied (**Figure 4. 12**), significantly enhanced gel contraction was seen from both mutant cell-populated gels compared to the WT gels across all time points, with Y740C cells showing a large increase in gel contraction compared with WT cells (**Figure 4. 12B**). These data suggested both disease mutant HDF cells exhibit high gel contractability in the model

representing the end stage of wound healing, during which the scarring and contracture could form.

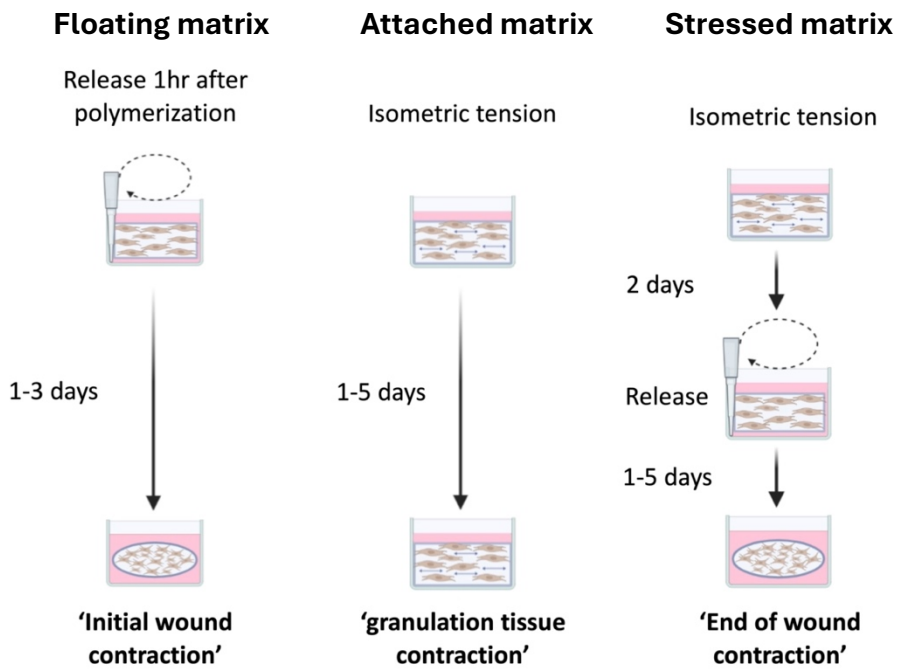


Figure 4. 10 Schematic diagram of three collagen gel contraction assay models.
Three standard models for collagen contraction assay are illustrated. In the floating matrix model, 3D collagen gel matrices populated with cells are manually released from the culture plate immediately after gel polymerization, which mimics the initial wound contraction. In contrast, gel matrices remain attached to the culture plate in the attached matrix model to mimic the granulation tissue contraction. In the stressed matrix model, gels are kept attached for two days before being released from the culture plate, which mimics the end of wound contraction. An adaptation of Figure 11 from (Howard et al., 2003).

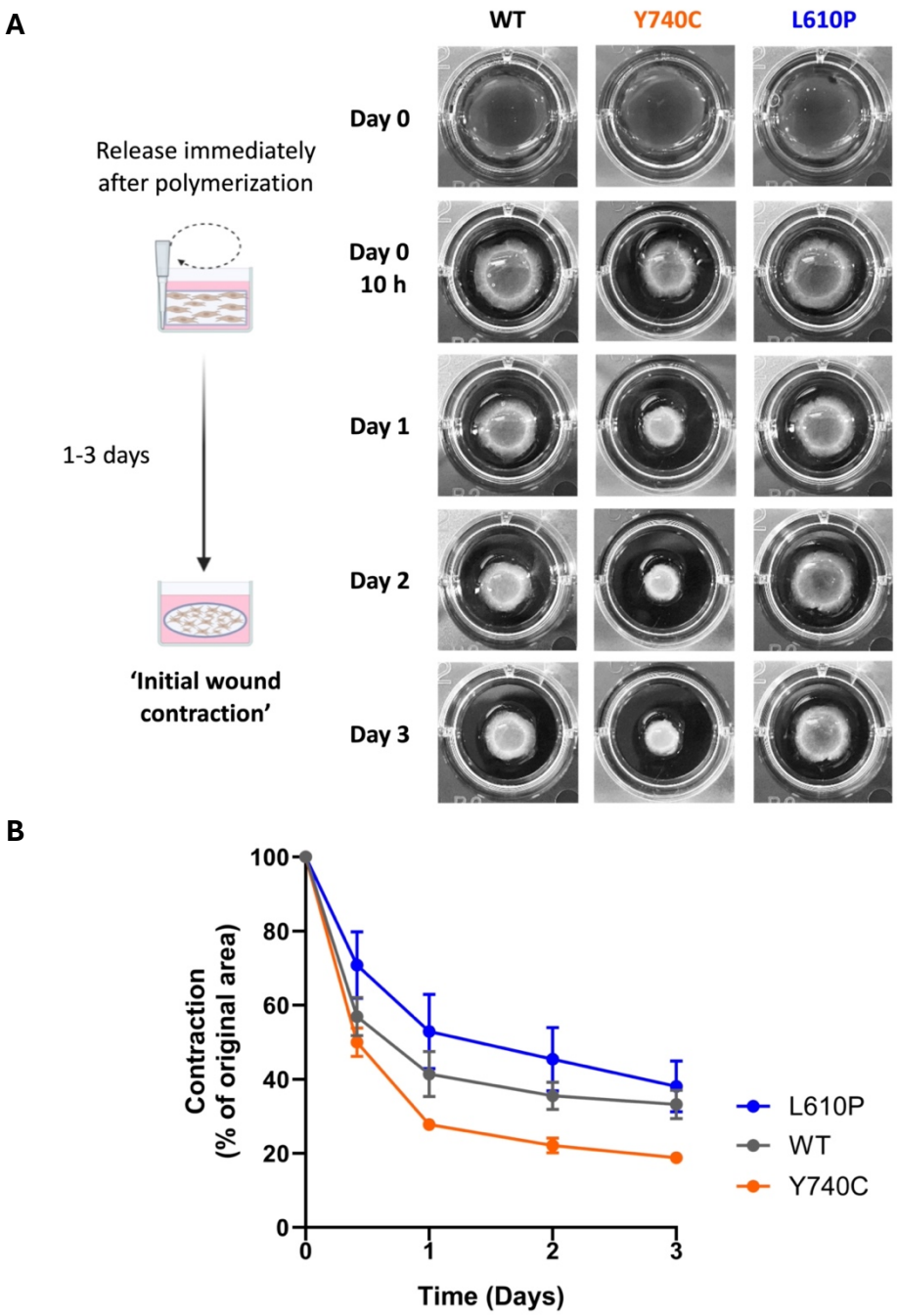


Figure 4. 11 Collagen gel contraction by HDF cells in the floating matrix model.
A. HDF cells were embedded into a 3D collagen gel matrix, which was then manually separated from the well plate surface immediately after gel polymerisation. Images were taken using an iPhone 11 Pro at regular intervals, up to 3 days after gel releasing. Images from one of the three biological replicate experiments are shown. Gel areas were measured using the 'Freehand selections' and 'Measure' functions in FIJI software.
B. Gel area size was normalised to the area size of the culture well border from the same image, and the data are presented as the percentage of the original gel area obtained on day zero, with mean and standard error of the mean shown (n=3). Two-way ANOVA with Tukey's multiple comparisons test was performed. No significant differences were found between WT and Y740C gel contractions and between WT and L610P gel contractions at all time points.

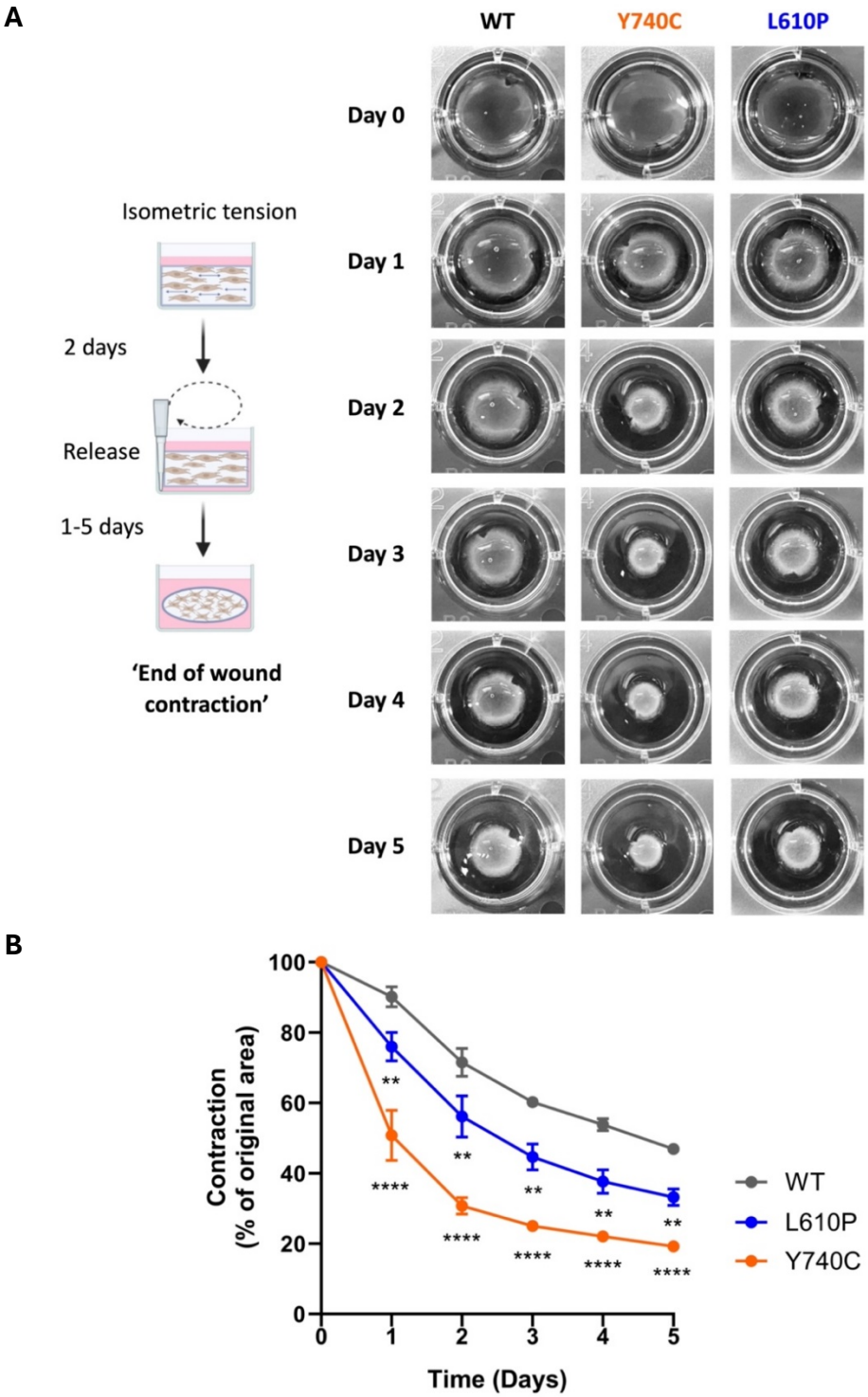


Figure 4. 12 Collagen gel contraction by HDF cells in the stressed matrix model.

A. HDF cells were embedded into a 3D collagen gel matrix, which was incubated for two days at 37°C before being separated from the well plate surface. Images were taken using an iPhone 11 Pro at regular intervals, up to 5 days after gel releasing. Images from one of the three biological replicate experiments are shown. Gel areas were measured using the 'Freehand selections' and 'Measure' functions in FIJI software.

B. Gel area size was normalised to the area size of the culture well border from the same image, and the data are presented as the percentage of the original gel area obtained on day zero, with mean and standard error of the mean shown (n=3). Two-way ANOVA with Tukey's multiple comparisons test was performed. Statistically significant differences between WT and L610P gel contractions were found among all time points (**, p=0.0063, p=0.0029, p=0.0026, p=0.0018, and p=0.0085, respectively). p<0.0001 statistically significant differences were found between WT and Y740C gel contractions at all time points (****, p<0.0001).

4.2.4 DDR2-Y740C expressing HDF cells induced collagen gel contraction via a DDR2 kinase activity-independent manner

I then examined whether DDR2 kinase activity is required for fibroblast-induced collagen gel contraction in the stressed matrix model. To this end, I applied the DDR-specific inhibitor VU6015929. HDF cell-populated collagen gels were cultured in the medium with a decreased amount of serum and containing either 100 nM VU6015929 or 0.01% DMSO during the two-day period where the gels were attached to the wells. Gels were then released from the wells and incubated with the same medium as before releasing for five days (**Figure 4. 13**). For WT cell-populated gels, the gel areas were significantly larger in the wells with inhibitor addition, compared to the wells incubated with vehicle control (**Figure 4. 14A**). This was particularly noticeable on day five where the gel area increased from 60% (vehicle control) to 80% (with inhibitor) of the original gel area (**Figure 4. 14A**). L610P cell-populated gel contraction was also reduced with VU6015929, but with high variance between replicates, as seen in the inhibitor-treated group (**Figure 4. 14C**). The differences of contraction between inhibitor and DMSO-treated L610P gels were not statistically significant. These data suggested that DDR2 kinase activity is involved in fibroblast-induced gel contraction with a stressed matrix model, as observed from the data with WT cells and indicated by the data obtained from the L610P cells. Surprisingly, no differences in Y740C gel areas were observed with or without DDR-specific kinase inhibitor treatment across all time points (**Figure 4. 14B**). As HDF cell autophosphorylation assay showed that VU6015929 inhibitor does block Y740C kinase activity (**Figure 4. 2B**), the absence of gel size change in inhibitor-treated Y740C gel suggested that factors other than constitutive DDR2 kinase activity primarily promote Y740C cell contractility. It is important to note that DDR2-Y740C protein could still be involved in mediating the increased gel contraction, as kinase-independent signalling has been demonstrated for both DDR1 and DDR2 (Juin et al., 2014, Barcus et al., 2021).

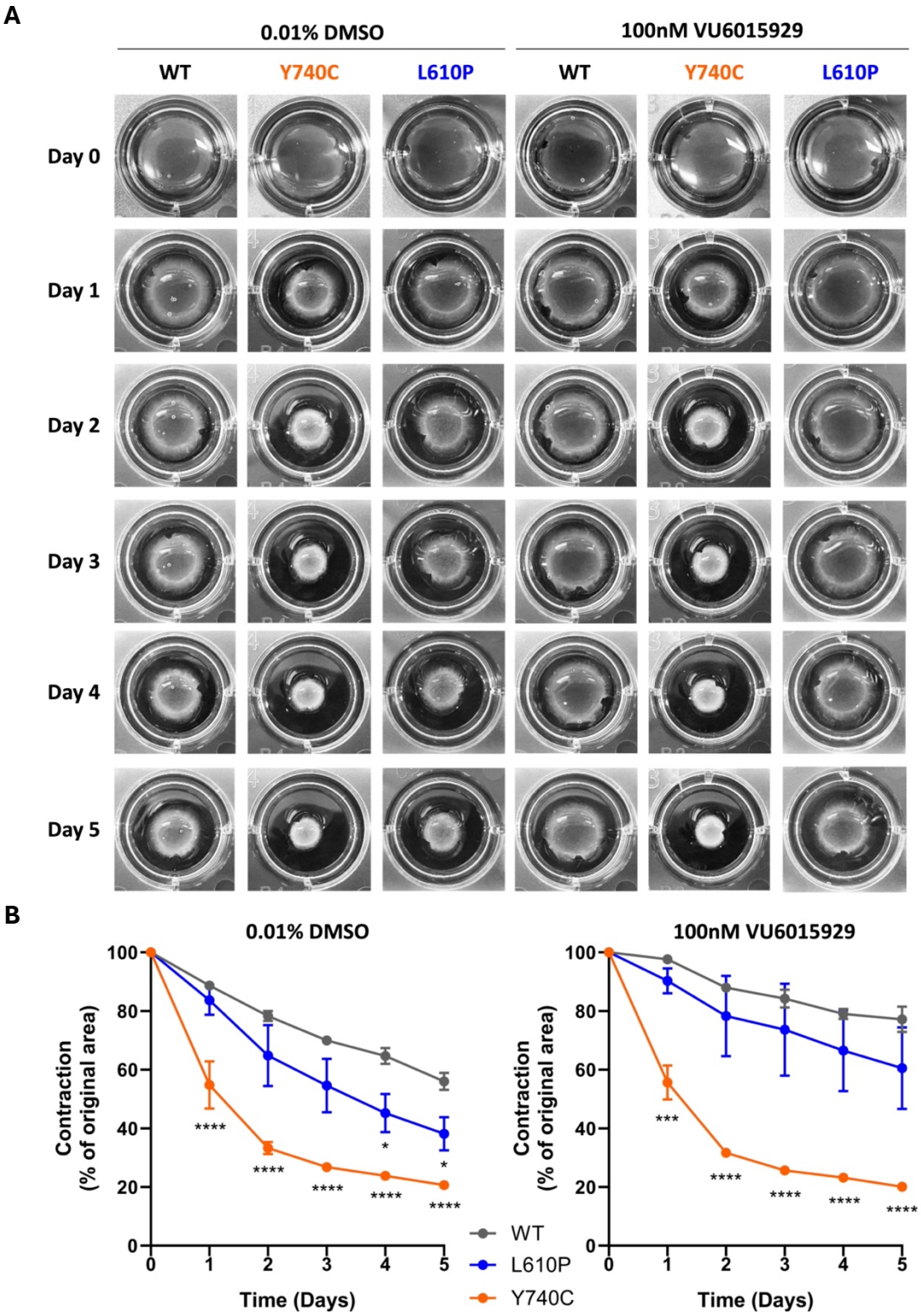


Figure 4. 13 Collagen gel contractions by HDF cells in the stressed matrix model in the presence of 100 nM VU6015929.

A. HDF cells were embedded into a 3D collagen gel matrix, which was incubated for two days at 37°C before being separated from the well plate surface. Gels were incubated with medium containing 0.01% DMSO (vehicle) or 100 nM VU6015929 for both the initial attached period and the period in which the gel was floating in the medium. Images were taken using an iPhone 11 Pro at regular intervals, up to 5 days after gel releasing. Images from one of the three biological replicate experiments are shown. Gel areas were measured using the 'Freehand selections' and 'Measure' functions in FIJI software.

Continued on the next page.

Figure 4.13. continued

B. Gel area size was normalised to the area size of the culture well border from the same image, and the data are presented as the percentage of the original gel area obtained on day zero, with mean and standard error of the mean shown (n=3). Two-way ANOVA with Tukey's multiple comparisons test was performed. In DMSO group, p<0.0001 statistically significant differences were found between WT and Y740C gel contractions among all time points (****, p<0.0001). Statistically significant differences were found between WT and L610P gel contractions on day 4 and 5 (*, p= 0.0137, p= 0.0251). In VU6015929 group, statistically significant differences were found between WT and Y740C gel contractions at all time points (***, p=0.0005 ; ****, p<0.0001)

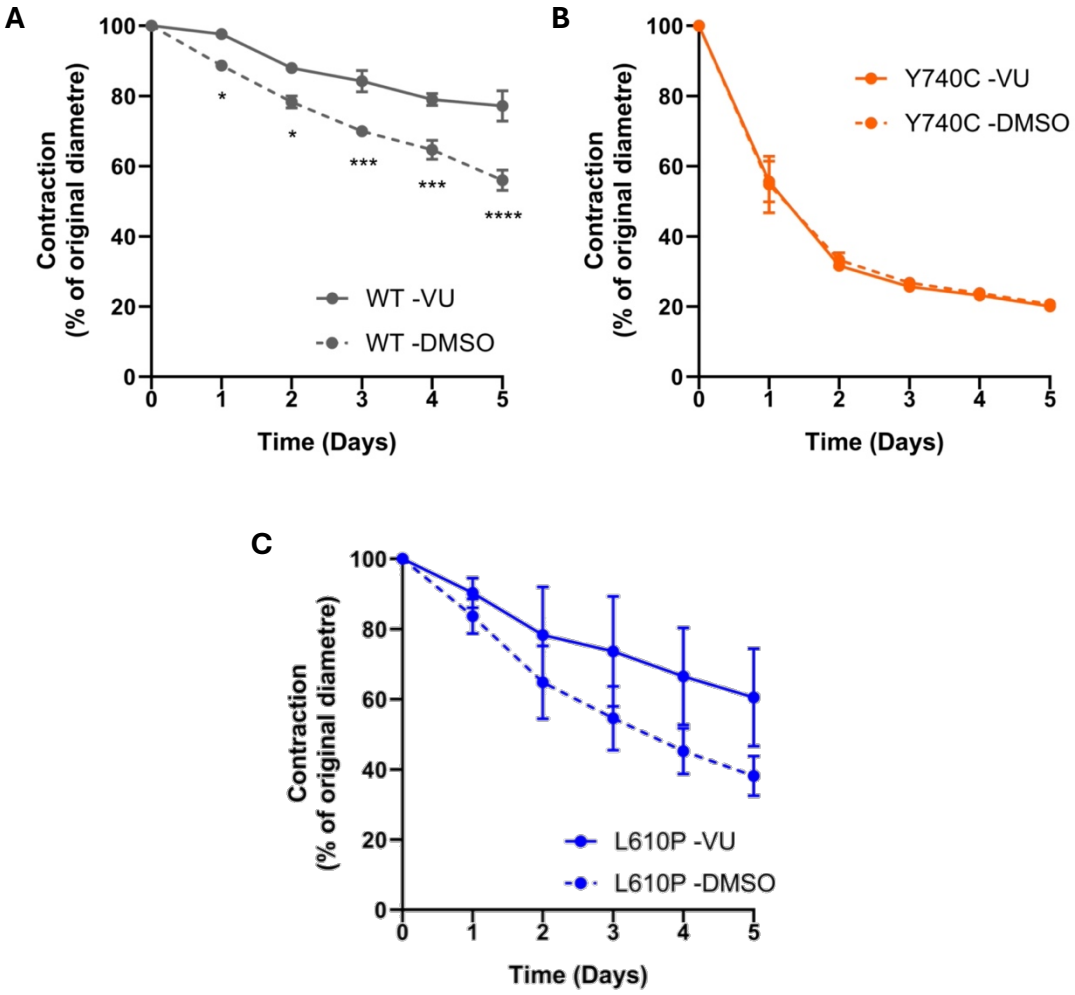


Figure 4. 14 Comparisons of the gel contraction between cells cultured in DMSO medium and 100 nM VU6015929 medium. (stressed matrix model)

Comparisons of the gel contraction between WT cells (**A**) or Y740C cells (**B**) or L610P cells (**C**) cultured in DMSO medium and medium containing 100 nM VU6015929. Two-way ANOVA with Šídák's multiple comparisons test was performed. For WT cells, significant differences were found between WT and Y740C gel contractions among all time points (*, p=0.0372, p=0.0208; ***, p=0.0004, p=0.0004; ****, p<0.0001). For Y740C and L610P cells, no significant differences were found at all time points.

During wound healing and contraction, fibroblasts respond to signals of the tissue microenvironment and differentiate into myofibroblasts, which is the predominant cell type present in the granulation tissue (Li and Wang, 2011, Tomasek et al., 2002). These two cell types can be easily distinguished, as myofibroblasts are known for adapting smooth muscle-like features, in particular, expressing the α-SMA protein (Tschumperlin, 2013). An intermediate fibroblast phenotype, termed proto-myofibroblasts, is known to exhibit myofibroblast morphological characteristics, such as expressions of stress fibre containing cytoplasmic actin, but in the absence of α-SMA expression (Tomasek et al., 2002). It is possible that the strongly enhanced contraction seen in Y740C cell-populated gels (**Figure 4. 12, Figure 4. 13**) may be due to the HDF fibroblasts having transitioned to proto-myofibroblasts or differentiated into myofibroblasts. To investigate whether the Y740C HDF cells comprises a proportion of differentiated myofibroblasts before being embedded into collagen gel, α-SMA gene and protein expression levels in HDF cells were assessed. HDF cells were either grown on coverslips and stained for α-SMA and F-actin or lysed to extract total RNA and proteins for qPCR and Western blotting analysis, respectively. For IF analysis, a similarly low proportion of cells expressing α-SMA were observed from both WT and Warburg Cinotti patient cell groups (**Figure 4. 15A**). However, a significant reduction of α-SMA gene expression was seen in Y740C cells compared with WT cells (**Figure 4. 15B**). Likewise, Y740C cells also showed a trend of producing less α-SMA protein than WT cells, as observed by Western blotting (**Figure 4. 15C**). However, the differences were not statistically significant. Altogether, data suggested that it is unlikely that fibroblast to fully differentiated myofibroblasts transition occurred in Y740C cells before embedding the cells into gels. Next, I asked whether the broad-range kinase inhibitor dasatinib could block Y740C gel contraction in the stressed matrix model. HDF cells were embedded into 3D collagen gels and cultured in the medium with a decreased amount of serum and containing 200 nM dasatinib, or vehicle control, for a two-day attached period and then a five-day period in which the gels were floating in the medium. Both WT and mutant-embedded gels with dasatinib treatment failed to contract at all (**Figure 4. 16B**). Cell viability was checked after dasatinib treatment, and neither HDF cell group showed apparent cell death (data not shown). This suggested that dasatinib-targeted kinase activities are required for fibroblast-induced gel contraction.

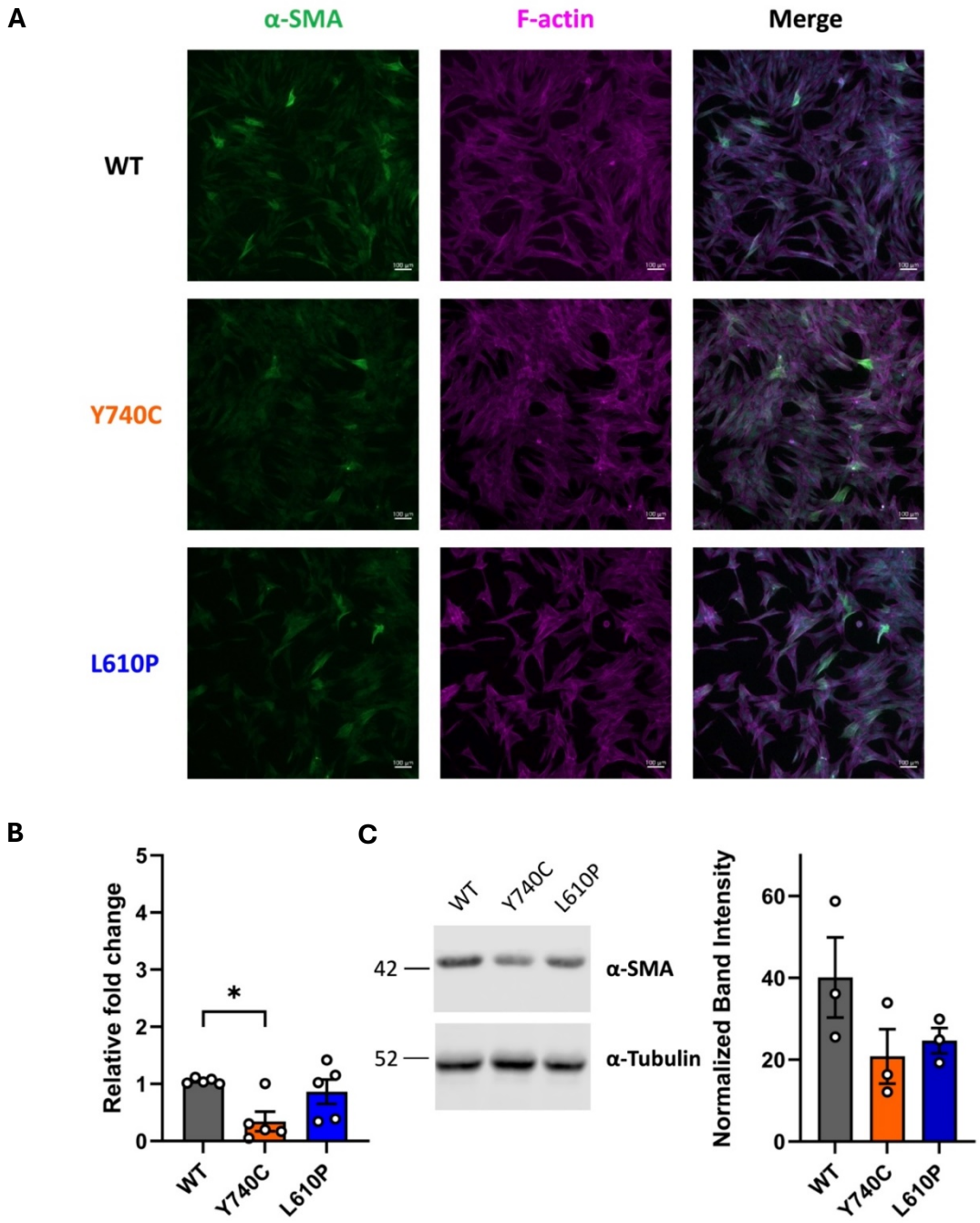


Figure 4. 15 Investigations of myofibroblast features.

A. HDF cells grew on coverslips were stained with anti-alpha-smooth muscle actin 1A4 antibody, followed by AlexaFluor 488 anti-mouse IgG (H+L) as well as Rhodamine-coupled phalloidin staining. Scale bar = 100 µm. Widefield images were acquired using Zeiss Axio Observer microscope equipped with an EC Plan-Neofluar 10X/0.30 Ph1 objective and Zen pro software. Images were prepared using Zen 3.5 blue edition software.

B. Total RNA was extracted from HDF cells, followed by reverse transcription and qPCR analysis. $\Delta\Delta C_T$ values were calculated by normalising the C_T values of the *ACTA2* gene to GAPDH. Data are presented as relative fold change of *ACTA2* gene expression levels from the patient samples *versus* the expression obtained from the WT cells using the $2^{-\Delta\Delta CT}$ methods. The final data is shown with mean and standard error of the mean (n=5). One-way ANOVA with Dunnett's multiple comparisons test was performed. WT vs Y740C; p=0.0152 (*).

C. HDF cell lysates were analysed by SDS-PAGE and Western Blotting with anti-alpha-smooth muscle actin 1A4 antibody and α-Tubulin antibody. The position of molecular weight markers (in kDa) is shown on the left. Quantification of the α-SMA signals normalised to respective Tubulin signals. The normalised signal is expressed as a percentage of the sum of all bands on a blot, with mean and standard error of the mean shown (n=3).

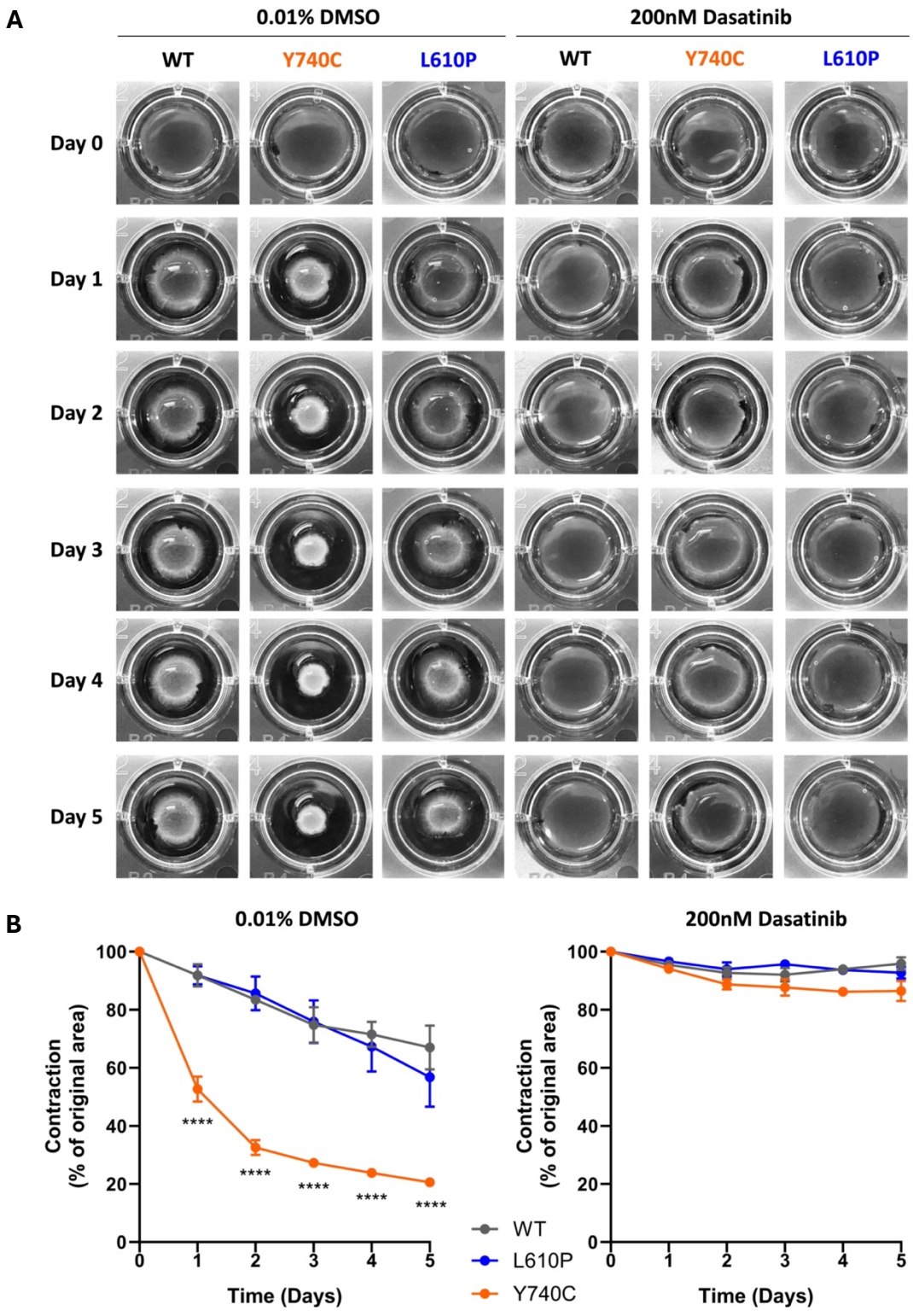


Figure 4. 16 Collagen gel contractions by HDF cells in the stressed matrix model in the presence of 200 nM dasatinib.

A. HDF cells were embedded into a 3D collagen gel matrix, which was incubated for two days at 37°C before being separated from the well plate surface. Gels were incubated with medium containing 0.01% DMSO (vehicle) or 200 nM dasatinib for both the initial attached period and the period in which the gel was floating in the medium. Images were taken using an iPhone 11 Pro at regular intervals, up to 5 days after gel releasing. Images from one of the three biological replicates are shown. Gel areas were measured using the 'Freehand selections' and 'Measure' functions in FIJI software.

Continued on the next page.

Figure 4.16. continued
B. Gel area size was normalized to the area size of the culture well border from the same image, and the data are presented as the percentage of the original gel area obtained on day zero, with mean and standard error of the mean shown (n=3). Two-way ANOVA with Tukey's multiple comparisons test was performed. Statistically significant differences between WT (-) dasatinib and Y740C (-) dasatinib gel contractions were found among all time points (****, $p<0.0001$). No statistically significant differences were found between WT (+) dasatinib and mutants (+) dasatinib gel contractions.

4.2.5 Investigation of β1 integrin activities in Patient HDF cells

Integrins are key ECM-binding receptors, which are obligate heterodimers comprising an α and a β subunit, in which combinations of two subunits generate 24 isoforms (Barczyk et al., 2010). Four isoforms containing the β1 subunit are collagen-binding receptors known to have cross-talk with DDRs (Leitinger, 2014, Leitinger, 2011). Several β1 integrins were also reported to play an important role in fibroblast-induced collagen contraction, myofibroblast differentiation, and dermal homeostasis (Schiro et al., 1991, Carracedo et al., 2010, Leask, 2013). To determine whether β1 integrin function is involved in HDF cell-induced collagen gel contraction, the β1 integrin function blocking mAb P5D2 (Xu et al., 2012) was used in the stressed matrix contraction assay. This experiment was only performed once, using WT and Y740C cells, due to the high amount of antibody needed in the experimental set-up. In brief, WT or Y740C-populated gels were incubated with medium containing 10 μg/mL P5D2 (saturation concentration for blocking β1 integrin function) for the initial attached period, as well as the period in which the gels are floating in the medium. In the absence of P5D2 antibody treatment (**Figure 4. 17B, left**), both WT and Y740C cell-populated gels contracted to a similar extent as observed in earlier contraction experiments (**Figure 4. 12B**). With antibody treatment, gels containing either WT or Y740C cells underwent minor contraction (**Figure 4. 17B, right**), indicating that HDF cell-induced gel contraction requires functional β1 integrins in both WT HDF cells and Y740C HDF cells.

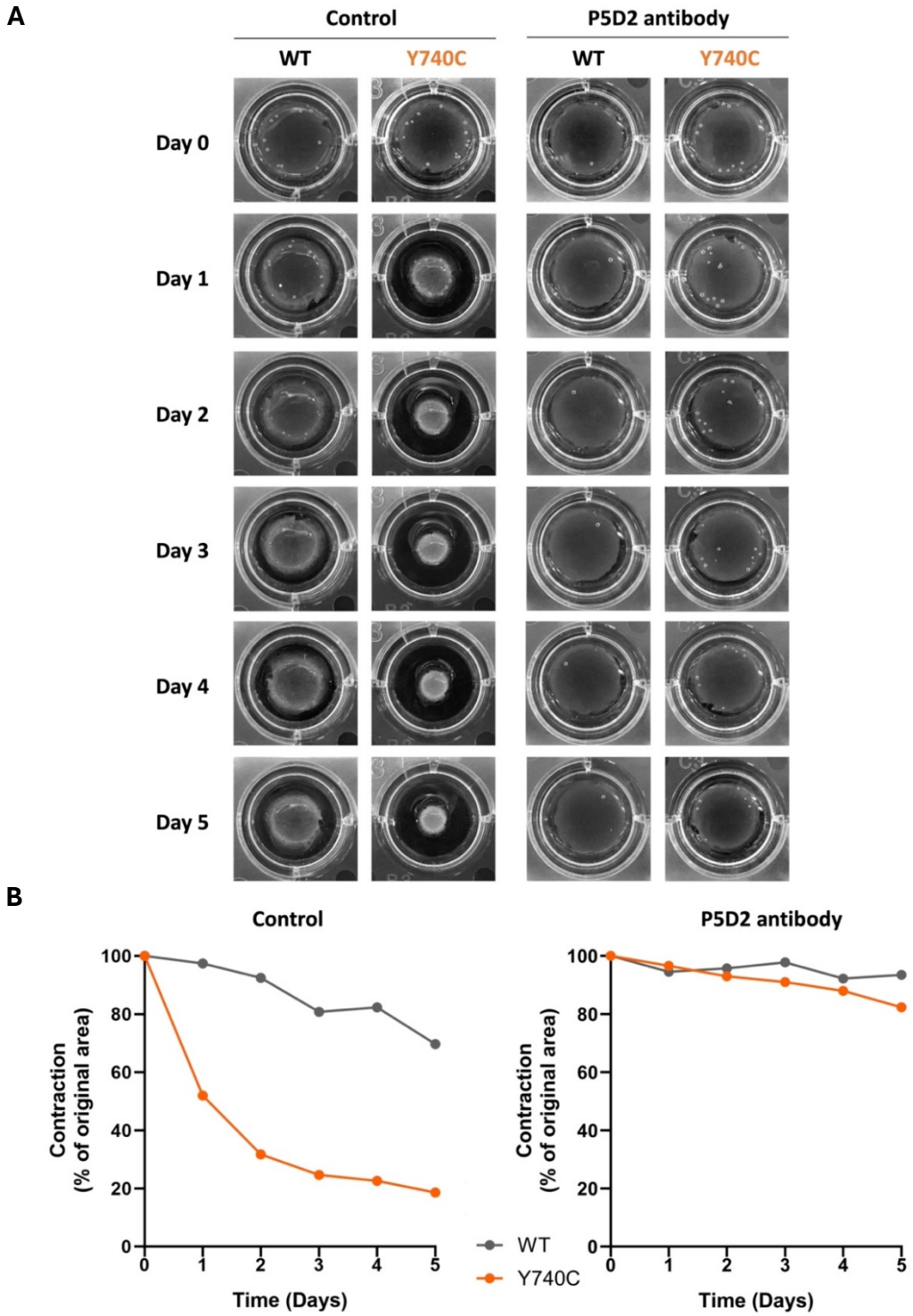


Figure 4. 17 Collagen gel contractions by HDF cells in the stressed matrix model in the presence of 10 µg/mL P5D2 antibody.

A. HDF cells were embedded into a 3D collagen gel matrix, which was incubated for two days at 37°C before being separated from the well plate surface. Gels were incubated with medium solution containing 10 µg/mL BSA (control) or 10 µg/mL P5D2 antibody for both the initial attached period and the period in which the gel was floating in the medium.

Images were taken using an iPhone 11 Pro at regular intervals, up to 5 days after gel releasing. Images from one of the three biological replicates are shown.

B. Gel areas were measured using the 'Freehand selections' and 'Measure' functions in FIJI software. Gel area size was normalized to the area size of the culture well border from the same image, and the data are presented as the percentage of the original gel area obtained on day zero (n=1).

Next, I asked whether β1 integrin activities were changed in patient HDF cells, compared to WT cells. Collagen-binding β1 integrins recognise and bind to specific amino acid motifs in fibrillar collagens. Synthetic triple-helical peptides encompassing various integrin binding motifs have been used for affinity studies and to evaluate the function of distinct collagen binding integrins in various cell-based assays (Xu and Kirchner, 2021). The α2β1 integrin binds to GxOGER motifs, in which the binding affinity decreases in order for x=F>L>M>A (Siljander et al., 2004). For α1β1 integrin, the most potent ligand was identified as the GLOGEN motif (Hamaia et al., 2012). Cell adhesion to collagen-mimetic peptides of various affinity towards distinct collagen-binding integrins provides insights into integrin activity (Siljander et al., 2004, Xu et al., 2012). A previous study using cell adhesion assays onto wells coated with integrin-binding peptides of varying affinity showed that DDR overexpression and/or activation enhances α1β1 and α2β1 integrin-induced cell adhesion (Xu et al., 2012). Therefore, five β1 integrin binding-peptides were used to measure integrin activities in HDF cells. GFOGER, GLOGER, GMOGER, and GAOGER are α2β1 integrin binding-peptides with the affinity decreasing in order, while GLOGEN has high affinity to α1β1 integrin. 96-well plates were coated with collagen I or β1 integrin-binding peptides, followed by incubating calcine-AM-stained HDF cells at 37°C for 40 minutes. The plate was washed four times to remove non-adherent cells before recording the fluorescence signal. As expected, the adhesion of both WT and mutant cells to collagen I and the high-affinity peptides α2β1-binding peptides GFOGER and GLOGER was similar for all tested cell groups (**Figure 4. 18**). Cell adhesion to α2β1-binding GMOGER and GAOGER was to a similar extent for WT and Y740C cells. However, Y740C cells displayed a significantly increased adhesion to α1β1 ligand GLOGEN compared with WT cells (**Figure 4. 18**). This showed a higher α1β1 integrin activity in Y740C cells than in WT cells. In contrast, compared with WT cells, L610P cells exhibited significant decreases in cell adhesion to α2β1 integrin ligands GMOGER and GAOGER, and to α1β1-binding peptide GLOGEN (**Figure 4. 18**), indicating that both α1β1 and α2β1 activity were lower in L610P cells, compared with WT cells. To determine whether the differences seen in cell adhesion were due to altered β1 integrin expression, flow cytometry was used to analyse β1 integrin surface expression levels. HDF cells were stained with antibodies against α1, α2, and β1 integrin subunits, followed by a FITC-labelled secondary antibody. Flow cytometry analysis showed that all three cell groups expressed comparable levels of α1, α2, and β1 subunits, with slightly

lower α2 expression found in L610P cells (**Figure 4. 19**). These data suggested that mutant HDF cells both exhibited changed integrin activity without regulating their expression levels.

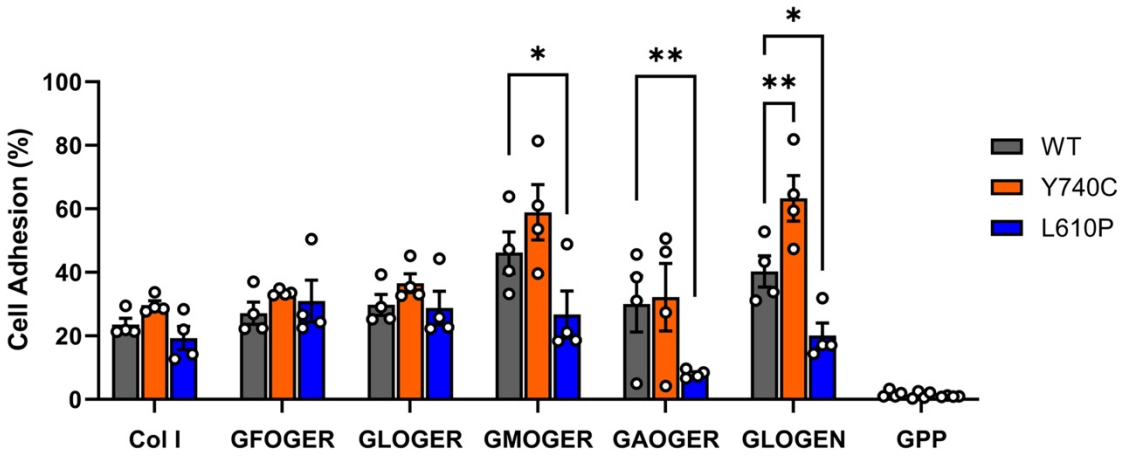


Figure 4. 18 Mutant HDF cells exhibited changed adhesion to medium- and low-affinity integrin-specific collagen peptides.
Immulon® 2HB plate was coated 10 μg/mL collagen I or 10 μg/mL β1 integrin-specific collagen peptides as well as non-receptor binding peptide GPP10 at 4°C overnight. The plate was then washed and blocked. Calcein-AM labelled HDF cells were allowed to adhere to the plate at 37°C for 40 minutes. Non-adherent cells were removed by washing. Fluorescence signals (485/520 nm) were measured using a Spark® plate reader. Data were normalized to the total fluorescence reading and presented as the percentage of cell adhesion.

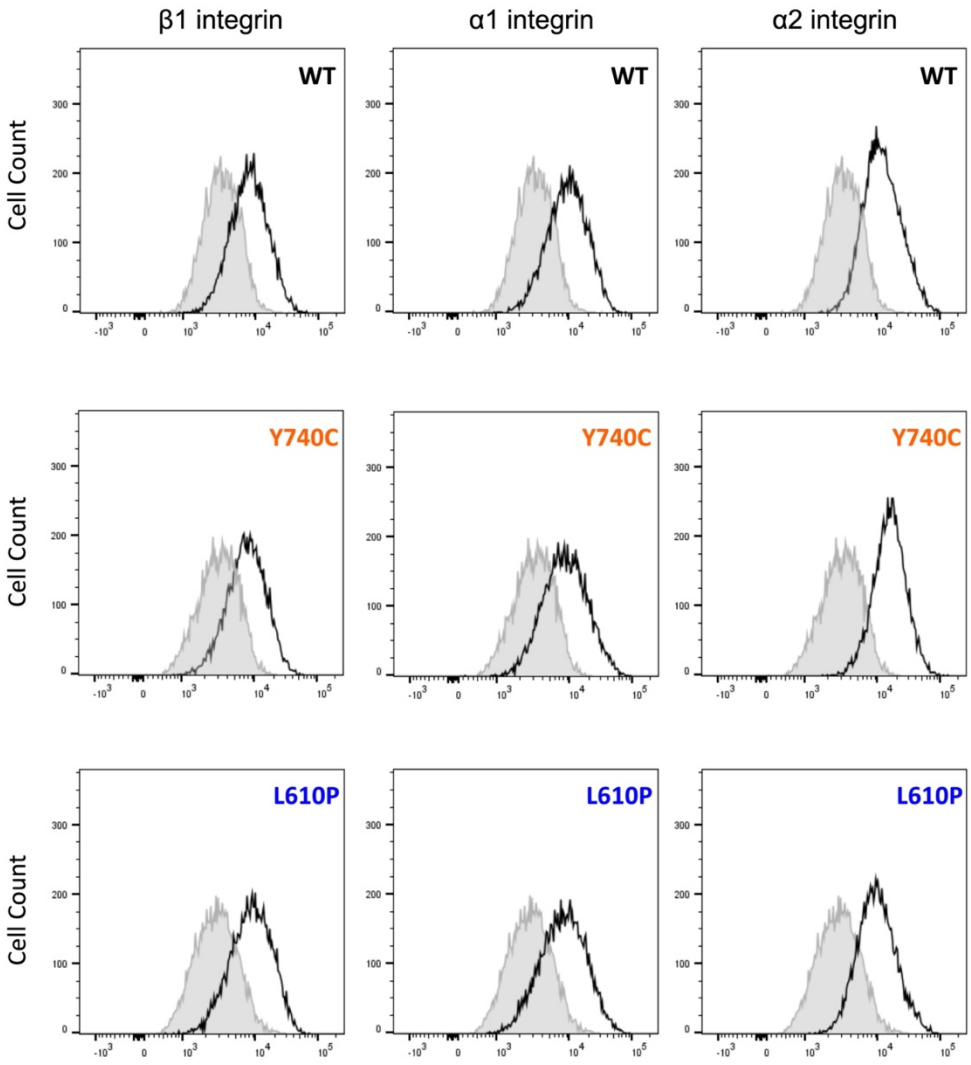


Figure 4. 19 HDF cell surface expressed collagen-binding integrin subunits detection by flow cytometry.
HDF cells were stained with anti-integrin β1 mAb P5D2, anti-integrin α1 mAb FB12 or anti-integrin α2 mAb AK7 antibodies, followed by FITC-labelled anti-mouse-Fc antibody and analysis by flow cytometry. The filled grey histograms represent secondary antibody only staining, while the open histograms represent anti-integrin and secondary antibody staining.

4.3 Discussion

In **Chapter 3**, I discovered that the soluble DDR2-Y740C kinase has higher catalytic activity than DDR2-WT kinase. Additionally, a full-length DDR2 study using an overexpression system revealed that DDR2-L610P and DDR2-Y740C lead to ligand-independent receptor activation. In this chapter, the constitutive DDR2 autophosphorylation was found in patient HDF cells (**Figure 4. 2**). Previous studies have shown that DDR2 regulates several cellular processes of fibroblasts, such as proliferation, migration, and fibroblast-induced contraction (Olaso et al., 2002, Olaso et al., 2011). Thus, I speculated that the constitutive DDR2 activity in patient HDF cells might result in changed cellular behaviours. The cell functions were investigated by wound healing (migration) assays and collagen gel contraction assays, with altered cellular behaviours observed in patient cells (**Figure 4. 3, Figure 4. 4, Figure 4. 12**). My data suggested that constitutive DDR2 activity in patient HDF cells was not the main factor that drove the changed patient HDF cell functions (**Figure 4. 6, Figure 4. 13**). Thus, as an additional target, the activity of collagen-binding receptor β1 integrin was assessed in HDF cells (**Figure 4. 18, Figure 4. 19**).

In this chapter, patient HDF cell lysates were analysed by Western blotting with anti-pY740 and anti-DDR2 antibodies. The cells were lysed in the lysis buffer with a non-ionic detergent, which previously showed impaired mutant DDR2 extraction from HEK293 cells (**Figure 3. 19A**). Although the DDR2 extraction from WT or mutant HDF cells was sufficient to detect total DDR2 and phosphorylated DDR2 by Western blotting, it would be beneficial to test HDF cell lysis in SDS loading buffer with β-mercaptoethanol to see if this method allows better detection of DDR2 by Western blotting. Concentrating endogenously expressed DDR2 proteins with anti-DDR2 antibody and IP was unsuccessful, presumably due to low affinity of the antibody for DDR2. A recent study has been able to immunoprecipitate DDR2 from lung fibroblasts (Ling et al., 2024). The anti-DDR2 antibody used in this study was not available when I performed IP; thus, it would be interesting to test this antibody in our cell system. Custom-made anti-pY antibodies against the JM4 region of DDRs, anti-pY569/538 and anti-pY586/538, were tested for detecting DDR2-specifc phosphorylation, with only weak signals obtained from Western blotting results. It was important to use an antibody that detects DDR-specific phosphorylation signals; hence I used the anti-pY740 antibody. Other phospho-proteins, such as FAK can migrate to the same region on SDS-PAGE as DDR2, which could cause signals to be

mistaken for one another (Herrera-Herrera and Quezada-Calvillo, 2012). The anti-pY740 antibody is the only commercially available antibody that has been used to detect DDR-specific phosphorylation (Sala et al., 2022, Barcus et al., 2021). In **Chapter 3**, although the anti-pY740 antibody was mainly targeting the tyrosine that has been mutated to cysteine in the DDR2-Y740C-K soluble construct, phosphorylation signals were still detectable from the *in vitro* autophosphorylation experiment (**Figure 3. 16A**); hence, this antibody must cross-react with other phosphorylated activation loop tyrosines (Y736, Y741). Here, the phosphorylation signals obtained from the Y740C patient cells would be predominantly from DDR2-WT but could also contain signals from phosphorylated DDR2-Y740C activation loop tyrosines. Alternative approaches can be considered for detecting DDR2 autophosphorylation. For instance, Xu et al. used a commercial human phospho-DDR2 DuoSet IC Elisa kit and successfully detected DDR2 phosphorylation signals from HDF cells (Xu et al., 2018). In this assay, an immobilised DDR2 capture antibody binds to DDR2 proteins regardless of their phosphorylation status, and a pY-specific antibody is used to detect phosphorylation signals from DDR2. The DDR2 antibody tested in my IP experiments did not provide high affinity to native DDR2, as very little DDR2 enrichment was observed in IP samples over cell lysate samples (data not shown); this commercial kit could be suitable for concentrating and detecting DDR2 phosphorylation. Alternatively, a small HiBiT tag could be knocked into immortalised control or patient HDF cells by using the CRISPR/Cas9 technique. This tag can be detected by an antibody or bind to a larger subunit LgBiT, resulting in a reconstituted luciferase enzyme complex that generates bright luminescence (Schwinn et al., 2020).

In the wound healing assay, patient cells exhibited a significantly higher gap closure rate compared with WT cells on the non-coated 2D surface (**Figure 4. 3C**), whilst all three cell groups showed similar gap closure rates on a collagen-coated surface (**Figure 4. 4B**). It is known that optimal cell-to-substratum adhesiveness and cell contractile forces contribute to maximal cell migration, under conditions which are suitable for forming new adhesion and breaking the trailing attachment (Tschumperlin, 2013). As discussed in **Chapter 3**, DDR2-L610P and DDR2-Y740C may have reduced protein solubility in non-ionic detergent (**Figure 3. 19**), indicating potential increases associations between the variant DDR2 proteins and the cytoskeleton. Thus, changed assembly and disassembly of the cytoskeleton or focal adhesion in patient cells may mediate HDF cell migration on the uncoated surface. Moreover, the DDR-

specific kinase inhibitor VU6015929 failed to block migration on the non-coated surface in all three HDF cell groups (**Figure 4. 6**), demonstrating that DDR2 kinase activity is not the critical regulator in HDF cell migration.

The gap closure of WT HDF cells was quicker on the collagen-coated surface than on the non-coated surface (**Figure 4. 4C**). This aligns with the finding that immobilised collagens can promote HDF migration by forming optimal integrin binding (Li et al., 2004). However, the gap closure rates of both mutant cells were similar on either non-coated or collagen-coated surfaces (**Figure 4. 5B, C**). It remains unclear why their migration rates were unaffected by the substratum they walked on. Fibroblasts are known to produce their own matrix to support the connective tissue (Fisher et al., 2008, Malakpour-Permlid et al., 2021). It is possible that patient cells secrete more matrix than WT cells on a non-coated surface, in which the secreted matrix provides support for mutant cell migration.

Interestingly, I observed a significant activity reduction of collagen-binding receptor β1 integrin in L610P cells compared with WT cells (**Figure 4. 18**). As discussed above, cell migration is mediated by cell-to-substratum adhesiveness (Tschumperlin, 2013), where strong adhesion can result in weak cell migration. It is possible that L610P cell migration is mediated by the downregulated α1β1 and α2β1 integrin adhesion activities. Integrin activation is regulated by the binding of talin and other scaffolding proteins, which facilitates integrin clustering and recruits other signalling proteins such as FAK and Src (Tadokoro et al., 2003, Hynes, 2002, Kenny and Connelly, 2015). A study has shown that fibroblast migration on fibronectin requires β1 integrin-recruited FAK activation (Zhao et al., 2016b). FAK is a non-receptor tyrosine kinase that undergoes phosphorylation in multiple steps to become catalytically active (Acebron et al., 2020). In brief, the FAK intramolecular autoinhibitory interactions are first disrupted to allow transphosphorylation to happen on Tyr397, followed by recruitment of Src kinase to further phosphorylate Tyr576 and 577, which results in a fully activated FAK (Zhou et al., 2021). Several studies have shown inhibition of FAK and Src phosphorylation by dasatinib treatment (Caccia et al., 2010, El Sayed et al., 2018, Tsukahara et al., 2017). Dasatinib treatment inhibited both WT and mutant cell migration on the non-coated surface (**Figure 4. 8**). This suggested that dasatinib may target the focal adhesion signalling pathways in HDF cells, resulting in the migration stop and cell morphology change. Interestingly, mutant cells showed resistance to continuous dasatinib treatment, and a clear

increase in mutant cell confluency was observed after two days of the treatment (**Figure 4. 9**). It remains unclear why mutant HDF cells reacted differently than WT cells to the long-term dasatinib treatment**.** However, dasatinib-induced FAK activation was observed in c-Myc-driven hepatocellular carcinoma (HCC), suggesting a paradoxical effect of dasatinib treatment in various disease models (Liu et al., 2018). Thus, it will therefore be important in future to explore the dasatinib effect in FAK activation using Warburg Cinotti patient samples.

In the collagen gel contraction assay, Y740C cells-populated collagen gels displayed strongly enhanced contraction in the stressed matrix model (**Figure 4. 12B**), compared with WT cells. However, the enhanced contraction caused by Y740C cells could be blocked only by broad-range kinase inhibitor dasatinib (**Figure 4. 16B**), but not the DDR-specific inhibitor VU6015929 (**Figure 4. 14B**). This suggested that dasatinib-targeted kinases are involved in regulating Y740C cell contraction. As discussed above, dasatinib can target proteins from β1 integrin signalling pathways. DDR1 expression levels have been shown to positively promote the interactions between β1 integrin and fibrillar collagen, which then subsequently recruited integrin binding partners and signalling molecules (Staudinger et al., 2013). Thus, it is possible that DDR2 in Y740C cells interacts with β1 integrin or its downstream signalling factors differently than in WT and L610P cells. Therefore, this relationship may play a role in the promotion of fibroblast-induced collagen gel contraction. From the cell adhesion assay, an increase in α1β1 integrin activity was observed in Y740C cells (**Figure 4. 18**). α1β1 has been shown as an important regulator for fibroblasts to myofibroblast differentiation (Rodriguez et al., 2009). This again emphasises the necessity of future research to focus on DDR2 and integrin-mediated focal adhesion. Apart from this, it would also be interesting to perform single-cell RNA sequencing (scRNA-seq) and single-cell proteomics (SCP) of HDF cells after incubating the cells in stressed gel contraction models, which would allow the investigation of HDF cells in response to mechanical forces (Ahmad and Budnik, 2023).

Primary cells from patient biopsies serve as a powerful tool to study molecular phenotypes, enabling a rational decision of which signalling pathway or cell functions to be further investigated in immortalised cell lines (Pan et al., 2009). However, not only does a limited lifespan lead to experimental inconvenience, but the cell characteristics may also change along with subsequent passages (Richter et al., 2021). Hence, HDF cells used in this report were limited to early culture passages to avoid potential genetic alterations caused by cell

culture (Neumann et al., 2010). One major limitation of these experiments is that WT cells were only obtained from a single donor, and primary cells derived from different donors can behave conflictingly even if they are identified as healthy (Kawecki et al., 2022). It is important to increase the diversity of control samples and minimise donor variability. Moreover, the patient cells were also obtained from single donors due to the rarity of the Warburg Cinotti syndrome. It was not possible to obtain biopsies from additional patients to expand the sample diversity. Alternatively, a better option would be using CRISPR/Cas9 with immortalised primary cells to engineer the DDR2 mutations into WT HDF cells. This approach allows the analysis of endogenously expressed DDR2 WT and mutations in the same genetic background, which would provide evidence that any biochemical or functional difference was conclusively due to the DDR2 mutations and not contingent on other concomitant variations. In addition, knocking down DDR2 expression in immortalised WT cells and identifying phenotype changes would provide insights into the cellular functions of the mutants. I was expecting to obtain immortalised HDF cells from our collaborator; however, due to technical difficulties, cell immortalisation was not finished before the end of this project. Besides the potential cell experiment, introducing heterozygous mutations using CRISPR/Cas9 generating mouse models of Warburg Cinotti syndrome would facilitate studies more relevant to humans.

In summary, constitutive DDR2 receptor activation has been demonstrated in patient HDF cells, in which the phosphorylation can be abolished by the DDR-specific inhibitor. Patient cells exhibited changed cell behaviours, with L610P cells migrating quicker on the non-coated surface and Y740C cells inducing enhanced collagen gel contraction, both compared to WT cells. Moreover, β1 integrin activities were different in patient cells than WT cells. Cell functional analysis in the presence of DDR2-specific inhibitor showed that DDR2 is not the only regulator in changed patient HDF cell behaviour (i.e. migration, cell-induced gel contraction), and whether DDR2 are involved in integrin-mediated focal adhesion remains to be determined.

Chapter 5 Regulation of signalling by Warburg Cinotti Syndrome DDR2 variants in patient primary dermal fibroblasts

5.1 Introduction

In previous chapters, it was shown through DDR2 autophosphorylation assays that Warburg Cinotti DDR2 variants showed constitutive receptor activation in both the DDR2 overexpression system (**Chapter 3**) and patient HDF cells (**Chapter 4**). Moreover, I discovered that HDF cells carrying different Warburg Cinotti variants displayed varying β1 integrin activities and the ability to induce collagen gel contraction. It is yet to be determined if these two variants influence different signalling pathways or regulate the expression levels of specific genes. Gain-of-function mutations in RTKs often induce aberrant downstream signalling transduction (Lahiry et al., 2010, Montor et al., 2018). For example, lung cancer-related EGFR missense mutation leads to receptor hyperphosphorylation which subsequently activates canonical EGFR signalling pathways (Red Brewer et al., 2013). Although my data suggested the DDR2 kinase activity was not the primary factor in causing changes in HDF cell functions, DDR1 and DDR2 have been shown to regulate other proteins in a kinase-independent way (Juin et al., 2014, Ling et al., 2023). Unlike RTKs that are well studied, less is known about DDR2 downstream proteins. Studies have shown that DDR2 can regulate the activities of some common signalling molecules (i.e. Src, Akt, and p38) and the expression level of MMPs (i.e. MMP2) (Ikeda et al., 2002, Jia et al., 2018, Zhu et al., 2021, Yu et al., 2021). Thus, exploring the phosphorylation status or expression levels of key signalling molecules in patient HDF cells is therefore important.

In this chapter, cell lysates and RNAs extracted from both WT and Warburg Cinotti patient HDF cells were used to investigate selected signalling molecule activities and gene expression levels. It was hypothesised that DDR2 variants induce enhanced cell signalling and regulate gene expression in Warburg Cinotti patient cells. The aims were: (1) to analyse a group of key signalling molecules' expression or phosphorylation status using a phospho-array kit or Western blotting; (2) to analyse the gene expression levels of selected genes known to influence cell signalling.

5.2 Results

5.2.1 Determination of signalling molecules' phosphorylation or expression levels in HDF cells

Considering the time and cost-effectiveness, a commercial membrane-based phospho-array kit was used to explore the phosphorylation/expression of signalling molecules in HDF cells. This kit contains membranes with phospho-specific antibodies targeting serine/threonine and tyrosine phosphorylation sites in 37 common signalling proteins. It also detects protein expression levels of β-catenin and heat shock protein 60 kDa (Hsp60). In brief, target-specific antibodies are embedded as duplicates on the membranes which capture the signalling proteins from the cell lysates. Then, a phospho-/protein- specific antibody cocktail is applied for the detection of phosphorylation/total expression levels. Information on signalling proteins and their phosphorylation sites can be found in Appendix (**Table 7. 1**). HDF cells were cultured in complete medium until 80% confluency, followed by 24 hours serum starvation with SFM. Cells were then stimulated with or without collagen I for 4 hours before lysis. Cell lysates were applied to the membranes, followed by antibody incubation, wash steps, and signal acquisition using the manufacturer's protocol. Average pixel intensity from the duplicate spots were determined and normalised against an average background signal from each membrane (**Figure 5. 1**). Although the signals for most of the tested sites were weak, both positive (**Figure 5. 1, p1-3**) and negative (**Figure 5. 1, n1-2**) reference spots showed expected intensity, indicating a valid assay was performed. For samples from different cell lines, data obtained at each tested site was very similar, with small changes seen in β-Catenin expression and Erk 1/2 phosphorylation (**Figure 5. 2**). WT and L610P cells expressed similar levels of β-Catenin, while a higher expression was seen in Y740C cells without collagen treatment (**Figure 5. 2, 1**). Moreover, β-Catenin expression was slightly enhanced in WT cells stimulated with collagen, compared with untreated WT samples (**Figure 5. 2, 1, grey bars)**. In contrast, Y740C cells treated with collagen expressed less β-Catenin than those without collagen treatment (**Figure 5. 2, 1, orange bars**). The β-Catenin expression was unaffected in L610P cells by collagen treatment (**Figure 5. 2, 1, blue bars**). In the untreated cells, the levels of Erk 1/2 phosphorylation were identical in WT and Y740C samples but slightly lower in L610P samples (**Figure 5. 2, 2**). Upon collagen treatment, the phosphorylation in Erk 1/2 increased slightly in WT and L610P cells, whereas it decreased in Y740C cells (**Figure 5. 2, 2**). This assay,

acting as an initial screening for the identification of potential downstream factors, was only performed once and provided preliminary data. As mentioned above, DDR2 signalling is much less explored than other RTKs. Although the phosphorylation/ expression levels of some signalling molecules were found somewhat different in WT and mutant cells, the results from this experiment did not highlight any obvious changes and therefore did not allow the identification of relevant downstream proteins for DDR2.

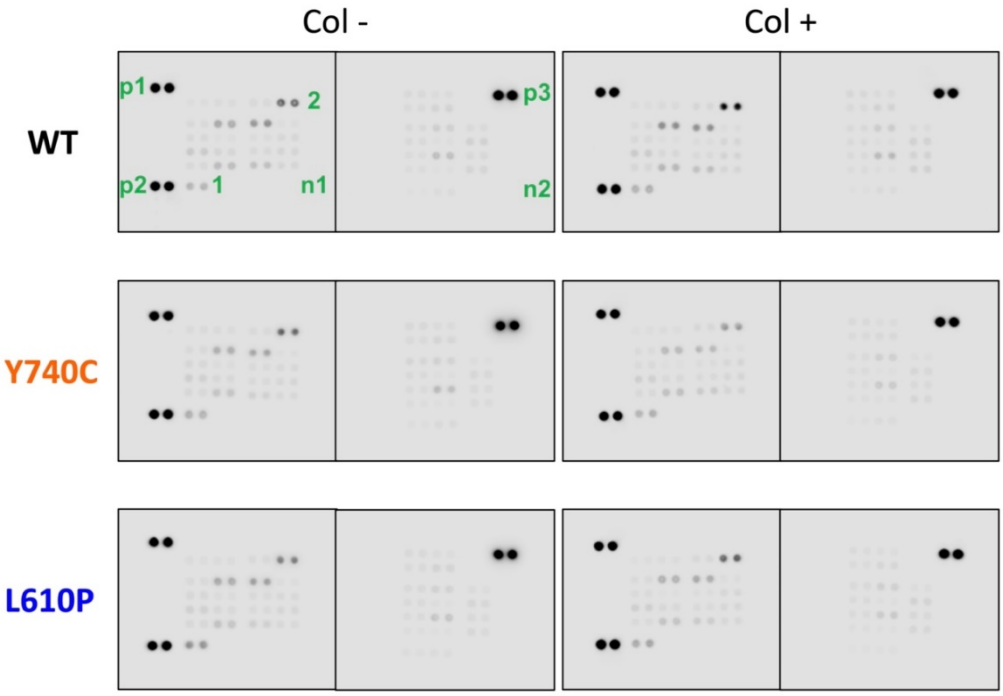


Figure 5. 1 Detection of phosphorylation or expression status of selected signalling molecules by phospho-array.

HDF cells were grown in multiple 100 mm dishes and serum starved for 24 hours before being incubated with or without 20 µg/mL collagen I for 4 hours at 37°C. Cells were then lysed and the cell lysates were applied to the phospho-array kit following the manufacturers' protocol. This experiment was only performed once. Phospho-array blots are shown with capture antibodies spotted in duplicates. p1-3 indicate the location of positive control spots and n1-2 indicate the location of negative control spots. 1 indicates the location of β-catenin capture spots, and 2 indicates the location of phospho-Erk1/2 capture spots. Col -, without collagen treatment; Col + with collagen treatment.

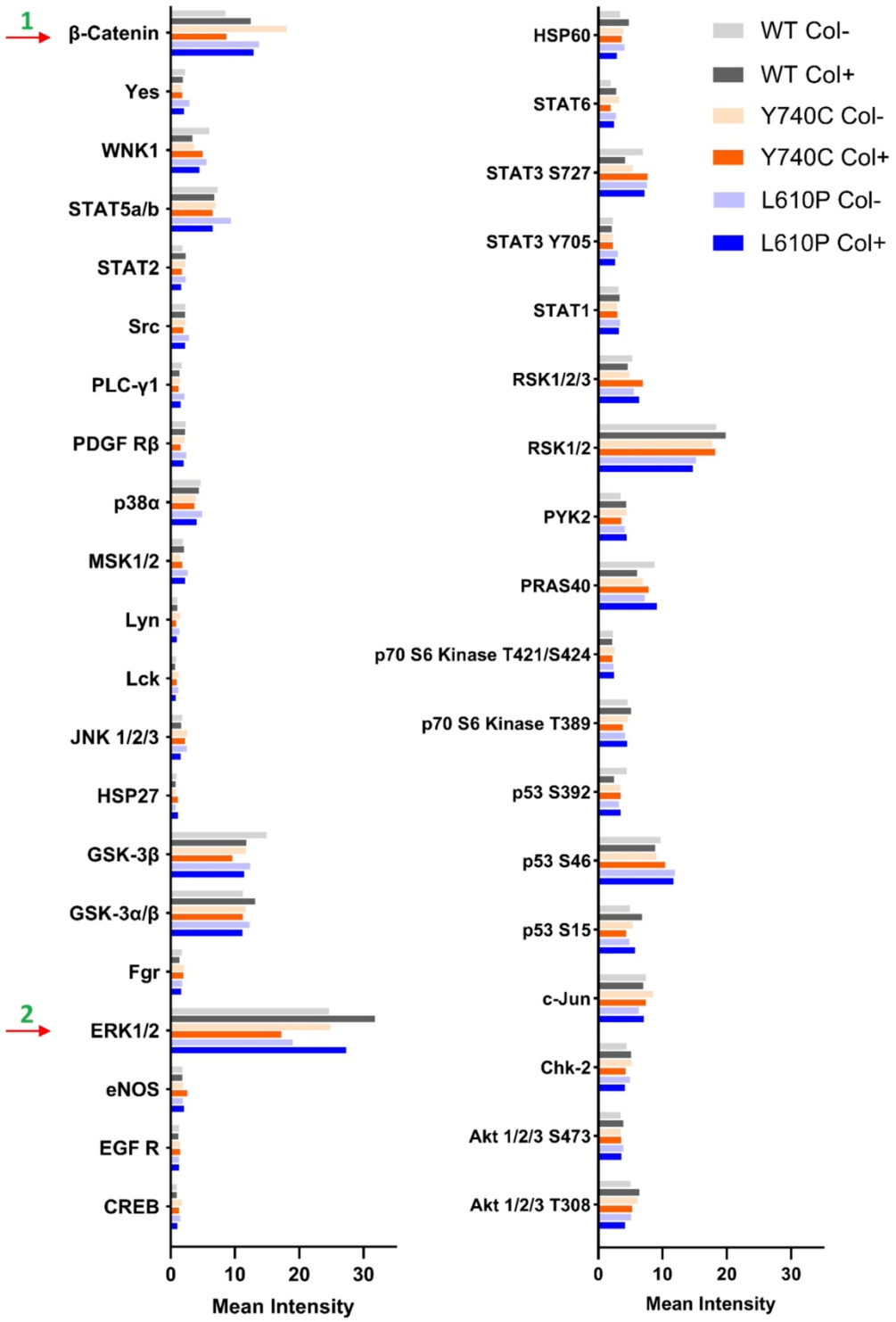


Figure 5. 2 Quantification of phosphorylation or expression signal intensity of selected signalling molecules by phospho-array.

Quantifications of the mean spot pixel intensity are shown. β-catenin and phospho-Erk1/2 signals are indicated with red arrows and the same numbers as labelled in Figure 3A. Col -, without collagen treatment; Col + with collagen treatment.

The single experiment using the commercial kit produced inconclusive results, making it difficult to rule out any natural variation in the tested samples. Thus, four common signalling molecules (Src, Akt, Erk 1/2, p38) were chosen to further investigate their protein expression and phosphorylation levels in HDF cells through Western blotting. Previous studies have identified Src as the binding partner for DDR2, in which DDR2 activation and signalling require Src activity (Ikeda et al., 2002, Yang et al., 2005, Terai et al., 2015). Akt is a major regulator of cell survival, and decreased Akt activation has been found in DDR2-null fibroblasts with greater apoptosis (Song et al., 2005, Jia et al., 2018). Erk 1/2 was included in this investigation as the initial screening provided some changes in different cell lines or treatment conditions, as described above. Moreover, DDR2 can upregulate MMP2 and MMP14 expression in HCC cells via Erk2/SNAIL1 signalling (Xie et al., 2015). The MAPK family member, p38, is the key co-ordinator in various cellular responses (Han et al., 2020). DDR2 activated p38/MAPK pathway has been shown to be involved in osteonectin (ON) mediated osteoblast mineralisation (Zhu et al., 2021). To assess these four signalling molecules, HDF cells were grown to 80% confluency in complete medium, and then further incubated in SFM for 24 hours. Cells were then lysed after serum starvation, and the lysates were analysed on SDS-PAGE, followed by Western blotting with phospho-specific antibodies and antibodies to detect total protein (**Figure 5. 3**). However, in contrast to what was expected, given that constitutive DDR2 activation of Warburg Cinotti mutants was found in patient cells and key molecules were studied as the downstream of DDR2, there were no significant changes in phosphorylation or expression of any of the selected signalling molecules in either of the patient cells, compared to the WT sample. It is possible that the signalling molecules selected in this investigation were not affected by Warburg Cinotti DDR2 variants. However, as discussed in **Chapter 4**, the sample diversity was limited due to narrowed donor selection. Due to time constraints, the phosphorylation and expression of signalling molecules were only assessed in HDF cells without collagen treatment. It will be important in future to stimulate HDF cells with collagen and check whether there is an increase of phospho-Src/phospho-Erk/phospho-Akt or phospho-p38. DDR-specific inhibitor treatment should also be included to verify that any changes are due to DDR2 signalling. Moreover, further assessment of DDR2 signalling using CRISPR/Cas9-engineered HDF cells is required to confirm whether there are any differences in the activation of these signalling molecules in cells with constitutive DDR2 activation.

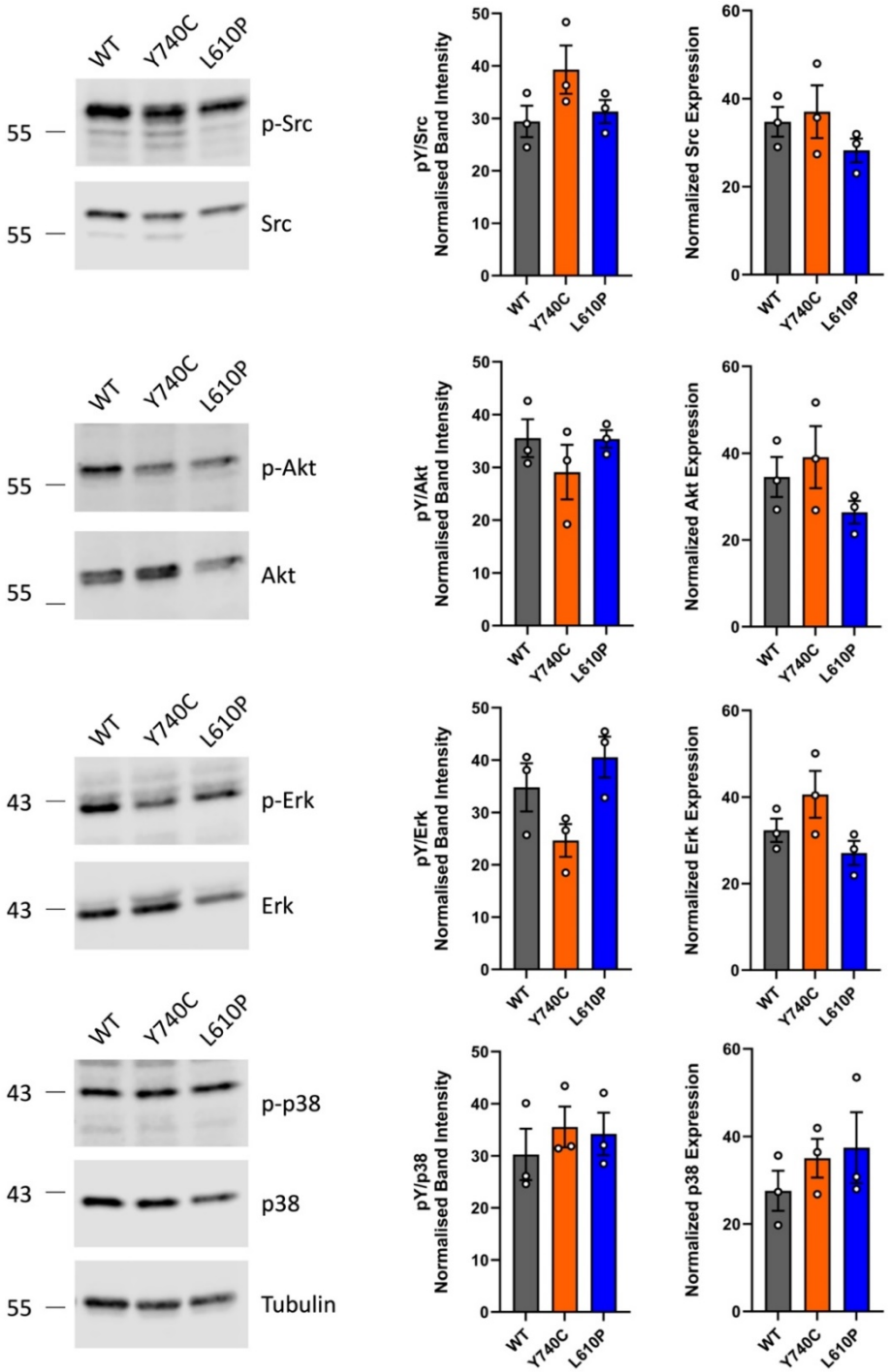


Figure 5. 3 Protein phosphorylation and expression analysis of key DDR2 downstream signalling molecules.
Left panels: HDF cell lysates were analysed by SDS-PAGE and Western Blotting with antibodies against phospho-sites or total protein of selected signalling molecules. Cell lysates were checked on different blots for the detection of each signalling molecule. Phosphorylation signals and total expression signals for each molecule were detected from the same blots by either stripping the membranes and re-probing with the other antibody or using coincubation with antibodies from different species. The position of molecular weight markers (in kDa) is shown on the left.
Right panels: quantification of the phosphorylation signals, normalised to respective total protein signals, which was then normalised to respective tubulin signals. The normalised signal is expressed as a percentage of the sum of all bands on a blot, with mean and standard error of the mean shown (n=3). One-way ANOVA with Dunnett's multiple comparisons test was performed.
No significant differences were found between WT and Y740C samples and between WT and L610P samples.

5.2.2 Determination of selected gene expression levels in HDF cells

Changes in cellular gene expression patterns associated with ligand-induced or mutation-driven RTK activation are now supported by an increasing number of studies (Frattini et al., 2004, Barbosa et al., 2021, Vasudevan et al., 2015). Therefore, a group of genes (*CTNNB, TNC*, *SMAD3, MMP2, MMP14, TIMP1*, and *ACTG2*) were selected to investigate whether their expression levels are changed in patient HDF cells. The *CTNNB* gene was included in this analysis as it encodes β-Catenin, whose expression was seemingly upregulated in non-collagen-stimulated Y740C cells compared with WT cells (**Figure 5. 2**). Studies have shown that the tenascin-C (TN-C; *TNC* gene) and tissue inhibitor of metalloproteinases 1 (TIMP1) expression levels were elevated in HDF cells derived from a systemic sclerosis patient biopsy (Bhattacharyya et al., 2016, Kikuchi et al., 1997). Moreover, overexpression of the TN-C downstream factor, mothers against decapentaplegic homolog 3 (SMAD3), was found to increase TN-C promoter activity in another study (Jinnin et al., 2004). In the case of Dupuytren's disease (DD), a fibrotic condition that leads to progressive flexion of the fingers (Shaw et al., 2007), similar to what is a key characteristic in Warburg Cinotti patients (Xu et al., 2018), knockdown of MMP2 and MMP14 inhibit DD patient cell-induced collagen gel contraction (Wilkinson et al., 2012). As mentioned in **Chapter 4**, fibroblasts can respond to signals from the environment of the wounded area and differentiate to myofibroblasts (Li and Wang, 2011, Tomasek et al., 2002). Interestingly, γ-2 actin (*ACTG2*) gene expression level was found to be upregulated by fibroblast to myofibroblast transdifferentiation (Untergasser et al., 2005). To study potential differential gene expression levels between WT and Warburg Cinotti patient HDF cells, cells were cultured in complete medium to 80%-90% confluency before cell lysis and total RNA extraction. This was followed by reverse transcription and qPCR analysis. Relative gene expression levels were computed as fold changes (**Chapter 2, Section 2.14**) compared to WT samples (**Figure 5. 4**). Compared with WT cells, no significant changes in *CTNNB* and *TNC* gene expression levels were observed from patient samples, although Y740C cells appeared to show reduced *TNC* expression (**Figure 5. 4A, B**). Y740C cells exhibited significantly upregulated gene expression, compared with WT cells, for *SMAD3*, *MMP14*, *TIMP1*, and *ACTG2,* while there were no significant changes in *MMP2* levels (**Figure 5. 4C, E-G**). For L610P cells, the only change, compared with WT cells, was for the *MMP2* gene, whose expression was found to be significantly increased (**Figure 5. 4D**). These data indicated that

select genes encoding proteins highly involved in ECM remodelling or myofibroblast transdifferentiation were elevated in patient HDF cells, but the two patient cell groups showed a very different expression pattern when compared to one another.

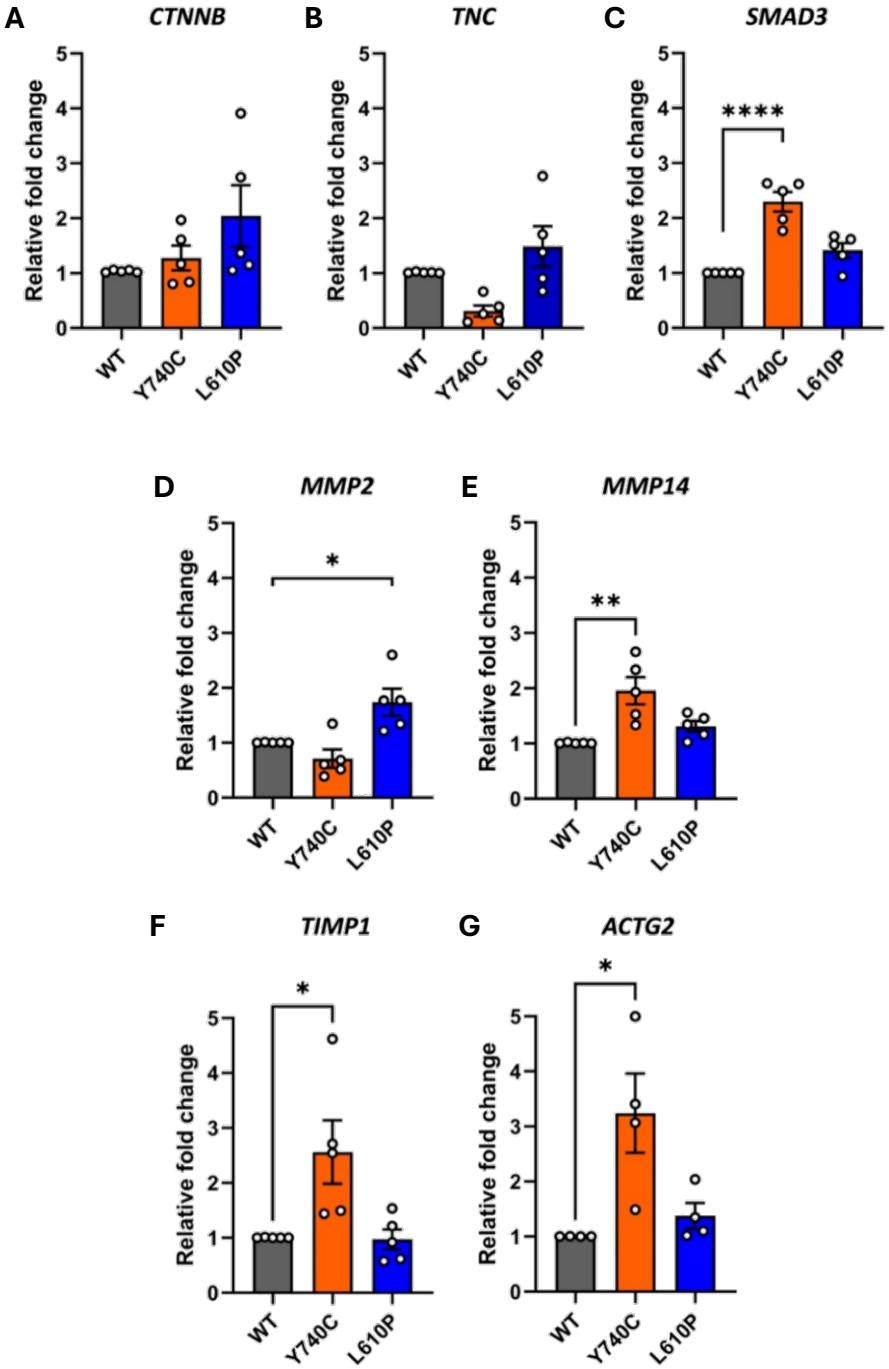


Figure 5. 4 Selected gene expression analysis in WT and Warburg Cinotti patient cells.
HDF cells were grown in multiple 100 mm dishes and serum starved for 24 hours before the extraction of total RNA. Total RNA was extracted from HDF cells, followed by reverse transcription and qPCR analysis. $\Delta\Delta C_T$ values were calculated by normalizing the C_T values of the target gene to GAPDH. Data are presented as relative fold change of target gene expression levels from the patient samples *versus* the expression obtained from the WT cells using the $2^{-\Delta\Delta CT}$ methods(Livak and Schmittgen, 2001). The data are shown with mean and standard error of the mean (n=4 or n=5). One-way ANOVA with Dunnett's multiple comparisons test was performed. *SMAD3*, WT vs Y740C; p<0.0001 (****). *MMP2*, WT vs L610P; p=0.0178 (*). *MMP14*, WT vs Y740C; p=0.0016 (**). *TIMP1*, WT vs Y740C; p=0.0153 (*). *ACTG2*, WT vs Y740C; p=0.0101 (*).

This Chapter presented preliminary data to explore the downstream effects of Warburg Cinotti DDR2 variants in HDF cells. Although no significant changes were observed in the phosphorylation or expression levels of selected signalling molecules, the assessment of gene expression provides an interesting avenue for further analysis. Due to time constraints, I was unable to pursue this further. The following experiment should focus on verifying gene-related protein production and activation levels and performing inhibitor treatment on HDF cells to confirm whether the differences are due to DDR2 activity-mediated signalling.

5.3 Discussion

In **Chapter 3** and **Chapter 4**, constitutive DDR2 activities caused by Warburg Cinotti variants (DDR2-L610P and DDR2-Y740C) were demonstrated in transiently transfected HEK293 cells and patient HDF cells. However, patient cells carrying individual DDR2 variants exhibited distinct changes in cellular behaviour, suggesting that different signalling pathways or unique changes in gene expression patterns are involved in regulating patient cell functions. In this chapter, the phosphorylation and expression of key signalling molecules from common pathways were assessed using a commercial phospho-array kit (**Figure 5. 1**) and Western blotting (**Figure 5. 2**), with no significant changes seen between WT and patient samples. However, the two patient samples displayed distinct changes in gene expression levels compared to one another (**Figure 5. 3**). My data suggested that although DDR2-L610P and DDR2-Y740C are both gain-of-function mutations and lead to the same genetic disorder, these individual mutations may regulate different gene expressions. Further studies are required to establish whether the data generally apply to HDF cells from these Warburg Cinotti syndrome patients.

In the gene expression study, the MMP2 expression levels were significantly upregulated in L610P cells but not Y740C cells, compared to the WT sample (**Figure 5. 3D**). MMP2 is a gelatinase involved in the secondary degradation of collagen and facilitates cell migration by ECM remodelling (Nikolov and Popovski, 2021). In cardiac fibroblasts, MMP2 has been found to stimulate collagen I expression through FAK activation (Hori et al., 2012). Moreover, reduced collagen expression by knocking down MMP2 in lung fibroblasts can be rescued by the addition of recombinant active MMP2 (Bates et al., 2015). As discussed in **Chapter 4**, L610P cells showed an increased gap closure rate on the non-coated 2D surface compared to

WT cells (**Figure 4. 3C**), which could be due to enhanced collagen production. Here, the upregulation of MMP2 in L610P cells supports this speculation.

As described and discussed in **Chapter 4**, enhanced Y740C cell-induced gel contraction compared to WT cells (**Figure 4. 12B**) could be linked to fibroblasts' transition to activated myofibroblasts, which express various contractile proteins (Hinz et al., 2001, Torr et al., 2015). A previous study has shown that assembled F-actin and increased cell contractility reduced MMP2 expression in fibroblasts (Howard et al., 2012). Together with the finding that Y740C cells expressed less *MMP2* than L610P cells, this suggests the possibility that the *MMP2* expression was inhibited in Y740C cells by increased F-actin (**Figure 4. 15A**) or contractile protein generation. However, future studies are required to assess MMP2 protein expression, as well as potential increases in MMP2 activity.

SMAD3, *TIMP1*, *ACTG2*, and *MMP14* expression levels were significantly increased in Y740C cells compared to WT (**Figure 5. 3**). These data provided possible explanations for enhanced Y740C gel contraction compared to WT (**Figure 4. 13B**). Upregulation of the *ACTG2* gene indicated a potential increase in cytoplasmic γ-actin expression level (**Figure 5. 3**G), which acts as an indicator for fibroblasts to proto-myofibroblasts transition (Hinz et al., 2004) and subsequently enhanced Y740C cell-populated gel contraction. The upregulation of *SMAD3* and *TIMP1* gene expression (**Figure 5. 3C, F**) indicates the potential involvement of TGF-β1 signalling in Y740C cells-induced contraction (**Figure 4. 13B**). TGF-β1 binds to TGF-β receptor I (TBRI) and induces phosphorylation on the receptor-activated SMADs, including SMAD3, which then transmits signals to the nucleus (Kim et al., 2018). In addition, TGF-β1 has been reported to induce TIMP1 expression, which then activates FAK signalling (Park et al., 2015). Moreover, differentiation from fibroblasts to myofibroblasts can also be induced by TGF-β1 activation (Vallee and Lecarpentier, 2019). Although further investigations for SMAD3 and TIMP1 protein expression are needed, TGF-β1 pathway could be an interesting direction for signalling research in Warburg Cinotti syndrome.

Another significant gene upregulation in Y740C cells was *MMP14* (**Figure 5. 3E**). DDR2, but not β1 integrin, has been reported to mediate collagen-induced *MMP14* gene expression in rheumatoid arthritis synovial fibroblasts (RASF) (Majkowska et al., 2017). Corneal vascularisation and reduced vision are symptoms recorded in the recent case report of

Warburg Cinotti syndrome (Xu et al., 2018). MMP14 was shown to be secreted by corneal fibroblast via exosomes to vascular endothelial cells, which then potentiate angiogenesis (Han et al., 2015). It is important to further study MMP14 protein expression and activity and determine the potential role or MMP14 in Warburg Cinotti Syndrome-induced corneal vascularisation.

My data for signalling pathway investigation did not show significant changes between WT and patient cell groups. As discussed in **Chapter 4**, Warburg Cinotti variants should be engineered into WT fibroblasts using the CRISPR/Cas9 technique to reduce donor-to-donor variability. Moreover, high-throughput methods such as scRNA-seq and SCP should be used to study DDR2 downstream factors more efficiently (Ahmad and Budnik, 2023).

In summary, while I was unable to identify differences in DDR2 downstream signalling, distinct gene expression patterns have been revealed in different Warburg Cinotti patient cells. Whether the protein levels and biological activities encoded by these tested genes are affected, and the roles of the genes/proteins in Warburg Cinotti syndrome disease progression remain to be determined.

Chapter 6 Final discussion

This thesis provides future directions for understanding the molecular mechanisms of Warburg Cinotti syndrome. My data demonstrate that DDR2-L610P and DDR2-Y740C are constitutively active on the cell surface. Autophosphorylation and substrate phosphorylation rates are enhanced in DDR2-Y740C kinase compared with WT DDR2 kinase. My data also show that patient HDF cells have altered cellular behaviours compare to the WT cells, including increased migration rate on non-coated 2D surfaces and enhanced cell-induced collagen gel contraction, in which neither change is primarily dependent on DDR2 kinase activity. Moreover, preliminary data suggest a potential relationship between DDR2 and integrin-mediated focal adhesion.

6.1 DDR2 kinase undergoes in *cis* activation loop autophosphorylation

In **Chapter 3**, structural analysis revealed the autoinhibitory role of the DDR2 kinase activation loop. Phosphorylation of the activation loop is considered the first step of kinase activation, in which the reaction can be accomplished in *cis* or in *trans* (Li and Miller, 2006, Reinhardt and Leonard, 2023). For nearly all RTKs, including DDR1, activation loop phosphorylation occurs in *trans*, with evidence from both structural and biochemical assessments (Lemmon and Schlessinger, 2010, Pellicena and Kuriyan, 2006, Binns et al., 2000, Sammon et al., 2020). The long exploration of InsR kinase autophosphorylation presented both in *cis* and in *trans* observations with kinetic analysis (Frattali et al., 1992, Shoelson et al., 1991), while activation loop *trans*-autophosphorylation was later confirmed by analysing the crystal structure of IGFR kinase (100% conserved activation loop) (Wu et al., 2008, Hubbard, 2013). For DDR2, belonging to the same RTK subfamily as DDR1, and containing a kinase that is highly homologous to InsR kinase, we would expect the activation loop to undergo *trans*-autophosphorylation (Bargal et al., 2009, Leitinger, 2014). However, *cis*-autophosphorylation was reported for the entire DDR2 cytosolic region (Yang et al., 2005), which was confirmed by my results, analysing specifically autophosphorylation of the activation loop middle tyrosine residue (**Figure 3. 15**). My results also showed faster autophosphorylation and substrate phosphorylation of DDR2 kinase compared with DDR1 kinase (**Figure 3. 13 and Figure 3. 14**) (Sammon et al., 2020). Collagen-induced receptor activation for both DDR1 and DDR2 is extraordinarily slow (Shrivastava et al., 1997, Vogel et al., 1997). How DDR2 exhibits a slow

overall activation, while its kinase displays a much higher autophosphorylation rate than DDR1 kinase is therefore an important question.

Whether and how kinase activation loop autophosphorylation can occur in *cis* remains highly controversial. Nevertheless, *cis*-autophosphorylation models for protein kinase D (PKD), glycogen synthase kinase 3β (GSK-3β), and p38α have been proposed. Different from the catalysis-promoting dimer formation found in most kinase *trans*-autophosphorylation models, PKD forms an inhibitory homodimer, in which the dimer dissociation is subsequently followed by activation loop *cis*-autophosphorylation (Reinhardt et al., 2023). Unlike PKD autophosphorylation that is regulated by its homodimer, both GSK-3β and p38α accomplish the intramolecular autophosphorylation with the help of protein-binding partners, heat shock protein 90 kD (Hsp90) and transforming growth factor-β-activated protein kinase 1-binding protein (TAB1), respectively (Lochhead, 2009, Lochhead et al., 2006, Ge et al., 2002). Based on the investigation between DDR2 and Src (Yang et al., 2005), it is possible that Src acts as the binding partner for DDR2 activation loop *cis*-autophosphorylation. Indeed, the JM4 residues Y569 and Y586, which are highly conserved between DDR1 and DDR2, have been identified as potential phosphosites that interact with Src (Lemeer et al., 2012). Thus, Src recruitment in cells could become a rate-limiting step for collagen-induced DDR2 activation. However, whether Src activity is essential for DDR1 or DDR2 activation in cells remains unclear. Future studies could investigate this further by using a Src knock-down or knock-out model to clarify the effect of loss of Src activity on DDR1 and DDR2 activation mechanisms.

6.2 Catalytic-independent functions of DDR2 kinase and potential issues in kinase inhibitor application for Warburg Cinotti syndrome

Protein kinases regulate essential cellular processes, primarily by their ability to catalyse phosphorylation (Ardito et al., 2017). However, compelling evidence suggests that catalytic-independent protein kinase functions are also crucial, which can result in sufficient biological outputs (Kung and Jura, 2016, Rauch et al., 2011). In **Chapter 3**, biochemical experiments using transiently transfected cells revealed ligand-independent receptor activation for DDR2-L610P and DDR2-Y740C (**Figure 3. 19**). In agreement with this finding, constitutive DDR2 activation was confirmed in Warburg Cinotti syndrome-derived HDF cells, in which a DDR-specific inhibitor VU6015929 can abolish the phosphorylation (**Figure 4. 2**). However, although

DDR2 kinase activity did participate in regulating HDF cell-induced collagen gel contraction of DDR2-WT and DDR2-L610P cells (**Figure 4. 14A**), the application of the DDR-specific inhibitor VU6015929 failed to induce gel size changes in Y740C cell-populated gels (**Figure 4. 14B**). This suggests that DDR2-Y740C might mediate cell functions in a kinase activity-independent way. While there is very little known about kinase-independent roles of DDR2, the non-catalytic function of DDR2 has been identified in regulating breast cancer cell invasion and resulting in kinase inhibitor resistance, but the underlying mechanism remains unclear (Barcus et al., 2021). Furthermore, a recent study found that DDR2 remains functional in IPF lung fibroblasts in the absence of its kinase activity, and that α2 integrin expression is regulated by the presence of DDR2 (Ling et al., 2023).

It is important to note that, besides the ligand-independent phosphorylation caused by the two Warburg Cinotti mutants studied in this thesis, the DDR2 kinase is likely to adopt the active conformation for both mutants, as predicted in **Figure 3. 3**. Structural transitions upon stimulation or inhibition have been proven to support non-catalytic kinase functions (Kung and Jura, 2016). For instance, activation loop phosphorylation-induced Erk2 conformational change is essential for Erk2 to activate topoisomerase IIα and poly(ADP-ribose)polymerase-1 (PARP1) in a non-catalytic manner (Shapiro et al., 1999, Cohen-Armon et al., 2007). Based on the structural studies of a serine/threonine kinase, inositol-requiring enzyme type 1 (IRE1), the kinase active conformation induces 'back-to-back' dimer/oligomerisation, which is essential for activating its RNase domain (Korennykh et al., 2009). In this case, applying type I ATP-competitive inhibitors stabilises the kinase active conformation, which then promotes the activation of signalling pathways (Korennykh et al., 2009, Papa et al., 2003). For EGFR, several studies have shown that loss of kinase activity does not result in equivalent phenotypes to the ablation of receptor expression, indicating a kinase activity-independent role for EGFR to participate in signalling transduction (Luetteke et al., 1994, Miettinen et al., 1995). Moreover, EGFR is found to interact with sodium/glucose cotransporter (SGLT1) without relying on receptor kinase activity, thus facilitating glucose uptake into cancer cells and consequently preventing cancer cell death (Weihua et al., 2008). Hereby, inhibitors that successfully block EGFR kinase activities cannot disrupt the receptor association with SGLT1, which fails to reduce cancer cell viability (Ren et al., 2013).

In **Chapter 5**, the expression and/or phosphorylation levels of a small range of signalling molecules were assessed, with no significant changes observed from the mutant cell samples compared to the WT cells (**Figure 5. 2 and Figure 5. 3**). Future studies should utilise techniques such as proteomics, phosphoproteomics, and transcriptomics to obtain extensive information on DDR2-mediated protein signalling. A recent study published after the completion of my lab work revealed that collagen stimulation leads to the formation of DDR2/phosphatidylinositol-4-phosphate 3-kinase C2 domain containing α polypeptide (PIK3C2α) complex in IPF patient-derived fibroblasts, where fibroblast activation and apoptosis are regulated by DDR2/PIK3C2α signalling (Ling et al., 2024). These findings provide an interesting avenue for future signalling research in Warburg Cinotti patient HDF cells.

As mentioned above, kinase inhibitor treatment might not be suitable for targeting RTKs that regulate disease progression in a kinase activity-independent fashion. Indeed, only dasatinib treatment significantly reduced mutant HDF cell-induced gel contraction (**Figure 4. 16**), potentially because dasatinib targets multiple kinases in its DFG-IN conformation (Roskoski, 2016). However, applying less selective inhibitors might result in unexpected effects on off-target proteins (Hantschel, 2015). Furthermore, inhibitor-caused paradoxical pathway activation is worth considering as a mechanism for kinase inhibitor resistance. For instance, a lung cancer cell line that carries the neurofibromatosis type 1 (*NF1*) splice site mutation displays dasatinib resistance by triggering a bypass pathway with increased Ras and Erk activity (Beauchamp et al., 2014). For Src protein, low-affinity ATP-competitive inhibitors abolish Src kinase activity but also induce Src association with FAK by stabilising an active Src conformation (Higuchi et al., 2021). Inhibitor washout and Src-FAK complex formation together initiate FAK-mediated signalling (Higuchi et al., 2021). As discussed in **Chapter 4**, unexpected FAK activation induced by dasatinib in c-Myc-driven HCC can be suppressed by a combination treatment of dasatinib and FAK inhibitors (Liu et al., 2018). To discover appropriate treatments for Warburg Cinotti syndrome, it will be paramount to further investigate DDR2 signalling targets and explore the potential of using inhibitor cocktails.

6.3 DDR2 association with cytoskeleton and focal adhesion

The cytoskeleton is a highly dynamic network that consists of three major types of components: microfilaments (actin), intermediate filaments, and microtubules (tubulin)

(Hohmann and Dehghani, 2019). It stays coordinated in normal cells and not only provides mechanical support but also acts as a platform for intracellular transportation (Wickstead and Gull, 2011). As the backbone of cells, the cytoskeleton is involved in multiple cellular processes, including adhesion, migration, and contraction (Balta et al., 2020, Tang and Gerlach, 2017). Dysregulated cytoskeleton undergoes dramatic remodelling in disease progression, leading to changes in cell behaviour and microenvironment homeostasis (Li et al., 2023). In **Chapter 3**, reduced Warburg Cinotti mutant protein solubility in non-ionic detergent implies the increased association between the mutant DDR2 variants and the cytoskeleton (**Figure 3. 19**). However, this finding should be further explored, in particular in patient HDF cells where the mutant DDR2 proteins are co-expressed with WT DDR2.

The unusually large intracellular JM region of DDRs likely provides high flexibility to the receptor cytoplasmic region, making it a suitable site for intermolecular interactions (Carafoli and Hohenester, 2013). For instance, DDR1, when stimulated by collagen, associates with the non-muscle myosin IIA heavy chain (NMIIA) and regulates cell spreading and migration (Huang et al., 2009). This association can also transmit cell-generated contractile forces to collagen, leading to collagen mechanical remodelling (Coelho et al., 2017). Although there is no evidence that DDR2 can associate with myosin motor, a recent study has shown that DDR2 can stabilise actin fibres and promote β1 integrin activation at focal adhesions in lung fibroblasts (McGowan, 2023). My data also showed enhanced α1β1 integrin activity in DDR2-Y740C cells compared to WT cells (**Figure 4. 18**). The mechanism behind DDR2-mediated β1 integrin activation remains poorly understood but appears to be related to inside-out signalling (Bayer et al., 2019). Integrin activation can occur through two mechanisms: outside-in and inside-out signalling (Harburger and Calderwood, 2009). The outside-in signalling occurs through α integrin binding to collagen, leading to conformational changes and reorientation of both α and β integrin domains for recruiting adhesion complexes (Pang et al., 2023, Michael and Parsons, 2020). The integrin activation by inside-out signalling is accomplished by β integrin interactions with scaffolding proteins and cytoskeleton proteins, such as talin and vinculin, which increase the integrin affinity to collagen (Pang et al., 2023, Klapholz and Brown, 2017). In CAFs, DDR2 has been found to control β1 integrin activation through inside-out signalling, in which the talin activation and recruitment to integrins are regulated by DDR2-mediated RAP1 activation (Bayer et al., 2019). Future studies should

establish whether DDR2 is associated with integrin or focal adhesion-related scaffolding and cytoskeleton proteins. Together with the proteomic analysis, inhibitors against focal adhesion-related proteins could be tested together with DDR-specific inhibitor VU6015929 in Warburg Cinotti patient HDF cells. This approach could provide a lower chance for inhibitor resistance than using broad-range kinase inhibitor dasatinib (Lovly and Shaw, 2014).

6.4 Summary

In conclusion, this thesis has provided insights into DDR2 activation and highlighted the future direction for understanding the molecular mechanisms of Warburg Cinotti Syndrome. As discussed in **Chapter 4**, both the WT and mutant HDF cells were from single donors, making it difficult to give solid conclusions. Thus, future studies should focus on: 1) using genome editing techniques to introduce single Warburg Cinotti DDR2 variants into immortalised WT HDF cells and mice (mouse knock-in model); 2) the kinase-independent role of DDR2 in regulating Warburg Cinotti Syndrome; 3) the signalling molecules that have been regulated by Warburg Cinotti DDR2 variants; 4) the relationship between Warburg Cinotti DDR2 variants and integrin/focal adhesion.

Chapter 7 Appendix

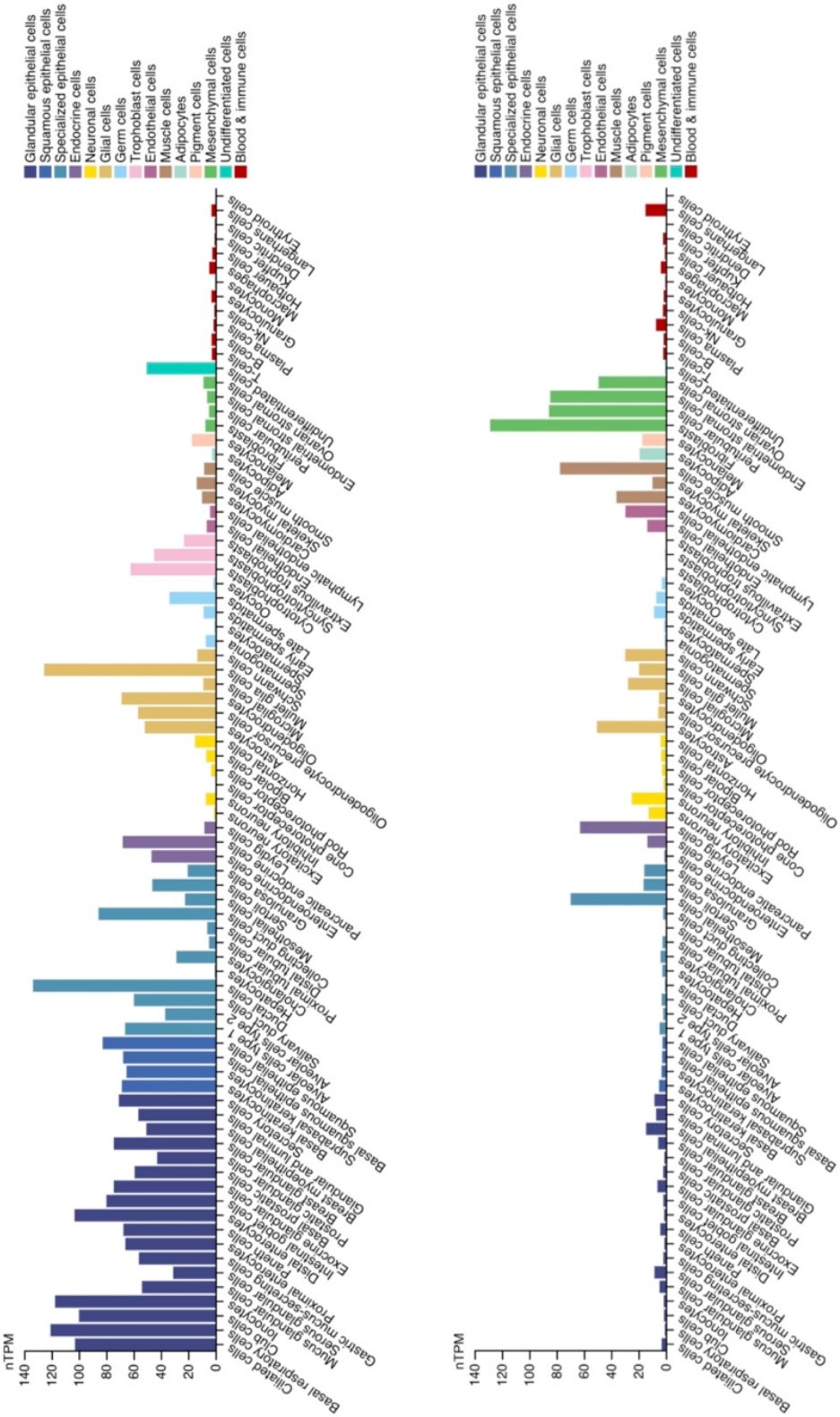


Figure 7. 1 Single cell RNA expressions for DDR1 and DDR2.
Data and figures were generated by The Human Protein Atlas based on normalized single cell RNA (nTPM, normalise transcripts per million) values for DDR1 (A.) and DDR2 (B.). Images are available from version 23.0.proteinatlas.org.
URL for DDR1: https://www.proteinatlas.org/ENSG00000204580-DDR1/single+cell+type.
URL for DDR2: https://www.proteinatlas.org/ENSG00000162733-DDR2/single+cell+type.

Table 7. 1 Signalling protein names and their phosphorylation sites

CREB, cAMP-response element binding protein; eNOS, endothelial nitric oxide synthase; Chk-2, checkpoint kinase-2; JNK, Jun N-terminal kinase; Lck, lymphocyte cell-specific protein-tyrosine kinase; MSK, mitogen- and stress-activated kinase; PRAS40, proline-rich Akt substrate of 40 kDa; PYK, Pyruvate kinase; RSK, ribosomal s6 kinase; WNK, lysine deficient protein kinase 1.

Signalling protein name	Phosphorylation site
Akt 1/2/3	T308
Akt 1/2/3	S473
CREB	S133
EGFR	Y1086
eNOS	S1177
ERK1/2	T202/Y204, T185/Y187
Chk-2	T68
c-Jun	S63
Fgr	Y412
GSK-3α/β	S21/S9
GSK-3β	S9
HSP27	S78/S82
p53	S15
p53	S46
p53	S392
JNK 1/2/3	T183/Y185, T221/Y223
Lck	Y394
Lyn	Y397
MSK1/2	S376/S360
p70 S6 Kinase	T389
p70 S6 Kinase	T421/S424
PRAS40	T246
p38α	T180/Y182
PDGFRβ	Y751
PLC-γ1	Y783
Src	Y419
PYK2	Y402
RSK1/2	S221/S227
RSK1/2/3	S380/S386/S377
STAT2	Y690
STAT5a/b	Y694/Y699
WNK1	T60
Yes	Y426
STAT1	Y701
STAT3	Y705
STAT3	S727
β-Catenin	-
STAT6	Y641
HSP60	-

Marketplace

This is a License Agreement between Ziteng Hao ("User") and Copyright Clearance Center, Inc. ("CCC") on behalf of the Rightsholder identified in the order details below. The license consists of the order details, the Marketplace Permissions General Terms and Conditions below, and any Rightsholder Terms and Conditions which are included below.

All payments must be made in full to CCC in accordance with the Marketplace Permissions General Terms and Conditions below.

Order Date	26-Mar-2024	Type of Use	Republish in a thesis/dissertation
Order License ID	1466317-1		
ISSN	0092-8674	Publisher	CELL PRESS
		Portion	Image/photo/illustration

LICENSED CONTENT

Publication Title	Cell	Rightsholder	Elsevier Science & Technology Journals
Article Title	Cell signaling by receptor tyrosine kinases.	Publication Type	Journal
Author/Editor	National Institute for Medical Research.	Start Page	1117
		End Page	1134
Date	01/01/1974	Issue	7
Language	English	Volume	141
Country	United States of America		

REQUEST DETAILS

Portion Type	Image/photo/illustration	Distribution	Worldwide
Number of Images / Photos / Illustrations	2	Translation	Original language of publication
Format (select all that apply)	Print, Electronic	Copies for the Disabled?	No
		Minor Editing Privileges?	Yes
Who Will Republish the Content?	Author of requested content	Incidental Promotional Use?	No
Duration of Use	Life of current edition	Currency	GBP
Lifetime Unit Quantity	Up to 499		
Rights Requested	Main product		

NEW WORK DETAILS

Title	Functional analysis of DDR2 mutations leading to Warburg Cinotti syndrome	Institution Name	Imperial College London
		Expected Presentation Date	2024-05-28
Instructor Name	Ziteng Hao		

ADDITIONAL DETAILS

Order Reference Number	N/A	The Requesting Person / Organization to Appear on the License	Ziteng Hao

REQUESTED CONTENT DETAILS

Title, Description or Numeric Reference of the Portion(s)	Figure 1 and Figure 2	**Title of the Article / Chapter the Portion Is From**	Cell signaling by receptor tyrosine kinases.
Editor of Portion(s)	Lemmon, Mark A.; Schlessinger, Joseph	**Author of Portion(s)**	Lemmon, Mark A.; Schlessinger, Joseph
Volume / Edition	141	**Issue, if Republishing an Article From a Serial**	7
Page or Page Range of Portion	1117-1134	**Publication Date of Portion**	2010-06-25

RIGHTSHOLDER TERMS AND CONDITIONS

Elsevier publishes Open Access articles in both its Open Access journals and via its Open Access articles option in subscription journals, for which an author selects a user license permitting certain types of reuse without permission. Before proceeding please check if the article is Open Access on http://www.sciencedirect.com and refer to the user license for the individual article. Any reuse not included in the user license terms will require permission. You must always fully and appropriately credit the author and source. If any part of the material to be used (for example, figures) has appeared in the Elsevier publication for which you are seeking permission, with credit or acknowledgement to another source it is the responsibility of the user to ensure their reuse complies with the terms and conditions determined by the rights holder. Please contact permissions@elsevier.com with any queries.

Marketplace Permissions General Terms and Conditions

The following terms and conditions ("General Terms"), together with any applicable Publisher Terms and Conditions, govern User's use of Works pursuant to the Licenses granted by Copyright Clearance Center, Inc. ("CCC") on behalf of the applicable Rightsholders of such Works through CCC's applicable Marketplace transactional licensing services (each, a "Service").

1) **Definitions.** For purposes of these General Terms, the following definitions apply:

"License" is the licensed use the User obtains via the Marketplace platform in a particular licensing transaction, as set forth in the Order Confirmation.

"Order Confirmation" is the confirmation CCC provides to the User at the conclusion of each Marketplace transaction. "Order Confirmation Terms" are additional terms set forth on specific Order Confirmations not set forth in the General Terms that can include terms applicable to a particular CCC transactional licensing service and/or any Rightsholder-specific terms.

"Rightsholder(s)" are the holders of copyright rights in the Works for which a User obtains licenses via the Marketplace platform, which are displayed on specific Order Confirmations.

"Terms" means the terms and conditions set forth in these General Terms and any additional Order Confirmation Terms collectively.

"User" or "you" is the person or entity making the use granted under the relevant License. Where the person accepting the Terms on behalf of a User is a freelancer or other third party who the User authorized to accept the General Terms on the User's behalf, such person shall be deemed jointly a User for purposes of such Terms.

"Work(s)" are the copyright protected works described in relevant Order Confirmations.

2) **Description of Service.** CCC's Marketplace enables Users to obtain Licenses to use one or more Works in accordance with all relevant Terms. CCC grants Licenses as an agent on behalf of the copyright rightsholder identified in the relevant Order Confirmation.

3) **Applicability of Terms.** The Terms govern User's use of Works in connection with the relevant License. In the event of any conflict between General Terms and Order Confirmation Terms, the latter shall govern. User acknowledges that Rightsholders have complete discretion whether to grant any permission, and whether to place any limitations on any grant, and that CCC has no right to supersede or to modify any such discretionary act by a Rightsholder.

4) **Representations; Acceptance.** By using the Service, User represents and warrants that User has been duly authorized by the User to accept, and hereby does accept, all Terms.

5) **Scope of License; Limitations and Obligations.** All Works and all rights therein, including copyright rights, remain the sole and exclusive property of the Rightsholder. The License provides only those rights expressly set forth in the terms and conveys no other rights in any Works

Marketplace

This is a License Agreement between Ziteng Hao ("User") and Copyright Clearance Center, Inc. ("CCC") on behalf of the Rightsholder identified in the order details below. The license consists of the order details, the Marketplace Permissions General Terms and Conditions below, and any Rightsholder Terms and Conditions which are included below.

All payments must be made in full to CCC in accordance with the Marketplace Permissions General Terms and Conditions below.

Order Date	26-Mar-2024	Type of Use	Republish in a thesis/dissertation
Order License ID	1466320-1		
ISSN	10972765	Publisher	CELL PRESS
		Portion	Image/photo/illustration

LICENSED CONTENT

Publication Title	Molecular cell	Publication Type	Journal
Article Title	Catalytic control in the EGF receptor and its connection to general kinase regulatory mechanisms.	Start Page	9
		End Page	22
		Issue	1
		Volume	42
Date	01/01/1998		
Language	English		
Country	United States of America		
Rightsholder	Elsevier Science & Technology Journals		

REQUEST DETAILS

Portion Type	Image/photo/illustration	Distribution	Worldwide
Number of Images / Photos / Illustrations	1	Translation	Original language of publication
Format (select all that apply)	Print, Electronic	Copies for the Disabled?	No
		Minor Editing Privileges?	No
Who Will Republish the Content?	Author of requested content	Incidental Promotional Use?	No
Duration of Use	Life of current edition	Currency	GBP
Lifetime Unit Quantity	Up to 499		
Rights Requested	Main product		

NEW WORK DETAILS

Title	Functional analysis of DDR2 mutations leading to Warburg Cinotti syndrome	Institution Name	Imperial College London
		Expected Presentation Date	2024-05-28
Instructor Name	Ziteng Hao		

ADDITIONAL DETAILS

Order Reference Number	N/A	The Requesting Person / Organization to Appear on the License	Ziteng Hao

REQUESTED CONTENT DETAILS

Title, Description or Numeric Reference of the Portion(s)	Figure 1	**Title of the Article / Chapter the Portion Is From**	Catalytic control in the EGF receptor and its connection to general kinase regulatory mechanisms.
Editor of Portion(s)	Jura, Natalia; Zhang, Xuewu; Endres, Nicholas F.; Seeliger, Markus A.; Schindler, Thomas; Kuriyan, John	**Author of Portion(s)**	Jura, Natalia; Zhang, Xuewu; Endres, Nicholas F.; Seeliger, Markus A.; Schindler, Thomas; Kuriyan, John
Volume / Edition	42		
Page or Page Range of Portion	9-22	**Issue, if Republishing an Article From a Serial**	1
		Publication Date of Portion	2011-04-08

RIGHTSHOLDER TERMS AND CONDITIONS

Elsevier publishes Open Access articles in both its Open Access journals and via its Open Access articles option in subscription journals, for which an author selects a user license permitting certain types of reuse without permission. Before proceeding please check if the article is Open Access on http://www.sciencedirect.com and refer to the user license for the individual article. Any reuse not included in the user license terms will require permission. You must always fully and appropriately credit the author and source. If any part of the material to be used (for example, figures) has appeared in the Elsevier publication for which you are seeking permission, with credit or acknowledgement to another source it is the responsibility of the user to ensure their reuse complies with the terms and conditions determined by the rights holder. Please contact permissions@elsevier.com with any queries.

Marketplace Permissions General Terms and Conditions

The following terms and conditions ("General Terms"), together with any applicable Publisher Terms and Conditions, govern User's use of Works pursuant to the Licenses granted by Copyright Clearance Center, Inc. ("CCC") on behalf of the applicable Rightsholders of such Works through CCC's applicable Marketplace transactional licensing services (each, a "Service").

1) **Definitions.** For purposes of these General Terms, the following definitions apply:

"License" is the licensed use the User obtains via the Marketplace platform in a particular licensing transaction, as set forth in the Order Confirmation.

"Order Confirmation" is the confirmation CCC provides to the User at the conclusion of each Marketplace transaction. "Order Confirmation Terms" are additional terms set forth on specific Order Confirmations not set forth in the General Terms that can include terms applicable to a particular CCC transactional licensing service and/or any Rightsholder-specific terms.

"Rightsholder(s)" are the holders of copyright rights in the Works for which a User obtains licenses via the Marketplace platform, which are displayed on specific Order Confirmations.

"Terms" means the terms and conditions set forth in these General Terms and any additional Order Confirmation Terms collectively.

"User" or "you" is the person or entity making the use granted under the relevant License. Where the person accepting the Terms on behalf of a User is a freelancer or other third party who the User authorized to accept the General Terms on the User's behalf, such person shall be deemed jointly a User for purposes of such Terms.

"Work(s)" are the copyright protected works described in relevant Order Confirmations.

2) **Description of Service.** CCC's Marketplace enables Users to obtain Licenses to use one or more Works in accordance with all relevant Terms. CCC grants Licenses as an agent on behalf of the copyright rightsholder identified in the relevant Order Confirmation.

3) **Applicability of Terms.** The Terms govern User's use of Works in connection with the relevant License. In the event of any conflict between General Terms and Order Confirmation Terms, the latter shall govern. User acknowledges that Rightsholders have complete discretion whether to grant any permission, and whether to place any limitations on any grant, and that CCC has no right to supersede or to modify any such discretionary act by a Rightsholder.

Marketplace

This is a License Agreement between Ziteng Hao ("User") and Copyright Clearance Center, Inc. ("CCC") on behalf of the Rightsholder identified in the order details below. The license consists of the order details, the Marketplace Permissions General Terms and Conditions below, and any Rightsholder Terms and Conditions which are included below.

All payments must be made in full to CCC in accordance with the Marketplace Permissions General Terms and Conditions below.

Order Date	26-Mar-2024	Type of Use	Republish in a thesis/dissertation
Order License ID	1466317-2		
ISSN	1937-6448	Publisher	Elsevier
		Portion	Image/photo/illustration

LICENSED CONTENT

Publication Title	International review of cell and molecular biology	Rightsholder	Elsevier Science & Technology Journals
Article Title	Discoidin Domain Receptor Functions in Physiological and Pathological Conditions	Publication Type	Journal
		Start Page	39
		End Page	87
Date	01/01/2008	Volume	310
Language	English		
Country	Netherlands		

REQUEST DETAILS

Portion Type	Image/photo/illustration	Distribution	Worldwide
Number of Images / Photos / Illustrations	3	Translation	Original language of publication
Format (select all that apply)	Print, Electronic	Copies for the Disabled?	No
		Minor Editing Privileges?	No
Who Will Republish the Content?	Author of requested content	Incidental Promotional Use?	No
Duration of Use	Life of current edition	Currency	GBP
Lifetime Unit Quantity	Up to 499		
Rights Requested	Main product		

NEW WORK DETAILS

Title	Functional analysis of DDR2 mutations leading to Warburg Cinotti syndrome	Institution Name	Imperial College London
		Expected Presentation Date	2024-05-28
Instructor Name	Ziteng Hao		

ADDITIONAL DETAILS

Order Reference Number	N/A	The Requesting Person / Organization to Appear on the License	Ziteng Hao

REQUESTED CONTENT DETAILS

Title, Description or Numeric Reference of the Portion(s)	Figure 2.1, Figure 2.2, and Figure 2.3	**Title of the Article / Chapter the Portion Is From**	Discoidin Domain Receptor Functions in Physiological and Pathological Conditions
Editor of Portion(s)	Leitinger, Birgit	**Author of Portion(s)**	Leitinger, Birgit
Volume / Edition	310	**Issue, if Republishing an Article From a Serial**	N/A
Page or Page Range of Portion	39-87	**Publication Date of Portion**	2014-01-01

RIGHTSHOLDER TERMS AND CONDITIONS

Elsevier publishes Open Access articles in both its Open Access journals and via its Open Access articles option in subscription journals, for which an author selects a user license permitting certain types of reuse without permission. Before proceeding please check if the article is Open Access on http://www.sciencedirect.com and refer to the user license for the individual article. Any reuse not included in the user license terms will require permission. You must always fully and appropriately credit the author and source. If any part of the material to be used (for example, figures) has appeared in the Elsevier publication for which you are seeking permission, with credit or acknowledgement to another source it is the responsibility of the user to ensure their reuse complies with the terms and conditions determined by the rights holder. Please contact permissions@elsevier.com with any queries.

Marketplace Permissions General Terms and Conditions

The following terms and conditions ("General Terms"), together with any applicable Publisher Terms and Conditions, govern User's use of Works pursuant to the Licenses granted by Copyright Clearance Center, Inc. ("CCC") on behalf of the applicable Rightsholders of such Works through CCC's applicable Marketplace transactional licensing services (each, a "Service").

1) **Definitions.** For purposes of these General Terms, the following definitions apply:

"License" is the licensed use the User obtains via the Marketplace platform in a particular licensing transaction, as set forth in the Order Confirmation.

"Order Confirmation" is the confirmation CCC provides to the User at the conclusion of each Marketplace transaction. "Order Confirmation Terms" are additional terms set forth on specific Order Confirmations not set forth in the General Terms that can include terms applicable to a particular CCC transactional licensing service and/or any Rightsholder-specific terms.

"Rightsholder(s)" are the holders of copyright rights in the Works for which a User obtains licenses via the Marketplace platform, which are displayed on specific Order Confirmations.

"Terms" means the terms and conditions set forth in these General Terms and any additional Order Confirmation Terms collectively.

"User" or "you" is the person or entity making the use granted under the relevant License. Where the person accepting the Terms on behalf of a User is a freelancer or other third party who the User authorized to accept the General Terms on the User's behalf, such person shall be deemed jointly a User for purposes of such Terms.

"Work(s)" are the copyright protected works described in relevant Order Confirmations.

2) **Description of Service.** CCC's Marketplace enables Users to obtain Licenses to use one or more Works in accordance with all relevant Terms. CCC grants Licenses as an agent on behalf of the copyright rightsholder identified in the relevant Order Confirmation.

3) **Applicability of Terms.** The Terms govern User's use of Works in connection with the relevant License. In the event of any conflict between General Terms and Order Confirmation Terms, the latter shall govern. User acknowledges that Rightsholders have complete discretion whether to grant any permission, and whether to place any limitations on any grant, and that CCC has no right to supersede or to modify any such discretionary act by a Rightsholder.

4) **Representations; Acceptance.** By using the Service, User represents and warrants that User has been duly authorized by the User to accept, and hereby does accept, all Terms.

5) **Scope of License; Limitations and Obligations.** All Works and all rights therein, including copyright rights, remain the sole and exclusive property of the Rightsholder. The License provides only those rights expressly set forth in the terms and conveys no other rights in any Works

Marketplace

This is a License Agreement between Ziteng Hao ("User") and Copyright Clearance Center, Inc. ("CCC") on behalf of the Rightsholder identified in the order details below. The license consists of the order details, the Marketplace Permissions General Terms and Conditions below, and any Rightsholder Terms and Conditions which are included below.

All payments must be made in full to CCC in accordance with the Marketplace Permissions General Terms and Conditions below.

Order Date	26-Mar-2024	Type of Use	Republish in a thesis/dissertation
Order License ID	1466317-3		
ISSN	1096-1186	Publisher	ACADEMIC PRESS
		Portion	Chart/graph/table/figure

LICENSED CONTENT

Publication Title	Pharmacological research	Rightsholder	Elsevier Science & Technology Journals
Article Title	Classification of small molecule protein kinase inhibitors based upon the structures of their drug-enzyme complexes.	Publication Type	e-Journal
		Start Page	26
		End Page	48
Author/Editor	Società italiana di farmacologia.	Volume	103
		URL	http://firstsearch.oclc.org
Date	01/01/1989		
Language	English		
Country	United Kingdom of Great Britain and Northern Ireland		

REQUEST DETAILS

Portion Type	Chart/graph/table/figure	Distribution	Worldwide
Number of Charts / Graphs / Tables / Figures Requested	1	Translation	Original language of publication
		Copies for the Disabled?	No
Format (select all that apply)	Print, Electronic	Minor Editing Privileges?	Yes
Who Will Republish the Content?	Author of requested content	Incidental Promotional Use?	No
Duration of Use	Life of current edition	Currency	GBP
Lifetime Unit Quantity	Up to 499		
Rights Requested	Main product		

NEW WORK DETAILS

Title	Functional analysis of DDR2 mutations leading to Warburg Cinotti syndrome	Institution Name	Imperial College London
		Expected Presentation Date	2024-05-28
Instructor Name	Ziteng Hao		

ADDITIONAL DETAILS

Order Reference Number	N/A

The Requesting Person / Organization to Appear on the License	Ziteng Hao

REQUESTED CONTENT DETAILS

Title, Description or Numeric Reference of the Portion(s)	Table 2
Editor of Portion(s)	Roskoski, Robert, Jr.
Volume / Edition	103
Page or Page Range of Portion	26-48
Title of the Article / Chapter the Portion Is From	Classification of small molecule protein kinase inhibitors based upon the structures of their drug-enzyme complexes.
Author of Portion(s)	Roskoski, Robert, Jr.
Issue, if Republishing an Article From a Serial	N/A
Publication Date of Portion	2016-01-01

RIGHTSHOLDER TERMS AND CONDITIONS

Elsevier publishes Open Access articles in both its Open Access journals and via its Open Access articles option in subscription journals, for which an author selects a user license permitting certain types of reuse without permission. Before proceeding please check if the article is Open Access on http://www.sciencedirect.com and refer to the user license for the individual article. Any reuse not included in the user license terms will require permission. You must always fully and appropriately credit the author and source. If any part of the material to be used (for example, figures) has appeared in the Elsevier publication for which you are seeking permission, with credit or acknowledgement to another source it is the responsibility of the user to ensure their reuse complies with the terms and conditions determined by the rights holder. Please contact permissions@elsevier.com with any queries.

Marketplace Permissions General Terms and Conditions

The following terms and conditions ("General Terms"), together with any applicable Publisher Terms and Conditions, govern User's use of Works pursuant to the Licenses granted by Copyright Clearance Center, Inc. ("CCC") on behalf of the applicable Rightsholders of such Works through CCC's applicable Marketplace transactional licensing services (each, a "Service").

1) **Definitions.** For purposes of these General Terms, the following definitions apply:

"License" is the licensed use the User obtains via the Marketplace platform in a particular licensing transaction, as set forth in the Order Confirmation.

"Order Confirmation" is the confirmation CCC provides to the User at the conclusion of each Marketplace transaction. "Order Confirmation Terms" are additional terms set forth on specific Order Confirmations not set forth in the General Terms that can include terms applicable to a particular CCC transactional licensing service and/or any Rightsholder-specific terms.

"Rightsholder(s)" are the holders of copyright rights in the Works for which a User obtains licenses via the Marketplace platform, which are displayed on specific Order Confirmations.

"Terms" means the terms and conditions set forth in these General Terms and any additional Order Confirmation Terms collectively.

"User" or "you" is the person or entity making the use granted under the relevant License. Where the person accepting the Terms on behalf of a User is a freelancer or other third party who the User authorized to accept the General Terms on the User's behalf, such person shall be deemed jointly a User for purposes of such Terms.

"Work(s)" are the copyright protected works described in relevant Order Confirmations.

2) **Description of Service.** CCC's Marketplace enables Users to obtain Licenses to use one or more Works in accordance with all relevant Terms. CCC grants Licenses as an agent on behalf of the copyright rightsholder identified in the relevant Order Confirmation.

3) **Applicability of Terms.** The Terms govern User's use of Works in connection with the relevant License. In the event of any conflict between General Terms and Order Confirmation Terms, the latter shall govern. User acknowledges that Rightsholders have complete discretion whether to grant any permission, and whether to place any limitations on any grant, and that CCC has no right to supersede or to modify any such discretionary act by a Rightsholder.

ELSEVIER LICENSE
TERMS AND CONDITIONS

Mar 27, 2024

This Agreement between Imperial College London -- Ziteng Hao ("You") and Elsevier ("Elsevier") consists of your license details and the terms and conditions provided by Elsevier and Copyright Clearance Center.

License Number	5756760602002
License date	Mar 26, 2024
Licensed Content Publisher	Elsevier
Licensed Content Publication	The American Journal of Human Genetics
Licensed Content Title	Recurrent, Activating Variants in the Receptor Tyrosine Kinase DDR2 Cause Warburg-Cinotti Syndrome
Licensed Content Author	Linda Xu,Hanne Jensen,Jennifer J. Johnston,Emilio Di Maria,Katja Kloth,Ileana Cristea,Julie C. Sapp,Thomas N. Darling,Laryssa A. Huryn,Lisbeth Tranebjærg,Elisa Cinotti,Christian Kubisch,Eyvind Rødahl,Ove Bruland,Leslie G. Biesecker,Gunnar Houge et al.
Licensed Content Date	Dec 6, 2018
Licensed Content Volume	103
Licensed Content Issue	6
Licensed Content Pages	8
Start Page	976
End Page	983

Type of Use	reuse in a thesis/dissertation
Portion	figures/tables/illustrations
Number of figures/tables/illustrations	1
Format	both print and electronic
Are you the author of this Elsevier article?	No
Will you be translating?	No
Title of new work	Functional analysis of DDR2 mutations leading to Warburg Cinotti syndrome
Institution name	Imperial College London
Expected presentation date	May 2024
Portions	Table 1
Requestor Location	Imperial College London Exhibition Road London, London SW7 2AZ United Kingdom Attn: Imperial College London
Publisher Tax ID	GB 494 6272 12
Total	0.00 GBP
Terms and Conditions	

INTRODUCTION

1. The publisher for this copyrighted material is Elsevier. By clicking "accept" in connection with completing this licensing transaction, you agree that the following terms and conditions apply to this transaction (along with the Billing and Payment terms and conditions established by Copyright Clearance Center, Inc. ("CCC"), at the time that you

Reference list

ABBONANTE, V., GRUPPI, C., RUBEL, D., GROSS, O., MORATTI, R. & BALDUINI, A. 2013. Discoidin domain receptor 1 protein is a novel modulator of megakaryocyte-collagen interactions. *J Biol Chem,* 288**,** 16738-16746.

ACEBRON, I., RIGHETTO, R. D., SCHOENHERR, C., DE BUHR, S., REDONDO, P., CULLEY, J., RODRIGUEZ, C. F., DADAY, C., BIYANI, N., LLORCA, O., BYRON, A., CHAMI, M., GRATER, F., BOSKOVIC, J., FRAME, M. C., STAHLBERG, H. & LIETHA, D. 2020. Structural basis of Focal Adhesion Kinase activation on lipid membranes. *EMBO J,* 39**,** e104743.

ADAMS, C. W., ALLISON, D. E., FLAGELLA, K., PRESTA, L., CLARKE, J., DYBDAL, N., MCKEEVER, K. & SLIWKOWSKI, M. X. 2006. Humanization of a recombinant monoclonal antibody to produce a therapeutic HER dimerization inhibitor, pertuzumab. *Cancer Immunol Immunother,* 55**,** 717-27.

AFONSO, P. V., MCCANN, C. P., KAPNICK, S. M. & PARENT, C. A. 2013. Discoidin domain receptor 2 regulates neutrophil chemotaxis in 3D collagen matrices. *Blood,* 121**,** 1644-50.

AGARWAL, G., KOVAC, L., RADZIEJEWSKI, C. & SAMUELSSON, S. J. 2002. Binding of discoidin domain receptor 2 to collagen I: an atomic force microscopy investigation. *Biochemistry,* 41**,** 11091-8.

AGARWAL, G., SMITH, A. W. & JONES, B. 2019. Discoidin domain receptors: Micro insights into macro assemblies. *Biochim Biophys Acta Mol Cell Res,* 1866**,** 118496.

AGGARWAL, B., CORREA, A. R. E., GUPTA, N., JANA, M. & KABRA, M. 2022. First case report of Penttinen syndrome from India. *Am J Med Genet A,* 188**,** 683-687.

AGUS, D. B., AKITA, R. W., FOX, W. D., LEWIS, G. D., HIGGINS, B., PISACANE, P. I., LOFGREN, J. A., TINDELL, C., EVANS, D. P., MAIESE, K., SCHER, H. I. & SLIWKOWSKI, M. X. 2002. Targeting ligand-activated ErbB2 signaling inhibits breast and prostate tumor growth. *Cancer Cell,* 2**,** 127-37.

AHMAD, R. & BUDNIK, B. 2023. A review of the current state of single-cell proteomics and future perspective. *Anal Bioanal Chem,* 415**,** 6889-6899.

ALI, B. R., XU, H., AKAWI, N. A., JOHN, A., KARUVANTEVIDA, N. S., LANGER, R., AL-GAZALI, L. & LEITINGER, B. 2010. Trafficking defects and loss of ligand binding are the underlying causes of all reported DDR2 missense mutations found in SMED-SL patients. *Hum Mol Genet,* 19**,** 2239-50.

ALVES, F., VOGEL, W., MOSSIE, K., MILLAUER, B., HOFLER, H. & ULLRICH, A. 1995. Distinct structural characteristics of discoidin I subfamily receptor tyrosine kinases and complementary expression in human cancer. *Oncogene,* 10**,** 609-18.

ARANDA, S., MUNTANE, G. & VILELLA, E. 2024. Coexpression network analysis of the adult brain sheds light on the pathogenic mechanism of DDR1 in schizophrenia and bipolar disorder. *Transl Psychiatry,* 14**,** 112.

ARDITO, F., GIULIANI, M., PERRONE, D., TROIANO, G. & LO MUZIO, L. 2017. The crucial role of protein phosphorylation in cell signaling and its use as targeted therapy (Review). *Int J Mol Med,* 40**,** 271-280.

ARNOULD, L., GELLY, M., PENAULT-LLORCA, F., BENOIT, L., BONNETAIN, F., MIGEON, C., CABARET, V., FERMEAUX, V., BERTHEAU, P., GARNIER, J., JEANNIN, J. F. & COUDERT, B. 2006. Trastuzumab-based treatment of HER2-positive breast cancer: an antibody-dependent cellular cytotoxicity mechanism? *Br J Cancer,* 94**,** 259-67.

ARTER, C., TRASK, L., WARD, S., YEOH, S. & BAYLISS, R. 2022. Structural features of the protein kinase domain and targeted binding by small-molecule inhibitors. *J Biol Chem,* 298**,** 102247.

AVIVI-GREEN, C., SINGAL, M. & VOGEL, W. F. 2006. Discoidin domain receptor 1-deficient mice are resistant to bleomycin-induced lung fibrosis. *Am J Respir Crit Care Med,* 174**,** 420-7.

BAINBRIDGE, P. 2013. Wound healing and the role of fibroblasts. *J Wound Care,* 22**,** 407-8, 410-12.

BALTA, E., KRAMER, J. & SAMSTAG, Y. 2020. Redox Regulation of the Actin Cytoskeleton in Cell Migration and Adhesion: On the Way to a Spatiotemporal View. *Front Cell Dev Biol,* 8**,** 618261.

BARBOSA, R., ACEVEDO, L. A. & MARMORSTEIN, R. 2021. The MEK/ERK Network as a Therapeutic Target in Human Cancer. *Mol Cancer Res,* 19**,** 361-374.

BARCUS, C. E., HWANG, P. Y., MORIKIS, V., BRENOT, A., PENCE, P., CLARKE, M. & LONGMORE, G. D. 2021. Tyrosine kinase-independent actions of DDR2 in tumor cells and cancer-associated fibroblasts influence tumor invasion, migration and metastasis. *J Cell Sci,* 134.

BARCZYK, M., CARRACEDO, S. & GULLBERG, D. 2010. Integrins. *Cell Tissue Res,* 339**,** 269-80.

BARGAL, R., CORMIER-DAIRE, V., BEN-NERIAH, Z., LE MERRER, M., SOSNA, J., MELKI, J., ZANGEN, D. H., SMITHSON, S. F., BOROCHOWITZ, Z., BELOSTOTSKY, R. & RAAS-ROTHSCHILD, A. 2009. Mutations in DDR2 gene cause SMED with short limbs and abnormal calcifications. *Am J Hum Genet,* 84**,** 80-4.

BARKAUSKAS, C. E. & NOBLE, P. W. 2014. Cellular mechanisms of tissue fibrosis. 7. New insights into the cellular mechanisms of pulmonary fibrosis. *Am J Physiol Cell Physiol,* 306**,** C987-96.

BATES, A. L., PICKUP, M. W., HALLETT, M. A., DOZIER, E. A., THOMAS, S. & FINGLETON, B. 2015. Stromal matrix metalloproteinase 2 regulates collagen expression and promotes the outgrowth of experimental metastases. *J Pathol,* 235**,** 773-83.

BAXTER, R. M., SECRIST, J. P., VAILLANCOURT, R. R. & KAZLAUSKAS, A. 1998. Full activation of the platelet-derived growth factor beta-receptor kinase involves multiple events. *J Biol Chem,* 273**,** 17050-5.

BAYER, S. V., GRITHER, W. R., BRENOT, A., HWANG, P. Y., BARCUS, C. E., ERNST, M., PENCE, P., WALTER, C., PATHAK, A. & LONGMORE, G. D. 2019. DDR2 controls breast tumor stiffness and metastasis by regulating integrin mediated mechanotransduction in CAFs. *Elife,* 8.

BAYLISS, R., HAQ, T. & YEOH, S. 2015. The Ys and wherefores of protein kinase autoinhibition. *Biochim Biophys Acta,* 1854**,** 1586-94.

BEAUCHAMP, E. M., WOODS, B. A., DULAK, A. M., TAN, L., XU, C., GRAY, N. S., BASS, A. J., WONG, K. K., MEYERSON, M. & HAMMERMAN, P. S. 2014. Acquired resistance to dasatinib in lung cancer cell lines conferred by DDR2 gatekeeper mutation and NF1 loss. *Mol Cancer Ther,* 13**,** 475-82.

BELLUS, G. A., MCINTOSH, I., SMITH, E. A., AYLSWORTH, A. S., KAITILA, I., HORTON, W. A., GREENHAW, G. A., HECHT, J. T. & FRANCOMANO, C. A. 1995. A recurrent mutation in the tyrosine kinase domain of fibroblast growth factor receptor 3 causes hypochondroplasia. *Nat Genet,* 10**,** 357-9.

BEN ARFI, K., SCHNEIDER, C., BENNASROUNE, A., BOULAND, N., WOLAK-THIERRY, A., COLLIN, G., LE, C. C., TOUSSAINT, K., HACHET, C., LEHRTER, V., DEDIEU, S., BOUCHE, O., MORJANI, H., BOULAGNON-ROMBI, C. & APPERT-COLLIN, A. 2022. Discoidin Domain Receptor 1 Expression in Colon Cancer: Roles and Prognosis Impact. *Cancers (Basel),* 14.

BERROW, N. S., ALDERTON, D., SAINSBURY, S., NETTLESHIP, J., ASSENBERG, R., RAHMAN, N., STUART, D. I. & OWENS, R. J. 2007. A versatile ligation-independent cloning method suitable for high-throughput expression screening applications. *Nucleic Acids Res,* 35**,** e45.

BHATTACHARYYA, S., WANG, W., MORALES-NEBREDA, L., FENG, G., WU, M., ZHOU, X., LAFYATIS, R., LEE, J., HINCHCLIFF, M., FEGHALI-BOSTWICK, C., LAKOTA, K., BUDINGER, G. R., RAPARIA, K., TAMAKI, Z. & VARGA, J. 2016. Tenascin-C drives persistence of organ fibrosis. *Nat Commun,* 7**,** 11703.

BHULLAR, K. S., LAGARON, N. O., MCGOWAN, E. M., PARMAR, I., JHA, A., HUBBARD, B. P. & RUPASINGHE, H. P. V. 2018. Kinase-targeted cancer therapies: progress, challenges and future directions. *Mol Cancer,* 17**,** 48.

BINNS, K. L., TAYLOR, P. P., SICHERI, F., PAWSON, T. & HOLLAND, S. J. 2000. Phosphorylation of tyrosine residues in the kinase domain and juxtamembrane region regulates the biological and catalytic activities of Eph receptors. *Mol Cell Biol,* 20**,** 4791-805.

BORZA, C. M., BOLAS, G., ZHANG, X., BROWNING MONROE, M. B., ZHANG, M. Z., MEILER, J., SKWARK, M. J., HARRIS, R. C., LAPIERRE, L. A., GOLDENRING, J. R., HOOK, M., RIVERA, J., BROWN, K. L., LEITINGER, B., TYSKA, M. J., MOSER, M., BOTTCHER, R. T., ZENT, R. & POZZI, A. 2022. The Collagen Receptor Discoidin Domain Receptor 1b Enhances Integrin beta1-Mediated Cell Migration by Interacting With Talin and Promoting Rac1 Activation. *Front Cell Dev Biol,* 10**,** 836797.

BORZA, C. M. & POZZI, A. 2014. Discoidin domain receptors in disease. *Matrix Biol,* 34**,** 185-92.

BORZA, C. M., POZZI, A. & PLOSA, E. J. 2018. Discoidin Domain Receptor 2, a Potential Therapeutic Target in Lung Fibrosis. *Am J Respir Cell Mol Biol,* 59**,** 277-278.

BOUSSIF, O., LEZOUALC'H, F., ZANTA, M. A., MERGNY, M. D., SCHERMAN, D., DEMENEIX, B. & BEHR, J. P. 1995. A versatile vector for gene and oligonucleotide transfer into cells in culture and in vivo: polyethylenimine. *Proc Natl Acad Sci U S A,* 92**,** 7297-301.

BRODSKY, B. & PERSIKOV, A. V. 2005. Molecular structure of the collagen triple helix. *Adv Protein Chem,* 70**,** 301-39.

BURGESS, A. W., CHO, H. S., EIGENBROT, C., FERGUSON, K. M., GARRETT, T. P., LEAHY, D. J., LEMMON, M. A., SLIWKOWSKI, M. X., WARD, C. W. & YOKOYAMA, S. 2003. An open-and-shut case? Recent insights into the activation of EGF/ErbB receptors. *Mol Cell,* 12**,** 541-52.

CACCIA, D., MICCICHE, F., CASSINELLI, G., MONDELLINI, P., CASALINI, P. & BONGARZONE, I. 2010. Dasatinib reduces FAK phosphorylation increasing the effects of RPI-1 inhibition in a RET/PTC1-expressing cell line. *Mol Cancer,* 9**,** 278.

CADER, F. Z., VOCKERODT, M., BOSE, S., NAGY, E., BRUNDLER, M. A., KEARNS, P. & MURRAY, P. G. 2013. The EBV oncogene LMP1 protects lymphoma cells from cell death through the collagen-mediated activation of DDR1. *Blood,* 122**,** 4237-45.

CANNING, P., TAN, L., CHU, K., LEE, S. W., GRAY, N. S. & BULLOCK, A. N. 2014. Structural mechanisms determining inhibition of the collagen receptor DDR1 by selective and multi-targeted type II kinase inhibitors. *J Mol Biol,* 426**,** 2457-70.

CARAFOLI, F., BIHAN, D., STATHOPOULOS, S., KONITSIOTIS, A. D., KVANSAKUL, M., FARNDALE, R. W., LEITINGER, B. & HOHENESTER, E. 2009. Crystallographic insight into collagen recognition by discoidin domain receptor 2. *Structure,* 17**,** 1573-1581.

CARAFOLI, F. & HOHENESTER, E. 2013. Collagen recognition and transmembrane signalling by discoidin domain receptors. *Biochim Biophys Acta,* 1834**,** 2187-94.

CARAFOLI, F., MAYER, M. C., SHIRAISHI, K., PECHEVA, M. A., CHAN, L. Y., NAN, R., LEITINGER, B. & HOHENESTER, E. 2012. Structure of the discoidin domain receptor 1 extracellular region bound to an inhibitory Fab fragment reveals features important for signaling. *Structure,* 20**,** 688-97.

CARIO, M. 2018. DDR1 and DDR2 in skin. *Cell Adh Migr,* 12**,** 386-393.

CARRACEDO, S., LU, N., POPOVA, S. N., JONSSON, R., ECKES, B. & GULLBERG, D. 2010. The fibroblast integrin alpha11beta1 is induced in a mechanosensitive manner involving activin A and regulates myofibroblast differentiation. *J Biol Chem,* 285**,** 10434-45.

CASTRO-SANCHEZ, L., SOTO-GUZMAN, A., GUADERRAMA-DIAZ, M., CORTES-REYNOSA, P. & SALAZAR, E. P. 2011. Role of DDR1 in the gelatinases secretion induced by native type IV collagen in MDA-MB-231 breast cancer cells. *Clin Exp Metastasis,* 28**,** 463-77.

CHETOUI, N., EL AZREQ, M. A., BOISVERT, M., BERGERON, M. E. & AOUDJIT, F. 2011. Discoidin domain receptor 1 expression in activated T cells is regulated by the ERK MAP kinase signaling pathway. *J Cell Biochem,* 112**,** 3666-74.

CHIARA, F., GOUMANS, M. J., FORSBERG, H., AHGREN, A., RASOLA, A., ASPENSTROM, P., WERNSTEDT, C., HELLBERG, C., HELDIN, C. H. & HEUCHEL, R. 2004. A gain of function mutation in the activation loop of platelet-derived growth factor beta-receptor deregulates its kinase activity. *J Biol Chem,* 279**,** 42516-27.

CHIN, G. S., LIU, W., STEINBRECH, D., HSU, M., LEVINSON, H. & LONGAKER, M. T. 2000. Cellular signaling by tyrosine phosphorylation in keloid and normal human dermal fibroblasts. *Plast Reconstr Surg,* 106**,** 1532-40.

CHITTURI, R. T., BALASUBRAMANIAM, A. M., PARAMESWAR, R. A., KESAVAN, G., HARIS, K. T. & MOHIDEEN, K. 2015. The role of myofibroblasts in wound healing, contraction and its clinical implications in cleft palate repair. *J Int Oral Health,* 7**,** 75-80.

CHOI, E. J. & MAYO, S. L. 2006. Generation and analysis of proline mutants in protein G. *Protein Eng Des Sel,* 19**,** 285-9.

CINOTTI, E., FERRERO, G., PAPARO, F., PAPADIA, M., FARAVELLI, F., RONGIOLETTI, F., TRAVERSO, C. & DI MARIA, E. 2013. Arthropathy, osteolysis, keloids, relapsing conjunctival pannus and gingival overgrowth: a variant of polyfibromatosis? *Am J Med Genet A,* 161A**,** 1214-20.

CLARK, P. 2014. Protease-mediated ectodomain shedding. *Thorax,* 69**,** 682-4.

COELHO, N. M., ARORA, P. D., VAN PUTTEN, S., BOO, S., PETROVIC, P., LIN, A. X., HINZ, B. & MCCULLOCH, C. A. 2017. Discoidin Domain Receptor 1 Mediates Myosin-Dependent Collagen Contraction. *Cell Rep,* 18**,** 1774-1790.

COELHO, N. M., WANG, A. & MCCULLOCH, C. A. 2019. Discoidin domain receptor 1 interactions with myosin motors contribute to collagen remodeling and tissue fibrosis. *Biochim Biophys Acta Mol Cell Res,* 1866**,** 118510.

COHEN-ARMON, M., VISOCHEK, L., ROZENSAL, D., KALAL, A., GEISTRIKH, I., KLEIN, R., BENDETZ-NEZER, S., YAO, Z. & SEGER, R. 2007. DNA-independent PARP-1 activation by phosphorylated ERK2 increases Elk1 activity: a link to histone acetylation. *Mol Cell,* 25**,** 297-308.

CORCORAN, D. S., JUSKAITE, V., XU, Y., GORLITZ, F., ALEXANDROV, Y., DUNSBY, C., FRENCH, P. M. W. & LEITINGER, B. 2019. DDR1 autophosphorylation is a result of aggregation into dense clusters. *Sci Rep,* 9**,** 17104.

CUELLO, M., ETTENBERG, S. A., CLARK, A. S., KEANE, M. M., POSNER, R. H., NAU, M. M., DENNIS, P. A. & LIPKOWITZ, S. 2001. Down-regulation of the erbB-2 receptor by trastuzumab (herceptin) enhances tumor necrosis factor-related apoptosis-inducing ligand-mediated apoptosis in breast and ovarian cancer cell lines that overexpress erbB-2. *Cancer Res,* 61**,** 4892-900.

CURAT, C. A. & VOGEL, W. F. 2002. Discoidin domain receptor 1 controls growth and adhesion of mesangial cells. *J Am Soc Nephrol,* 13**,** 2648-56.

DAS, R., CHOITHRAMANI, A. & SHARD, A. 2022. A molecular perspective for the use of type IV tyrosine kinase inhibitors as anticancer therapeutics. *Drug Discov Today,* 27**,** 808-821.

DAY, E., WATERS, B., SPIEGEL, K., ALNADAF, T., MANLEY, P. W., BUCHDUNGER, E., WALKER, C. & JARAI, G. 2008. Inhibition of collagen-induced discoidin domain receptor 1 and 2 activation by imatinib, nilotinib and dasatinib. *Eur J Pharmacol,* 599**,** 44-53.

DE MEYTS, P. 2000. The Insulin Receptor and Its Signal Transduction Network. *In:* FEINGOLD, K. R., ANAWALT, B., BLACKMAN, M. R., BOYCE, A., CHROUSOS, G., CORPAS, E., DE HERDER, W. W., DHATARIYA, K., DUNGAN, K., HOFLAND, J., KALRA, S., KALTSAS, G., KAPOOR, N., KOCH, C., KOPP, P., KORBONITS, M., KOVACS, C. S., KUOHUNG, W., LAFERRERE, B., LEVY, M., MCGEE, E. A., MCLACHLAN, R., NEW, M., PURNELL, J., SAHAY, R., SHAH, A. S., SINGER, F., SPERLING, M. A., STRATAKIS, C. A., TRENCE, D. L. & WILSON, D. P. (eds.) *Endotext*. South Dartmouth (MA).

DEJMEK, J., DIB, K., JONSSON, M. & ANDERSSON, T. 2003. Wnt-5a and G-protein signaling are required for collagen-induced DDR1 receptor activation and normal mammary cell adhesion. *Int J Cancer,* 103**,** 344-51.

DENG, Y., ZHAO, F., HUI, L., LI, X., ZHANG, D., LIN, W., CHEN, Z. & NING, Y. 2017. Suppressing miR-199a-3p by promoter methylation contributes to tumor aggressiveness and cisplatin resistance of ovarian cancer through promoting DDR1 expression. *J Ovarian Res,* 10**,** 50.

DESOGUS, A., SCHENONE, S., BRULLO, C., TINTORI, C. & MUSUMECI, F. 2015. Bcr-Abl tyrosine kinase inhibitors: a patent review. *Expert Opin Ther Pat,* 25**,** 397-412.

DI MARCO, E., CUTULI, N., GUERRA, L., CANCEDDA, R. & DE LUCA, M. 1993. Molecular cloning of trkE, a novel trk-related putative tyrosine kinase receptor isolated from normal human keratinocytes and widely expressed by normal human tissues. *J Biol Chem,* 268**,** 24290-5.

DI MARTINO, J. S., NOBRE, A. R., MONDAL, C., TAHA, I., FARIAS, E. F., FERTIG, E. J., NABA, A., AGUIRRE-GHISO, J. A. & BRAVO-CORDERO, J. J. 2022. A tumor-derived type III collagen-rich ECM niche regulates tumor cell dormancy. *Nat Cancer,* 3**,** 90-107.

DIWANJI, D., THAKER, T. & JURA, N. 2019. More than the sum of the parts: Toward full-length receptor tyrosine kinase structures. *IUBMB Life,* 71**,** 706-720.

DU, Z. & LOVLY, C. M. 2018. Mechanisms of receptor tyrosine kinase activation in cancer. *Mol Cancer,* 17**,** 58.

DUMONT, J. E., DREMIER, S., PIRSON, I. & MAENHAUT, C. 2002. Cross signaling, cell specificity, and physiology. *Am J Physiol Cell Physiol,* 283**,** C2-28.

EL AZREQ, M. A., KADIRI, M., BOISVERT, M., PAGE, N., TESSIER, P. A. & AOUDJIT, F. 2016. Discoidin domain receptor 1 promotes Th17 cell migration by activating the RhoA/ROCK/MAPK/ERK signaling pathway. *Oncotarget,* 7**,** 44975-44990.

EL SAYED, I., HELMY, M. W. & EL-ABHAR, H. S. 2018. Inhibition of SRC/FAK cue: A novel pathway for the synergistic effect of rosuvastatin on the anti-cancer effect of dasatinib in hepatocellular carcinoma. *Life Sci,* 213**,** 248-257.

ELKAMHAWY, A., LU, Q., NADA, H., WOO, J., QUAN, G. & LEE, K. 2021. The Journey of DDR1 and DDR2 Kinase Inhibitors as Rising Stars in the Fight Against Cancer. *Int J Mol Sci,* 22.

ENDICOTT, J. A., NOBLE, M. E. & JOHNSON, L. N. 2012. The structural basis for control of eukaryotic protein kinases. *Annu Rev Biochem,* 81**,** 587-613.

ENDRES, N. F., DAS, R., SMITH, A. W., ARKHIPOV, A., KOVACS, E., HUANG, Y., PELTON, J. G., SHAN, Y., SHAW, D. E., WEMMER, D. E., GROVES, J. T. & KURIYAN, J. 2013. Conformational coupling across the plasma membrane in activation of the EGF receptor. *Cell,* 152**,** 543-56.

ESPOSITO, D. & CHATTERJEE, D. K. 2006. Enhancement of soluble protein expression through the use of fusion tags. *Curr Opin Biotechnol,* 17**,** 353-8.

FAN, Y., XU, Z., FAN, J., HUANG, L., YE, M., SHI, K., HUANG, Z., LIU, Y., HE, L., HUANG, J., WANG, Y. & LI, Q. 2016. Prognostic significance of discoidin domain receptor 2 (DDR2) expression in ovarian cancer. *Am J Transl Res,* 8**,** 2845-50.

FARACI-ORF, E., MCFADDEN, C. & VOGEL, W. F. 2006. DDR1 signaling is essential to sustain Stat5 function during lactogenesis. *J Cell Biochem,* 97**,** 109-21.

FARNDALE, R. W., LISMAN, T., BIHAN, D., HAMAIA, S., SMERLING, C. S., PUGH, N., KONITSIOTIS, A., LEITINGER, B., DE GROOT, P. G., JARVIS, G. E. & RAYNAL, N. 2008. Cell-collagen interactions: the use of peptide Toolkits to investigate collagen-receptor interactions. *Biochem Soc Trans,* 36**,** 241-50.

FAUVEL, B. & YASRI, A. 2014. Antibodies directed against receptor tyrosine kinases: current and future strategies to fight cancer. *MAbs,* 6**,** 838-51.

FINGER, C., ESCHER, C. & SCHNEIDER, D. 2009. The single transmembrane domains of human receptor tyrosine kinases encode self-interactions. *Sci Signal,* 2**,** ra56.

FISHER, G. J., VARANI, J. & VOORHEES, J. J. 2008. Looking older: fibroblast collapse and therapeutic implications. *Arch Dermatol,* 144**,** 666-72.

FOX, J. D., ROUTZAHN, K. M., BUCHER, M. H. & WAUGH, D. S. 2003. Maltodextrin-binding proteins from diverse bacteria and archaea are potent solubility enhancers. *FEBS Lett,* 537**,** 53-7.

FRANCESCHI, R. T., HALLETT, S. A. & GE, C. 2023. Discoidin domain receptors; an ancient family of collagen receptors has major roles in bone development, regeneration and metabolism. *Front Dent Med,* 4.

FRANTZ, C., STEWART, K. M. & WEAVER, V. M. 2010. The extracellular matrix at a glance. *J Cell Sci,* 123**,** 4195-200.

FRATTALI, A. L., TREADWAY, J. L. & PESSIN, J. E. 1992. Transmembrane signaling by the human insulin receptor kinase. Relationship between intramolecular beta subunit trans- and cis-autophosphorylation and substrate kinase activation. *J Biol Chem,* 267**,** 19521-8.

FRATTINI, M., FERRARIO, C., BRESSAN, P., BALESTRA, D., DE CECCO, L., MONDELLINI, P., BONGARZONE, I., COLLINI, P., GARIBOLDI, M., PILOTTI, S., PIEROTTI, M. A. & GRECO, A. 2004. Alternative mutations of BRAF, RET and NTRK1 are associated with similar but distinct gene expression patterns in papillary thyroid cancer. *Oncogene,* 23**,** 7436-40.

FREED, D. M., BESSMAN, N. J., KIYATKIN, A., SALAZAR-CAVAZOS, E., BYRNE, P. O., MOORE, J. O., VALLEY, C. C., FERGUSON, K. M., LEAHY, D. J., LIDKE, D. S. & LEMMON, M. A. 2017. EGFR Ligands Differentially Stabilize Receptor Dimers to Specify Signaling Kinetics. *Cell,* 171**,** 683-695 e18.

FREEZE, H. H. & KRANZ, C. 2010. Endoglycosidase and glycoamidase release of N-linked glycans. *Curr Protoc Mol Biol,* Chapter 17**,** Unit 17 13A.

FU, H. L., SOHAIL, A., VALIATHAN, R. R., WASINSKI, B. D., KUMARASIRI, M., MAHASENAN, K. V., BERNARDO, M. M., TOKMINA-ROSZYK, D., FIELDS, G. B., MOBASHERY, S. & FRIDMAN, R. 2013a. Shedding of discoidin domain receptor 1 by membrane-type matrix metalloproteinases. *J Biol Chem,* 288**,** 12114-29.

FU, H. L., VALIATHAN, R. R., ARKWRIGHT, R., SOHAIL, A., MIHAI, C., KUMARASIRI, M., MAHASENAN, K. V., MOBASHERY, S., HUANG, P., AGARWAL, G. & FRIDMAN, R. 2013b. Discoidin domain receptors: unique receptor tyrosine kinases in collagen-mediated signaling. *J Biol Chem,* 288**,** 7430-7.

FU, H. L., VALIATHAN, R. R., PAYNE, L., KUMARASIRI, M., MAHASENAN, K. V., MOBASHERY, S., HUANG, P. & FRIDMAN, R. 2014. Glycosylation at Asn211 regulates the activation state of the discoidin domain receptor 1 (DDR1). *J Biol Chem,* 289**,** 9275-87.

GADIYA, M. & CHAKRABORTY, G. 2018. Signaling by discoidin domain receptor 1 in cancer metastasis. *Cell Adh Migr,* 12**,** 315-323.

GAJRIA, D. & CHANDARLAPATY, S. 2011. HER2-amplified breast cancer: mechanisms of trastuzumab resistance and novel targeted therapies. *Expert Rev Anticancer Ther,* 11**,** 263-75.

GARBUZENKO, E., NAGLER, A., PICKHOLTZ, D., GILLERY, P., REICH, R., MAQUART, F. X. & LEVI-SCHAFFER, F. 2002. Human mast cells stimulate fibroblast proliferation, collagen synthesis and lattice contraction: a direct role for mast cells in skin fibrosis. *Clin Exp Allergy,* 32**,** 237-46.

GARRETT, J. T., OLIVARES, M. G., RINEHART, C., GRANJA-INGRAM, N. D., SANCHEZ, V., CHAKRABARTY, A., DAVE, B., COOK, R. S., PAO, W., MCKINELY, E., MANNING, H. C., CHANG, J. & ARTEAGA, C. L. 2011. Transcriptional and posttranslational up-regulation of HER3 (ErbB3) compensates for inhibition of the HER2 tyrosine kinase. *Proc Natl Acad Sci U S A,* 108**,** 5021-6.

GARRETT, T. P., MCKERN, N. M., LOU, M., ELLEMAN, T. C., ADAMS, T. E., LOVRECZ, G. O., ZHU, H. J., WALKER, F., FRENKEL, M. J., HOYNE, P. A., JORISSEN, R. N., NICE, E. C., BURGESS, A. W. & WARD, C. W. 2002. Crystal structure of a truncated

epidermal growth factor receptor extracellular domain bound to transforming growth factor alpha. *Cell,* 110**,** 763-73.

GE, B., GRAM, H., DI PADOVA, F., HUANG, B., NEW, L., ULEVITCH, R. J., LUO, Y. & HAN, J. 2002. MAPKK-independent activation of p38alpha mediated by TAB1-dependent autophosphorylation of p38alpha. *Science,* 295**,** 1291-4.

GIBSON, T. J., SEILER, M. & VEITIA, R. A. 2013. The transience of transient overexpression. *Nat Methods,* 10**,** 715-21.

GOLDBERG, A. L. 2003. Protein degradation and protection against misfolded or damaged proteins. *Nature,* 426**,** 895-9.

GOMES, R. N., MANUEL, F. & NASCIMENTO, D. S. 2021. The bright side of fibroblasts: molecular signature and regenerative cues in major organs. *NPJ Regen Med,* 6**,** 43.

GRIMMINGER, F., SCHERMULY, R. T. & GHOFRANI, H. A. 2010. Targeting non-malignant disorders with tyrosine kinase inhibitors. *Nat Rev Drug Discov,* 9**,** 956-70.

GRITHER, W. R. & LONGMORE, G. D. 2018. Inhibition of tumor-microenvironment interaction and tumor invasion by small-molecule allosteric inhibitor of DDR2 extracellular domain. *Proc Natl Acad Sci U S A,* 115**,** E7786-E7794.

GROSS, O., BEIROWSKI, B., HARVEY, S. J., MCFADDEN, C., CHEN, D., TAM, S., THORNER, P. S., SMYTH, N., ADDICKS, K., BLOCH, W., NINOMIYA, Y., SADO, Y., WEBER, M. & VOGEL, W. F. 2004. DDR1-deficient mice show localized subepithelial GBM thickening with focal loss of slit diaphragms and proteinuria. *Kidney Int,* 66**,** 102-11.

HACHEHOUCHE, L. N., CHETOUI, N. & AOUDJIT, F. 2010. Implication of discoidin domain receptor 1 in T cell migration in three-dimensional collagen. *Mol Immunol,* 47**,** 1866-9.

HALAWA, M., ABU-HASAN, M. N. & ELMALLAH, M. K. 2015. Hereditary mucoepithelial dysplasia and severe respiratory distress. *Respir Med Case Rep,* 15**,** 27-9.

HAMAIA, S. W., PUGH, N., RAYNAL, N., NEMOZ, B., STONE, R., GULLBERG, D., BIHAN, D. & FARNDALE, R. W. 2012. Mapping of potent and specific binding motifs, GLOGEN and GVOGEA, for integrin alpha1beta1 using collagen toolkits II and III. *J Biol Chem,* 287**,** 26019-28.

HAN, J., WU, J. & SILKE, J. 2020. An overview of mammalian p38 mitogen-activated protein kinases, central regulators of cell stress and receptor signaling. *F1000Res,* 9.

HAN, K. Y., DUGAS-FORD, J., SEIKI, M., CHANG, J. H. & AZAR, D. T. 2015. Evidence for the Involvement of MMP14 in MMP2 Processing and Recruitment in Exosomes of Corneal Fibroblasts. *Invest Ophthalmol Vis Sci,* 56**,** 5323-9.

HANSON, S. M., GEORGHIOU, G., THAKUR, M. K., MILLER, W. T., REST, J. S., CHODERA, J. D. & SEELIGER, M. A. 2019. What Makes a Kinase Promiscuous for Inhibitors? *Cell Chem Biol,* 26**,** 390-399 e5.

HANTSCHEL, O. 2015. Unexpected off-targets and paradoxical pathway activation by kinase inhibitors. *ACS Chem Biol,* 10**,** 234-45.

HARBURGER, D. S. & CALDERWOOD, D. A. 2009. Integrin signalling at a glance. *J Cell Sci,* 122**,** 159-63.

HARJUNPAA, H., LLORT ASENS, M., GUENTHER, C. & FAGERHOLM, S. C. 2019. Cell Adhesion Molecules and Their Roles and Regulation in the Immune and Tumor Microenvironment. *Front Immunol,* 10**,** 1078.

HARPER, S. & SPEICHER, D. W. 2011. Purification of proteins fused to glutathione S-transferase. *Methods Mol Biol,* 681**,** 259-80.

HELDIN, C. H., LU, B., EVANS, R. & GUTKIND, J. S. 2016. Signals and Receptors. *Cold Spring Harb Perspect Biol,* 8**,** a005900.

HERRERA-HERRERA, M. L. & QUEZADA-CALVILLO, R. 2012. DDR2 plays a role in fibroblast migration independent of adhesion ligand and collagen activated DDR2 tyrosine kinase. *Biochem Biophys Res Commun,* 429**,** 39-44.

HEY, S. & LINDER, S. 2024. Matrix metalloproteinases at a glance. *J Cell Sci,* 137.

HIGUCHI, M., ISHIYAMA, K., MARUOKA, M., KANAMORI, R., TAKAORI-KONDO, A. & WATANABE, N. 2021. Paradoxical activation of c-Src as a drug-resistant mechanism. *Cell Rep,* 34**,** 108876.

HILGER, D., MASUREEL, M. & KOBILKA, B. K. 2018. Structure and dynamics of GPCR signaling complexes. *Nat Struct Mol Biol,* 25**,** 4-12.

HILTON, H. N., STANFORD, P. M., HARRIS, J., OAKES, S. R., KAPLAN, W., DALY, R. J. & ORMANDY, C. J. 2008. KIBRA interacts with discoidin domain receptor 1 to modulate collagen-induced signalling. *Biochim Biophys Acta,* 1783**,** 383-93.

HIMANEN, J. P., YERMEKBAYEVA, L., JANES, P. W., WALKER, J. R., XU, K., ATAPATTU, L., RAJASHANKAR, K. R., MENSINGA, A., LACKMANN, M., NIKOLOV, D. B. & DHE-PAGANON, S. 2010. Architecture of Eph receptor clusters. *Proc Natl Acad Sci U S A,* 107**,** 10860-5.

HINZ, B., CELETTA, G., TOMASEK, J. J., GABBIANI, G. & CHAPONNIER, C. 2001. Alpha-smooth muscle actin expression upregulates fibroblast contractile activity. *Mol Biol Cell,* 12**,** 2730-41.

HINZ, B., PITTET, P., SMITH-CLERC, J., CHAPONNIER, C. & MEISTER, J. J. 2004. Myofibroblast development is characterized by specific cell-cell adherens junctions. *Mol Biol Cell,* 15**,** 4310-20.

HOFMANN, M., WINZER, M., WEBER, C. & GIESELER, H. 2018. Low-volume solubility assessment during high-concentration protein formulation development. *J Pharm Pharmacol,* 70**,** 636-647.

HOHMANN, T. & DEHGHANI, F. 2019. The Cytoskeleton-A Complex Interacting Meshwork. *Cells,* 8.

HOMMELGAARD, A. M., LERDRUP, M. & VAN DEURS, B. 2004. Association with membrane protrusions makes ErbB2 an internalization-resistant receptor. *Mol Biol Cell,* 15**,** 1557-67.

HORI, Y., KASHIMOTO, T., YONEZAWA, T., SANO, N., SAITOH, R., IGARASHI, S., CHIKAZAWA, S., KANAI, K., HOSHI, F., ITOH, N. & HIGUCHI, S. 2012. Matrix metalloproteinase-2 stimulates collagen-I expression through phosphorylation of focal adhesion kinase in rat cardiac fibroblasts. *Am J Physiol Cell Physiol,* 303**,** C947-53.

HOWARD, E. W., CRIDER, B. J., UPDIKE, D. L., BULLEN, E. C., PARKS, E. E., HAAKSMA, C. J., SHERRY, D. M. & TOMASEK, J. J. 2012. MMP-2 expression by fibroblasts is suppressed by the myofibroblast phenotype. *Exp Cell Res,* 318**,** 1542-53.

HOWARD, J. C., VARALLO, V. M., ROSS, D. C., ROTH, J. H., FABER, K. J., ALMAN, B. & GAN, B. S. 2003. Elevated levels of beta-catenin and fibronectin in three-dimensional collagen cultures of Dupuytren's disease cells are regulated by tension in vitro. *BMC Musculoskelet Disord,* 4**,** 16.

HUANG, Y., ARORA, P., MCCULLOCH, C. A. & VOGEL, W. F. 2009. The collagen receptor DDR1 regulates cell spreading and motility by associating with myosin IIA. *J Cell Sci,* 122**,** 1637-46.

HUBBARD, S. R. 1997. Crystal structure of the activated insulin receptor tyrosine kinase in complex with peptide substrate and ATP analog. *EMBO J,* 16**,** 5572-81.

HUBBARD, S. R. 2002. Autoinhibitory mechanisms in receptor tyrosine kinases. *Front Biosci,* 7**,** d330-40.

HUBBARD, S. R. 2004. Juxtamembrane autoinhibition in receptor tyrosine kinases. *Nat Rev Mol Cell Biol,* 5**,** 464-71.

HUBBARD, S. R. 2013. The insulin receptor: both a prototypical and atypical receptor tyrosine kinase. *Cold Spring Harb Perspect Biol,* 5**,** a008946.

HUBBARD, S. R. & MILLER, W. T. 2007. Receptor tyrosine kinases: mechanisms of activation and signaling. *Curr Opin Cell Biol,* 19**,** 117-23.

HUBBARD, S. R. & TILL, J. H. 2000. Protein tyrosine kinase structure and function. *Annu Rev Biochem,* 69**,** 373-98.

HUBBARD, S. R., WEI, L., ELLIS, L. & HENDRICKSON, W. A. 1994. Crystal structure of the tyrosine kinase domain of the human insulin receptor. *Nature,* 372**,** 746-54.

HYNES, R. O. 2002. Integrins: bidirectional, allosteric signaling machines. *Cell,* 110**,** 673-87.

HYNES, R. O. 2009. The extracellular matrix: not just pretty fibrils. *Science,* 326**,** 1216-9.

ICHIKAWA, O., OSAWA, M., NISHIDA, N., GOSHIMA, N., NOMURA, N. & SHIMADA, I. 2007. Structural basis of the collagen-binding mode of discoidin domain receptor 2. *EMBO J,* 26**,** 4168-76.

IKEDA, K., WANG, L. H., TORRES, R., ZHAO, H., OLASO, E., ENG, F. J., LABRADOR, P., KLEIN, R., LOVETT, D., YANCOPOULOS, G. D., FRIEDMAN, S. L. & LIN, H. C. 2002. Discoidin domain receptor 2 interacts with Src and Shc following its activation by type I collagen. *J Biol Chem,* 277**,** 19206-12.

ITOH, Y. 2018. Discoidin domain receptors: Microenvironment sensors that promote cellular migration and invasion. *Cell Adh Migr,* 12**,** 378-385.

ITOH, Y. 2021. Modulation of Microenvironment Signals by Proteolytic Shedding of Cell Surface Extracellular Matrix Receptors. *Front Cell Dev Biol,* 9**,** 736735.

IWAI, L. K., CHANG, F. & HUANG, P. H. 2013a. Phosphoproteomic analysis identifies insulin enhancement of discoidin domain receptor 2 phosphorylation. *Cell Adh Migr,* 7**,** 161-4.

IWAI, L. K., PAYNE, L. S., LUCZYNSKI, M. T., CHANG, F., XU, H., CLINTON, R. W., PAUL, A., ESPOSITO, E. A., GRIDLEY, S., LEITINGER, B., NAEGLE, K. M. & HUANG, P. H. 2013b. Phosphoproteomics of collagen receptor networks reveals SHP-2 phosphorylation downstream of wild-type DDR2 and its lung cancer mutants. *Biochem J,* 454**,** 501-13.

IWATA, T., CHEN, L., LI, C., OVCHINNIKOV, D. A., BEHRINGER, R. R., FRANCOMANO, C. A. & DENG, C. X. 2000. A neonatal lethal mutation in FGFR3 uncouples proliferation and differentiation of growth plate chondrocytes in embryos. *Hum Mol Genet,* 9**,** 1603-13.

IZARZUGAZA, J. M., REDFERN, O. C., ORENGO, C. A. & VALENCIA, A. 2009. Cancer-associated mutations are preferentially distributed in protein kinase functional sites. *Proteins,* 77**,** 892-903.

JEFFRIES, D. E., BORZA, C. M., BLOBAUM, A. L., POZZI, A. & LINDSLEY, C. W. 2020. Discovery of VU6015929: A Selective Discoidin Domain Receptor 1/2 (DDR1/2) Inhibitor to Explore the Role of DDR1 in Antifibrotic Therapy. *ACS Med Chem Lett,* 11**,** 29-33.

JIA, S., AGARWAL, M., YANG, J., HOROWITZ, J. C., WHITE, E. S. & KIM, K. K. 2018. Discoidin Domain Receptor 2 Signaling Regulates Fibroblast Apoptosis through PDK1/Akt. *Am J Respir Cell Mol Biol,* 59**,** 295-305.

JIA, Y., YUN, C. H., PARK, E., ERCAN, D., MANUIA, M., JUAREZ, J., XU, C., RHEE, K., CHEN, T., ZHANG, H., PALAKURTHI, S., JANG, J., LELAIS, G., DIDONATO, M., BURSULAYA, B., MICHELLYS, P. Y., EPPLE, R., MARSILJE, T. H., MCNEILL, M., LU, W., HARRIS, J., BENDER, S., WONG, K. K., JANNE, P. A. & ECK, M. J. 2016. Overcoming EGFR(T790M) and EGFR(C797S) resistance with mutant-selective allosteric inhibitors. *Nature,* 534**,** 129-32.

JINNIN, M., IHN, H., ASANO, Y., YAMANE, K., TROJANOWSKA, M. & TAMAKI, K. 2004. Tenascin-C upregulation by transforming growth factor-beta in human dermal fibroblasts involves Smad3, Sp1, and Ets1. *Oncogene,* 23**,** 1656-67.

JOHNSON, J. D., EDMAN, J. C. & RUTTER, W. J. 1993. A receptor tyrosine kinase found in breast carcinoma cells has an extracellular discoidin I-like domain. *Proc Natl Acad Sci U S A,* 90**,** 10891.

JOHNSTON, J. J., SANCHEZ-CONTRERAS, M. Y., KEPPLER-NOREUIL, K. M., SAPP, J., CRENSHAW, M., FINCH, N. A., CORMIER-DAIRE, V., RADEMAKERS, R., SYBERT, V. P. & BIESECKER, L. G. 2015. A Point Mutation in PDGFRB Causes Autosomal-Dominant Penttinen Syndrome. *Am J Hum Genet,* 97**,** 465-74.

JUIN, A., BILLOTTET, C., MOREAU, V., DESTAING, O., ALBIGES-RIZO, C., ROSENBAUM, J., GENOT, E. & SALTEL, F. 2012. Physiological type I collagen organization induces the formation of a novel class of linear invadosomes. *Mol Biol Cell,* 23**,** 297-309.

JUIN, A., DI MARTINO, J., LEITINGER, B., HENRIET, E., GARY, A. S., PAYSAN, L., BOMO, J., BAFFET, G., GAUTHIER-ROUVIERE, C., ROSENBAUM, J., MOREAU, V. & SALTEL, F. 2014. Discoidin domain receptor 1 controls linear invadosome formation via a Cdc42-Tuba pathway. *J Cell Biol,* 207**,** 517-33.

JURA, N., ZHANG, X., ENDRES, N. F., SEELIGER, M. A., SCHINDLER, T. & KURIYAN, J. 2011. Catalytic control in the EGF receptor and its connection to general kinase regulatory mechanisms. *Mol Cell,* 42**,** 9-22.

JUSKAITE, V., CORCORAN, D. S. & LEITINGER, B. 2017. Collagen induces activation of DDR1 through lateral dimer association and phosphorylation between dimers. *Elife,* 6.

KADLER, K. E., BALDOCK, C., BELLA, J. & BOOT-HANDFORD, R. P. 2007. Collagens at a glance. *J Cell Sci,* 120**,** 1955-8.

KAMOHARA, H., YAMASHIRO, S., GALLIGAN, C. & YOSHIMURA, T. 2001. Discoidin domain receptor 1 isoform-a (DDR1alpha) promotes migration of leukocytes in three-dimensional collagen lattices. *FASEB J,* 15**,** 2724-6.

KAMRANI, P., MARSTON, G., ARBOR, T. C. & JAN, A. 2024. Anatomy, Connective Tissue. *StatPearls*. Treasure Island (FL).

KANDA, T., FUNATO, N., BABA, Y. & KURODA, T. 2003. Evidence for fibroblast growth factor receptors in myofibroblasts during palatal mucoperiosteal repair. *Arch Oral Biol,* 48**,** 213-21.

KARN, T., HOLTRICH, U., BRAUNINGER, A., BOHME, B., WOLF, G., RUBSAMEN-WAIGMANN, H. & STREBHARDT, K. 1993. Structure, expression and chromosomal mapping of TKT from man and mouse: a new subclass of receptor tyrosine kinases with a factor VIII-like domain. *Oncogene,* 8**,** 3433-40.

KAVRAN, J. M., MCCABE, J. M., BYRNE, P. O., CONNACHER, M. K., WANG, Z., RAMEK, A., SARABIPOUR, S., SHAN, Y., SHAW, D. E., HRISTOVA, K., COLE, P. A. & LEAHY, D. J. 2014. How IGF-1 activates its receptor. *Elife,* 3.

KAWECKI, F., GLUAIS, M., CLAVEROL, S., DUSSERRE, N., MCALLISTER, T. & L'HEUREUX, N. 2022. Inter-donor variability of extracellular matrix production in long-term cultures of human fibroblasts. *Biomater Sci,* 10**,** 3935-3950.

KENNY, F. N. & CONNELLY, J. T. 2015. Integrin-mediated adhesion and mechano-sensing in cutaneous wound healing. *Cell Tissue Res,* 360**,** 571-82.

KIKUCHI, K., KADONO, T., FURUE, M. & TAMAKI, K. 1997. Tissue inhibitor of metalloproteinase 1 (TIMP-1) may be an autocrine growth factor in scleroderma fibroblasts. *J Invest Dermatol,* 108**,** 281-4.

KIM, K. K., SHEPPARD, D. & CHAPMAN, H. A. 2018. TGF-beta1 Signaling and Tissue Fibrosis. *Cold Spring Harb Perspect Biol,* 10.

KIM, S. H., TURNBULL, J. & GUIMOND, S. 2011. Extracellular matrix and cell signalling: the dynamic cooperation of integrin, proteoglycan and growth factor receptor. *J Endocrinol,* 209**,** 139-51.

KLAPHOLZ, B. & BROWN, N. H. 2017. Talin - the master of integrin adhesions. *J Cell Sci,* 130**,** 2435-2446.

KLUG, L. R., KENT, J. D. & HEINRICH, M. C. 2018. Structural and clinical consequences of activation loop mutations in class III receptor tyrosine kinases. *Pharmacol Ther,* 191**,** 123-134.

KNIGHTON, D. R., ZHENG, J. H., TEN EYCK, L. F., ASHFORD, V. A., XUONG, N. H., TAYLOR, S. S. & SOWADSKI, J. M. 1991. Crystal structure of the catalytic subunit of cyclic adenosine monophosphate-dependent protein kinase. *Science,* 253**,** 407-14.

KONITSIOTIS, A. D., RAYNAL, N., BIHAN, D., HOHENESTER, E., FARNDALE, R. W. & LEITINGER, B. 2008. Characterization of high affinity binding motifs for the discoidin domain receptor DDR2 in collagen. *J Biol Chem,* 283**,** 6861-8.

KOO, D. H., MCFADDEN, C., HUANG, Y., ABDULHUSSEIN, R., FRIESE-HAMIM, M. & VOGEL, W. F. 2006. Pinpointing phosphotyrosine-dependent interactions downstream of the collagen receptor DDR1. *FEBS Lett,* 580**,** 15-22.

KORENNYKH, A. V., EGEA, P. F., KOROSTELEV, A. A., FINER-MOORE, J., ZHANG, C., SHOKAT, K. M., STROUD, R. M. & WALTER, P. 2009. The unfolded protein response signals through high-order assembly of Ire1. *Nature,* 457**,** 687-93.

KORNEV, A. P., HASTE, N. M., TAYLOR, S. S. & EYCK, L. F. 2006. Surface comparison of active and inactive protein kinases identifies a conserved activation mechanism. *Proc Natl Acad Sci U S A,* 103**,** 17783-8.

KORNEV, A. P. & TAYLOR, S. S. 2010. Defining the conserved internal architecture of a protein kinase. *Biochim Biophys Acta,* 1804**,** 440-4.

KRAMPERT, M., HELDIN, C. H. & HEUCHEL, R. L. 2008. A gain-of-function mutation in the PDGFR-beta alters the kinetics of injury response in liver and skin. *Lab Invest,* 88**,** 1204-14.

KRIS, M. G., NATALE, R. B., HERBST, R. S., LYNCH, T. J., JR., PRAGER, D., BELANI, C. P., SCHILLER, J. H., KELLY, K., SPIRIDONIDIS, H., SANDLER, A., ALBAIN, K. S., CELLA,

D., WOLF, M. K., AVERBUCH, S. D., OCHS, J. J. & KAY, A. C. 2003. Efficacy of gefitinib, an inhibitor of the epidermal growth factor receptor tyrosine kinase, in symptomatic patients with non-small cell lung cancer: a randomized trial. *JAMA,* 290**,** 2149-58.

KULAR, J. K., BASU, S. & SHARMA, R. I. 2014. The extracellular matrix: Structure, composition, age-related differences, tools for analysis and applications for tissue engineering. *J Tissue Eng,* 5**,** 2041731414557112.

KUNG, J. E. & JURA, N. 2016. Structural Basis for the Non-catalytic Functions of Protein Kinases. *Structure,* 24**,** 7-24.

LABRADOR, J. P., AZCOITIA, V., TUCKERMANN, J., LIN, C., OLASO, E., MANES, S., BRUCKNER, K., GOERGEN, J. L., LEMKE, G., YANCOPOULOS, G., ANGEL, P., MARTINEZ, C. & KLEIN, R. 2001. The collagen receptor DDR2 regulates proliferation and its elimination leads to dwarfism. *EMBO Rep,* 2**,** 446-52.

LAHIRY, P., TORKAMANI, A., SCHORK, N. J. & HEGELE, R. A. 2010. Kinase mutations in human disease: interpreting genotype-phenotype relationships. *Nat Rev Genet,* 11**,** 60-74.

LAI, C. & LEMKE, G. 1994. Structure and expression of the Tyro 10 receptor tyrosine kinase. *Oncogene,* 9**,** 877-83.

LAURINI, E., POSOCCO, P., FERMEGLIA, M., GIBBONS, D. L., QUINTAS-CARDAMA, A. & PRICL, S. 2013. Through the open door: Preferential binding of dasatinib to the active form of BCR-ABL unveiled by in silico experiments. *Mol Oncol,* 7**,** 968-75.

LAVAL, S., BUTLER, R., SHELLING, A. N., HANBY, A. M., POULSOM, R. & GANESAN, T. S. 1994. Isolation and characterization of an epithelial-specific receptor tyrosine kinase from an ovarian cancer cell line. *Cell Growth Differ,* 5**,** 1173-83.

LEASK, A. 2013. Integrin beta1: A Mechanosignaling Sensor Essential for Connective Tissue Deposition by Fibroblasts. *Adv Wound Care (New Rochelle),* 2**,** 160-166.

LEE, C. R., PARK, Y. H., MIN, H., KIM, Y. R. & SEOK, Y. J. 2019. Determination of protein phosphorylation by polyacrylamide gel electrophoresis. *J Microbiol,* 57**,** 93-100.

LEITINGER, B. 2003. Molecular analysis of collagen binding by the human discoidin domain receptors, DDR1 and DDR2. Identification of collagen binding sites in DDR2. *J Biol Chem,* 278**,** 16761-9.

LEITINGER, B. 2011. Transmembrane collagen receptors. *Annu Rev Cell Dev Biol,* 27**,** 265-90.

LEITINGER, B. 2014. Discoidin domain receptor functions in physiological and pathological conditions. *Int Rev Cell Mol Biol,* 310**,** 39-87.

LEITINGER, B. 2022. Pulling the strings of tumor collagen. *Nat Cancer,* 3**,** 9-10.

LEITINGER, B. & KWAN, A. P. 2006. The discoidin domain receptor DDR2 is a receptor for type X collagen. *Matrix Biol,* 25**,** 355-64.

LEITINGER, B., STEPLEWSKI, A. & FERTALA, A. 2004. The D2 period of collagen II contains a specific binding site for the human discoidin domain receptor, DDR2. *J Mol Biol,* 344**,** 993-1003.

LEMEER, S., BLUWSTEIN, A., WU, Z., LEBERFINGER, J., MULLER, K., KRAMER, K. & KUSTER, B. 2012. Phosphotyrosine mediated protein interactions of the discoidin domain receptor 1. *J Proteomics,* 75**,** 3465-77.

LEMMON, M. A. & SCHLESSINGER, J. 2010. Cell signaling by receptor tyrosine kinases. *Cell,* 141**,** 1117-34.

LENDAHL, U., MUHL, L. & BETSHOLTZ, C. 2022. Identification, discrimination and heterogeneity of fibroblasts. *Nat Commun,* 13**,** 3409.
LEVI-SCHAFFER, F., GARBUZENKO, E., RUBIN, A., REICH, R., PICKHOLZ, D., GILLERY, P., EMONARD, H., NAGLER, A. & MAQUART, F. A. 1999. Human eosinophils regulate human lung- and skin-derived fibroblast properties in vitro: a role for transforming growth factor beta (TGF-beta). *Proc Natl Acad Sci U S A,* 96**,** 9660-5.
LI, B. & WANG, J. H. 2011. Fibroblasts and myofibroblasts in wound healing: force generation and measurement. *J Tissue Viability,* 20**,** 108-20.
LI, C., WEN, A., SHEN, B., LU, J., HUANG, Y. & CHANG, Y. 2011. FastCloning: a highly simplified, purification-free, sequence- and ligation-independent PCR cloning method. *BMC Biotechnol,* 11**,** 92.
LI, E. & HRISTOVA, K. 2006. Role of receptor tyrosine kinase transmembrane domains in cell signaling and human pathologies. *Biochemistry,* 45**,** 6241-51.
LI, E., WIMLEY, W. C. & HRISTOVA, K. 2012. Transmembrane helix dimerization: beyond the search for sequence motifs. *Biochim Biophys Acta,* 1818**,** 183-93.
LI, M., PENG, L., WANG, Z., LIU, L., CAO, M., CUI, J., WU, F. & YANG, J. 2023. Roles of the cytoskeleton in human diseases. *Mol Biol Rep,* 50**,** 2847-2856.
LI, S., WONG, A. H. & LIU, F. 2014. Ligand-gated ion channel interacting proteins and their role in neuroprotection. *Front Cell Neurosci,* 8**,** 125.
LI, W., FAN, J., CHEN, M., GUAN, S., SAWCER, D., BOKOCH, G. M. & WOODLEY, D. T. 2004. Mechanism of human dermal fibroblast migration driven by type I collagen and platelet-derived growth factor-BB. *Mol Biol Cell,* 15**,** 294-309.
LI, W. & MILLER, W. T. 2006. Role of the activation loop tyrosines in regulation of the insulin-like growth factor I receptor-tyrosine kinase. *J Biol Chem,* 281**,** 23785-91.
LIANG, L., YAN, X. E., YIN, Y. & YUN, C. H. 2016. Structural and biochemical studies of the PDGFRA kinase domain. *Biochem Biophys Res Commun,* 477**,** 667-672.
LING, S., KWAK, D. & KIM, K. K. 2023. Inhibition of discoidin domain receptor 2 reveals kinase-dependent and kinase-independent functions in regulating fibroblast activity. *Am J Physiol Lung Cell Mol Physiol,* 325**,** L342-L351.
LING, S., KWAK, D., TAKUWA, Y., GE, C., FRANCESCHI, R. & KIM, K. K. 2024. Discoidin domain receptor 2 signaling through PIK3C2alpha in fibroblasts promotes lung fibrosis. *J Pathol,* 262**,** 505-516.
LIU, H., CHEN, X., FOCIA, P. J. & HE, X. 2007. Structural basis for stem cell factor-KIT signaling and activation of class III receptor tyrosine kinases. *EMBO J,* 26**,** 891-901.
LIU, H. & NAISMITH, J. H. 2008. An efficient one-step site-directed deletion, insertion, single and multiple-site plasmid mutagenesis protocol. *BMC Biotechnol,* 8**,** 91.
LIU, J., CHIANG, H. C., XIONG, W., LAURENT, V., GRIFFITHS, S. C., DULFER, J., DENG, H., SUN, X., YIN, Y. W., LI, W., AUDOLY, L. P., AN, Z., SCHURPF, T., LI, R. & ZHANG, N. 2023. A highly selective humanized DDR1 mAb reverses immune exclusion by disrupting collagen fiber alignment in breast cancer. *J Immunother Cancer,* 11.
LIU, M., ZHANG, J., LI, X. & WANG, Y. 2024. Research progress of DDR1 inhibitors in the treatment of multiple human diseases. *Eur J Med Chem,* 268**,** 116291.
LIU, X., SONG, X., ZHANG, J., XU, Z., CHE, L., QIAO, Y., ORTIZ PEDRAZA, Y., CIGLIANO, A., PASCALE, R. M., CALVISI, D. F., LIU, Y. & CHEN, X. 2018. Focal adhesion kinase activation limits efficacy of Dasatinib in c-Myc driven hepatocellular carcinoma. *Cancer Med,* 7**,** 6170-6181.

LIVAK, K. J. & SCHMITTGEN, T. D. 2001. Analysis of relative gene expression data using real-time quantitative PCR and the 2(-Delta Delta C(T)) Method. *Methods,* 25**,** 402-8.

LOCHHEAD, P. A. 2009. Protein kinase activation loop autophosphorylation in cis: overcoming a Catch-22 situation. *Sci Signal,* 2**,** pe4.

LOCHHEAD, P. A., KINSTRIE, R., SIBBET, G., RAWJEE, T., MORRICE, N. & CLEGHON, V. 2006. A chaperone-dependent GSK3beta transitional intermediate mediates activation-loop autophosphorylation. *Mol Cell,* 24**,** 627-33.

LOVLY, C. M. & SHAW, A. T. 2014. Molecular pathways: resistance to kinase inhibitors and implications for therapeutic strategies. *Clin Cancer Res,* 20**,** 2249-56.

LU, K. K., TRCKA, D. & BENDECK, M. P. 2011a. Collagen stimulates discoidin domain receptor 1-mediated migration of smooth muscle cells through Src. *Cardiovasc Pathol,* 20**,** 71-6.

LU, P., TAKAI, K., WEAVER, V. M. & WERB, Z. 2011b. Extracellular matrix degradation and remodeling in development and disease. *Cold Spring Harb Perspect Biol,* 3.

LUETTEKE, N. C., PHILLIPS, H. K., QIU, T. H., COPELAND, N. G., EARP, H. S., JENKINS, N. A. & LEE, D. C. 1994. The mouse waved-2 phenotype results from a point mutation in the EGF receptor tyrosine kinase. *Genes Dev,* 8**,** 399-413.

LUO, B. H., CARMAN, C. V. & SPRINGER, T. A. 2007. Structural basis of integrin regulation and signaling. *Annu Rev Immunol,* 25**,** 619-47.

LUO, Z., LIU, H., SUN, X., GUO, R., CUI, R., MA, X. & YAN, M. 2013. RNA interference against discoidin domain receptor 2 ameliorates alcoholic liver disease in rats. *PLoS One,* 8**,** e55860.

MA, Y. S., WU, Z. J., BAI, R. Z., DONG, H., XIE, B. X., WU, X. H., HANG, X. S., LIU, A. N., JIANG, X. H., WANG, G. R., JIANG, J. J., XU, W. H., CHEN, X. P., TAN, G. H., FU, D., LIU, J. B. & LIU, Q. 2018. DRR1 promotes glioblastoma cell invasion and epithelial-mesenchymal transition via regulating AKT activation. *Cancer Lett,* 423**,** 86-94.

MAJKOWSKA, I., SHITOMI, Y., ITO, N., GRAY, N. S. & ITOH, Y. 2017. Discoidin domain receptor 2 mediates collagen-induced activation of membrane-type 1 matrix metalloproteinase in human fibroblasts. *J Biol Chem,* 292**,** 6633-6643.

MAJO, S. & AUGUSTE, P. 2021. The Yin and Yang of Discoidin Domain Receptors (DDRs): Implications in Tumor Growth and Metastasis Development. *Cancers (Basel),* 13.

MAKINO, K., JINNIN, M., AOI, J., HIRANO, A., KAJIHARA, I., MAKINO, T., SAKAI, K., FUKUSHIMA, S., INOUE, Y. & IHN, H. 2013. Discoidin domain receptor 2-microRNA 196a-mediated negative feedback against excess type I collagen expression is impaired in scleroderma dermal fibroblasts. *J Invest Dermatol,* 133**,** 110-9.

MALAKPOUR-PERMLID, A., BUZZI, I., HEGARDT, C., JOHANSSON, F. & OREDSSON, S. 2021. Identification of extracellular matrix proteins secreted by human dermal fibroblasts cultured in 3D electrospun scaffolds. *Sci Rep,* 11**,** 6655.

MANNING, L. B., LI, Y., CHICKMAGALUR, N. S., LI, X. & XU, L. 2016. Discoidin Domain Receptor 2 as a Potential Therapeutic Target for Development of Disease-Modifying Osteoarthritis Drugs. *Am J Pathol,* 186**,** 3000-3010.

MARIADOSS, A. V. A. & WANG, C. Z. 2023. Exploring the Cellular and Molecular Mechanism of Discoidin Domain Receptors (DDR1 and DDR2) in Bone Formation, Regeneration, and Its Associated Disease Conditions. *Int J Mol Sci,* 24.

MARSHALL, C. J. 1995. Specificity of receptor tyrosine kinase signaling: transient versus sustained extracellular signal-regulated kinase activation. *Cell,* 80**,** 179-85.
MARUYAMA, I. N. 2014. Mechanisms of activation of receptor tyrosine kinases: monomers or dimers. *Cells,* 3**,** 304-30.
MCCLENDON, C. L., KORNEV, A. P., GILSON, M. K. & TAYLOR, S. S. 2014. Dynamic architecture of a protein kinase. *Proc Natl Acad Sci U S A,* 111**,** E4623-31.
MCDONELL, L. M., KERNOHAN, K. D., BOYCOTT, K. M. & SAWYER, S. L. 2015. Receptor tyrosine kinase mutations in developmental syndromes and cancer: two sides of the same coin. *Hum Mol Genet,* 24**,** R60-6.
MCGOWAN, S. E. 2023. Discoidin domain receptor-2 enhances secondary alveolar septation in mice by activating integrins and modifying focal adhesions. *Am J Physiol Lung Cell Mol Physiol,* 324**,** L307-L324.
MCKEE, T. J., PERLMAN, G., MORRIS, M. & KOMAROVA, S. V. 2019. Extracellular matrix composition of connective tissues: a systematic review and meta-analysis. *Sci Rep,* 9**,** 10542.
MCLARTY, K., CORNELISSEN, B., CAI, Z., SCOLLARD, D. A., COSTANTINI, D. L., DONE, S. J. & REILLY, R. M. 2009. Micro-SPECT/CT with 111In-DTPA-pertuzumab sensitively detects trastuzumab-mediated HER2 downregulation and tumor response in athymic mice bearing MDA-MB-361 human breast cancer xenografts. *J Nucl Med,* 50**,** 1340-8.
MEDVES, S. & DEMOULIN, J. B. 2012. Tyrosine kinase gene fusions in cancer: translating mechanisms into targeted therapies. *J Cell Mol Med,* 16**,** 237-48.
MELNIKOV, S., MAILLIOT, J., RIGGER, L., NEUNER, S., SHIN, B. S., YUSUPOVA, G., DEVER, T. E., MICURA, R. & YUSUPOV, M. 2016. Molecular insights into protein synthesis with proline residues. *EMBO Rep,* 17**,** 1776-1784.
MEYER ZUM GOTTESBERGE, A. M., GROSS, O., BECKER-LENDZIAN, U., MASSING, T. & VOGEL, W. F. 2008. Inner ear defects and hearing loss in mice lacking the collagen receptor DDR1. *Lab Invest,* 88**,** 27-37.
MICHAEL, M. & PARSONS, M. 2020. New perspectives on integrin-dependent adhesions. *Curr Opin Cell Biol,* 63**,** 31-37.
MIETTINEN, P. J., BERGER, J. E., MENESES, J., PHUNG, Y., PEDERSEN, R. A., WERB, Z. & DERYNCK, R. 1995. Epithelial immaturity and multiorgan failure in mice lacking epidermal growth factor receptor. *Nature,* 376**,** 337-41.
MIHAI, C., CHOTANI, M., ELTON, T. S. & AGARWAL, G. 2009. Mapping of DDR1 distribution and oligomerization on the cell surface by FRET microscopy. *J Mol Biol,* 385**,** 432-45.
MILLER, E. J. & LAPPIN, S. L. 2024. Physiology, Cellular Receptor. *StatPearls*. Treasure Island (FL).
MILLER, M. A., SULLIVAN, R. J. & LAUFFENBURGER, D. A. 2017. Molecular Pathways: Receptor Ectodomain Shedding in Treatment, Resistance, and Monitoring of Cancer. *Clin Cancer Res,* 23**,** 623-629.
MOHAMED, F. F., GE, C., COWLING, R. T., LUCAS, D., HALLETT, S. A., ONO, N., BINRAYES, A. A., GREENBERG, B. & FRANCESCHI, R. T. 2022. The collagen receptor, discoidin domain receptor 2, functions in Gli1-positive skeletal progenitors and chondrocytes to control bone development. *Bone Res,* 10**,** 11.

MOHAMMADI, M., SCHLESSINGER, J. & HUBBARD, S. R. 1996. Structure of the FGF receptor tyrosine kinase domain reveals a novel autoinhibitory mechanism. *Cell,* 86**,** 577-87.

MOL, C. D., DOUGAN, D. R., SCHNEIDER, T. R., SKENE, R. J., KRAUS, M. L., SCHEIBE, D. N., SNELL, G. P., ZOU, H., SANG, B. C. & WILSON, K. P. 2004. Structural basis for the autoinhibition and STI-571 inhibition of c-Kit tyrosine kinase. *J Biol Chem,* 279**,** 31655-63.

MOL, C. D., LIM, K. B., SRIDHAR, V., ZOU, H., CHIEN, E. Y., SANG, B. C., NOWAKOWSKI, J., KASSEL, D. B., CRONIN, C. N. & MCREE, D. E. 2003. Structure of a c-kit product complex reveals the basis for kinase transactivation. *J Biol Chem,* 278**,** 31461-4.

MONTOR, W. R., SALAS, A. & MELO, F. H. M. 2018. Receptor tyrosine kinases and downstream pathways as druggable targets for cancer treatment: the current arsenal of inhibitors. *Mol Cancer,* 17**,** 55.

MORI, S., RONNSTRAND, L., YOKOTE, K., ENGSTROM, A., COURTNEIDGE, S. A., CLAESSON-WELSH, L. & HELDIN, C. H. 1993. Identification of two juxtamembrane autophosphorylation sites in the PDGF beta-receptor; involvement in the interaction with Src family tyrosine kinases. *EMBO J,* 12**,** 2257-64.

MULLER, A. K., MEYER, M. & WERNER, S. 2012. The roles of receptor tyrosine kinases and their ligands in the wound repair process. *Semin Cell Dev Biol,* 23**,** 963-70.

MUNTANE, G., CHILLIDA, M., ARANDA, S., NAVARRO, A. & VILELLA, E. 2021. Coexpression of the discoidin domain receptor 1 gene with oligodendrocyte-related and schizophrenia risk genes in the developing and adult human brain. *Brain Behav,* 11**,** e2309.

NAIR, A., CHAUHAN, P., SAHA, B. & KUBATZKY, K. F. 2019. Conceptual Evolution of Cell Signaling. *Int J Mol Sci,* 20.

NANGOLE, F. W. & AGAK, G. W. 2019. Keloid pathophysiology: fibroblast or inflammatory disorders? *JPRAS Open,* 22**,** 44-54.

NATARAJAN, K. & BERK, B. C. 2006. Crosstalk coregulation mechanisms of G protein-coupled receptors and receptor tyrosine kinases. *Methods Mol Biol,* 332**,** 51-77.

NAWROTEK, A., TALAGAS, A., VUILLARD, L.M., MIALLAU, L. 2020. Structure of DDR2 Kinase domain in complex with IBZ3. *To be published*.

NEBEN, C. L., LO, M., JURA, N. & KLEIN, O. D. 2019. Feedback regulation of RTK signaling in development. *Dev Biol,* 447**,** 71-89.

NEDELEC, A., GUERIT, E. M., DACHY, G., LENGLEZ, S., WONG, L. S., ARTS, F. A. & DEMOULIN, J. B. 2022. Penttinen syndrome-associated PDGFRB Val665Ala variant causes aberrant constitutive STAT1 signalling. *J Cell Mol Med,* 26**,** 3902-3912.

NEUMANN, E., RIEPL, B., KNEDLA, A., LEFEVRE, S., TARNER, I. H., GRIFKA, J., STEINMEYER, J., SCHOLMERICH, J., GAY, S. & MULLER-LADNER, U. 2010. Cell culture and passaging alters gene expression pattern and proliferation rate in rheumatoid arthritis synovial fibroblasts. *Arthritis Res Ther,* 12**,** R83.

NGO, P., RAMALINGAM, P., PHILLIPS, J. A. & FURUTA, G. T. 2006. Collagen gel contraction assay. *Methods Mol Biol,* 341**,** 103-9.

NIKOLOV, A. & POPOVSKI, N. 2021. Role of Gelatinases MMP-2 and MMP-9 in Healthy and Complicated Pregnancy and Their Future Potential as Preeclampsia Biomarkers. *Diagnostics (Basel),* 11.

NIU, X. L., PETERS, K. G. & KONTOS, C. D. 2002. Deletion of the carboxyl terminus of Tie2 enhances kinase activity, signaling, and function. Evidence for an autoinhibitory mechanism. *J Biol Chem,* 277**,** 31768-73.

NOBLE, M. E., ENDICOTT, J. A. & JOHNSON, L. N. 2004. Protein kinase inhibitors: insights into drug design from structure. *Science,* 303**,** 1800-5.

NOORDEEN, N. A., CARAFOLI, F., HOHENESTER, E., HORTON, M. A. & LEITINGER, B. 2006. A transmembrane leucine zipper is required for activation of the dimeric receptor tyrosine kinase DDR1. *J Biol Chem,* 281**,** 22744-51.

OGISO, H., ISHITANI, R., NUREKI, O., FUKAI, S., YAMANAKA, M., KIM, J. H., SAITO, K., SAKAMOTO, A., INOUE, M., SHIROUZU, M. & YOKOYAMA, S. 2002. Crystal structure of the complex of human epidermal growth factor and receptor extracellular domains. *Cell,* 110**,** 775-87.

OLASO, E., IKEDA, K., ENG, F. J., XU, L., WANG, L. H., LIN, H. C. & FRIEDMAN, S. L. 2001. DDR2 receptor promotes MMP-2-mediated proliferation and invasion by hepatic stellate cells. *J Clin Invest,* 108**,** 1369-78.

OLASO, E., LABRADOR, J. P., WANG, L., IKEDA, K., ENG, F. J., KLEIN, R., LOVETT, D. H., LIN, H. C. & FRIEDMAN, S. L. 2002. Discoidin domain receptor 2 regulates fibroblast proliferation and migration through the extracellular matrix in association with transcriptional activation of matrix metalloproteinase-2. *J Biol Chem,* 277**,** 3606-13.

OLASO, E., LIN, H. C., WANG, L. H. & FRIEDMAN, S. L. 2011. Impaired dermal wound healing in discoidin domain receptor 2-deficient mice associated with defective extracellular matrix remodeling. *Fibrogenesis Tissue Repair,* 4**,** 5.

ONGUSAHA, P. P., KIM, J. I., FANG, L., WONG, T. W., YANCOPOULOS, G. D., AARONSON, S. A. & LEE, S. W. 2003. p53 induction and activation of DDR1 kinase counteract p53-mediated apoptosis and influence p53 regulation through a positive feedback loop. *EMBO J,* 22**,** 1289-301.

OURS, C. A., BIESECKER, L. G. & DARLING, T. N. 2022. Progression of skin lesions in Warburg-Cinotti syndrome. *JAAD Case Rep,* 20**,** 47-49.

PAGANI, C. A., BANCROFT, A. C., TOWER, R. J., LIVINGSTON, N., SUN, Y., HONG, J. Y., KENT, R. N., 3RD, STRONG, A. L., NUNEZ, J. H., MEDRANO, J. M. R., PATEL, N., NANES, B. A., DEAN, K. M., LI, Z., GE, C., BAKER, B. M., JAMES, A. W., WEISS, S. J., FRANCESCHI, R. T. & LEVI, B. 2022. Discoidin domain receptor 2 regulates aberrant mesenchymal lineage cell fate and matrix organization. *Sci Adv,* 8**,** eabq6152.

PAN, C., KUMAR, C., BOHL, S., KLINGMUELLER, U. & MANN, M. 2009. Comparative proteomic phenotyping of cell lines and primary cells to assess preservation of cell type-specific functions. *Mol Cell Proteomics,* 8**,** 443-50.

PANG, X., HE, X., QIU, Z., ZHANG, H., XIE, R., LIU, Z., GU, Y., ZHAO, N., XIANG, Q. & CUI, Y. 2023. Targeting integrin pathways: mechanisms and advances in therapy. *Signal Transduct Target Ther,* 8**,** 1.

PAPA, F. R., ZHANG, C., SHOKAT, K. & WALTER, P. 2003. Bypassing a kinase activity with an ATP-competitive drug. *Science,* 302**,** 1533-7.

PARASKEVOPOULOU, V. & FALCONE, F. H. 2018. Polyionic Tags as Enhancers of Protein Solubility in Recombinant Protein Expression. *Microorganisms,* 6.

PARK, K., JAYADEV, R., PAYNE, S. G., KENNY-GANZERT, I. W., CHI, Q., COSTA, D. S., RAMOS-LEWIS, W., THENDRAL, S. B. & SHERWOOD, D. R. 2023. Reciprocal

discoidin domain receptor signaling strengthens integrin adhesion to connect adjacent tissues. *Elife,* 12.

PARK, S. A., KIM, M. J., PARK, S. Y., KIM, J. S., LIM, W., NAM, J. S. & YHONG SHEEN, Y. 2015. TIMP-1 mediates TGF-beta-dependent crosstalk between hepatic stellate and cancer cells via FAK signaling. *Sci Rep,* 5**,** 16492.

PATEL, S. D., CHEN, C. P., BAHNA, F., HONIG, B. & SHAPIRO, L. 2003. Cadherin-mediated cell-cell adhesion: sticking together as a family. *Curr Opin Struct Biol,* 13**,** 690-8.

PAWSON, T. 2004. Specificity in signal transduction: from phosphotyrosine-SH2 domain interactions to complex cellular systems. *Cell,* 116**,** 191-203.

PELLICENA, P. & KURIYAN, J. 2006. Protein-protein interactions in the allosteric regulation of protein kinases. *Curr Opin Struct Biol,* 16**,** 702-9.

PEREZ, J. L., SHEN, X., FINKERNAGEL, S., SCIORRA, L., JENKINS, N. A., GILBERT, D. J., COPELAND, N. G. & WONG, T. W. 1994. Identification and chromosomal mapping of a receptor tyrosine kinase with a putative phospholipid binding sequence in its ectodomain. *Oncogene,* 9**,** 211-9.

PIEZ, K. A. 1997. History of extracellular matrix: a personal view. *Matrix Biol,* 16**,** 85-92.

PLAYFORD, M. P., BUTLER, R. J., WANG, X. C., KATSO, R. M., COOKE, I. E. & GANESAN, T. S. 1996. The genomic structure of discoidin receptor tyrosine kinase. *Genome Res,* 6**,** 620-7.

PLIKUS, M. V., WANG, X., SINHA, S., FORTE, E., THOMPSON, S. M., HERZOG, E. L., DRISKELL, R. R., ROSENTHAL, N., BIERNASKIE, J. & HORSLEY, V. 2021. Fibroblasts: Origins, definitions, and functions in health and disease. *Cell,* 184**,** 3852-3872.

POOLE, S., FIRTEL, R. A., LAMAR, E. & ROWEKAMP, W. 1981. Sequence and expression of the discoidin I gene family in Dictyostelium discoideum. *J Mol Biol,* 153**,** 273-89.

POTTIER, C., FRESNAIS, M., GILON, M., JERUSALEM, G., LONGUESPEE, R. & SOUNNI, N. E. 2020. Tyrosine Kinase Inhibitors in Cancer: Breakthrough and Challenges of Targeted Therapy. *Cancers (Basel),* 12.

POUDEL, B., KI, H. H., LEE, Y. M. & KIM, D. K. 2013. Induction of IL-12 production by the activation of discoidin domain receptor 2 via NF-kappaB and JNK pathway. *Biochem Biophys Res Commun,* 434**,** 584-8.

PRELICH, G. 2012. Gene overexpression: uses, mechanisms, and interpretation. *Genetics,* 190**,** 841-54.

PULSATELLI, L., ADDIMANDA, O., BRUSI, V., PAVLOSKA, B. & MELICONI, R. 2013. New findings in osteoarthritis pathogenesis: therapeutic implications. *Ther Adv Chronic Dis,* 4**,** 23-43.

QUAN, J., YAHATA, T., ADACHI, S., YOSHIHARA, K. & TANAKA, K. 2011. Identification of receptor tyrosine kinase, discoidin domain receptor 1 (DDR1), as a potential biomarker for serous ovarian cancer. *Int J Mol Sci,* 12**,** 971-82.

RADSTAKE, W. E., GAUTAM, K., VAN ROMPAY, C., VERMEESEN, R., TABURY, K., VERSLEGERS, M., BAATOUT, S. & BASELET, B. 2023. Comparison of in vitro scratch wound assay experimental procedures. *Biochem Biophys Rep,* 33**,** 101423.

RAUCH, J., VOLINSKY, N., ROMANO, D. & KOLCH, W. 2011. The secret life of kinases: functions beyond catalysis. *Cell Commun Signal,* 9**,** 23.

RAYNAL, N., HAMAIA, S. W., SILJANDER, P. R., MADDOX, B., PEACHEY, A. R., FERNANDEZ, R., FOLEY, L. J., SLATTER, D. A., JARVIS, G. E. & FARNDALE, R. W. 2006. Use of synthetic peptides to locate novel integrin alpha2beta1-binding motifs in human collagen III. *J Biol Chem,* 281**,** 3821-31.

RED BREWER, M., YUN, C. H., LAI, D., LEMMON, M. A., ECK, M. J. & PAO, W. 2013. Mechanism for activation of mutated epidermal growth factor receptors in lung cancer. *Proc Natl Acad Sci U S A,* 110**,** E3595-604.

REGER DE MOURA, C., BATTISTELLA, M., SOHAIL, A., CAUDRON, A., FEUGEAS, J. P., PODGORNIAK, M. P., PAGES, C., MAZOUZ DORVAL, S., MARCO, O., MENASHI, S., FRIDMAN, R., LEBBE, C., MOURAH, S. & JOUENNE, F. 2019. Discoidin domain receptors: A promising target in melanoma. *Pigment Cell Melanoma Res,* 32**,** 697-707.

REINHARDT, R., HIRZEL, K., LINK, G., EISLER, S. A., HAGELE, T., PARSON, M. A. H., BURKE, J. E., HAUSSER, A. & LEONARD, T. A. 2023. PKD autoinhibition in trans regulates activation loop autophosphorylation in cis. *Proc Natl Acad Sci U S A,* 120**,** e2212909120.

REINHARDT, R. & LEONARD, T. A. 2023. A critical evaluation of protein kinase regulation by activation loop autophosphorylation. *Elife,* 12.

REN, J., BOLLU, L. R., SU, F., GAO, G., XU, L., HUANG, W. C., HUNG, M. C. & WEIHUA, Z. 2013. EGFR-SGLT1 interaction does not respond to EGFR modulators, but inhibition of SGLT1 sensitizes prostate cancer cells to EGFR tyrosine kinase inhibitors. *Prostate,* 73**,** 1453-61.

REN, T., ZHANG, W., LIU, X., ZHAO, H., ZHANG, J., ZHANG, J., LI, X., ZHANG, Y., BU, X., SHI, M., YAO, L. & SU, J. 2014. Discoidin domain receptor 2 (DDR2) promotes breast cancer cell metastasis and the mechanism implicates epithelial-mesenchymal transition programme under hypoxia. *J Pathol,* 234**,** 526-37.

RICHARDSON, J. S. & RICHARDSON, D. C. 2002. Natural beta-sheet proteins use negative design to avoid edge-to-edge aggregation. *Proc Natl Acad Sci U S A,* 99**,** 2754-9.

RICHTER, M., PIWOCKA, O., MUSIELAK, M., PIOTROWSKI, I., SUCHORSKA, W. M. & TRZECIAK, T. 2021. From Donor to the Lab: A Fascinating Journey of Primary Cell Lines. *Front Cell Dev Biol,* 9**,** 711381.

RIKOVA, K., GUO, A., ZENG, Q., POSSEMATO, A., YU, J., HAACK, H., NARDONE, J., LEE, K., REEVES, C., LI, Y., HU, Y., TAN, Z., STOKES, M., SULLIVAN, L., MITCHELL, J., WETZEL, R., MACNEILL, J., REN, J. M., YUAN, J., BAKALARSKI, C. E., VILLEN, J., KORNHAUSER, J. M., SMITH, B., LI, D., ZHOU, X., GYGI, S. P., GU, T. L., POLAKIEWICZ, R. D., RUSH, J. & COMB, M. J. 2007. Global survey of phosphotyrosine signaling identifies oncogenic kinases in lung cancer. *Cell,* 131**,** 1190-203.

RODRIGUEZ, A., KAREN, J., GARDNER, H., GERDIN, B., RUBIN, K. & SUNDBERG, C. 2009. Integrin alpha1beta1 is involved in the differentiation into myofibroblasts in adult reactive tissues in vivo. *J Cell Mol Med,* 13**,** 3449-62.

ROMAYOR, I., GARCIA-VAQUERO, M. L., MARQUEZ, J., ARTETA, B., BARCELO, R. & BENEDICTO, A. 2022. Discoidin Domain Receptor 2 Expression as Worse Prognostic Marker in Invasive Breast Cancer. *Breast J,* 2022**,** 5169405.

ROSENBAUM, D. M., RASMUSSEN, S. G. & KOBILKA, B. K. 2009. The structure and function of G-protein-coupled receptors. *Nature,* 459**,** 356-63.

ROSKOSKI, R., JR. 2016. Classification of small molecule protein kinase inhibitors based upon the structures of their drug-enzyme complexes. *Pharmacol Res,* 103**,** 26-48.

RUBIN, I. & YARDEN, Y. 2001. The basic biology of HER2. *Ann Oncol,* 12 Suppl 1**,** S3-8.

SALA, M., ALLAIN, N., MOREAU, M., JABOUILLE, A., HENRIET, E., ABOU-HAMMOUD, A., UGUEN, A., DI-TOMMASO, S., DOURTHE, C., RAYMOND, A. A., DUPUY, J. W., GERARD, E., DUGOT-SENANT, N., ROUSSEAU, B., MERLIO, J. P., PHAM-LEDART, A., VERGIER, B., TARTARE-DECKERT, S., MOREAU, V. & SALTEL, F. 2022. Discoidin Domain Receptor 2 orchestrates melanoma resistance combining phenotype switching and proliferation. *Oncogene,* 41**,** 2571-2586.

SAMMON, D., HOHENESTER, E. & LEITINGER, B. 2020. Two-step release of kinase autoinhibition in discoidin domain receptor 1. *Proc Natl Acad Sci U S A,* 117**,** 22051-22060.

SANDOVAL-PEREZ, A., WINGER, B. A. & JACOBSON, M. P. 2022. Assessing the Activation of Tyrosine Kinase KIT through Free Energy Calculations. *J Chem Theory Comput,* 18**,** 6251-6258.

SCHIRO, J. A., CHAN, B. M., ROSWIT, W. T., KASSNER, P. D., PENTLAND, A. P., HEMLER, M. E., EISEN, A. Z. & KUPPER, T. S. 1991. Integrin alpha 2 beta 1 (VLA-2) mediates reorganization and contraction of collagen matrices by human cells. *Cell,* 67**,** 403-10.

SCHLESSINGER, J., PLOTNIKOV, A. N., IBRAHIMI, O. A., ELISEENKOVA, A. V., YEH, B. K., YAYON, A., LINHARDT, R. J. & MOHAMMADI, M. 2000. Crystal structure of a ternary FGF-FGFR-heparin complex reveals a dual role for heparin in FGFR binding and dimerization. *Mol Cell,* 6**,** 743-50.

SCHMINKE, B., MUHAMMAD, H., BODE, C., SADOWSKI, B., GERTER, R., GERSDORFF, N., BURGERS, R., MONSONEGO-ORNAN, E., ROSEN, V. & MIOSGE, N. 2014. A discoidin domain receptor 1 knock-out mouse as a novel model for osteoarthritis of the temporomandibular joint. *Cell Mol Life Sci,* 71**,** 1081-96.

SCHWINN, M. K., STEFFEN, L. S., ZIMMERMAN, K., WOOD, K. V. & MACHLEIDT, T. 2020. A Simple and Scalable Strategy for Analysis of Endogenous Protein Dynamics. *Sci Rep,* 10**,** 8953.

SEIRADAKE, E., HARLOS, K., SUTTON, G., ARICESCU, A. R. & JONES, E. Y. 2010. An extracellular steric seeding mechanism for Eph-ephrin signaling platform assembly. *Nat Struct Mol Biol,* 17**,** 398-402.

SHAMSIR, M. S. & DALBY, A. R. 2007. Beta-sheet containment by flanking prolines: molecular dynamic simulations of the inhibition of beta-sheet elongation by proline residues in human prion protein. *Biophys J,* 92**,** 2080-9.

SHAPIRO, P. S., WHALEN, A. M., TOLWINSKI, N. S., WILSBACHER, J., FROELICH-AMMON, S. J., GARCIA, M., OSHEROFF, N. & AHN, N. G. 1999. Extracellular signal-regulated kinase activates topoisomerase IIalpha through a mechanism independent of phosphorylation. *Mol Cell Biol,* 19**,** 3551-60.

SHAW, R. B., JR., CHONG, A. K. S., ZHANG, A., HENTZ, V. R. & CHANG, J. 2007. Dupuytren's disease: history, diagnosis, and treatment. *Plast Reconstr Surg,* 120**,** 44e-54e.

SHENOY, G. P., PAL, R., PURWARGA MATADA, G. S., SINGH, E., RAGHAVENDRA, N. M. & DHIWAR, P. S. 2023. Discoidin domain receptor inhibitors as anticancer agents: A systematic review on recent development of DDRs inhibitors, their resistance and structure activity relationship. *Bioorg Chem,* 130**,** 106215.

SHEWCHUK, L. M., HASSELL, A. M., ELLIS, B., HOLMES, W. D., DAVIS, R., HORNE, E. L., KADWELL, S. H., MCKEE, D. D. & MOORE, J. T. 2000. Structure of the Tie2 RTK

domain: self-inhibition by the nucleotide binding loop, activation loop, and C-terminal tail. *Structure,* 8**,** 1105-13.

SHIN, D. & MINN, K. W. 2004. The effect of myofibroblast on contracture of hypertrophic scar. *Plast Reconstr Surg,* 113**,** 633-40.

SHINTANI, Y., FUKUMOTO, Y., CHAIKA, N., SVOBODA, R., WHEELOCK, M. J. & JOHNSON, K. R. 2008. Collagen I-mediated up-regulation of N-cadherin requires cooperative signals from integrins and discoidin domain receptor 1. *J Cell Biol,* 180**,** 1277-89.

SHITOMI, Y., THOGERSEN, I. B., ITO, N., LEITINGER, B., ENGHILD, J. J. & ITOH, Y. 2015. ADAM10 controls collagen signaling and cell migration on collagen by shedding the ectodomain of discoidin domain receptor 1 (DDR1). *Mol Biol Cell,* 26**,** 659-73.

SHOELSON, S. E., BONI-SCHNETZLER, M., PILCH, P. F. & KAHN, C. R. 1991. Autophosphorylation within insulin receptor beta-subunits can occur as an intramolecular process. *Biochemistry,* 30**,** 7740-6.

SHRIVASTAVA, A., RADZIEJEWSKI, C., CAMPBELL, E., KOVAC, L., MCGLYNN, M., RYAN, T. E., DAVIS, S., GOLDFARB, M. P., GLASS, D. J., LEMKE, G. & YANCOPOULOS, G. D. 1997. An orphan receptor tyrosine kinase family whose members serve as nonintegrin collagen receptors. *Mol Cell,* 1**,** 25-34.

SILJANDER, P. R., HAMAIA, S., PEACHEY, A. R., SLATTER, D. A., SMETHURST, P. A., OUWEHAND, W. H., KNIGHT, C. G. & FARNDALE, R. W. 2004. Integrin activation state determines selectivity for novel recognition sites in fibrillar collagens. *J Biol Chem,* 279**,** 47763-72.

SONG, G., OUYANG, G. & BAO, S. 2005. The activation of Akt/PKB signaling pathway and cell survival. *J Cell Mol Med,* 9**,** 59-71.

STAUDINGER, L. A., SPANO, S. J., LEE, W., COELHO, N., RAJSHANKAR, D., BENDECK, M. P., MORIARTY, T. & MCCULLOCH, C. A. 2013. Interactions between the discoidin domain receptor 1 and beta1 integrin regulate attachment to collagen. *Biol Open,* 2**,** 1148-59.

STEFL, S., NISHI, H., PETUKH, M., PANCHENKO, A. R. & ALEXOV, E. 2013. Molecular mechanisms of disease-causing missense mutations. *J Mol Biol,* 425**,** 3919-36.

STEIN, E., LANE, A. A., CERRETTI, D. P., SCHOECKLMANN, H. O., SCHROFF, A. D., VAN ETTEN, R. L. & DANIEL, T. O. 1998. Eph receptors discriminate specific ligand oligomers to determine alternative signaling complexes, attachment, and assembly responses. *Genes Dev,* 12**,** 667-78.

SUN, X., WU, B., CHIANG, H. C., DENG, H., ZHANG, X., XIONG, W., LIU, J., ROZEBOOM, A. M., HARRIS, B. T., BLOMMAERT, E., GOMEZ, A., GARCIA, R. E., ZHOU, Y., MITRA, P., PREVOST, M., ZHANG, D., BANIK, D., ISAACS, C., BERRY, D., LAI, C., CHALDEKAS, K., LATHAM, P. S., BRANTNER, C. A., POPRATILOFF, A., JIN, V. X., ZHANG, N., HU, Y., PUJANA, M. A., CURIEL, T. J., AN, Z. & LI, R. 2021. Tumour DDR1 promotes collagen fibre alignment to instigate immune exclusion. *Nature,* 599**,** 673-678.

SUNK, I. G., BOBACZ, K., HOFSTAETTER, J. G., AMOYO, L., SOLEIMAN, A., SMOLEN, J., XU, L. & LI, Y. 2007. Increased expression of discoidin domain receptor 2 is linked to the degree of cartilage damage in human knee joints: a potential role in osteoarthritis pathogenesis. *Arthritis Rheum,* 56**,** 3685-92.

TADOKORO, S., SHATTIL, S. J., ETO, K., TAI, V., LIDDINGTON, R. C., DE PEREDA, J. M., GINSBERG, M. H. & CALDERWOOD, D. A. 2003. Talin binding to integrin beta tails: a final common step in integrin activation. *Science,* 302**,** 103-6.

TAKAI, K., DRAIN, A. P., LAWSON, D. A., LITTLEPAGE, L. E., KARPUJ, M., KESSENBROCK, K., LE, A., INOUE, K., WEAVER, V. M. & WERB, Z. 2018. Discoidin domain receptor 1 (DDR1) ablation promotes tissue fibrosis and hypoxia to induce aggressive basal-like breast cancers. *Genes Dev,* 32**,** 244-257.

TANG, D. D. & GERLACH, B. D. 2017. The roles and regulation of the actin cytoskeleton, intermediate filaments and microtubules in smooth muscle cell migration. *Respir Res,* 18**,** 54.

TERAI, H., TAN, L., BEAUCHAMP, E. M., HATCHER, J. M., LIU, Q., MEYERSON, M., GRAY, N. S. & HAMMERMAN, P. S. 2015. Characterization of DDR2 Inhibitors for the Treatment of DDR2 Mutated Nonsmall Cell Lung Cancer. *ACS Chem Biol,* 10**,** 2687-96.

TERPE, K. 2003. Overview of tag protein fusions: from molecular and biochemical fundamentals to commercial systems. *Appl Microbiol Biotechnol,* 60**,** 523-33.

TILL, J. H., BECERRA, M., WATTY, A., LU, Y., MA, Y., NEUBERT, T. A., BURDEN, S. J. & HUBBARD, S. R. 2002. Crystal structure of the MuSK tyrosine kinase: insights into receptor autoregulation. *Structure,* 10**,** 1187-96.

TOKI, F., HONKURA, N., SHIRAKATA, Y., IMAMURA, T., HIGASHIYAMA, S. & NANBA, D. 2013. Second harmonic generation reveals collagen fibril remodeling in fibroblast-populated collagen gels. *Cell Struct Funct,* 38**,** 227-36.

TOMASEK, J. J., GABBIANI, G., HINZ, B., CHAPONNIER, C. & BROWN, R. A. 2002. Myofibroblasts and mechano-regulation of connective tissue remodelling. *Nat Rev Mol Cell Biol,* 3**,** 349-63.

TORR, E. E., NGAM, C. R., BERNAU, K., TOMASINI-JOHANSSON, B., ACTON, B. & SANDBO, N. 2015. Myofibroblasts exhibit enhanced fibronectin assembly that is intrinsic to their contractile phenotype. *J Biol Chem,* 290**,** 6951-61.

TRENKER, R., CALL, M. J. & CALL, M. E. 2016. Progress and prospects for structural studies of transmembrane interactions in single-spanning receptors. *Curr Opin Struct Biol,* 39**,** 115-123.

TRENKER, R. & JURA, N. 2020. Receptor tyrosine kinase activation: From the ligand perspective. *Curr Opin Cell Biol,* 63**,** 174-185.

TRONO, P., OTTAVI, F. & ROSANO, L. 2024. Novel insights into the role of Discoidin domain receptor 2 (DDR2) in cancer progression: a new avenue of therapeutic intervention. *Matrix Biol,* 125**,** 31-39.

TSCHUMPERLIN, D. J. 2013. Fibroblasts and the ground they walk on. *Physiology (Bethesda),* 28**,** 380-90.

TSUKAHARA, R., UMAZUME, K., MCDONALD, K., KAPLAN, H. J. & TAMIYA, S. 2017. Focal adhesion kinase family is involved in matrix contraction by transdifferentiated Muller cells. *Exp Eye Res,* 164**,** 90-94.

ULLO, M. F. & CASE, L. B. 2023. How cells sense and integrate information from different sources. *WIREs Mech Dis,* 15**,** e1604.

UNTERGASSER, G., GANDER, R., LILG, C., LEPPERDINGER, G., PLAS, E. & BERGER, P. 2005. Profiling molecular targets of TGF-beta1 in prostate fibroblast-to-myofibroblast transdifferentiation. *Mech Ageing Dev,* 126**,** 59-69.

VAGENENDE, V., YAP, M. G. & TROUT, B. L. 2009. Mechanisms of protein stabilization and prevention of protein aggregation by glycerol. *Biochemistry,* 48**,** 11084-96.

VALIATHAN, R. R., MARCO, M., LEITINGER, B., KLEER, C. G. & FRIDMAN, R. 2012. Discoidin domain receptor tyrosine kinases: new players in cancer progression. *Cancer Metastasis Rev,* 31**,** 295-321.

VALLEE, A. & LECARPENTIER, Y. 2019. TGF-beta in fibrosis by acting as a conductor for contractile properties of myofibroblasts. *Cell Biosci,* 9**,** 98.

VAN DE WATER, L., VARNEY, S. & TOMASEK, J. J. 2013. Mechanoregulation of the Myofibroblast in Wound Contraction, Scarring, and Fibrosis: Opportunities for New Therapeutic Intervention. *Adv Wound Care (New Rochelle),* 2**,** 122-141.

VASUDEVAN, H. N., MAZOT, P., HE, F. & SORIANO, P. 2015. Receptor tyrosine kinases modulate distinct transcriptional programs by differential usage of intracellular pathways. *Elife,* 4.

VIJAYAN, R. S., HE, P., MODI, V., DUONG-LY, K. C., MA, H., PETERSON, J. R., DUNBRACK, R. L., JR. & LEVY, R. M. 2015. Conformational analysis of the DFG-out kinase motif and biochemical profiling of structurally validated type II inhibitors. *J Med Chem,* 58**,** 466-79.

VILELLA, E., GAS, C., GARCIA-RUIZ, B. & RIVERA, F. J. 2019. Expression of DDR1 in the CNS and in myelinating oligodendrocytes. *Biochim Biophys Acta Mol Cell Res,* 1866**,** 118483.

VOGEL, W., GISH, G. D., ALVES, F. & PAWSON, T. 1997. The discoidin domain receptor tyrosine kinases are activated by collagen. *Mol Cell,* 1**,** 13-23.

VOGEL, W. F. 2002. Ligand-induced shedding of discoidin domain receptor 1. *FEBS Lett,* 514**,** 175-80.

VOGEL, W. F., ASZODI, A., ALVES, F. & PAWSON, T. 2001. Discoidin domain receptor 1 tyrosine kinase has an essential role in mammary gland development. *Mol Cell Biol,* 21**,** 2906-17.

VOLINSKY, N. & KHOLODENKO, B. N. 2013. Complexity of receptor tyrosine kinase signal processing. *Cold Spring Harb Perspect Biol,* 5**,** a009043.

WANG, C. Z., HSU, Y. M. & TANG, M. J. 2005. Function of discoidin domain receptor I in HGF-induced branching tubulogenesis of MDCK cells in collagen gel. *J Cell Physiol,* 203**,** 295-304.

WANG, C. Z., SU, H. W., HSU, Y. C., SHEN, M. R. & TANG, M. J. 2006. A discoidin domain receptor 1/SHP-2 signaling complex inhibits alpha2beta1-integrin-mediated signal transducers and activators of transcription 1/3 activation and cell migration. *Mol Biol Cell,* 17**,** 2839-52.

WANG, Z., LONGO, P. A., TARRANT, M. K., KIM, K., HEAD, S., LEAHY, D. J. & COLE, P. A. 2011. Mechanistic insights into the activation of oncogenic forms of EGF receptor. *Nat Struct Mol Biol,* 18**,** 1388-93.

WARBURG, M., ULLMAN, S., JENSEN, H., PEDERSEN, H., KOBAYASHI, T., RUSSELL, B., TRANEBJAERG, L., RICHARD, G. & BRONDUM-NIELSEN, K. 2006. Blepharophimosis, corneal vascularization, deafness, and acroosteolysis: a "new" syndrome? *Am J Med Genet A,* 140**,** 2709-13.

WAUDBY, C. A., DOBSON, C. M. & CHRISTODOULOU, J. 2019. Nature and Regulation of Protein Folding on the Ribosome. *Trends Biochem Sci,* 44**,** 914-926.

WAY, T. D. & LIN, J. K. 2005. Role of HER2/HER3 co-receptor in breast carcinogenesis. *Future Oncol,* 1**,** 841-9.

WEHRMAN, T., HE, X., RAAB, B., DUKIPATTI, A., BLAU, H. & GARCIA, K. C. 2007. Structural and mechanistic insights into nerve growth factor interactions with the TrkA and p75 receptors. *Neuron,* 53**,** 25-38.

WEIHUA, Z., TSAN, R., HUANG, W. C., WU, Q., CHIU, C. H., FIDLER, I. J. & HUNG, M. C. 2008. Survival of cancer cells is maintained by EGFR independent of its kinase activity. *Cancer Cell,* 13**,** 385-93.

WENDLER, F., PURICE, T. M., SIMON, T., STEBBING, J. & GIAMAS, G. 2021. The LMTK-family of kinases: Emerging important players in cell physiology and pathogenesis. *Biochim Biophys Acta Mol Basis Dis,* 1867**,** 165372.

WICKSTEAD, B. & GULL, K. 2011. The evolution of the cytoskeleton. *J Cell Biol,* 194**,** 513-25.

WIEDUWILT, M. J. & MOASSER, M. M. 2008. The epidermal growth factor receptor family: biology driving targeted therapeutics. *Cell Mol Life Sci,* 65**,** 1566-84.

WIESMANN, C., ULTSCH, M. H., BASS, S. H. & DE VOS, A. M. 1999. Crystal structure of nerve growth factor in complex with the ligand-binding domain of the TrkA receptor. *Nature,* 401**,** 184-8.

WILKINSON, J. M., DAVIDSON, R. K., SWINGLER, T. E., JONES, E. R., CORPS, A. N., JOHNSTON, P., RILEY, G. P., CHOJNOWSKI, A. J. & CLARK, I. M. 2012. MMP-14 and MMP-2 are key metalloproteases in Dupuytren's disease fibroblast-mediated contraction. *Biochim Biophys Acta,* 1822**,** 897-905.

WOLTERSDORF, C., BONK, M., LEITINGER, B., HUHTALA, M., KAPYLA, J., HEINO, J., GIL GIROL, C., NILAND, S., EBLE, J. A., BRUCKNER, P., DREIER, R. & HANSEN, U. 2017. The binding capacity of alpha1beta1-, alpha2beta1- and alpha10beta1-integrins depends on non-collagenous surface macromolecules rather than the collagens in cartilage fibrils. *Matrix Biol,* 63**,** 91-105.

WOUTERS, V., LIMAYE, N., UEBELHOER, M., IRRTHUM, A., BOON, L. M., MULLIKEN, J. B., ENJOLRAS, O., BASELGA, E., BERG, J., DOMPMARTIN, A., IVARSSON, S. A., KANGESU, L., LACASSIE, Y., MURPHY, J., TEEBI, A. S., PENINGTON, A., RIEU, P. & VIKKULA, M. 2010. Hereditary cutaneomucosal venous malformations are caused by TIE2 mutations with widely variable hyper-phosphorylating effects. *Eur J Hum Genet,* 18**,** 414-20.

WU, J., LI, W., CRADDOCK, B. P., FOREMAN, K. W., MULVIHILL, M. J., JI, Q. S., MILLER, W. T. & HUBBARD, S. R. 2008. Small-molecule inhibition and activation-loop trans-phosphorylation of the IGF1 receptor. *EMBO J,* 27**,** 1985-94.

WU, L., ZHAO, X., MA, H., ZHANG, L. & LI, X. 2022. Discoidin Domain Receptor 1, a Potential Biomarker and Therapeutic Target in Hepatocellular Carcinoma. *Int J Gen Med,* 15**,** 2037-2044.

WU, P.-H., GILKES, D. M. & WIRTZ, D. 2018. The Biophysics of 3D Cell Migration. *Annual Review of Biophysics,* 47**,** 549-567.

WYBENGA-GROOT, L. E., BASKIN, B., ONG, S. H., TONG, J., PAWSON, T. & SICHERI, F. 2001. Structural basis for autoinhibition of the Ephb2 receptor tyrosine kinase by the unphosphorylated juxtamembrane region. *Cell,* 106**,** 745-57.

XIAO, L., LIU, C., WANG, B., FEI, W., MU, Y., XU, L. & LI, Y. 2021. Targeting Discoidin Domain Receptor 2 for the Development of Disease-Modifying Osteoarthritis Drugs. *Cartilage,* 13**,** 1285S-1291S.

XIE, B., LIN, W., YE, J., WANG, X., ZHANG, B., XIONG, S., LI, H. & TAN, G. 2015. DDR2 facilitates hepatocellular carcinoma invasion and metastasis via activating ERK signaling and stabilizing SNAIL1. *J Exp Clin Cancer Res,* 34**,** 101.

XU, H., ABE, T., LIU, J. K., ZALIVINA, I., HOHENESTER, E. & LEITINGER, B. 2014. Normal activation of discoidin domain receptor 1 mutants with disulfide cross-links, insertions, or deletions in the extracellular juxtamembrane region: mechanistic implications. *J Biol Chem,* 289**,** 13565-74.

XU, H., BIHAN, D., CHANG, F., HUANG, P. H., FARNDALE, R. W. & LEITINGER, B. 2012. Discoidin domain receptors promote alpha1beta1- and alpha2beta1-integrin mediated cell adhesion to collagen by enhancing integrin activation. *PLoS One,* 7**,** e52209.

XU, H., RAYNAL, N., STATHOPOULOS, S., MYLLYHARJU, J., FARNDALE, R. W. & LEITINGER, B. 2011. Collagen binding specificity of the discoidin domain receptors: binding sites on collagens II and III and molecular determinants for collagen IV recognition by DDR1. *Matrix Biol,* 30**,** 16-26.

XU, L., JENSEN, H., JOHNSTON, J. J., DI MARIA, E., KLOTH, K., CRISTEA, I., SAPP, J. C., DARLING, T. N., HURYN, L. A., TRANEBJAERG, L., CINOTTI, E., KUBISCH, C., RODAHL, E., BRULAND, O., BIESECKER, L. G., HOUGE, G. & BREDRUP, C. 2018. Recurrent, Activating Variants in the Receptor Tyrosine Kinase DDR2 Cause Warburg-Cinotti Syndrome. *Am J Hum Genet,* 103**,** 976-983.

XU, L., PENG, H., GLASSON, S., LEE, P. L., HU, K., IJIRI, K., OLSEN, B. R., GOLDRING, M. B. & LI, Y. 2007. Increased expression of the collagen receptor discoidin domain receptor 2 in articular cartilage as a key event in the pathogenesis of osteoarthritis. *Arthritis Rheum,* 56**,** 2663-73.

XU, L., PENG, H., WU, D., HU, K., GOLDRING, M. B., OLSEN, B. R. & LI, Y. 2005. Activation of the discoidin domain receptor 2 induces expression of matrix metalloproteinase 13 associated with osteoarthritis in mice. *J Biol Chem,* 280**,** 548-55.

XU, L., SERVAIS, J., POLUR, I., KIM, D., LEE, P. L., CHUNG, K. & LI, Y. 2010. Attenuation of osteoarthritis progression by reduction of discoidin domain receptor 2 in mice. *Arthritis Rheum,* 62**,** 2736-44.

XU, Y. & KIRCHNER, M. 2021. Collagen Mimetic Peptides. *Bioengineering (Basel),* 8.

YAMAOKA, T., KUSUMOTO, S., ANDO, K., OHBA, M. & OHMORI, T. 2018. Receptor Tyrosine Kinase-Targeted Cancer Therapy. *Int J Mol Sci,* 19.

YANG, J. C., ZHANG, Y., HE, S. J., LI, M. M., CAI, X. L., WANG, H., XU, L. M. & CAO, J. 2017. TM4SF1 Promotes Metastasis of Pancreatic Cancer via Regulating the Expression of DDR1. *Sci Rep,* 7**,** 45895.

YANG, K., KIM, J. H., KIM, H. J., PARK, I. S., KIM, I. Y. & YANG, B. S. 2005. Tyrosine 740 phosphorylation of discoidin domain receptor 2 by Src stimulates intramolecular autophosphorylation and Shc signaling complex formation. *J Biol Chem,* 280**,** 39058-66.

YEH, Y. C., WANG, C. Z. & TANG, M. J. 2009. Discoidin domain receptor 1 activation suppresses alpha2beta1 integrin-dependent cell spreading through inhibition of Cdc42 activity. *J Cell Physiol,* 218**,** 146-56.

YEUNG, D., CHMIELEWSKI, D., MIHAI, C. & AGARWAL, G. 2013. Oligomerization of DDR1 ECD affects receptor-ligand binding. *J Struct Biol,* 183**,** 495-500.

YEUNG, D. A., SHANKER, N., SOHAIL, A., WEISS, B. A., WANG, C., WELLMERLING, J., DAS, S., GANJU, R. K., MILLER, J. L. C., HERR, A. B., FRIDMAN, R. & AGARWAL, G. 2019. Clustering, Spatial Distribution, and Phosphorylation of Discoidin Domain Receptors 1 and 2 in Response to Soluble Collagen I. *J Mol Biol,* 431**,** 368-390.

YU, Q., LIU, R., CHEN, Y., WAQAR, A. B., LIU, F., YANG, J., LIAN, T., ZHANG, G., GUAN, H., CUI, Y. & XU, C. 2021. Discoidin Domain-Containing Receptor 2 Is Present in Human Atherosclerotic Plaques and Involved in the Expression and Activity of MMP-2. *Oxid Med Cell Longev,* 2021**,** 1010496.

YUNN, N. O., KIM, J., RYU, S. H. & CHO, Y. 2023. A stepwise activation model for the insulin receptor. *Exp Mol Med,* 55**,** 2147-2161.

YUZAWA, S., OPATOWSKY, Y., ZHANG, Z., MANDIYAN, V., LAX, I. & SCHLESSINGER, J. 2007. Structural basis for activation of the receptor tyrosine kinase KIT by stem cell factor. *Cell,* 130**,** 323-34.

ZAKERI, B., FIERER, J. O., CELIK, E., CHITTOCK, E. C., SCHWARZ-LINEK, U., MOY, V. T. & HOWARTH, M. 2012. Peptide tag forming a rapid covalent bond to a protein, through engineering a bacterial adhesin. *Proc Natl Acad Sci U S A,* 109**,** E690-7.

ZHANG, G. & IGNATOVA, Z. 2011. Folding at the birth of the nascent chain: coordinating translation with co-translational folding. *Curr Opin Struct Biol,* 21**,** 25-31.

ZHANG, K., CORSA, C. A., PONIK, S. M., PRIOR, J. L., PIWNICA-WORMS, D., ELICEIRI, K. W., KEELY, P. J. & LONGMORE, G. D. 2013. The collagen receptor discoidin domain receptor 2 stabilizes SNAIL1 to facilitate breast cancer metastasis. *Nat Cell Biol,* 15**,** 677-87.

ZHANG, Q., WANG, P., FANG, X., LIN, F., FANG, J. & XIONG, C. 2022. Collagen gel contraction assays: From modelling wound healing to quantifying cellular interactions with three-dimensional extracellular matrices. *Eur J Cell Biol,* 101**,** 151253.

ZHANG, Y., SU, J., YU, J., BU, X., REN, T., LIU, X. & YAO, L. 2011. An essential role of discoidin domain receptor 2 (DDR2) in osteoblast differentiation and chondrocyte maturation via modulation of Runx2 activation. *J Bone Miner Res,* 26**,** 604-17.

ZHAO, H., BIAN, H., BU, X., ZHANG, S., ZHANG, P., YU, J., LAI, X., LI, D., ZHU, C., YAO, L. & SU, J. 2016a. Targeting of Discoidin Domain Receptor 2 (DDR2) Prevents Myofibroblast Activation and Neovessel Formation During Pulmonary Fibrosis. *Mol Ther,* 24**,** 1734-1744.

ZHAO, X. K., CHENG, Y., LIANG CHENG, M., YU, L., MU, M., LI, H., LIU, Y., ZHANG, B., YAO, Y., GUO, H., WANG, R. & ZHANG, Q. 2016b. Focal Adhesion Kinase Regulates Fibroblast Migration via Integrin beta-1 and Plays a Central Role in Fibrosis. *Sci Rep,* 6**,** 19276.

ZHAO, Y., CHAPMAN, D. A. & JONES, I. M. 2003. Improving baculovirus recombination. *Nucleic Acids Res,* 31**,** E6-6.

ZHAO, Z., XIE, L. & BOURNE, P. E. 2017. Insights into the binding mode of MEK type-III inhibitors. A step towards discovering and designing allosteric kinase inhibitors across the human kinome. *PLoS One,* 12**,** e0179936.

ZHOU, D. W., FERNANDEZ-YAGUE, M. A., HOLLAND, E. N., GARCIA, A. F., CASTRO, N. S., O'NEILL, E. B., EYCKMANS, J., CHEN, C. S., FU, J., SCHLAEPFER, D. D. & GARCIA, A. J. 2021. Force-FAK signaling coupling at individual focal adhesions coordinates mechanosensing and microtissue repair. *Nat Commun,* 12**,** 2359.

ZHOU, J., LIN, J., LEUNG, W. T. & WANG, L. 2020. A basic understanding of mucopolysaccharidosis: Incidence, clinical features, diagnosis, and management. *Intractable Rare Dis Res,* 9**,** 1-9.

ZHU, Y. S., ZHANG, J. N., MO, T. T., JIANG, C., MA, R. C. & CHEN, L. 2021. Discoidin domain receptor 2 activation of p38 mitogen-activated protein kinase as an important pathway for osteonectin-regulating osteoblast mineralization. *J Orthop Surg Res,* 16**,** 711.